

**Nitric oxide formation in nitrosation reactions, with  
applications in the sensitisation of emulsion explosives**

**Submitted for the Degree of  
DOCTOR OF PHILOSOPHY**

**Mark Stuart Rayson, BEng (Hons), BBus**

**June, 2012**

## STATEMENT OF ORIGINALITY

*The thesis contains no material which has been accepted for the award of any other degree or diploma in any university or other tertiary institution and, to the best of my knowledge and belief, contains no material previously published or written by another person, except where due reference has been made in the text. I give consent to this copy of my thesis, when deposited in the University Library, being made available for loan and photocopying subject to the provisions of the Copyright Act 1968.*

Date:

---

Mark Rayson

## STATEMENT OF AUTHORSHIP

*I hereby certify that the work embodied in this thesis contains published papers of which I am a joint author. I have included as part of the thesis a written statement, endorsed by my supervisor, attesting to my contribution to the joint publications.*

Date:

---

Mark Rayson

## STATEMENT OF CONTRIBUTION OF OTHERS

*We, the undersigned, attest that the Research Higher Degree candidate, Mark Rayson, has devised the experimental program, conducted experiments, analysed data, performed computational chemistry calculations and has written all papers included in this thesis. Professors Bogdan Dlugogorski, Eric Kennedy and John Mackie provided advice on the experimental program, project direction and assisted with editing the papers, consistent with normal supervisor-candidate relations.*

---

Bogdan Dlugogorski

Date:

---

Eric Kennedy

Date:

---

John Mackie

Date:

## **ACKNOWLEDGEMENTS**

I would like to express my sincere thanks to my colleagues, family and friends for their support throughout my studies. In particular, the continued guidance and encouragement from my supervisors, Professors Bogdan Dlugogorski, Eric Kennedy and John Mackie has been greatly appreciated. I would also like to thank the staff at the Dyno Nobel Mt Thorley Technical Centre who assisted in the project. Financial support from the Australian Research Council and Dyno Nobel Asia Pacific Pty. Ltd is gratefully acknowledged.

## TABLE OF CONTENTS

DECLARATION		ii
STATEMENT OF AUTHORSHIP		iii
STATEMENT OF CONTRIBUTION OF OTHERS		iv
ACKNOWLEDGMENTS		v
TABLE OF CONTENTS		vi
ABSTRACT		viii
Chapter 1	Introduction and hypothesis	1
Chapter 2	Literature review	11
Chapter 3	Experimental and computational methods	35
Chapter 4	Accurate rate constants for the decomposition of aqueous nitrous acid	69
Chapter 5	Experimental study of decomposition of aqueous nitrosyl thiocyanate	101
Chapter 6	Quantum chemistry study of nitrosyl thiocyanate decomposition mechanism	149
Chapter 7	Solubility of nitric oxide in concentrated solutions of ammonium and sodium nitrates	193
Chapter 8	Decomposition of nitrous acid in solutions of sodium and ammonium nitrates	217
Chapter 9	Kinetic model of NO <sub>x</sub> and N <sub>2</sub> formation reactions and comparison to observed NO <sub>x</sub> formation during chemical gassing of emulsion explosives	243
Chapter 10	Conclusions and recommendations	295
Appendix A	Supporting information for Chapter 4	307
Appendix B	Supporting information for Chapter 5	323

<b>Appendix C</b>	Supporting information for Chapter 6	<b>341</b>
<b>Appendix D</b>	Supporting information for Chapter 8	<b>357</b>
<b>Appendix E</b>	Supporting information for Chapter 9	<b>367</b>
<b>Appendix F</b>	Publications arising from the present study	<b>379</b>

## ABSTRACT

This thesis examines the rates and mechanisms of chemical reactions leading to production of nitrogen oxides during nitrosation reactions and, in particular, those occurring under conditions relevant to the sensitisation of emulsion explosives, where these toxic gases pose a hazard to explosive users. The decomposition of nitrous acid and nitrosyl thiocyanate were identified in the literature review as likely sources of nitrogen oxides during nitrosation reactions and were subjected to detailed experimental and computational studies.

Stopped-flow spectrophotometry was employed to study the decomposition of nitrous acid in order to resolve discrepancies in the rate constants reported in the literature. The decomposition reactions were examined under conditions where the rate limiting step comprised the hydrolysis of nitrogen dioxide ( $\text{NO}_2$ ), enabling the derivation of a simplified rate law based on the known elementary reaction mechanism. The rate constant,  $1.34 \times 10^{-6} \text{ M}^{-1}\text{s}^{-1}$ , is thought to be of higher accuracy than those in the literature as it does not depend on the rate of parallel reaction pathways or on the rate of interphase mass transfer of gaseous reaction products. The activation energy for the simplified rate law was established to be  $107 \text{ kJ mol}^{-1}$ . Quantum chemistry calculations indicate that the majority of the large activation energy results from the endothermic nature of the equilibrium  $2\text{HNO}_2 \rightleftharpoons \text{NO} + \text{NO}_2 + \text{H}_2\text{O}$ . The rate constant for the reaction between nitrate ions and nitrous acid, which inhibits  $\text{HNO}_2$  decomposition, was also determined.



The decomposition of nitrosyl thiocyanate (ONSCN) comprises a complex sequence of reaction steps involving three reaction pathways, and results in the formation of NO and (SCN)<sub>2</sub>, with the latter undergoing a series of disproportion and hydrolysis reactions to ultimately yield SO<sub>4</sub><sup>2-</sup>, HCN and SCN<sup>-</sup>. The first reaction pathway involves an irreversible reaction second order in ONSCN, producing NO and (SCN)<sub>2</sub> directly, whilst the second pathway constitutes a reversible reaction between ONSCN and SCN<sup>-</sup> to yield NO and an (SCN)<sub>2</sub><sup>-</sup> intermediate. The rate limiting step of the second pathway involves the reaction between (SCN)<sub>2</sub><sup>-</sup> and ONSCN, which could occur via S-nitrosation of (SCN)<sub>2</sub><sup>-</sup> by ONSCN or through a radical substitution mechanism. The third reaction pathway, which becomes significant at low thiocyanate concentrations, involves the formation of a previously unreported species, ONOSCN, via reaction between ONSCN and HOSCN, the latter being an intermediate in the hydrolysis of (SCN)<sub>2</sub>. The proposed kinetic mechanism provides an excellent fit to the experimental measurements, and enables accurate modelling of the ONSCN decomposition reactions. Comparison of the HNO<sub>2</sub> and ONSCN decomposition kinetics showed that HNO<sub>2</sub> decomposition is the dominant NO<sub>x</sub> formation pathway under conditions relevant to explosive sensitisation.

A quantum chemistry study was undertaken to determine the thermodynamic feasibility of the nitrosyl thiocyanate decomposition mechanism proposed on the basis of kinetic experiments. The procedure involved combining the results of accurate gas phase calculations, performed with the G3B3 and CBS-QB3 methods, with solvation free energies computed using continuum solvent models. Eight different procedures for calculating the solvation free energy were benchmarked against a set of six reactions with established reaction free energies, with the combination of the B3LYP/6-

31+G(d,p) method and the PCM solvation model with either UAHF or UFF atomic radii yielding the best results, with a mean absolute deviation on the order of 6 kJ mol<sup>-1</sup>. The quantum chemistry results support the experimentally determined reaction mechanism, and confirmed the formation and subsequent decomposition of the previously unreported species, ONOSCN, to be thermodynamically feasible.

The solubility of nitric oxide in ammonium and sodium nitrate solutions was examined at temperatures ranging from 25 to 55 °C, at salt concentrations up to 7.5 and 10 mol L<sup>-1</sup> for the sodium and ammonium salts, respectively. The solubility decreased significantly with increasing salt concentration, as predicted from the Sechenov equation. The enthalpy of solvation of NO decreased considerably with increasing salt concentration, indicating that the effect of temperature on the solubility diminishes with increasing salt concentration. The effect of sodium nitrate on NO solubility was significantly greater than that of ammonium nitrate, in agreement with previous literature results, which show that sodium ions have a much greater effect on gas solubility than ammonium ions. A model was developed to describe the solubility of NO as a function of salt concentration and temperature. The model predicted the solubility of NO in 13 mol L<sup>-1</sup> NH<sub>4</sub>NO<sub>3</sub> (as found in emulsion explosives) to be 5 times lower than in water at 25 °C, and largely independent of temperature.

A novel membrane inlet reactor was employed to examine the effect of ammonium and sodium nitrate concentrations on the decomposition equilibrium of nitrous acid. An increase in the observed equilibrium constant was recorded at low salt concentrations (up to 1 mol L<sup>-1</sup>) owing to the initial rapid decline in the nitrate activity coefficient with increasing salt concentration, whilst a steady decline in the observed equilibrium

constant at high salt concentrations was attributed to the relative increase in the activity coefficients of NO and  $H^+$  compared to that of  $HNO_2$ . Modelling of the activity coefficients of species involved in nitrous acid decomposition permitted extrapolation of the results to supersaturated solutions of ammonium nitrate relevant to emulsion explosives. Owing to cancellation effects among the activity coefficients of species involved in the decomposition equilibrium, the model predicts a similar aqueous NO concentration in concentrated salt solution to that observed in dilute acid. However, owing to the salting out effect, under the conditions of the present study, the equilibrium partial pressure of nitric oxide is approximately four times higher in concentrated ammonium nitrate compared to dilute acid solution.

A kinetic model was developed to predict the rate of  $N_2$  and NO formation from the nitrosation of ammonia under conditions relevant to emulsion explosives. Experiments in ammonium nitrate solution showed that the model correctly predicts the rates of both  $N_2$  and NO formation, including the catalytic effect of thiocyanate ions. The kinetic model was then employed to predict the amount of NO produced during the gassing of an emulsion explosive, and the results compared to laboratory measurements. Simulations showed that inclusion of sulfamate ions in the emulsion could significantly reduce the amount of NO formed, whilst addition of urea was predicted to have a negligible effect owing to its poor reactivity with nitrous acid. The levels of NO predicted by the model were similar to those observed experimentally, confirming nitrous acid decomposition as the sole source of  $NO_x$  during explosive sensitisation.

A common commercial chemical gassing technology involves sequential addition of concentrated acid and nitrite solutions to the explosive. Both experiments and

simulations showed that, provided the components required to effect nitrosation are well mixed into the explosive, nitric oxide constitutes less than 1 % of the reaction products. However, during large scale explosive sensitisation, inadequate mixing could lead to direct contact between the concentrated acid and nitrite solutions. Experiments showed that direct contact between concentrated acetic acid and sodium nitrite solutions results in rapid nitrous acid decomposition, with the stoichiometric amount of nitric oxide produced within 5 min. As such, direct contact between these solutions is the likely cause of visible  $\text{NO}_x$  emissions during explosive sensitisation. The amount of NO formed can be reduced by inclusion of a nitrous acid scavenger in the acid solution to convert nitrous acid into harmless  $\text{N}_2$ , however, owing to the rapid rate of nitrous acid decomposition in concentrated solutions, NO formation cannot be completely eliminated.

## **CHAPTER 1**

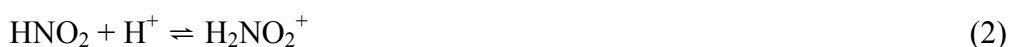
### **Introduction and hypothesis**

## **Table of Contents**

1.1	Background	3
1.2	Objectives, hypothesis and focussing questions	6
1.3	Thesis structure	8
1.4	References	9

## 1.1 Background

Nitrosation reactions, in which the nitroso ( $\text{NO}^+$ ) group is transferred from a nitrosating agent to a substrate, are important in a diverse range of industrial, environmental and biological settings. Industrially, nitrosation reactions find application in the synthesis of azo dyes<sup>1</sup>, the production of hydroxylamine<sup>2</sup>, the sensitisation of emulsion explosives<sup>3</sup> and have potential to assist in removal of wax deposits in oil pipelines<sup>4</sup>. In biology, nitrosation reactions have received great attention owing to the importance of S-nitrosothiols as a source of nitric oxide in the human body<sup>5, 6</sup>, and due to the potential for formation of carcinogenic N-nitrosamines, which can occur under acidic conditions in the human body or in the environment<sup>7</sup>. Under acidic conditions, nitrosation reactions occur via the nitrosating agents  $\text{N}_2\text{O}_3$  and  $\text{H}_2\text{NO}_2^+$ , derived from nitrous acid<sup>8</sup>.  $\text{N}_2\text{O}_3$  is the primary nitrosating agent under mildly acidic conditions, ( $\text{pH} > 1$ ), whilst  $\text{H}_2\text{NO}_2^+$  dominates under highly acidic conditions.



In the presence of added nucleophiles, such as  $\text{Cl}^-$ ,  $\text{Br}^-$ ,  $\text{I}^-$  and  $\text{SCN}^-$ , a new nitrosation pathway is introduced due to the formation of nitrosyl halides, denoted ONX (where  $\text{X} = \text{Cl}^-$ ,  $\text{Br}^-$ ,  $\text{I}^-$  or  $\text{SCN}^-$ ). The formation of nitrosyl halides catalyses a wide range of nitrosation reactions, owing to an increase in the concentration of nitrosating agents in the system. Thiocyanate ions, in particular, are a powerful catalyst owing to the large equilibrium constant for the formation of nitrosyl thiocyanate,  $\text{ONSCN}$ , and in many

cases the catalysed rate of nitrosation can be many orders of magnitude faster than the uncatalysed rate.<sup>9-11</sup> For a wide variety of substrates, the formation of ONSCN is sufficiently fast that it can be considered to be at equilibrium as shown below<sup>12</sup>:

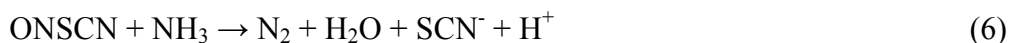


$$K_{ONSCN} = \frac{[ONSCN]}{[H^+][HNO_2][SCN^-]} \quad (4)$$

The interest in nitrosation reactions in the present study originates from their application in the sensitisation of emulsion explosives. Emulsion explosives consist of discrete droplets of super-saturated ammonium nitrate solution dispersed within a continuous hydrocarbon phase, usually diesel. This type of explosive is deployed extensively for mineral extraction in both open cut and underground mining due to the advantages of low cost, high water resistance and improved safety compared to high explosives such as trinitrotoluene, nitroglycerine and nitrocellulose<sup>13</sup>. Owing to their high stability, emulsion explosives must be sensitised prior to detonation via the introduction of small voids within the emulsion matrix. These voids undergo adiabatic compression during detonation, raising their temperature and propagating the explosion through the bulk explosive<sup>14</sup>. The voids can be introduced physically in the form of hollow, light weight materials such as glass micro-balloons, grain hulls or polystyrene foam. Alternatively, voids can be introduced in the form of gas bubbles generated from a chemical reaction inside the emulsion. The latter process, known as chemical gassing, is the most common sensitisation method and involves adding one or more chemicals to the emulsion which react to generate gas bubbles within the explosive. A popular chemical



gassing technique involves the generation of nitrogen gas in the explosive via the nitrosation of ammonia, which is present in solutions of ammonium nitrate<sup>15</sup>. The reaction is effected by the addition of a concentrated solution of a nitrite salt to the explosive, which can contain added nucleophiles such as thiocyanate ions, forming nitrosating agents in situ according to Equations 1-3. These nitrosating agents react with ammonia to form nitrogen gas, N<sub>2</sub>, as shown below:



This method, however, suffers from several drawbacks, including slow reaction rates at ambient temperatures (particularly for Reaction 5) and the generation of toxic nitrogen oxides (NO<sub>x</sub>) via side reactions<sup>16</sup>. The formation of NO<sub>x</sub> poses a safety hazard to mine workers prior to explosive detonation as a consequence of their high toxicity, particularly nitrogen dioxide (NO<sub>2</sub>), which can cause severe respiratory problems including lung oedema, and aggravate existing respiratory illnesses such as asthma<sup>17</sup>. Despite the significant dangers presented by NO<sub>x</sub> formation, the mechanisms for the generation of NO<sub>x</sub> during chemical gassing are unknown.

## 1.2 Objectives, hypothesis and focussing questions

The aim of this study is to determine the rates and mechanisms of the chemical reactions leading to  $\text{NO}_x$  formation during nitrosation reactions, and in particular, those relevant to explosive sensitisation. Knowledge of the rates and mechanisms of  $\text{NO}_x$  formation will enable selection of reaction conditions, such as reagent concentrations, pH and temperatures to minimise the formation of  $\text{NO}_x$  during chemical gassing. Furthermore, knowledge of the source of  $\text{NO}_x$  will assist in the development of new intrinsically safe gassing technologies, such as the deployment of new reaction substrates that eliminate or reduce the prevalence of  $\text{NO}_x$  formation pathways.

It is hypothesised that the formation of  $\text{NO}_x$  during chemical gassing results from the decomposition of chemical species associated with the explosive sensitisation process, in particular, the nitrosating agents nitrous acid and nitrosyl thiocyanate. The aim of the thesis is to investigate these reaction pathways and to address the following focussing questions:

1. What are the mechanisms for the decomposition of nitrosyl thiocyanate and nitrous in acidic aqueous solution, what are the products of the reaction and how fast do these reactions occur? How do variables such as reactant concentrations, temperature and pH affect the rate of these processes?
2. What corrections are required to enable models developed for nitrous acid and nitrosyl thiocyanate decomposition in aqueous solution to be applied to

predict the rates in solutions containing high concentrations (>60% wt) of ammonium nitrate?

3. Are the results of (1) – (2) consistent with the levels of  $\text{NO}_x$  observed when gassing emulsion explosives? What are the optimum conditions (i.e., pH, composition and temperature) for explosive sensitisation with respect to minimising  $\text{NO}_x$  formation? Could the formation of  $\text{NO}_x$  be reduced or avoided by employing an alternate reaction substrate or other modifications of the gassing chemistry?

### 1.3 Thesis structure

This thesis presents a comprehensive study on the  $\text{NO}_x$  formation reactions associated with nitrous acid and nitrosyl thiocyanate and the incidence of these reactions during the chemical gassing of emulsion explosives. The literature related to nitrous acid, nitrosyl thiocyanate and nitrosation chemistry is reviewed in the following chapter, whilst Chapter 3 provides an overview of the experimental and computational methods employed in the study. Chapters 4, 5 and 6 are concerned with the first focussing question and present experimental and computational chemistry studies on the decomposition of nitrous acid and nitrosyl thiocyanate in dilute acid solution. The second focussing question is addressed in Chapters 7 and 8, which relate to the effect of ammonium nitrate concentration on the solubility of nitric oxide and the equilibria associated with the decomposition of nitrous acid. Chapter 9 addresses the third focussing question by developing a kinetic model describing the concurrent formation of  $\text{NO}_x$  and  $\text{N}_2$  during ammonia nitrosation, including the effect of pH, temperature, and the addition of alternate reaction substrates. Simulation results are compared to experimental  $\text{NO}_x$  measurements during explosives sensitisation to confirm the source of  $\text{NO}_x$  during this process. Finally, Chapter 10 summarises the conclusions of the thesis and presents recommendations for further research efforts in this area.

## 1.4 References

1. Hunger, K.; Mischke, P.; Rieper, W.; Raue, R.; Kunde, K.; Engel, A., *Azo Dyes*. Wiley-VCH Verlag GmbH & Co. KGaA: 2000.
2. Rollefson, G. K.; Oldershaw, C. F., The reduction of nitrites to hydroxylamine by sulfites. *J. Am. Chem. Soc.* **1932**, *54* (3), 977-979.
3. da Silva, G.; Dlugogorski, B. Z.; Kennedy, E. M., Water-in-oil emulsion foaming by thiourea nitrosation: Reaction and mass transfer. *AIChE J.* **2006**, *52* (4), 1558-1565.
4. Nguyen, D. A.; Iwaniw, M. A.; Fogler, H. S., Kinetics and mechanism of the reaction between ammonium and nitrite ions: experimental and theoretical studies. *Chem. Eng. Sci.* **2003**, *58* (19), 4351-4362.
5. Stamler, J. S.; Singel, D. J.; Loscalzo, J., Biochemistry of nitric oxide and its redox-activated forms. *Science* **1992**, *258* (5090), 1898-1902.
6. Williams, D. L. H., The chemistry of S-nitrosothiols. *Acc. Chem. Res.* **1999**, *32* (10), 869-876.
7. Choi, J.; Valentine, R. L., N-Nitrosodimethylamine formation by free-chlorine-enhanced nitrosation of dimethylamine. *Environ. Sci. Technol.* **2003**, *37* (21), 4871-4876.
8. Ridd, J. H., Nitrosation, diazotisation, and deamination. *Q. Rev., Chem. Soc.* **1961**, *15* (4), 418-441.
9. Meyer, T. A.; Williams, D. L. H., Nucleophilic catalysis in the nitrosation of sarcosine and proline. *J. Chem. Soc., Perkin Trans. 2* **1988**, (4), 517-521.

10. Amado, S.; Blakelock, L.; Holmes, A. J.; Williams, D. L. H., Kinetics and mechanism of the formation and reactions of S-nitroso derivatives of some heterocyclic thiones. *J. Chem. Soc., Perkin Trans. 2* **2001**, (4), 441-447.
11. Hughes, E. D.; Ridd, J. H., 17. Nitrosation, diazotisation, and deamination. Part V. Catalysis by anions of strong acids in the diazotisation of aniline and of o-chloroaniline in dilute perchloric acid. *J. Chem. Soc.* **1958**, 82-88.
12. Williams, D. L. H., *Nitrosation Reactions and the Chemistry of Nitric Oxide*. Elsevier B. V.: Amsterdam, 2004.
13. Sudweeks, W. B., Physical and chemical properties of industrial slurry explosives. *Ind. Eng. Chem. Prod. Res. Dev.* **1985**, 24 (3), 432-6.
14. Bourne, N. K.; Field, J. E., Bubble collapse and the initiation of explosion. *Proc. R. Soc. London, Ser. A* **1991**, 435 (1894), 423-435.
15. da Silva, G.; Dlugogorski, B. Z.; Kennedy, E. M., An experimental and theoretical study of the nitrosation of ammonia and thiourea. *Chem. Eng. Sci.* **2006**, 61 (10), 3186-3197.
16. Vestre, J. *A Method for Preparing a Sensitised Emulsion Explosive* 2003. WO 03/055830 A1
17. Nitschke, M.; Smith, B. J.; Pilotto, L. S.; Pisaniello, D. L.; Abramson, M. J.; Ruffin, R. E., Respiratory health effects of nitrogen dioxide exposure and current guidelines. *Int. J. Environ. Health Res.* **1999**, 9 (1), 39-53.

## **CHAPTER 2**

**Literature Review: Nitrosation chemistry and the decomposition of nitrous acid and nitrosyl thiocyanate**

## Table of Contents

2.1	Nitrosation chemistry	13
2.2	Decomposition of nitrous acid and related reactions	17
2.3	Decomposition of nitrosyl thiocyanate	25
2.2.1	Formation of ONSCN	25
2.3.2	Decomposition of ONSCN: Background and potential pathways	27
2.4	References	31



## 2.1 Nitrosation chemistry

Nitrosation reactions represent a class of chemical reactions involving the formation of a nitrosyl compound<sup>1</sup>. Nitrosation reactions typically comprise the transfer of the nitrosyl cation ( $\text{NO}^+$ ) from one species to another and are usually undertaken using nitrous acid, formed in situ via the protonation of an inorganic nitrite salt, frequently sodium nitrite (Reaction 1). Nitrous acid constitutes a weak acid, exhibiting a  $\text{p}K_a$  of 3.16 at 25 °C<sup>2</sup>.



In most cases, the reaction does not occur with nitrous acid itself, but with species derived from nitrous acid which act as better  $\text{NO}^+$  donors<sup>3</sup>. At low acidity ( $\text{pH} > 2$ ), the predominant nitrosating species is dinitrogen trioxide ( $\text{N}_2\text{O}_3$ ) which typically exists in equilibrium with nitrous acid (Reaction 2)<sup>4</sup>. Formation of  $\text{N}_2\text{O}_3$  has been interpreted as the nitrosation of nitrite ions by  $\text{H}_2\text{NO}_2^+$ .<sup>5</sup> Experiments performed under conditions of rate limiting  $\text{N}_2\text{O}_3$  formation suggest that reaction between  $\text{H}_2\text{NO}_2^+$  and  $\text{HNO}_2$  is also possible.<sup>6</sup> At higher acidities ( $\text{pH} < 2$ ), the equilibrium concentration of the nitrous acidium ion (i.e. protonated nitrous acid)<sup>7</sup> increases, and an additional nitrosation pathway, referred to as the acid catalysed pathway, becomes significant. There is debate in the literature as to whether the nitrosating species is  $\text{H}_2\text{NO}_2^+$  or the  $\text{NO}^+$  cation itself; however, from a practical perspective the distinction is irrelevant as the species are kinetically indistinguishable.

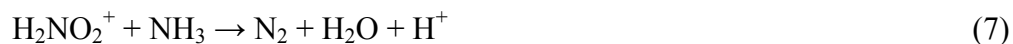
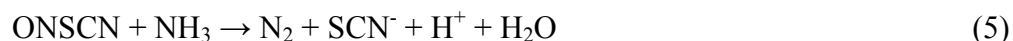




In the presence of nucleophilic species, such as thiocyanate ions, a parallel nitrosation pathway becomes possible. The mechanism involves the formation of an additional nitrosating agent, ONSCN, which exists in equilibrium with the thiocyanate ions and nitrous acid<sup>8</sup>. As such, thiocyanate ions can act as a catalyst for nitrosation reactions as they increase the concentration of active nitrosating agents. Analogous reactions have been reported for  $\text{Cl}^-$ ,  $\text{Br}^-$ ,  $\text{I}^-$  and thiourea.



Nitrosating agents such as ONSCN,  $\text{N}_2\text{O}_3$  and  $\text{H}_2\text{NO}_2^+$  react with ammonia to generate nitrogen gas as outlined in Reactions 5-7<sup>9</sup>:



As can be seen in Reactions 5-7, the reactive form of ammonia is  $\text{NH}_3$ , owing to the lone pair of electrons which make  $\text{NH}_3$  a much better nucleophile than its protonated form,  $\text{NH}_4^+$ .<sup>10</sup> However,  $\text{NH}_3$  is a weak base, and under conditions relevant to explosive sensitisation, the overwhelming majority of  $\text{NH}_3$  is in the form of unreactive  $\text{NH}_4^+$  ions ( $\text{p}K_a \text{ NH}_4^+ = 9.2$ )<sup>11</sup>. Thus, under the low pH conditions required to generate nitrosating

agents, the concentration of reactive  $\text{NH}_3$  is very low, resulting in a slow reaction rate.

The rate expressions for each nitrosating agent are shown in Equations 5a-7a<sup>7</sup>.

$$\frac{d[\text{N}_2]}{dt} = k_5 K_4 [\text{H}^+][\text{HNO}_2][\text{SCN}^-][\text{NH}_3] \quad (5a)$$

$$\frac{d[\text{N}_2]}{dt} = k_6 K_2 [\text{HNO}_2][\text{NO}_2^-][\text{H}^+][\text{NH}_3] \quad (6a)$$

$$\frac{d[\text{N}_2]}{dt} = k_7 K_3 [\text{H}^+][\text{HNO}_2][\text{NH}_3] \quad (7a)$$

where square brackets denote the concentration of the species in solution. It can be seen that the rate of the ONSCN pathway is first order in nitrous acid, hydrogen ion and thiocyanate concentrations. The  $\text{N}_2\text{O}_3$  reaction rate is second order in nitrous acid, whilst the  $\text{H}_2\text{NO}_2^+$  pathway is first order in both nitrous acid and hydrogen ion concentrations. Equations 5a-7a, in conjunction with the known reaction equilibria of 1-4 can be employed to determine both the rate of nitrogen formation and the concentrations of species present in the solution. Knowledge of the species present during ammonia nitrosation under various reaction conditions is important, because it is likely that  $\text{NO}_x$  formation results from parallel reactions of the same species responsible for  $\text{N}_2$  production. As such, this literature review focuses on  $\text{NO}_x$  formation from species present during explosive sensitisation. This review identified that nitrous acid and nitrosyl thiocyanate were both capable of undergoing decomposition reactions at room temperature leading to  $\text{NO}_x$ <sup>12, 13</sup>. The following sections provide a detailed discussion of the prior literature on these reactions.



## 2.2 Decomposition of nitrous acid and related reactions

Motivation for the study of nitrous acid decomposition is diverse, with the reactions playing important roles in many industrial and environmental processes. Industrially, the decomposition of nitrous acid is a significant process occurring in the manufacture of nitric acid, wherein a gaseous  $\text{NO}_x$  stream is absorbed in water<sup>14, 15</sup> and in synthesis reactions involving nitrous acid (i.e., nitrosation reactions) where the  $\text{NO}_x$  side products pose a toxicity hazard<sup>1, 16</sup>. In atmospheric chemistry, the reactions of nitrous acid and  $\text{NO}_x$  have received attention owing to their importance in acid deposition on the earth's surface and their role in smog formation<sup>17</sup>, whilst the reactions may be of biological importance under certain conditions where nitrous acid decomposition could contribute to NO production in the body<sup>18</sup>. The decomposition of nitrous acid can be employed as a source of NO in the laboratory<sup>19</sup>, and has been implicated in the release of nitrogen oxides from plants<sup>20</sup>. Because of these considerations, the kinetics of nitrous acid decomposition have received considerable attention in the literature, however, the reported rate constants exhibit significant disagreement.

The decomposition of nitrous acid was first examined by Abel and Schmidt<sup>21</sup>, who studied the reaction in a well mixed gas-liquid reactor assuming that dissolved NO was in equilibrium with the gas phase in accordance with Henry's law. The reaction was discovered to have a stoichiometry of three moles of nitrous acid decomposing to produce two moles of NO and one mole of nitric acid, and to have a rate law fourth order in nitrous acid and inversely proportional to the square of the NO partial pressure.



$$\frac{d[HNO_2]}{dt} = \frac{k_{fwd}[HNO_2]^4}{P_{NO}^2} \quad (8a)$$

This rate law can be rationalised by assuming that nitrous acid is in equilibrium with dissolved NO and NO<sub>2</sub> (Reaction 9) and that the hydrolysis of NO<sub>2</sub> is rate limiting (Reaction 10). A derivation of Equation 8a is provided in Appendix A. The hydrolysis of NO<sub>2</sub> comprises a reaction second order in NO<sub>2</sub> concentration, whilst two moles of nitrous acid are required to produce one mole each of NO and NO<sub>2</sub>, yielding an overall rate law that is fourth order in HNO<sub>2</sub> (Equation 11).



$$\frac{d[HNO_2]}{dt} = -\frac{3k_{10}K_9^2[HNO_2]^4}{[NO]^2} \quad (11)$$

Reactions (9) and (10) proceed via N<sub>2</sub>O<sub>3</sub> and N<sub>2</sub>O<sub>4</sub> intermediates, respectively, however, this distinction is not important kinetically provided that these species are at equilibrium. Under typical conditions of explosive gassing, the formation of N<sub>2</sub>O<sub>3</sub> has been shown to be sufficiently rapid for N<sub>2</sub>O<sub>3</sub> to be in equilibrium with HNO<sub>2</sub><sup>9</sup>, whilst the rate of formation of N<sub>2</sub>O<sub>4</sub> is considerably faster than the hydrolysis of NO<sub>2</sub> and as such, NO<sub>2</sub> exists in equilibrium with N<sub>2</sub>O<sub>4</sub>.<sup>22</sup> This mechanism has been confirmed in a

number of independent studies, which have been reviewed in detail by Schwartz and White<sup>23</sup>.

Schwartz and White<sup>23</sup> performed a comprehensive review of experimental studies related to the absorption of NO and NO<sub>2</sub> in water. Part of that study reviewed the decomposition of nitrous acid, which is the reverse process of NO<sub>x</sub> hydrolysis. The review by Schwartz & White recommended a set of values for the rate constants of (9) and (10) based on a consensus of literature values. A major deficiency of the values recommended by Schwartz and White for determining the rate of nitrous acid decomposition is that many of the studies reviewed were concerned with either Reaction 9 or 10 occurring in isolation. Thus, the recommended value of  $k_9$  comes from the isotope exchange experiments of Bunton and Stedman<sup>24</sup> and the diazotisation experiments of Hughes and Ridd<sup>25</sup> and assumes that the reaction proceeds through an N<sub>2</sub>O<sub>3</sub> intermediate, with NO and NO<sub>2</sub> in equilibrium with N<sub>2</sub>O<sub>3</sub>. The value of  $k_{10}$  was recommended based on a consensus of rate constants from studies concerned with the dissolution of gaseous NO<sub>2</sub> in water and the pulse radiolysis or flash photolysis of nitrite solutions, for which different estimates of the rate constants varied over an order of magnitude. Although the selection of the “recommended” values in themselves appears quite reasonable, it is unclear whether the combination of rate constants determined by different methods will result in the correct value of  $K_9^2 k_{10}$ . For example, the quantity  $K_9^2 k_{10}$  determined from the individual rate constants of Schwartz and White is  $2.4 \times 10^{-6} \text{ M}^{-1} \text{ s}^{-1}$ , which is a factor of 2.5 larger than the value of  $9.4 \times 10^{-7} \text{ M}^{-1} \text{ s}^{-1}$  inferred from the data of Abel and Schmidt<sup>21</sup> assuming a Henry’s constant for NO of  $1.9 \times 10^{-3} \text{ M atm}^{-1}$ .<sup>26</sup> Thus, it is unclear which rate constants should be selected when attempting to accurately model the formation of NO from nitrous acid decomposition.

A number of studies have been published since the review of Schwartz and White, the results of which are summarised in Table 2.1. There are considerable differences in the reported rate constants, which has a dramatic effect on the predicted rate of NO production. In addition, the hydrolysis of NO<sub>2</sub> has been recently studied with  $k_5$  determined as  $4.8 \times 10^7 \text{ M}^{-1}\text{s}^{-1}$ .<sup>27</sup> Figure 1 illustrates the discrepancies in the literature rate constants, wherein the production of NO from the decomposition of a 0.01 M nitrous acid solution has been simulated based on the rate constants of the studies in Table 2.1.

**Table 2.1. Summary of rate constants for nitrous acid decomposition**

	<b>Park and Lee<sup>12</sup> (22 °C)</b>	<b>Beake and Moodie<sup>28</sup> (25 °C)</b>	<b>Schwarz and White<sup>23</sup> (25 °C)</b>	<b>Ram and Stanbury<sup>29</sup> (25 °C)</b>
$k_9 (\text{M}^{-1}\text{s}^{-1})$	$13.4 \pm 1$	15	5.6	10-25
$k_{-9} (\text{M}^{-1}\text{s}^{-1})$	$1.58 \pm 0.13$ $\times 10^8$	$9.00 \times 10^7$	$3.00 \times 10^7$	$1.75 \times 10^8$
$K_9$	$8.38 \times 10^{-8}$	$1.67 \times 10^{-7}$	$1.87 \times 10^{-7}$	$5.7\text{-}14.3 \times 10^{-8}$
$k_{10} (\text{M}^{-1}\text{s}^{-1})$	$8.40 \pm 1.5$ $\times 10^7$	$1.00 \times 10^8$	$7.00 \times 10^7$	$5.00 \times 10^7$
$k_{-10} (\text{M}^{-2}\text{s}^{-1})$	0	0.005	0.0089	0.0122
$k_{10}K_9^2 (\text{M}^{-1}\text{s}^{-1})$	<b><math>5.9 \times 10^{-7}</math></b>	<b><math>2.8 \times 10^{-6}</math></b>	<b><math>2.4 \times 10^{-6}</math></b>	<b><math>0.16\text{-}1.0 \times 10^{-6}</math></b>



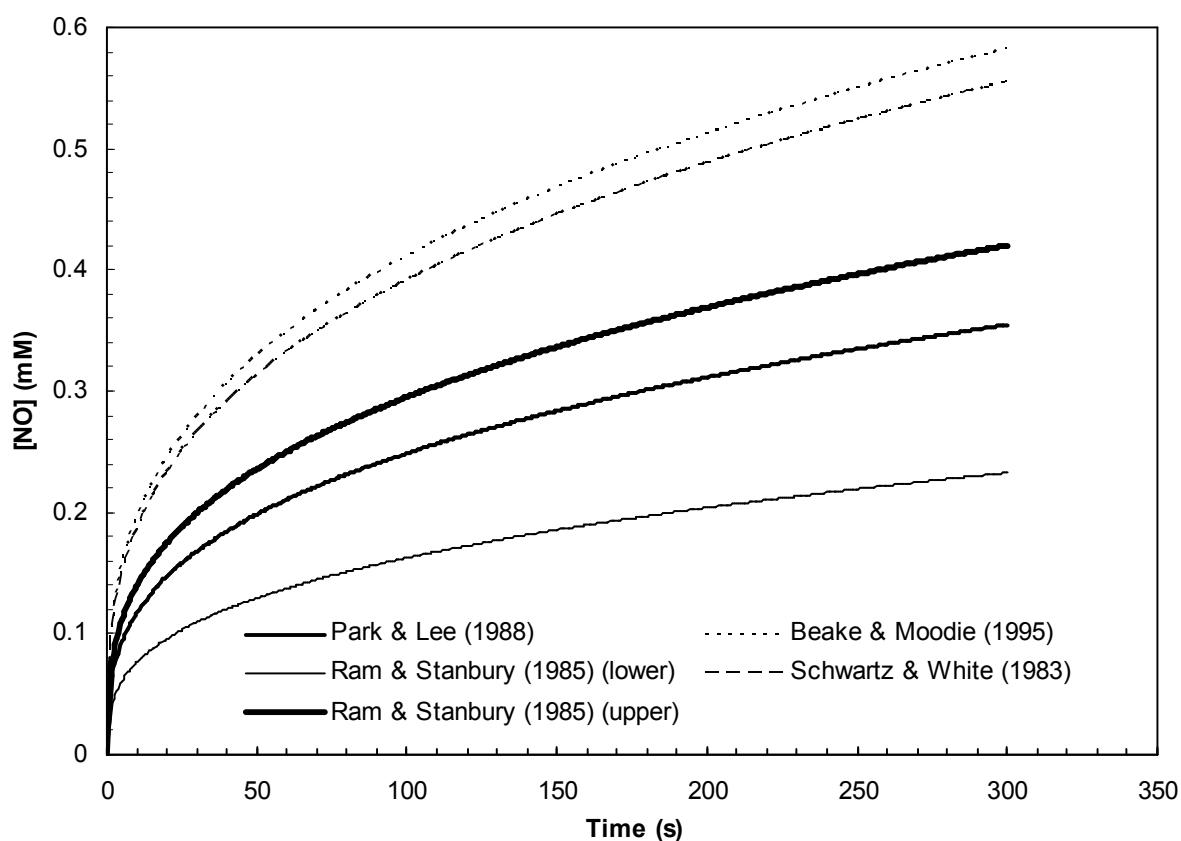


**Figure 2.1: Formation of nitric oxide predicted using different rate constants for  $HNO_2$  decomposition**

As demonstrated in Table 2.1, there are significant differences in the rate constants determined for nitrous acid decomposition reported in the literature, which could cause significant error when attempting to model the formation of NO from these reactions. It is therefore of great interest to determine the correct values of the rate constants that are required to accurately model the formation of NO from nitrous acid decomposition. The studies cited in Table 2.1 and Figure 2.1 are discussed below, with potential reasons given for the discrepancies in the reported rate constants.

Perhaps the most comprehensive individual study to date is that of Park & Lee,<sup>12</sup> who determined both the forward and reverse rate constants of Reaction 9 and the forward

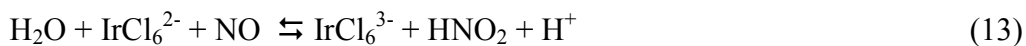
rate constant of Reaction 10. The decomposition of  $\text{HNO}_2$  was studied using a gas-liquid reactor with the gas phase concentrations of  $\text{NO}$ ,  $\text{NO}_2$  and  $\text{HNO}_2$  measured using a chemiluminescence  $\text{NO}_x$  detector. The decomposition kinetics were analysed by assuming steady state concentrations of  $\text{NO}$  and  $\text{NO}_2$ , and by determining the convective mass transfer coefficient of their reactor setup by measuring the rate of  $\text{CO}_2$  dissolution in separate experiments. These authors also studied the temperature dependence of the reactions, but did not calculate activation energies owing to uncertainties in the measurements at temperatures other than  $22\text{ }^\circ\text{C}$ , because the mass transfer coefficient was only measured at that temperature. The rate constants determined in this study are considerably lower than those recommended by Schwartz and White, being smaller by a factor of four. The rate constants would be expected to be marginally smaller due to the slightly lower temperature used in this study ( $22\text{ }^\circ\text{C}$  versus  $25\text{ }^\circ\text{C}$  for the others), however, this would not account for the size of the discrepancy.

Beake & Moodie<sup>28</sup> have studied the decomposition of  $\text{HNO}_2$  in the presence of dissolved oxygen, determining the change in nitrous acid concentration with time from the UV absorbance of nitrous acid at  $385\text{ nm}$ . In the presence of oxygen, the oxidation of  $\text{NO}$  by  $\text{O}_2$  also occurs, which will influence the reaction kinetics by reducing the  $\text{NO}$  concentration.



The approach taken was to assume values of the rate constants  $k_9$ ,  $k_{10}$  and  $k_{12}$  from the literature and to determine the value of  $k_9$  by solving the set of ordinary differential equations describing the reaction mechanism and varying  $k_9$  to provide the best fit to their experimental data. The results provide a value of  $K_9^2 k_{10}$  that is similar to that of Schwartz & White, and considerably larger than that of Park & Lee. It is important to note, that whilst Beake & Moodie claim to be determining  $k_9$ , the result would actually depend on the initially chosen value for  $k_9$  as Reaction 9 is at equilibrium under these conditions. The rate constants determined in this study would be sensitive to the value of  $k_{12}$  chosen, as under these conditions, Reaction 12 is partially rate limiting.

Ram and Stanbury<sup>29</sup> examined the reactions of the  $\text{IrCl}_6^{2-/3-}$  redox couple in nitrous acid over a variety of nitrous acid, nitrate and hydrogen ion concentrations. Reaction 13, shown below, was found to occur in parallel with Reactions 9 and 10.



The rate and equilibrium constants for Reaction 13 were determined under conditions where the rate did not depend on the rates of Reactions 9 and 10. The reactions were then studied under a range of conditions where Reactions 9 and 10 influence the kinetics, including a range of acidities (pH 0-7), initially starting with either  $\text{IrCl}_6^{2-}$  or  $\text{IrCl}_6^{3-}$  and also in the presence of nitric acid to promote the reverse of (10). The value for the rate constant  $k_9$  was adjusted to give the best fit to the data, with values of  $k_9$  and  $k_{10}$  chosen from the literature and adjusted slightly to improve the fit. The resulting values of  $k_9$  ranged from 10 to 25  $\text{M}^{-1}\text{s}^{-1}$  depending on the experimental conditions,

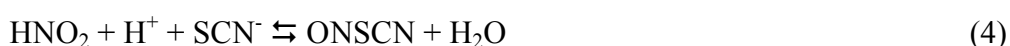
leading to  $K_9^2 k_{10}$  values of  $0.16 - 1 \times 10^{-6} \text{ M}^{-1} \text{ s}^{-1}$ . These values are considerably lower than those of Schwartz and White, but bracket the value of Park and Lee.

Despite the widespread interest in the decomposition of nitrous acid and agreement on the reaction mechanism, there is no general consensus on the correct values of the rate constants, with differences in the reported values of about an order of magnitude (for  $K_9^2 k_{10}$ ). Discrepancies in the results reported are likely caused by the differences in the methods used for studying the reaction and the assumptions employed when analysing the data, for example, Park and Lee assumed that the concentrations of NO and NO<sub>2</sub> were in steady state and that the mass transfer characteristics of NO and NO<sub>2</sub> were the same (and equal to that of CO<sub>2</sub>), the results of Ram and Stanbury depended on the values employed for rate constants of parallel reactions pathways (i.e. Reaction 13), whilst the results of Beake and Moodie depended on the assumed initial concentration of oxygen and value of  $k_{12}$ . Therefore, it would be desirable to study the decomposition of nitrous acid without the following complications (1) mass transfer between the aqueous and gas phase and (2) the presence of parallel reaction pathways that influence the reaction kinetics. This can be achieved by monitoring the decomposition of nitrous acid spectrophotometrically, with precautions taken to prevent any transfer of gases in or out of the reacting solution. Such conditions can be readily achieved in a stopped flow mixing device, wherein two reactant solutions contained in gas tight syringes are mixed together rapidly before flowing to a UV-Vis observation cuvette. Such a study may yield an accurate value for the quantity  $K_9^2 k_{10}$  to be used for modelling NO formation from nitrous acid decomposition during nitrosation reactions.

## 2.3 Decomposition of nitrosyl thiocyanate

### 2.2.1 Formation of ONSCN

The evidence for the existence of ONSCN originates from spectroscopic and kinetic studies, which both indicate the presence of a species formed according to Equation 4 in acidic aqueous solutions containing nitrous acid and thiocyanate ions. These solutions have a characteristic red colour, the intensity of which is dependent on the concentrations of  $H^+$ ,  $SCN^-$  and  $HNO_2$ . The red coloured species has a broad absorption band with a maximum at 460 nm ( $\epsilon_{460} = 100 \text{ M}^{-1}\text{cm}^{-1}$ ), and an equilibrium constant of  $32 \text{ M}^{-1}$  has been determined in perchloric acid medium<sup>8</sup>. The kinetic evidence for ONSCN comes from the observation that a wide variety of nitrosation reactions are catalysed by the presence of thiocyanate ions. The rate of the catalytic reaction is also first order in the concentrations of  $H^+$ ,  $SCN^-$  and  $HNO_2$ , indicating that the same species is responsible for the UV absorption and the catalysis caused by thiocyanate ions<sup>1</sup>.



$$K_{ONSCN} = \frac{[ONSCN]}{[H^+][HNO_2][SCN^-]} \quad (14)$$

The high value of the equilibrium constant for formation of nitrosyl thiocyanate ( $K_{ONSCN}$ ) makes thiocyanate ions a powerful catalyst for nitrosation reactions. Similar catalytic mechanisms are observed for other nucleophilic species, including  $Cl^-$ , and  $Br^-$ , which form the corresponding nitrosyl halides ONCl and ONBr, although the catalytic effect is less pronounced due to their smaller formation constants<sup>5</sup>. The apparent value

of  $K_{ONSCN}$  varies considerably with ionic strength and has been reported as 21.0, 28.6, 36.3 and 44  $M^{-2}$  for ionic strengths of 0.42, 1.02, 1.42 and 2 M respectively<sup>13</sup>. Jones et al.<sup>30</sup> also measured the equilibrium constant in perchloric acid and found similar increases in the equilibrium constant with increasing perchloric acid concentrations. In the cases above, the reported equilibrium constant is an apparent equilibrium constant. That is, it is determined classically from the concentrations, and does not take into account the changes in activity coefficients of the species involved. The apparent increase in the equilibrium constant is therefore postulated to be caused by changes to the activity coefficients<sup>30</sup>, however, the activity coefficients have not been estimated due to absence of data for the activities of  $SCN^-$  in  $HClO_4$ .

An alternate explanation posed by Bazsa and Epstein<sup>31</sup> is that the red species observed is in fact  $ONSCNH^+$  not  $ONSCN$ . A species of this stoichiometry gives an approximately constant value of  $K_{ONSCN}$  for perchloric acid concentrations ranging from 1 to 6  $M^{-1}$ . This claim is strongly refuted by Jones et al. (1996)<sup>30</sup> who cite the kinetic evidence that the species is  $ONSCN$  (i.e., the rate law for its formation is  $k[H^+][SCN^-][HNO_2]$ ) and note that, owing to changes in activity coefficients, there is no requirement for the observed equilibrium constant to remain the same with increasing ionic strength. The activity coefficient of hydrogen ions in concentrated acids is substantially higher than unity<sup>32</sup>, explaining the increase in apparent equilibrium constant with ionic strength, showing that the formula  $ONSCN$  is indeed correct.

### 2.3.2 Decomposition of ONSCN: Background and potential pathways

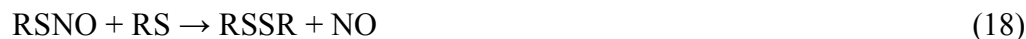
ONSCN is known to be unstable in pure form, decomposing readily even at temperatures approaching -60 °C to form nitric oxide and thiocyanogen<sup>33</sup>.



Dilute aqueous solutions of ONSCN are relatively stable, however, the red colour of the solutions is observed to fade over time with evolution of bubbles of NO<sup>13</sup>. Despite its widespread application as a catalyst for nitrosation reactions, the kinetics and mechanism of ONSCN decomposition appear not to have been previously studied. Thus, it is of interest to determine the kinetics and mechanism of ONSCN decomposition in order to assess the contribution of ONSCN to the formation of NO<sub>x</sub> during explosive sensitisation.

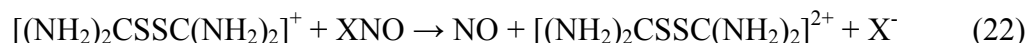
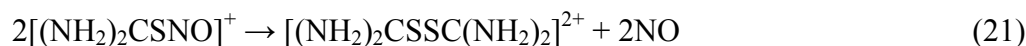
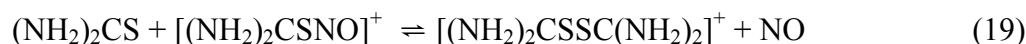
Whilst the mechanism for the decomposition of ONSCN in particular has not been studied, the mechanisms for decomposition of other related species, including thionitrites (i.e. RSNO), nitroso thioureas and nitrosyl halides have received some attention in the literature. RSNO compounds, in particular, have been of considerable interest to biochemists, owing to their importance as a source of nitric oxide in the body. The decomposition of these species is known to yield the disulfide and NO, the formation of which has been postulated to occur via two parallel pathways<sup>34</sup>.





The first pathway involves the homolytic fission of the S-NO bond to form NO and a thiyl radical. Two thiyl radicals then combine, forming the disulfide. The second pathway for disulfide formation involves the substitution of NO for RS in the thionitrite.

The decomposition of nitroso-thioureas has also been studied. Two pathways have been proposed, the first involving the reaction between a thiourea molecule and nitroso-thiourea (Reactions 19 & 20), which generates a positively charged disulfide radical. The second pathway involves a bimolecular reaction between two nitroso-thiourea molecules (Reaction 21) yielding the products, formamidine disulfide, and two molecules of NO<sup>35</sup>.



By analogy with the decomposition of thionitrites and nitroso-thioureas, three possible decomposition pathways for ONSCN could be expected. Pathway 1 involves the homolytic fission of the S-N bond of ONSCN to generate NO and SCN radicals, with



SCN reacting either by a radical combination reaction to generate (SCN)<sub>2</sub>, or via substitution with NO in ONSCN, to yield (SCN)<sub>2</sub> and NO. Both routes of SCN consumption lead to the same overall stoichiometry given in Equation 15. Pathway 2 involves the reaction between SCN<sup>-</sup> and ONSCN to generate NO and (SCN)<sub>2</sub><sup>-</sup> radicals, which is analogous to the reaction between thiourea and nitrosothiourea (19). The third potential pathway is a second order reaction in ONSCN, directly generating NO and (SCN)<sub>2</sub>. This pathway is analogous to Reaction (21) in the decomposition of nitrosothiourea<sup>35, 36</sup> and the oxidation of iodide ions by HNO<sub>2</sub><sup>37, 38</sup> which has a term that is second order in nitrosyl iodide concentration.

Pathway 1:



Pathway 2:



Pathway 3:



Pathways 1 and 2 are both inhibited by nitric oxide, pathway 2 depends on the concentration of thiocyanate ion whilst Pathway 3 depends only on the concentration of

nitrosyl thiocyanate. It should therefore be possible to determine which, if any, of these pathways are significant by examining the decomposition of ONSCN over a range of  $\text{SCN}^-$ , ONSCN and NO concentrations.

## 2.4 References

1. Williams, D. L. H., *Nitrosation reactions and the chemistry of nitric oxide*. Elsevier B. V.: Amsterdam, 2004.
2. da Silva, G.; Kennedy, E. M.; Dlugogorski, B. Z., Ab Initio procedure for aqueous-phase pKa calculation: The acidity of nitrous acid. *J. Phys. Chem. A* **2006**, *110*, 11371-11376.
3. Ridd, J. H., Nitrosation, diazotisation, and deamination. *Q. Rev., Chem. Soc.* **1961**, *15* (4), 418-441.
4. Markovits, G. Y.; Schwartz, S. E.; Newman, L., Hydrolysis equilibrium of dinitrogen trioxide in dilute aqueous solution. *Inorg. Chem.* **1981**, *20*, 445-450.
5. da Silva, G. Experimental and theoretical study of nitrosation reactions: Applications in the chemical foaming of concentrated water-in-oil emulsions. PhD Thesis. The University of Newcastle, Australia, Newcastle, 2005.
6. Pestovsky, O.; Bakac, A., Nitrous acid as a source of NO and NO<sub>2</sub> in the reaction with a macrocyclic superoxorhodium(III) complex. *Inorg. Chem.* **2002**, (41), 901-905.
7. da Silva, G. R.; Dlugogorski, B. Z.; Kennedy, E. M., Elementary reaction step model of the N-nitrosation of ammonia. *Int. J. Chem. Kinet.* **2007**, *39* (12), 645-656.
8. Stedman, G.; Whincup, P. A. E., The equilibrium constant for the formation of nitrosyl thiocyanate in aqueous solution. *J. Chem. Soc.* **1963**, 5796-5799.
9. da Silva, G.; Dlugogorski, B. Z.; Kennedy, E. M., An experimental and theoretical study of the nitrosation of ammonia and thiourea. *Chem. Eng. Sci.* **2006**, *61* (10), 3186-3197.

10. Nguyen, D. A.; Iwaniw, M. A.; Fogler, H. S., Kinetics and mechanism of the reaction between ammonium and nitrite ions: experimental and theoretical studies. *Chem. Eng. Sci.* **2003**, *58* (19), 4351-4362.
11. Everett, D. H.; Wynne-Jones, W. F., The dissociation of the ammonium ion and the basic strength of ammonia in water. *Proc. R. Soc. London, Ser. A* **1938**, *169*, 190-204.
12. Park, J. Y.; Lee, Y. N., Solubility and decomposition kinetics of nitrous acid in aqueous solution. *J. Phys. Chem.* **1988**, *92* (22), 6294-302.
13. Doherty, A. M.; Garley, M. S.; Haine, N.; Stedman, G., Formation of an adduct between thiocyanate ion and nitrosyl thiocyanate. *J. Chem. Soc., Dalton Trans.* **1997**, 2163-2166.
14. Patwardhan, J.; Joshi, J., Unified model for NO<sub>x</sub> absorption in aqueous alkaline and dilute acidic solutions. *AIChE J.* **2003**, *49* (11), 2728-2748.
15. Ingale, N. D.; Chatterjee, I. B.; Joshi, J. B., Role of nitrous acid decomposition in absorber and bleacher in nitric acid plant. *Chem. Eng. J. (Amsterdam, Neth.)* **2009**, *155* (3), 851-858.
16. Zollinger, H., *Azo and diazo chemistry: Aliphatic and aromatic compounds*. Interscience Publishers Inc.: New York, 1961.
17. Finlayson-Pitts, B. J.; Pitts, J. N. J., *Atmospheric chemistry: Fundamentals and experimental techniques*. Wiley: New York, 1986.
18. Butler, A. R.; Ridd, J. H., Formation of nitric oxide from nitrous acid in ischemic tissue and skin. *Nitric Oxide* **2004**, *10* (1), 20-24.
19. Aga, R. G.; Hughes, M. N., The preparation and purification of NO gas and the use of NO releasers: The application of NO donors and other agents of nitrosative stress in biological systems. *Methods Enzymol.* **2008**, *436*, 35-48.

20. Klepper, L., Comparison between NO<sub>x</sub> evolution mechanisms of wild-type and nr1 mutant soybean leaves. *Plant Physiol.* **1990**, *93*, 26-32.
21. Abel, E.; Schmid, H., The kinetics of nitrous acid. III. Kinetics of the decomposition of nitrous acid. *Z. physik. Chem.* **1928**, *134*, 279-300.
22. Treinin, A.; Hayon, E., Absorption spectra and reaction kinetics of NO<sub>2</sub>, N<sub>2</sub>O<sub>3</sub>, and N<sub>2</sub>O<sub>4</sub> in aqueous solution. *J. Amer. Chem. Soc.* **1970**, *92* (20), 5821-8.
23. Schwartz, S. E.; White, W. H., Kinetics of reactive dissolution of nitrogen oxides into aqueous solution. *Adv. Environ. Sci. Technol.* **1983**, *12*, 1-116.
24. Bunton, C. A.; Llewellyn, D. R.; Stedman, G., Oxygen exchange between nitrous acid and water. *J. Chem. Soc.* **1959**, 568-573.
25. Hughes, E. E.; Ridd, J. H., Nitrosation, diazotisation, and deamination. Part III. Zeroth order diazotisation of aromatic amines in carboxylic acid buffers. *J. Chem. Soc.* **1958**, 70-76.
26. Armor, J. N., Influence of pH and ionic strength upon solubility of NO in aqueous solution. *J. Chem. Eng. Data* **1974**, *19* (1), 82-84.
27. Becker, R. H.; Nicoson, J. S.; Margerum, D. W., Nucleophile assistance of electron-transfer reactions between nitrogen dioxide and chlorine dioxide concurrent with the nitrogen dioxide disproportionation. *Inorg. Chem.* **2003**, *42* (24), 7938-7944.
28. Beake, B. D.; Moodie, R. B., Role of the reaction of nitric oxide with oxygen in the decomposition of nitrous acid in aqueous acid solution. *J. Chem. Soc., Perkin Trans. 2* **1995**, (6), 1045-8.
29. Ram, M. S.; Stanbury, D. M., Kinetics and equilibria for reactions of the hexachloroiridate redox couple in nitrous acid. *Inorg. Chem.* **1985**, *24* (19), 2954-62.

30. Jones, E.; Munkley, C. G.; Phillips, E. D.; Stedman, G., Kinetics and equilibria in the nitric acid-nitrous acid-sodium thiocyanate system. *J. Chem. Soc., Dalton Trans.* **1996**, 1915-1920.
31. Bazsa, G.; Epstein, I. R., Autocatalysis and bistability in the reaction between nitric acid and thiocyanate. *Int. J. Chem. Kinet.* **1985**, *17*, 601-612.
32. Davis, W.; De Bruin, H. J., New activity coefficients of 0-100 per cent aqueous nitric acid. *J. Inorg. Nucl. Chem.* **1964**, *26* (6), 1069-1083.
33. Lecher, H.; Graf, F., Nitrosyl derivatives of bivalent sulfur. III. Nitrosyl thiocyanate. *Ber. Dtsch. Chem. Ges. B* **1926**, *59B*, 2601-2.
34. Stamler, J. S.; Toone, E. J., The decomposition of thionitrites. *Curr. Opin. Chem. Biol.* **2002**, *6* (6), 779-785.
35. Collings, P.; Garley, M. S.; Stedman, G., Kinetics and mechanism of the decomposition of nitrosyl thiourea. *J. Chem. Soc., Dalton Trans.* **1981**, 331-335.
36. Garley, M. S.; Stedman, G.; Miller, H., Kinetics and mechanism of the decomposition of thionitrites derived from thioureas. *J. Chem. Soc., Dalton Trans.* **1984**, 1959-1963.
37. Dózsa, L.; Szilassy, I.; Beck, M. T., Mechanism of the nitrite-iodide reaction. *Inorg. Chim. Acta* **1976**, *17*, 147-153.
38. Ferranti, F.; Indelli, A., Kinetics and mechanism of the reaction of nitrous acid with iodide ion in acid medium at 25 C. *Gazz. Chim. Ital.* **1980**, *110*, 273-277.

## **CHAPTER 3**

### **Experimental and computational methods**

## Table of Contents

3.1	Experimental methods	37
3.1.1	Stopped flow UV-Vis spectrophotometry	37
3.1.2	Gas analysis	39
3.1.3	Aqueous and membrane inlet reactors	41
3.1.4	Measurement of NO solubility in concentrated nitrate solutions	46
3.1.5	Emulsion preparation and NO <sub>x</sub> measurements	48
3.2	Computational methods	51
3.2.1	Ab-initio methods and basis sets	51
3.2.2	Density functional theory	55
3.2.3	Compound methods	57
3.2.4	Solvation modelling	59
3.2.6	Optimisation, frequency and transition state theory calculations	61
3.3	References	64



### 3.1 Experimental methods

#### 3.1.1 Stopped flow UV-Vis spectrophotometry

Stopped flow UV-Visible spectrophotometry was employed to examine the kinetics and equilibria associated with nitrous acid and nitrosyl thiocyanate decomposition. The stopped flow apparatus affords a mechanism for rapidly mixing two solutions, as well as providing an anaerobic environment. The flow circuit of the stopped flow apparatus consists of two drive syringes, a mixing tee, observation cell and a stopping syringe. For a kinetic run, the drive syringes are loaded with solutions containing the species to be reacted. The drive syringes can be actuated either pneumatically or by hand, propelling the solutions through a section of tubing to a mixing tee, before the solution flows through the observation cell to the stopping syringe. The piston in the stopping syringe expands until it contacts a rigid barrier, preventing further flow of fluid through the system. At the instant immediately prior to stopping, the flowing solution has achieved a high velocity and only a small time period elapses between the mixing point and the observation cell, thereby enabling measurement of rapid reactions. The dead time of a stopped flow instrument is defined as the time elapsed between the mixing point and observation cell and governs the maximum reaction rate that can be observed in a particular instrument. Typical dead times are on the order of a few milliseconds, affording kinetic measurements of reactions with first order rate constants up to approximately  $200 - 2000 \text{ s}^{-1}$ .<sup>1</sup> Figure 1 shows a schematic of the stopped flow circuit.

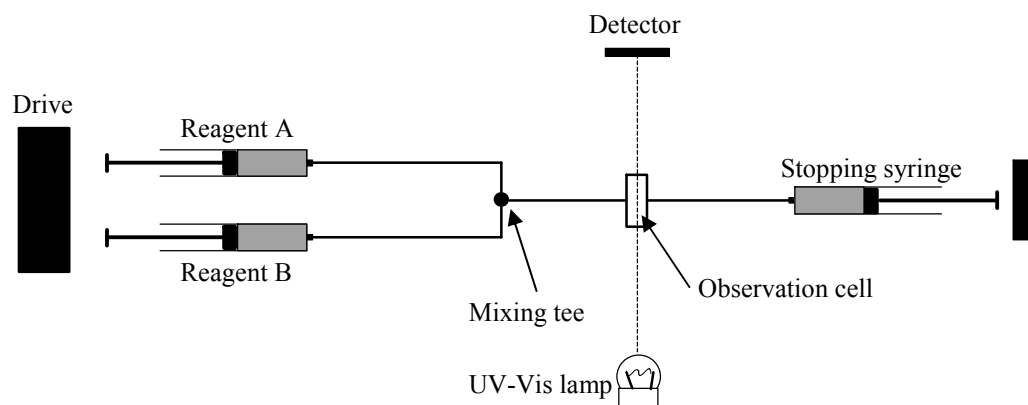
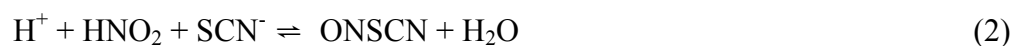


**Figure 1: Diagram of stopped-flow apparatus**

Nitrous acid and nitrosyl thiocyanate exhibit characteristic UV or visible spectra<sup>2,3</sup>, allowing their concentrations to be determined from absorbance readings in accordance with Beer's Law, which states that the absorbance at a particular wavelength is proportional to the concentration of the species and the distance that the light travels through the solution (i.e., the cell path length)<sup>4</sup>. In the case of nitrous acid decomposition, solutions of nitrous acid were generated in situ using the stopped flow, by mixing a solution of sodium nitrite and a solution of perchloric acid (Reaction 1). Similarly, for the study of nitrosyl thiocyanate decomposition, nitrosyl thiocyanate was generated by mixing a solution containing both sodium nitrite and sodium thiocyanate with a solution of perchloric acid, forming ONSCN in accordance with Reaction 2. Both nitrous acid and nitrosyl thiocyanate are formed rapidly, and the kinetics of their decomposition can be monitored by the decreasing absorbance at specific wavelengths.



The apparatus employed in the present study consisted of a RX-2000 stopped flow rapid mixing accessory equipped with anaerobic accessory from Applied Photophysics, coupled to a Varian Cary50 UV-Visible spectrometer. The spectrometer was operated with a data acquisition rate in single wavelength mode of 80 Hz and had a spectral resolution of 0.15 nm. The drive syringes of the RX-2000 were surrounded by water connected to a constant temperature circulating water bath at the desired reaction temperature, whilst the observation cell was housed in a thermostatted cell holder regulated by a Varian Cary single cell Peltier temperature controller to within  $\pm 0.1$  °C. The procedure for an experiment involved firstly removing oxygen from the reactant solutions by bubbling with nitrogen gas for at least 15 min. Degassing for longer times produced identical results. Prior to each experiment, the stopped flow apparatus was flushed with de-oxygenated water and a baseline absorbance reading taken and stored in the Varian software to be automatically subtracted from subsequent readings.

### 3.1.2 Gas analysis

Analysis of gases was performed by Fourier transform infrared spectroscopy (FTIR), membrane inlet mass spectroscopy (MIMS)<sup>5</sup> and a nitric oxide chemiluminescence detector. The FTIR was a Varian IR-600 with  $0.5\text{ cm}^{-1}$  resolution used in conjunction with a 10 m path length gas cell. The long path length of the gas cell permitted reliable measurement of low gas concentrations and of weakly absorbing species. To collect the gaseous products of ONSCN decomposition, a  $50\text{ cm}^3$  round bottomed glass reactor containing a solution of  $\text{SCN}^-$  and  $\text{NO}_2^-$  at  $\text{pH} > 7$  was de-oxygenated by flushing with nitrogen for 30 min, prior to adding a small volume of 2 M  $\text{HClO}_4$  through a septum side port in the reactor, forming ONSCN in-situ. The product gases were purged from the reactor with high purity nitrogen gas, dried by passage over a column of silica gel and

collected in a 3 L gas transfer bag for analysis. Removal of water vapour from the sample for the FTIR analysis was essential owing to the interference of the water spectrum with other products of interest. It was established in separate experiments that silica gel did not adsorb NO, by comparing the spectrum of a 1000 ppm NO calibration gas before and after passage over the column.

Prior to analysis, the FTIR gas cell was evacuated and flushed with high purity nitrogen three times before taking a background spectrum. The cell was subsequently loaded with the sample for scanning, with the background being automatically subtracted from the sample spectrum by the Varian software. The QASoft program (Infrared Analysis Inc.) was employed to determine the concentrations of gaseous species from the FTIR spectrum. The program utilises a region integration and subtraction (RIAS) method to determine the concentrations based on standard spectra from the QASoft database. The absorbance of traces of water vapour was subtracted from the sample spectrum prior to the analysis, by employing a water spectrum recorded on the same instrument.

Membrane inlet mass spectroscopy experiments were performed using a Pfeifer Thermostar quadrupole mass spectrometer. The end of the capillary from the MS was housed within a 1 cm length of semi-permeable Silastic tubing mounted on a stainless steel tube as described by Tu et al.<sup>5</sup> The Silastic tubing permitted diffusion of dissolved gases whilst excluding water, thereby enabling direct measurement of dissolved gas concentrations. In particular, this method was employed to determine if nitrogen was a product of the ONSCN decomposition reaction. This was necessary because N<sub>2</sub> does not absorb infrared radiation and hence cannot be detected by FTIR. In these

experiments, the solution was degassed with high purity argon to remove oxygen and nitrogen present from air. The purge gas was turned off at the start of the experiment.

Analysis of gaseous nitric oxide concentrations was performed with a Thermo 42i-HL nitric oxide analyser. The analyser utilises the chemiluminescent reaction between nitric oxide and ozone to quantify the concentration of nitric oxide in a gas stream. The reaction between NO and O<sub>3</sub> produces electronically excited molecules of NO<sub>2</sub>, which release light upon relaxation to the ground state, with the intensity of light emitted being proportional to the concentration of NO<sup>6</sup>:



The analyser was calibrated weekly with a cylinder of 1016 ppm nitric oxide in nitrogen, supplied by Coregas Pty Ltd. Linearity of the response was confirmed by accurately diluting the calibration gas with high purity nitrogen by means of two mass flow controllers.

### 3.1.3 Aqueous and membrane inlet reactors

The stopped flow UV-Vis apparatus was unsuitable for studying the decomposition of nitrous acid in concentrated ammonium nitrate solutions, owing to the production of nitrogen bubbles formed by the reaction between nitrous acid and ammonia and the high concentration of nitrate ions. The formation of nitrogen bubbles within the stopped flow cell results in light scattering, producing an artificial increase in absorbance, whilst the high nitrate ion concentration reduces the rate and extent of the decomposition

reaction. Consequently, an alternate method was required in order to study the decomposition of nitrous acid in concentrated ammonium nitrate solutions. For this purpose, two reactor setups were trialled, comprising a partially filled gas-liquid reactor with gas phase analysis of NO concentrations, and a novel membrane inlet chemiluminescence detector setup.

The first apparatus comprised a 125 cm<sup>3</sup> round bottomed flask with septum side port, operated partially filled with ammonium nitrate solution, and agitated by means of a magnetic stirrer. The reactor was immersed in a water bath to maintain the desired reaction temperature. To initiate reaction, 1 cm<sup>3</sup> of concentrated sodium nitrate solution was added to an acidified solution of ammonium nitrate. Nitrogen gas was supplied to the headspace of the reactor and the flow regulated to between 40 and 100 cm<sup>3</sup> min<sup>-1</sup> by means of a mass flow controller. The gaseous concentration of NO was determined with the Thermo 42i-HL chemiluminescence nitric oxide analyser. The transport of nitric oxide from the aqueous to gas phase was modelled by means of an overall mass transfer coefficient<sup>7</sup> as outlined in Equation 5.

$$R_{MT} = K_{MT} ([NO] - [NO]_{EQ}) \quad (5)$$

where  $R_{MT}$  is the rate of mass transfer (mol s<sup>-1</sup>),  $K_{MT}$  is the overall mass transfer coefficient (L s<sup>-1</sup>),  $[NO]$  is the concentration of nitric oxide (mol L<sup>-1</sup>) and  $[NO]_{EQ}$  is the aqueous concentration of nitric oxide that would exist in equilibrium with a given gas phase partial pressure of NO.  $[NO]_{EQ}$  can be determined by employing Henry's law, which states that the concentration of a dissolved gas is proportional to the gas phase partial pressure of that species:

$$[NO]_{EQ} = k_{NO}P_{NO} = k_{NO}C_{NO}RT \quad (6)$$

where  $k_{NO}$  is the Henry's law constant for nitric oxide ( $\text{mol m}^{-3} \text{ Pa}^{-1}$ ),  $P_{NO}$  is the partial pressure of nitric oxide (Pa),  $C_{NO}$  is the gas phase concentration of nitric oxide ( $\text{mol m}^{-3}$ ),  $R$  is the gas constant ( $\text{J mol}^{-1} \text{ K}^{-1}$ ) and  $T$  is the absolute temperature (K). Substituting Equations 5 and 6 into a mass balance over the gas and liquid phases of the reactor yields Equations 7 and 8.

$$\frac{d[NO]}{dt} = \frac{k_{NO}RTK_{MT}}{V_{aq}}C_{NO} - \frac{K_{MT}}{V_{aq}}[NO] + r_{NO} \quad (7)$$

$$\frac{dC_{NO}}{dt} = \frac{K_{MT}}{V_{gas}}[NO] - \frac{(v + k_{NO}K_{MT}RT)}{V_{gas}}C_{NO} \quad (8)$$

where  $V_{aq}$  is the volume of solution in the reactor (L),  $r_{NO}$  is the rate of nitric oxide generation by chemical reaction ( $\text{mol L}^{-1} \text{ s}^{-1}$ ),  $V_{gas}$  is the volume of gas in the reactor (L) and  $v$  is the volumetric gas flowrate into the reactor ( $\text{L s}^{-1}$ ). If the mass transfer coefficient for the reaction is known, Equations 7 and 8 can be solved simultaneously for a given set of initial conditions to yield  $r_{NO}$  versus time. Equations 7 and 8 consist of a coupled set of ordinary differential equations and were solved numerically using the Polymath 5.0 stiff ordinary differential equation solver. In the absence of chemical reaction,  $K_{MT}$  represents the only unknown term in Equations 7 and 8. As such, the mass transfer coefficient was determined in separate experiments by injecting a small volume of a solution saturated with nitric oxide into the reactor. The parameter  $K_{MT}$

was determined by adjusting this variable in the Polymath simulations to provide the best fit to the experimental data. The length of tubing connecting the reactor to the analyser resulted in a delay between the injection of NO and the first NO reading. This delay was accounted for by shifting the times of each data point by a constant amount.

The second apparatus employed to study nitrous acid decomposition in concentrated ammonium nitrate solution comprised a novel membrane inlet reactor coupled to the Thermo 42i-HL nitric oxide analyser. The apparatus consisted of a 125 cm<sup>3</sup> round bottomed flask with septum side port containing a magnetic stirrer and was mounted in a water bath to maintain a temperature of 25 °C in all experiments. Measurements of nitric oxide in the reactor were performed using a membrane inlet NO probe. A similar system has previously been employed for the measurement of nitric oxide by mass spectrometry<sup>5,8</sup>. The reactor was partially filled with liquid, and the probe positioned in the centre of the vessel such that the membrane section was exposed to the gas phase. The motion of the magnetic stirrer created a vortex, with the probe located in the centre. The probe consisted of a section of Dow Corning laboratory silastic tubing (catalogue number 508-006) mounted on 1/16" (1.588 mm) stainless steel tubing. The stainless steel tubes were mounted in a rubber stopper inserted in the top of the reactor. The silastic tubing acts as a selective membrane that allows passage of nitric oxide whilst being relatively impermeable to water. Nitric oxide diffusing through the membrane was collected by a flowing stream of nitrogen gas for analysis using the Thermo 42i-HL chemiluminescence NO<sub>x</sub> analyser.

The advantage of the membrane inlet setup over direct gas phase measurements of NO was that it enabled the concentration of NO in the gas phase of the reactor to be



established without the need for a purge gas to pass through the headspace. This permitted the accumulation of NO in the gas phase over time to a point where the gas and aqueous phase NO concentrations reached equilibrium, at which time the aqueous NO concentration was determined using Henry's law. To maintain a constant pressure in the reactor, a syringe was mounted in the rubber stopper at the top of the reactor, and the plunger allowed to expand with the increase in the gas volume (owing to the production of gaseous NO, and N<sub>2</sub>). The reactor-probe setup was calibrated by generating a known concentration of nitric oxide via the reaction between nitrous and ascorbic acids<sup>9</sup>. Figure 2 presents a diagram of the membrane inlet reactor apparatus, whilst Figure 3 provides a typical calibration plot.

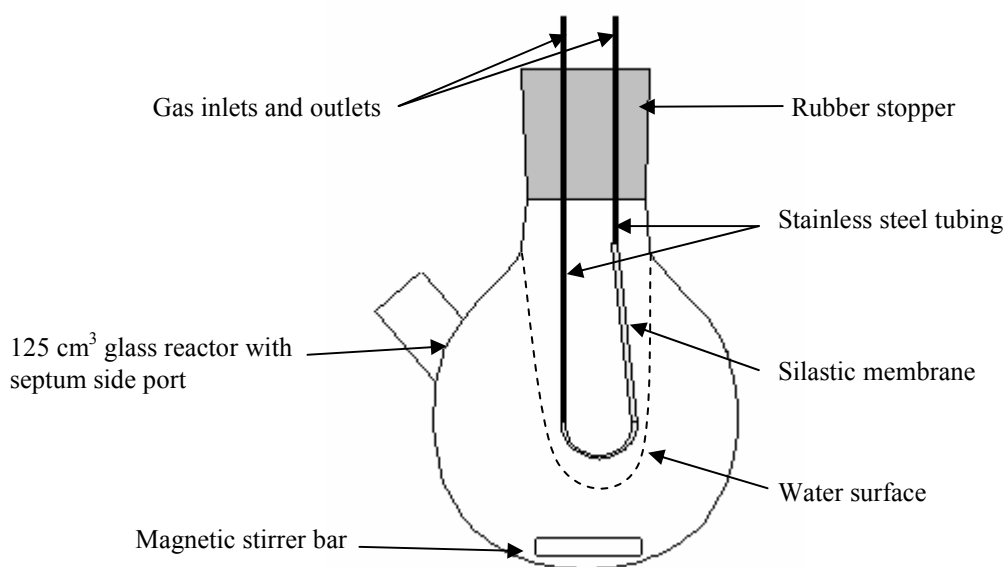


***Figure 2: Diagram of membrane inlet reactor apparatus for measurement***

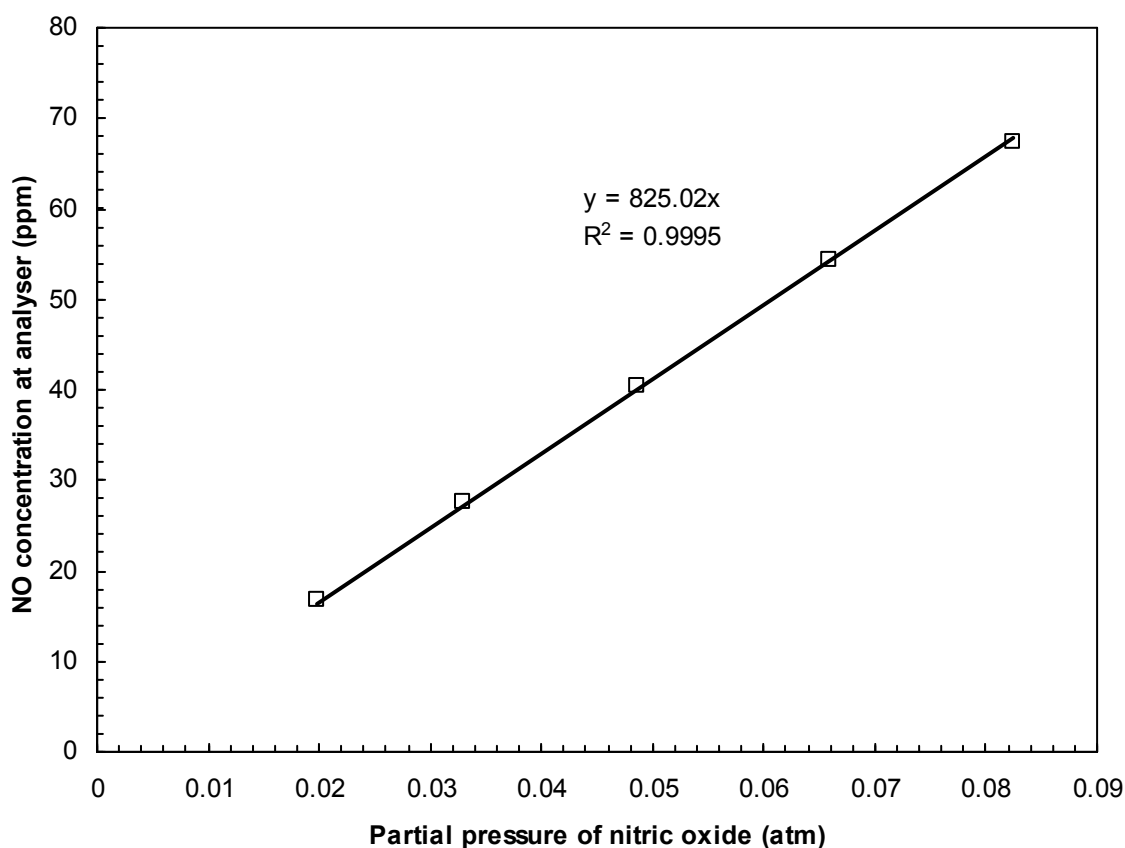
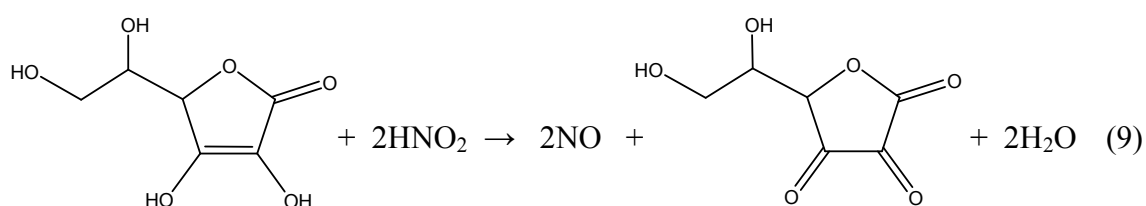


*Figure 3: Calibration plot for membrane inlet reactor*

### 3.1.4 Measurement of NO solubility in concentrated nitrate solutions

The solubility of nitric oxide in solutions of  $\text{NaNO}_3$  and  $\text{NH}_4\text{NO}_3$  was established by first saturating the solutions with nitric oxide, and determining the concentration of dissolved NO using the chemiluminescence analyser, as described below. Saturated solutions of nitric oxide (NO) were generated by first flushing the target solution with  $\text{N}_2$  to remove oxygen, prior to bubbling with NO generated via the reduction of nitrous acid by ascorbate<sup>10</sup>. The reaction of ascorbic and nitrous acids produces two moles of nitric oxide per mole of ascorbic acid.



The apparatus employed to generate the NO solutions consisted of a 50 cm<sup>3</sup> reaction flask, with the inlet connected to a supply of high purity nitrogen. The reactor was filled with 40 cm<sup>3</sup> of a solution containing approximately 0.375 mol L<sup>-1</sup> ascorbic acid and 0.75 mol L<sup>-1</sup> HClO<sub>4</sub>, prior to purging the system of air using N<sub>2</sub>. The N<sub>2</sub> purge was stopped after 30 min and a steady flow of NO initiated by adding a 25% solution of sodium nitrite dropwise to the reactor via a syringe inserted through a rubber stopper. The NO flowed through a scrubber containing a 0.1 M NaOH solution to trap any traces of NO<sub>2</sub> formed in the first reactor, before bubbling through the target solution contained within a 10 cm<sup>3</sup> reaction flask with septum side port. The reaction flask containing the salt solution was placed in a water bath at the desired temperature, and the NO allowed to bubble through the solution for a period of approx 20 min. Over this time, 0.7 L of NO was produced, corresponding to an average flow rate of 35 cm<sup>3</sup> min<sup>-1</sup>. After half of the NO had been produced (i.e., 10 min), a 0.5 cm<sup>3</sup> sample of NO saturated solution was withdrawn from the reactor by means of a gas tight syringe.

The NO solution was injected into a second reactor that was continually purged with nitrogen gas supplied through a mass flow controller, with the outlet of the reactor connected to the Thermo 42i-HL nitric oxide analyser. This enabled the total amount of NO contained in the solution to be determined, allowing calculation of the NO solubility at a particular ammonium nitrate concentration. A second sample of solution

was taken and analysed with the same method just before the production of NO ceased (after approx 20 min). Comparison of the concentration determined in the two samples taken after different exposure times provided confirmation that the solutions were indeed saturated with NO, as identical concentrations were determined. Figure 4 shows a diagram of the apparatus.

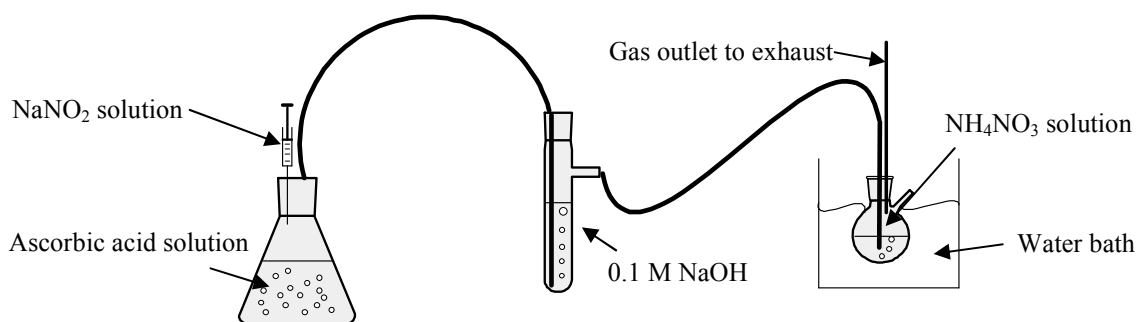


**Figure 4: Diagram of apparatus employed to generate salt solutions saturated with nitric oxide**

### 3.1.5 Emulsion preparation and $\text{NO}_x$ measurements

Emulsion explosives consist of a concentrated ammonium nitrate solution dispersed within a continuous hydrocarbon phase. The oxidiser phase of the emulsion (discontinuous phase) typically constitutes approximately 94 % of the emulsion mass and comprises a 75 % w/w ammonium nitrate solution. The continuous phase (fuel phase) constitutes the remaining 6% of the emulsion mass and typically contains a mixture of diesel fuel and a polyisobutylene succinic anhydride (PIBSA) based emulsifier<sup>11</sup>. To prepare the emulsion, the oxidiser phase components were weighed into a stainless steel jug, and heated to 80 °C with continuous stirring to dissolve all of

the ammonium nitrate. Once the ammonium nitrate was dissolved, the pH of the solution was adjusted to 5 by addition of concentrated sodium hydroxide solution. The fuel phase was weighed out in a separate stainless steel container and heated to 60 °C. The emulsion was formed by slowly pouring the oxidiser phase solution into the fuel phase with continual stirring by an overhead mixer, over a period of 60 s. The speed of the mixer was increased gradually from 600 to 1700 rpm over a further 120 s, or until the viscosity had reached between 22 – 28 Pa s. Viscosity measurements were performed on a Brookfield RVDVII+ viscometer with no. 7 spindle at 20 rpm.

The standard process for gassing an emulsion explosive in the laboratory involves consecutive addition of concentrated acetic acid (45 % w/w solution in water) and sodium nitrate solutions (25 % w/w solution in water) to the emulsion, mixing each solution for a period of 30 s. The emulsion is then weighed into a stainless steel cup of known mass and volume. A spatula is used to scrape the emulsion from the top of the cup, such that the emulsion is level with the rim of the cup, and the initial mass recorded. As gas is produced, the emulsion expands over the rim of the cup, and the excess emulsion is removed with a spatula and the cup re-weighed. The density change of the gassed emulsion can then be determined from the change in the mass of emulsion held within the cup. This type of experiment enabled determination of the time taken for complete gassing to occur.

A similar procedure was employed to determine the level of NO<sub>x</sub> produced during gassing, except that in this case the gassing process occurred within a sealed glove box. The apparatus consisted of the Thermo 42i-HL NO<sub>x</sub> analyser connected to a plastic glove box with a volume of 50 L, similar to the apparatus described by Vestre (2003)<sup>12</sup>.

A cylinder of nitrogen gas and a flow meter enabled the box to be purged with nitrogen prior to the start of experiments. A container holding a known mass of emulsion, along with syringes holding the gassing chemicals were loaded into the glove box. The box was then sealed to the atmosphere, and flushed with nitrogen for at least 15 min at a flow of  $10 \text{ L min}^{-1}$ . After this time, the gas flow was reduced to  $25 \text{ cm}^3 \text{ min}^{-1}$ , and the gassing chemicals were added sequentially to the emulsion. The concentration of nitrogen oxides in the box was continually monitored using the  $\text{NO}_x$  analyser. After gassing was substantially complete (typically around 90 min), the gas was stirred out of the emulsion using a spatula, liberating any  $\text{NO}_x$  contained within the emulsion gas bubbles, and a final  $\text{NO}_x$  reading taken. Figure 5 shows a diagram of the apparatus.

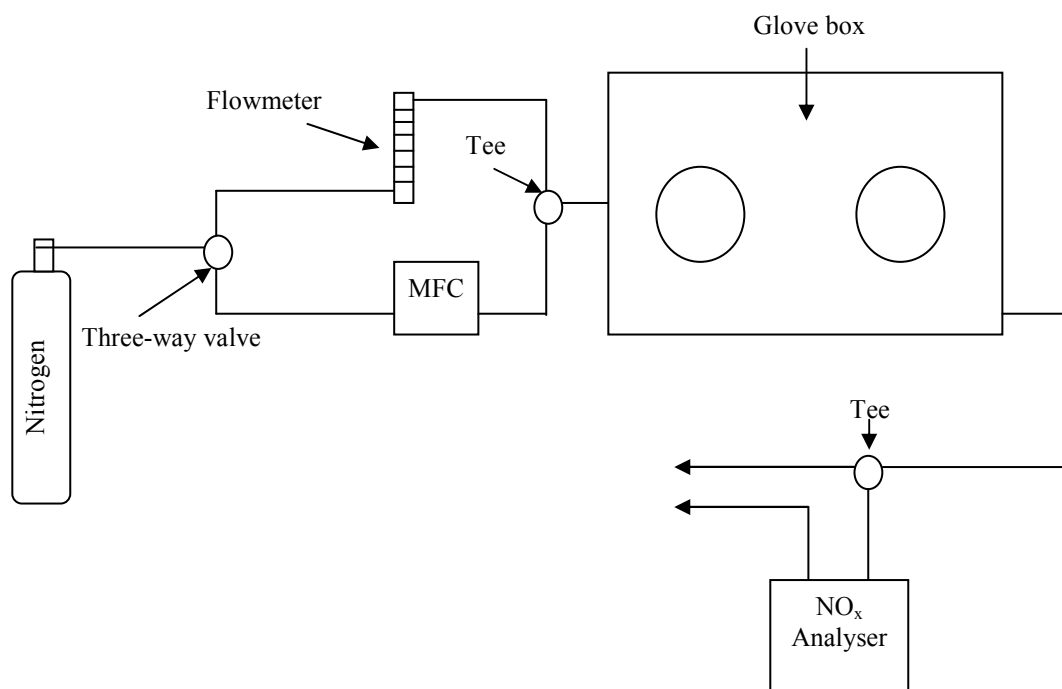


**Figure 5: Diagram of apparatus for  $\text{NO}_x$  measurements during emulsion gassing**

### 3.2 Computational methods

This study employed computational chemistry to examine the reaction mechanisms of the decomposition of nitrous acid and nitrosyl thiocyanate. Computational chemistry utilises the principles of quantum mechanics to determine the structure, energy and reactivity of molecules. It is particularly useful for studying systems or species that are difficult to observe experimentally, including short lived intermediates and transition structures. The overall decomposition reactions of nitrous acid and nitrosyl thiocyanate comprise complex sequences of elementary reaction steps. Many of these reactions involve intermediate species present at very low concentrations, making them near impossible to observe experimentally. In this manner, computational chemistry has been employed to explore the elementary reactions involved in nitrous acid and nitrosyl thiocyanate decomposition, to study the properties of proposed intermediate species that could not be experimentally observed, and to investigate the thermodynamic feasibility of reaction mechanisms proposed to explain the experimental results. This section provides a discussion of the types of computational methods available including key assumptions and limitations. Detailed descriptions of specific computational procedures are provided in the associated thesis chapters.

#### 3.2.1 Ab-initio methods and basis sets

*Ab initio*, or first principles methods, determine the structure and energy of molecules by solving the Schrödinger equation<sup>13</sup>.

$$H\Psi(q_i, q_k) = E_{Tot} \Psi(q_i, q_k) \quad (10)$$

where  $H$  is the Hamiltonian operator,  $E_{tot}$  is the systems energy,  $\Psi$  is the wave function and  $q_i$  and  $q_k$  are the electronic and nuclear coordinates, respectively. The Hamiltonian is composed of terms representing the electronic kinetic energy, the nuclear kinetic energy and the potential energy. In practice, exact solutions to the Schrödinger equation are possible only for systems with one electron and a series of approximations are required in order to solve the Schrödinger equation for multi-electron systems of practical interest.

The Hamiltonian contains pairwise attraction and repulsion terms describing the fact that the motion of the particles is interdependent, or correlated. To simplify this situation, the Born-Oppenheimer approximation<sup>14</sup> can be invoked to separate out the motion of the nuclei and the electrons. Owing to the larger mass of the nucleus, the electrons in a molecule are moving much faster than the nucleus and, consequently, it is assumed that the electrons in the system react instantaneously to changes in nuclear position. As such, the nuclear positions are treated as parameters, reducing the dimensionality of the problem and eliminating the difficulty in describing the nuclear component of the wave function. Invoking the Born-Oppenheimer approximation yields the electronic Schrödinger Equation<sup>13</sup>:

$$(H_{el} + V_N)\Psi_{el}(q_i; q_k) = E_{el}\Psi_{el}(q_i; q_k) \quad (11)$$

where  $H_{el}$  is the electronic Hamiltonian,  $V_N$  is a constant for a given set of fixed nuclear coordinates,  $\Psi_{el}$  is the electronic wave function,  $E_{el}$  is the electronic energy,  $q_i$  denotes



the electronic coordinates which are independent variables and  $q_k$  denotes the nuclear coordinates which are parameters.

The earliest *ab-initio* technique is the Hartree-Fock (HF) method, which forms the basis of subsequent more accurate procedures<sup>15</sup>. The HF method takes advantage of the variational principle, that is, the computed energy of the system will always be higher than the true energy, and solves the Schrödinger equation iteratively using a self consistent field (SCF) method. The SCF process involves making an initial guess for the molecular orbital coefficients, then solves the HF equations to yield a new set of coefficients. The HF equations are then solved with the new coefficients and the process iterated to convergence<sup>13</sup>. The primary approximation employed in Hartree-Fock calculations is the mean-field approximation, wherein the instantaneous coulombic electron-electron repulsion (known as electron correlation) is not explicitly taken into account; rather, the method considers the interaction of each electron with the average charge distribution of all the other electrons in the molecule.

To solve the HF equations, the molecular orbitals are expressed as a linear combination of atomic orbitals which describe the distribution of an electron around an atom. A linear combination of atomic orbitals yields molecular orbitals, and a molecular wave function corresponds to an antisymmetric combination of molecular orbitals. For computational reasons, the atomic orbitals are approximated by a linear combination of Gaussian basis functions. This combination of basis functions is known as the *basis set*. The better the basis functions describe the true atomic orbitals, the more accurate will be the calculations. However, to accurately describe the true atomic orbitals requires a very large number of basis functions. The time taken to perform a calculation is highly

dependant on the size of the basis set, and as such, there is a trade-off between the accuracy of a calculation and the time required to perform it.

Basis functions are derived from atomic orbitals of hydrogen. They are combined in sets to describe atomic orbitals of an element, with basis sets containing one, two and three basis functions per atomic orbital denoted as single- $\zeta$ , double- $\zeta$  and triple- $\zeta$  basis sets respectively. In practice, chemical interactions between atoms affect the outer valence electrons much more than inner core electrons, and it is common to use a larger number of basis functions to describe the valence orbitals than the core orbitals. For example, the 6-31G basis set<sup>16</sup> uses two basis functions to describe the valence orbital and one basis function for each core orbital. In this notation, the number 6 preceding the hyphen denotes that each core basis function is constructed from six primitive Gaussian functions, whilst the numbers 3 and 1 after the hyphen indicates that the valence orbitals are described by two basis functions, one composed of three primitive Gaussians and a second composed of a single primitive. Further additions to the basis set include polarisation functions<sup>17</sup> and diffuse functions<sup>18</sup>. Polarization functions allow greater flexibility in the shape of the orbitals and are necessary to take into account the distortion of atomic orbitals which occurs as a result of bond formation. These are denoted by letters appearing in parentheses following the basis function information. For example, the 6-31G(d,p) basis set denotes that a d function is added to heavy atoms and a p function to light atoms. Diffuse functions on the other hand are essential for describing situations where there is a high electron density away from the nucleus, including molecules with lone electron pairs or those carrying a negative charge. Diffuse functions applied to heavy atoms are denoted by a plus sign (+), whilst two plus sign indicate that diffuse functions are added to both light (i.e. hydrogen) and heavy atoms.

The errors introduced by neglecting electron correlation mean that the results of HF calculations can be in significant error. With an infinite basis set, the difference between the true energy and the HF computed energy results solely from the effect of neglecting electron correlation. As such, significant effort has been expended in developing methods that take into account electron correlation, including Møller-Plesset (MP) perturbation theory<sup>19</sup>, configuration interaction (CI)<sup>20</sup> and coupled cluster (CC) methods<sup>21</sup>. These methods attempt to modify the HF wave function to account for the effect of electron correlation, and as such, have considerably improved accuracy. However, the complexity of these calculations means that these procedures are significantly more computationally expensive than the HF method. The CCSD(T) method with a large basis set is considered the “gold standard” of the *ab initio* methods and is capable of calculating enthalpies of reaction to within 4 kJ mol<sup>-1</sup>.<sup>13</sup> The CCSD(T) method employs an exponential cluster operator to account for electron correlation, with the notation signifying that both single and double excitations are included with triple excitations accounted for perturbatively.

### 3.2.2 Density functional theory

The *ab initio* methods described in the preceding section attempt to determine a molecule's energy by calculating its wave function. An alternative approach is the density functional theory (DFT), which determines the energy of a molecule based on the electron density. The foundations for DFT are the Hohenberg-Kohn theorems<sup>22</sup>, which demonstrate that the energy of the ground state can be uniquely determined by the electron density, and that the density obeys a variational principle (that is, the

calculated energy is always greater than the true ground state energy). The total energy of a system can be expressed as a function of the electron density,  $\rho(\mathbf{r})$ :

$$E(\rho) = E_T(\rho) + E_V(\rho) + E_J(\rho) + E_{XC}(\rho) \quad (12)$$

where  $E_T$  is the kinetic energy of the electrons,  $E_V$  is the potential energy of the nuclear-electron attraction,  $E_J$  is the electron-electron repulsion and  $E_{XC}$  is the exchange-correlation energy. The exchange energy arises from the antisymmetry of the quantum mechanical wave function whilst the correlation energy arises from the interactions between individual electrons. Modern implementations of DFT employ the Kohn-Sham theory<sup>23</sup> and calculate the electron density from the molecular orbitals, which are solved iteratively to find the electron density that yields the lowest energy. These molecular orbitals are constructed from the same basis sets described in Section 3.2.2. The primary challenge in the development of DFT is the description of the exchange-correlation term of Equation 12,  $E_{XC}$ . A variety of exchange correlation functionals have been proposed, ranging from those dependant on the electron density and derived from the localised density approximation (LDA), those that depend on the electron density and the gradient of the density (e.g., those employing the generalised gradient approximation, GGA) and hybrid methods<sup>24</sup>, wherein  $E_{XC}$  includes a proportion of the Hartree Fock exchange energy.

The advantage of DFT methods is that they achieve significantly greater accuracy than Hartree Fock methods for a similar computational cost. In addition, DFT methods produce very accurate molecular geometries and vibrational frequencies, at a fraction of the computational cost of correlated *ab initio* methods such as MP2 and CCSD(T). However, the results of energy calculations are relatively poor compared to accurate *ab*

*initio* methods, and particularly large errors can result for the calculation of energies of non-equilibrium structures, including transition states. For this reason, the primary use of DFT is for calculating accurate geometries for subsequent energy calculations by accurate *ab initio* methods, and for studying large systems where high level molecular orbital theory calculations are unfeasible. A wide variety of DFT methods have also been optimised to yield accurate results for a particular class of chemical species. As such, it is essential to confirm that a chosen method is suitable for studying a particular system. This is typically achieved by performing benchmarking calculations on similar species or reactions with experimentally determined properties/energies, before proceeding to the study of unknown compounds.

### 3.2.3 Compound methods

A series of multi-level methods have been developed for very accurate energy calculations. These methods perform several calculations at different levels of theory and with a variety of basis sets, and combine the results to calculate accurate thermochemical parameters. A typical multi-level method optimises the geometry of the molecule using DFT, HF or an MP2 method with a relatively small basis set. Møller-Plesset (MP $n$ ) methods attempt to account for dynamic electron correlation by treating electron-electron repulsion as a perturbation of the HF Hamiltonian<sup>19</sup>. The perturbation is expressed as a power series with  $n=2,3,4$  or 5 denoting truncation at the second, third, fourth or fifth order term. Subsequent calculations are performed with increasing levels of theory and/or basis set size on the previously optimised geometries (known as a single-point energy calculation). For example, the G3B3 method employs B3LYP geometries in conjunction with single point MP2, MP4 and QCISD(T)

(denoting a quadratic configuration interaction calculation including single, double and perturbed triple excitations<sup>25</sup>) calculations, which are combined in accordance with Equations 13-18<sup>26</sup>:

***Table 1: Calculations employed in G3B3 method***

<b><i>Calculation</i></b>	<b><i>Method</i></b>
Geometry	B3LYP/6-31G(d)
Single point energies	MP4/6-31G(d)
	MP4/6-31+G(d)
	MP4/6-31G(2df,p)
	QCISD(T)/6-31G(d)
	MP2(Full)/G3large
Higher level correction	$A = 6.760$
	$B = 3.233$
Zero point energy	B3LYP/6-31G(d)

$$E_o(G3) = E[\text{MP4/6-31G(d)}] + \Delta(+) + 2\Delta(2\text{df,p}) + \Delta\text{QCI} + \Delta + \Delta\text{HLC} + \text{ZPE} \quad (13)$$

$$\Delta(+) = E[\text{MP4/6-31+G(d)} - \text{MP4/6-31G(d)}] \quad (14)$$

$$\Delta(2df,p) = E[MP4/6-31G(2df,p) - MP4/6-31G(d)] \quad (15)$$

$$\Delta QCI = E[QCISD(T)/6-31G(2df,p) - MP4/6-31G(d)] \quad (16)$$

$$\Delta = E[MP2(Full)/G3large - MP2/6-31G(2df,p) - MP2/6-31+G(d) + MP2/6-31G(d)] \quad (17)$$

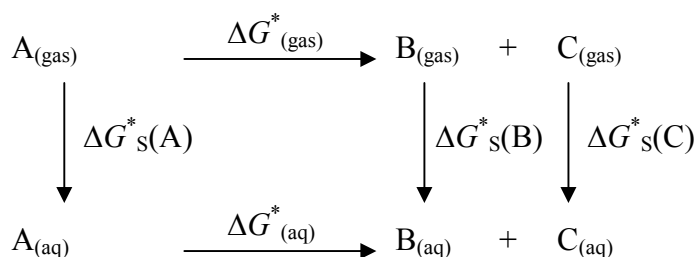
$$\Delta HLC = -An_{\beta} - B(n_{\alpha} - n_{\beta}) \quad (18)$$

where  $n_{\alpha}$  and  $n_{\beta}$  are the number of  $\alpha$  and  $\beta$  valence electrons, respectively. The G3B3 and CBS-QB3 multilevel methods have been employed in the present study for accurate calculation of gas phase reaction enthalpies and free energies. These methods have average absolute errors of 4.14 and 3.64 kJ mol<sup>-1</sup> for G3B3 and CBS-QB3 respectively<sup>26,27</sup>.

### 3.2.4 Solvation modelling

The methods discussed so far pertain to the calculation of molecular energies in the gas phase, where molecules are treated as isolated, non-interacting entities. However, the decomposition of nitrous acid and nitrosyl thiocyanate are aqueous processes, in which the interaction between the reactants and the solvent, water, must be taken into account. Generally, the target for calculations is to compute the aqueous Gibbs Free Energy change of reaction, enabling calculation of the equilibrium constant. Such a calculation can be achieved by accurately determining the gas phase free energy of solvation with methods such as G3B3 or CBS-QB3, and combining these results with a calculated free

energy of solvation using a thermodynamic cycle and making appropriate corrections for changes in standard states, as depicted in Figure 6.<sup>28</sup>



$$\Delta G^*_{(\text{gas})} = \Delta G^0_{(\text{gas}, 1 \text{ atm})} + \Delta n RT \ln(24.46)^a$$

$$\Delta G^*_{(\text{aq})} = \Delta G^*_{(\text{gas})} + \Delta G^*_s(B) + \Delta G^*_s(C) - \Delta G^*_s(A).$$

**Figure 6. Thermochemical cycle for determining aqueous free energy change of reaction, for reaction  $A \rightarrow B + C$ . <sup>a</sup>The value 24.46 reflects the ratio of the molar volume of a gas at 1 atm to that at 1 M**

where  $\Delta G^*_s$  is the free energy of solvation and  $\Delta n$  is the difference in the number of moles of products and reactants. Computational chemistry programs typically calculate gas phase reaction free energies assuming a standard state of 1 atm or 1 bar, whilst aqueous free energies employ a 1 mol L<sup>-1</sup> standard state. As such, if the number of moles of species changes in the course of a reaction, a correction must be applied to account for the difference in the entropy component of the free energy for the 1 mol L<sup>-1</sup> standard state compared to the one based on 1 atm. Figure 6 demonstrates that it is possible to calculate the aqueous reaction free energy by combining the gas phase reaction free energy and the free energy of solvation. As such, most solvation models are concerned with the calculation of  $\Delta G^*_s$ .



The solvation free energy is composed of electrostatic, cavitation, dispersion and solvent rearrangement components. Owing to the complexity of describing solvation by explicit inclusion of water molecules, which require consideration of hundreds if not thousands of individual water molecules, a family of solvation models has been developed which treat the solvent as a homogeneous continuum of uniform dielectric constant. These models, known as the self consistent reaction field (SCRF) or polarisable continuum models (PCM), place the solute inside a cavity surrounded by the continuum and use an iterative procedure to calculate the electrostatic interaction between the solvent and solute. A variety of different models have been presented, differing primarily in their description of the solvent cavity, including its shape and size/radius<sup>29</sup>, and the calculation of non-electrostatic components of the solvation free energy<sup>30</sup>. Typically, the solvent models are optimised to reproduce experimental free energies of solvation. For neutral species, typical accuracies for polarization continuum models are on the order of  $\pm 4 \text{ kJ mol}^{-1}$ , but are much higher for ionic species, on average  $\pm 20\text{-}30 \text{ kJ mol}^{-1}$ . More recent methods which address short range interactions through analysis of the solvent accessible area afford a slight improvement in accuracy to  $\pm 2$  and  $\pm 17 \text{ kJ mol}^{-1}$  for neutrals and charged species, respectively<sup>30</sup>. In the present work, a variety of solvent models were investigated to calculate the reaction free energies of reactions where experimental data is available, to select the best solvent model for a particular reaction system.

### **3.2.6 Optimisation, frequency and transition state theory calculations**

The present study utilises the Gaussian03 and Gaussian09 software packages for electronic structure calculations<sup>31</sup>. The first step in determining the reaction free

energies is to optimise the geometry of the reactant and product species<sup>32</sup>. From a practical perspective, this involves supplying an initial guess of the molecular geometry, and performing an “optimisation” calculation, which minimises the energy of the molecule with respect to the molecules internal coordinates (that is, bond angles and bond lengths). Because the potential energy surface can contain many local minima, it is necessary to trial different initial guesses for the initial geometry to ensure that the optimised structure is a global minimum.

Once the minimum energy structure is located, a “frequency” calculation is performed. This calculation yields thermodynamic quantities of interest including the enthalpy and free energy at a specified temperature, usually 298.15 K, and assists in the characterisation of the stationary point. The vibrational frequencies of stable structures will all be positive, whilst those for transition structures will contain one negative vibrational mode<sup>32</sup>. The transition structure is the point of highest energy on the path connecting the reactants to products known as the reaction coordinate. Location of the transition structure of a reaction is of great interest because it enables the calculation of the reaction rate constant via transition state theory. Transition state theory states that there is a thermodynamic equilibrium between the reactants and the transition state and that the rate of reaction is proportional to the concentration of the transition state<sup>33</sup>. The rate constant is calculated as:

$$k = \frac{k_B T}{h} \exp\left(\frac{-\Delta G^\ddagger}{RT}\right) \quad (19)$$

where  $k$  is the reaction rate constant,  $k_B$  is the Boltzmann constant,  $h$  is the Planck constant,  $\Delta G^\ddagger$  is the free energy of activation (the difference between the transition state free energy and the reactant free energy),  $R$  is the gas constant and  $T$  is the absolute temperature.

### 3.3 References

1. Dickson, P. N.; Margerum, D. W., Extension of accessible first-order rate constants and accurate dead-time determinations for stopped-flow spectroscopy. *Analytical Chemistry* **1986**, 58 (14), 3153-3158.
2. Stedman, G.; Whincup, P. A. E., The equilibrium constant for the formation of nitrosyl thiocyanate in aqueous solution. *J. Chem. Soc.* **1963**, 5796-5799.
3. da Silva, G.; Kennedy, E. M.; Dlugogorski, B. Z., Ab Initio procedure for aqueous-phase pKa calculation: The acidity of nitrous acid. *J. Phys. Chem. A* **2006**, 110, 11371-11376.
4. Clark, J.; Frost, T.; Russell, M. A., *UV spectroscopy: Techniques, instrumentation and data handling*. Chapman & Hall: London, 1993.
5. Tu, C.; Swenson, E. R.; Silverman, D. N., Membrane inlet for mass spectrometric measurement of nitric oxide. *Free Radical Biol. Med.* **2007**, 43, 1453-1457.
6. Fontijn, A.; Sabadell, A. J.; Ronco, R. J., Homogeneous chemiluminescent measurement of nitric oxide with ozone. Implications for continuous selective monitoring of gaseous air pollutants. *Analytical Chemistry* **1970**, 42 (6), 575-579.
7. McCabe, W.; Smith, J.; Harriott, P., *Unit operations of chemical engineering*. McGraw Hill: New York, 2004.
8. Davey, N. G.; Krogh, E. T.; Gill, C. G., Membrane-introduction mass spectrometry (MIMS). *TrAC, Trends Anal. Chem.* **2011**, 30 (9), 1477-1485.
9. Williams, D. L. H., *Nitrosation reactions and the chemistry of nitric oxide*. Elsevier B. V.: Amsterdam, 2004.

10. Bunton, C. A.; Dahn, H.; Loewe, L., Oxidation of ascorbic acid and similar reductones by nitrous acid. *Nature* **1959**, *183* (4655), 163-165.
11. Turner, D.; Dlugogorski, B.; Palmer, T., Factors affecting the stability of foamed concentrated emulsions. *Colloids Surf., A* **1999**, *150* (1-3), 171-184.
12. Vestre, J. *A Method for Preparing a Sensitised Emulsion Explosive* 2003. WO 03/055830 A1
13. Cramer, C. J., *Essentials of computational chemistry, Second Eddition*. John Wiley & Sons Ltd: Chichester, England, 2004.
14. Born, M.; Oppenheimer, R., Quantum theory of the molecules. *Ann. Phys. (Berlin, Ger.)* **1927**, *84*, 457-84.
15. Jensen, F., *Introduction to computational chemistry*. 2nd ed.; John Wiley & Sons Ltd: Chichester, UK, 2007.
16. Ditchfield, R.; Hehre, W. J.; Pople, J. A., Self-consistent molecular-orbital methods. IX. An extended gaussian-type basis for molecular-orbital studies of organic molecules. *J. Chem. Phys.* **1971**, *54* (2), 724-728.
17. Hariharan, P. C.; Pople, J. A., The influence of polarization functions on molecular orbital hydrogenation energies. *Theoretical Chemistry Accounts: Theory, Computation, and Modeling (Theoretica Chimica Acta)* **1973**, *28* (3), 213-222.
18. Clark, T.; Chandrasekhar, J.; Spitznagel, G. W.; Schleyer, P. V. R., Efficient diffuse function-augmented basis sets for anion calculations. III. The 3-21+G basis set for first-row elements, Li–F. *J. Comput. Chem.* **1983**, *4* (3), 294-301.
19. Moller, C.; Plesset, M. S., Note on an approximation treatment for many-electron systems. *Physical Review* **1934**, *46* (7), 618-622.

20. Foresman, J. B.; Head-Gordon, M.; Pople, J. A.; Frisch, M. J., Toward a systematic molecular orbital theory for excited states. *The Journal of Physical Chemistry* **1992**, *96* (1), 135-149.
21. Pople, J. A.; Head-Gordon, M.; Raghavachari, K., Quadratic configuration interaction. A general technique for determining electron correlation energies. *The Journal of Chemical Physics* **1987**, *87* (10), 5968-5975.
22. Hohenberg, P.; Kohn, W., Inhomogeneous electron gas. *Physical Review* **1964**, *136* (3B), B864-B871.
23. Kohn, W.; Sham, L. J., Self-consistent equations including exchange and correlation effects. *Physical Review* **1965**, *140* (4A), A1133-A1138.
24. Becke, A. D., Density-functional thermochemistry. III. The role of exact exchange. *J. Chem. Phys.* **1993**, *98* (7), 5648-5652.
25. Pople, J. A.; Head-Gordon, M.; Raghavachari, K., Quadratic configuration interaction. A general technique for determining electron correlation energies. *J. Chem. Phys.* **1987**, *87* (10), 5968.
26. Baboul, A. G.; Curtiss, L. A.; Redfern, P. C.; Raghavachari, K., Gaussian-3 theory using density functional geometries and zero-point energies. *J. Chem. Phys.* **1999**, *110* (16), 7650-7657.
27. Montgomery, J. J. A.; Frisch, M. J.; Ochterski, J. W.; Petersson, G. A., A complete basis set model chemistry. VI. Use of density functional geometries and frequencies. *J. Chem. Phys.* **1999**, *110* (6), 2822-2827.
28. Liptak, M. D.; Shields, G. C., Experimentation with different thermodynamic cycles used for pKa calculations on carboxylic acids using complete basis set and Gaussian-n models combined with CPCM continuum solvation methods. *International Journal of Quantum Chemistry* **2001**, *85* (6), 727-741.

29. Tomasi, J.; Mennucci, B.; Cancès, E., The IEF version of the PCM solvation method: an overview of a new method addressed to study molecular solutes at the QM ab initio level. *THEOCHEM* **1999**, *464* (1-3), 211-226.
30. Marenich, A. V.; Cramer, C. J.; Truhlar, D. G., Universal solvation model based on solute electron density and on a continuum model of the solvent defined by the bulk dielectric constant and atomic surface tensions. *J. Phys. Chem. B* **2009**, *113* (18), 6378-6396.
31. Frisch, M. J.; Trucks, G. W.; Schlegel, H. B.; Scuseria, G. E.; Robb, M. A.; Cheeseman, J. R.; Montgomery, J., J. A.; Vreven, T. K., K. N.; Burant, J. C.; Millam, J. M.; Iyengar, S. S.; Tomasi, J.; Barone, V.; Mennucci, B.; Cossi, M.; Scalmani, G.; Kudin, K. N.; Rega, N.; Petersson, G. A.; Nakatsuji, H.; Hada, M.; Ehara, M.; Toyota, K.; Fukuda, R.; Hasegawa, J.; Ishida, M.; Nakajima, T.; Honda, Y.; Kitao, O.; Nakai, H.; Klene, M.; Li, X. K., J. E; Hratchian, H. P.; Cross, J. B.; Bakken, V.; Adamo, C.; Jaramillo, J.; Gomperts, R.; Stratmann, R. E.; Yazyev, O.; Austin, A. J.; Cammi, R.; Pomelli, C.; Ochterski, J. W.; Ayala, P. Y.; Morokuma, K.; Voth, G. A.; Salvador, P.; Dannenberg, J. J.; Zakrzewski, V. G.; Dapprich, S.; Daniels, A. D.; Strain, M. C.; Farkas, O.; Malick, D. K.; Rabuck, A. D.; Raghavachari, K.; Foresman, J. B.; Ortiz, J. V.; Cui, Q.; Baboul, A. G.; Clifford, S.; Cioslowski, J.; Stefanov, B. B.; Liu, G.; Liashenko, A.; Piskorz, P.; Komaromi, I.; Martin, R. L.; Fox, D. J.; Keith, T.; Al-Laham, M. A.; Peng, C. Y.; Nanayakkara, A.; Challacombe, M.; Gill, P. M. W.; Johnson, B.; Chen, W.; Wong, M. W.; Gonzalez, C.; Pople, J. A. *Gaussian 03, Revision B.05*, Gaussian Inc: Pittsburgh PA, 2003.
32. Foresman, J. B.; Frisch, A., *Exploring chemistry with electronic structure methods*. Gaussian, Inc.: Pittsburgh, PA, USA, 1996.

33. Eyring, H., The activated complex in chemical reactions. *The Journal of Chemical Physics* **1935**, 3 (2), 107-115.



## CHAPTER 4

**Accurate rate constants for the decomposition of aqueous nitrous acid**

## **Table of Contents**

4.1	Introduction	71
4.2	Experimental	78
4.3	Results and discussion	82
4.3.1	Kinetics at 25 °C in anaerobic solution	82
4.3.2	Kinetics at 25 °C in the presence of oxygen	84
4.3.3	Kinetics of reverse reaction	86
4.3.4	Temperature dependence and thermochemical analysis of the elementary reaction mechanism	89
4.4	Conclusion	95
4.5	References	96

## 1.1 Introduction

Interest in the decomposition of nitrous acid decomposition is widespread, with the reactions playing important roles in many industrial and environmental processes. Industrially, the decomposition of nitrous acid is a significant process occurring in the manufacture of nitric acid, wherein a gaseous  $\text{NO}_x$  stream is absorbed in water<sup>1,2</sup> and in synthesis reactions involving nitrous acid (i.e., nitrosation reactions) where the  $\text{NO}_x$  side products pose a toxicity hazard<sup>3,4</sup>. In atmospheric chemistry, the reactions of nitrous acid and  $\text{NO}_x$  have received attention owing to their importance in acid deposition on the earth's surface and their role in smog formation<sup>5</sup>, whilst the reactions may be of biological importance under certain conditions where nitrous acid decomposition could contribute to NO production in the body<sup>6</sup>. The decomposition of nitrous acid can be employed as a source of NO in the laboratory<sup>7</sup>, and has been implicated in the release of nitrogen oxides from plants<sup>8</sup>. Because of these considerations, the kinetics of nitrous acid decomposition have received considerable attention in the literature, however, the reported rate constants exhibit significant disagreement.

The present study aims to establish accurate rate constants for the decomposition of nitrous acid to enable kinetic modeling of  $\text{NO}_x$  formation that results as a side reaction during nitrosation reactions, in particular, the sensitisation of emulsion blasting agents via ammonia nitrosation. The nitrosation of ammonia (Reaction 1) aims to produce small nitrogen bubbles within the explosive which act as hot spots to propagate the explosion front through the bulk explosive, and result in more reliable and efficient detonation<sup>9</sup>. Formation of  $\text{NO}_x$  as a side product of ammonia nitrosation, however, poses a hazard to miners prior to explosive detonation, particularly in confined underground mines. For industrial applications such as this, accurate knowledge of the

kinetics of the decomposition of nitrous acid is essential to safely implementing nitrosation reactions.



The reaction kinetics of the decomposition of nitrous acid were first elucidated by Abel and Schmidt<sup>10</sup>, who discovered a rate law fourth order in nitrous acid concentration and inversely proportional to the square of the NO concentration (Equation 2). The reaction was demonstrated to have a stoichiometry of three moles of nitrous acid decomposing to produce two moles of NO and one mole of nitric acid (Reaction 3).

$$-\frac{d[\text{HNO}_2]_T}{dt} = \frac{k_{fwd} [\text{HNO}_2]^4}{[\text{NO}]^2} \quad (2)$$



where  $[\text{HNO}_2]_T = [\text{HNO}_2] + [\text{NO}_2^-]$ . Equation 2 can be rationalised by assuming that an equilibrium establishes rapidly between nitrous acid, dissolved NO and NO<sub>2</sub> (Reaction 4), and that the hydrolysis of NO<sub>2</sub> (Reaction 5) comprises the rate limiting reaction step. The hydrolysis of NO<sub>2</sub> consists of a reaction second order in NO<sub>2</sub> concentration, whilst two moles of nitrous acid are required to produce one mole each of NO and NO<sub>2</sub>. This yields an overall rate law fourth order in HNO<sub>2</sub> concentration and gives  $k_{fwd} = 3K_4^2 k_5$ . Combining Reactions 4 and 5 yields the stoichiometry identified in Reaction 3. Derivations are provided in Appendix A.



Reactions 4 and 5 proceed via  $\text{N}_2\text{O}_3$  and  $\text{N}_2\text{O}_4$  intermediates, respectively, which typically exist in equilibrium with NO and  $\text{NO}_2$ . Reactions 6-9 below describe the commonly accepted elementary mechanism<sup>11, 12</sup>:



Schwartz and White<sup>12</sup> performed a comprehensive review of experimental studies related to the absorption of NO and  $\text{NO}_2$  in water. Part of that study reviewed the decomposition of nitrous acid, which constitutes the reverse process of  $\text{NO}_x$  hydrolysis. Further details of that study are discussed in Chapter 2. The quantity  $K_4^2 k_5$  determined from the individual rate constants of Schwartz and White is  $2.4 \times 10^{-6} \text{ L mol}^{-1} \text{ s}^{-1}$ , which is a factor of 2.5 larger than the value of  $9.4 \times 10^{-7} \text{ L mol}^{-1} \text{ s}^{-1}$  inferred from the data of Abel and Schmidt<sup>10</sup> assuming a Henry's constant for NO of  $1.9 \times 10^{-3} \text{ mol L}^{-1} \text{ atm}^{-1}$ .<sup>13</sup>

Thus, it is unclear which rate constants should be selected when attempting to accurately model the formation of NO and NO<sub>2</sub> from nitrous acid decomposition.

Three studies relating to nitrous acid decomposition have been published since the review of Schwartz and White, the results of which are summarised in Table 1. There are considerable differences in the reported rate constants; these have a dramatic effect on the predicted rate of NO<sub>x</sub> production. In addition, the hydrolysis of NO<sub>2</sub> has been recently studied with  $k_5$  determined as  $4.8 \times 10^7 \text{ L mol}^{-1} \text{ s}^{-1}$ .<sup>14</sup> Figure 1 illustrates the discrepancies in the literature rate constants, wherein the production of NO from the decomposition of a 0.01 mol L<sup>-1</sup> nitrous acid solution has been simulated based on the rate constants of the studies in Table 1.

**Table 1. Summary of rate constants for nitrous acid decomposition**

	<b>Park and Lee<sup>15</sup> (22 °C)</b>	<b>Beake and Moodie<sup>16</sup> (25 °C)</b>	<b>Schwarz and White<sup>12</sup> (25 °C)</b>	<b>Ram and Stanbury<sup>17</sup> (25 °C)</b>
$k_4 \text{ (L mol}^{-1} \text{ s}^{-1}\text{)}$	13.4	15	5.6	10-25
$k_{-4} \text{ (L mol}^{-1} \text{ s}^{-1}\text{)}$	$1.60 \times 10^8$	$9.00 \times 10^7$	$3.00 \times 10^7$	$1.75 \times 10^8$
$K_4$	$8.38 \times 10^{-8}$	$1.67 \times 10^{-7}$	$1.87 \times 10^{-7}$	$5.7\text{-}14.3 \times 10^{-8}$
$k_5 \text{ (L mol}^{-1} \text{ s}^{-1}\text{)}$	$8.40 \times 10^7$	$1.00 \times 10^8$	$7.00 \times 10^7$	$5.00 \times 10^7$
$k_{-5} \text{ (L}^2 \text{ mol}^{-2} \text{ s}^{-1}\text{)}$	0	0.005	0.0089	0.0122
$k_5 K_4^2$ $\text{(L mol}^{-1} \text{ s}^{-1}\text{)}$	<b><math>5.9 \times 10^{-7}</math></b> <b><math>(9.2 \times 10^{-7})^a</math></b>	<b><math>2.8 \times 10^{-6}</math></b>	<b><math>2.4 \times 10^{-6}</math></b>	<b><math>0.16\text{-}1.0 \times 10^{-6}</math></b>

<sup>a</sup>Value in parentheses corrected from 22 °C to 25 °C using the activation energy calculated in the present work

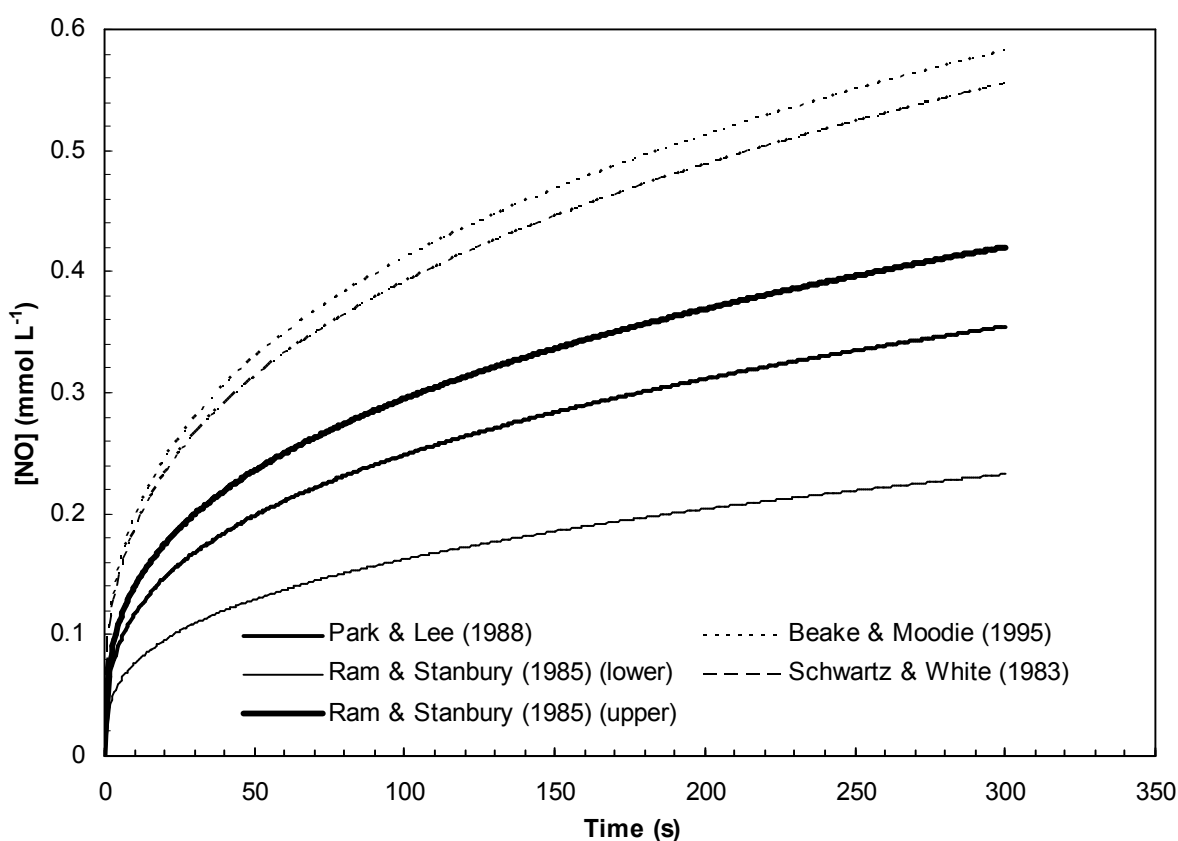


**Figure 1: Formation of nitric oxide predicted using different rate constants for  $\text{HNO}_2$  decomposition**

Discrepancies in the reported results are likely caused by the differences in the methods deployed to study the reaction and the assumptions employed when analysing the data. Park and Lee<sup>15</sup> studied Reactions 4 and 5 by employing a chemiluminescence  $\text{NO}_x$  analyser to measure the gaseous concentrations of NO,  $\text{NO}_2$  and  $\text{HNO}_2$  sparged from a solution of nitrous acid. That study assumed that the concentrations of NO and  $\text{NO}_2$  were in steady state and that the mass transfer characteristics of NO and  $\text{NO}_2$  were the same (and equal to those of  $\text{CO}_2$ ). The rate constant (i.e.  $K_4^2 k_5$ ) derived from this study is four times smaller than the recommended values provided by Schwartz and White. A small portion of this difference could be attributed to the slightly lower temperature of the experiments in that study (22 °C versus 25 °C).

Ram and Stanbury<sup>17</sup> examined the reactions of the  $\text{IrCl}_6^{2-/3-}$  redox couple in nitrous acid over a variety of nitrous acid, nitrate and hydrogen ion concentrations under conditions where the overall reaction rate was dependent on the rate of Reactions 4 and 5. The results of that study depended on the values employed for rate constants of parallel reactions pathways, hence any errors in the rate constants assumed for parallel reaction pathways in simulations would result in errors in the rate constants for Reactions 4 and 5. The resulting values of  $k_4$  ranged from 10 to 25  $\text{L mol}^{-1} \text{s}^{-1}$  depending on the experimental conditions, leading to  $K_4^2 k_5$  values ranging from  $1.6 \times 10^{-7} \text{L mol}^{-1} \text{s}^{-1}$  to  $1 \times 10^{-6} \text{L mol}^{-1} \text{s}^{-1}$ .

Beake and Moodie<sup>16</sup> studied the decomposition of  $\text{HNO}_2$  by UV spectrophotometry at 385 nm in solutions saturated with atmospheric oxygen. The presence of oxygen results in the oxidation of NO to  $\text{NO}_2$  via Reaction 10, which influences the reaction kinetics by reducing the NO concentration, hence driving Reaction 4 to the right.



The approach taken was to assume values of the rate constants  $k_4$ ,  $k_5$  and  $k_{10}$  from the literature and to determine the value of  $k_4$  by solving the set of ordinary differential equations describing the reaction mechanism and varying  $k_4$  to provide the best fit to their experimental data. The results provide a value of  $K_4^2 k_5$  similar to that of Schwartz and White, and considerably larger than that of Park and Lee. An important distinction, as outlined by Butler in Ridd<sup>6</sup>, should be made regarding the rate limiting reaction step in gas-liquid systems versus purely liquid phase experiments. In gas-liquid



experiments, rapid removal of reaction products can result in rate limiting formation of  $\text{N}_2\text{O}_3$ , (Reaction 6) whilst in purely aqueous systems Reaction 4 rapidly reaches equilibrium and the dissolution of  $\text{NO}_2$  via Reaction 5 becomes the rate limiting step. Thus, whilst Beake and Moodie<sup>16</sup> claim to be determining  $k_{-4}$ , the result would actually depend on the initially chosen values for  $k_4$  and  $k_5$ .

Owing to the discrepancies between reported values for rate constants for nitrous acid decomposition, it is desirable to study the reaction kinetics without the complications of (i) mass transfer between the aqueous and gas phase and (ii) the presence of parallel reaction pathways that influence the reaction kinetics. This can be established by monitoring the decomposition of nitrous acid spectrophotometrically, with precautions taken to prevent any transfer of gases in or out of the reacting solution. Such conditions can be readily achieved in a stopped flow mixing device, wherein two reactant solutions contained in gas tight syringes are mixed together rapidly before flowing to a UV-Vis observation cuvette. Such a study may yield an accurate value for the quantity  $K_4^2 k_5$  suitable for modeling NO formation from nitrous acid decomposition during nitrosation reactions.

## 1.2 Experimental

The decomposition of nitrous acid was studied at concentrations ranging from 2.5 to 100 mmol L<sup>-1</sup> using UV-Vis stopped flow spectrophotometry. The setup comprised an Applied Photophysics RX-2000 rapid mixing accessory coupled to a Varian Cary50 spectrophotometer. The temperature of the stopped flow cell was regulated via a Varian Cary peltier thermostated cell holder, whilst the drive syringes of the rapid mixing accessory were surrounded by water connected to a circulating cooling/heating bath at the desired reaction temperature. Nitrous acid was generated in situ by reacting a solution of sodium nitrite with a solution of perchloric acid, with an excess of perchloric acid of at least 0.02 mol L<sup>-1</sup>, providing near complete conversion of nitrite ions into nitrous acid. The precise fraction of nitrite converted to nitrous acid was determined by examining the absorbance at 371 and 386 nm as outlined in Appendix A.

The ionic strength ranged from 0.08 to 0.2 mol L<sup>-1</sup>, with increasing concentrations of NaNO<sub>2</sub> necessitating higher HClO<sub>4</sub> concentrations for complete protonation of NO<sub>2</sub><sup>-</sup>. Small changes in the ionic strength do not affect the reaction rate because the rate depends only on the concentration of neutral species, whose activity changes minimally with increasing ionic strength. Prior to each kinetic experiment, oxygen was removed from the solutions by sparging them with high purity nitrogen for at least 20 min. Degassing for longer time periods produced identical results. The reaction kinetics were determined based on the decrease in absorbance at 357.5, 371, and 386 nm. The absorbance at 500 nm (where neither NO or HNO<sub>2</sub> absorbs) was monitored in each experiment to confirm that gas bubbles of nitric oxide were not forming in the solution. Had gas bubbles formed, an increase in absorbance at 500 nm would be observed due to

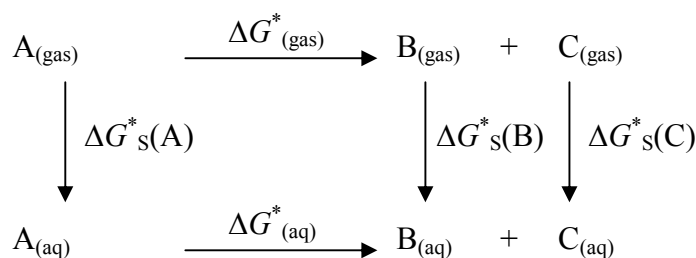
light scattering. The 10 mm path length of the RX-2000 dual path cell was employed for concentrations of 20 mmol L<sup>-1</sup> and below, and the 2 mm length utilised for higher concentrations. The total concentration of nitrous acid ([NO<sub>2</sub><sup>-</sup>] + [HNO<sub>2</sub>]) was determined using Equation 11, where  $A$  is the absorbance at a particular wavelength:

$$[HNO_2]_{Total} = [HNO_2]_{Total,initial} \frac{A}{A_{initial}} \quad (11)$$

Equation 11 is valid provided that the ratio of the nitrous acid to nitrite ion concentration remains constant. Employing an excess of hydrogen ions in the experiments ensures that this criteria is met. The reaction kinetics were analysed by fitting the data from individual experiments over the first 1200 s of reaction to the integrated form of Equation 2, which is provided in Appendix A. The fitting procedure was performed by employing the solver function in Microsoft Excel to find the value of  $K_4^2 k_5$  that produced the minimum error between the experimental data and that predicted from the integrated rate equation. In the case of the experiments involving dissolved oxygen at low HNO<sub>2</sub> concentrations, a system of ordinary differential equations describing the reaction mechanism was solved in Polymath 5.1 for different values of  $K_4^2 k_5$ .

Quantum chemistry calculations were performed with the Gaussian 03 software package<sup>18</sup> to investigate the thermochemistry of nitrous acid decomposition. The G3B3<sup>19</sup> and CBS-QB3<sup>20</sup> methods were employed for accurate determination of gas phase reaction free energies, whilst enthalpies and free energies of solvation were determined at the B3LYP/6-31G(d,p) level<sup>21</sup> with the PCM model (UAHF radii)<sup>22</sup>. This was established by comparing the PCM energies to those calculated for the gas phase

with the same method and basis sets. Combination of the calculated solvation free energies with the gas phase free energy of reaction by means of the thermochemical cycle depicted in Figure 2 enabled calculation of the aqueous phase reaction free energies.



$$\Delta G^*_{(\text{gas})} = \Delta G^0_{(\text{gas}, 1 \text{ atm})} + \Delta nRT \ln(24.46)^a$$

$$\Delta G^*_{(\text{aq})} = \Delta G^*_{(\text{gas})} + \Delta G^*_s(B) + \Delta G^*_s(C) - \Delta G^*_s(A).$$

**Figure 2. Thermochemical cycle for determining aqueous free energy change of reaction, for reaction  $A \rightarrow B + C$ . <sup>a</sup>The value 24.46 reflects the ratio of the molar volume of a gas at 1 atm to that at 1 mol L<sup>-1</sup>**

Thermochemical parameters calculated in Gaussian are based on a standard state pressure of 1 atm, whilst aqueous free energies of reaction employ the 1 mol L<sup>-1</sup> standard state. Results for reaction free energies must therefore be corrected for the change in entropy associated with the transition from a pressure of 1 atm to the concentration of 1 mol L<sup>-1</sup>. This correction has been discussed by Bryantsev et al.,<sup>23</sup> and acts to make the free energy of each species 7.9 kJ/mol more positive. Thus, there is no net correction for reactions where there is no change in the number of moles in a

reaction, whilst reactions exhibiting a greater number of moles of products than reactants become less favorable in the  $1 \text{ mol L}^{-1}$  standard state, and *vice-versa*.

### 1.3 Results and discussion

#### 4.3.1 Kinetics at 25 °C in anaerobic solution

Over the concentration range of interest, Reaction 4 is sufficiently rapid to be at equilibrium and the rate of nitrous acid decomposition is therefore dependent on the rate of hydrolysis of  $\text{NO}_2$ , leading to the simplified rate law given in Equation 2. Equation 2 provided an excellent fit to the data, with the value of  $K_4^2 k_5$  remaining constant at  $1.34 (\pm 0.06) \times 10^{-6} \text{ L mol}^{-1} \text{ s}^{-1}$  for nitrous acid concentrations ranging from 0.02 to 0.1 mol  $\text{L}^{-1}$ , demonstrating the validity of this rate law under the present experimental conditions. The kinetics show an initial period of rapid decomposition, after which the accumulation of nitric oxide in the solution causes a continued decline in the reaction rate. The importance of completely removing oxygen from the reaction medium cannot be stressed enough, particularly at low nitrous acid concentrations where small amounts of oxygen have a significant impact on the reaction kinetics and cause a deviation from the simplified rate equation. As expected from Equation 2, the rate of decomposition increases significantly with increasing nitrous acid concentration. At low concentrations of nitrous acid, the rate of reaction declines such that the fraction of nitrous acid decomposed in the time frame of the experiments becomes quite low, leading to small changes in absorbance. Thus, we place the highest confidence in the results obtained for nitrous acid concentrations of 20 mmol  $\text{L}^{-1}$  or greater. Figure 3 shows kinetic traces for 0.02-0.1 mol  $\text{L}^{-1}$   $\text{HNO}_2$  including the best fit of Equation 2 to the data, whilst Table 2 provides the results of the individual experiments.

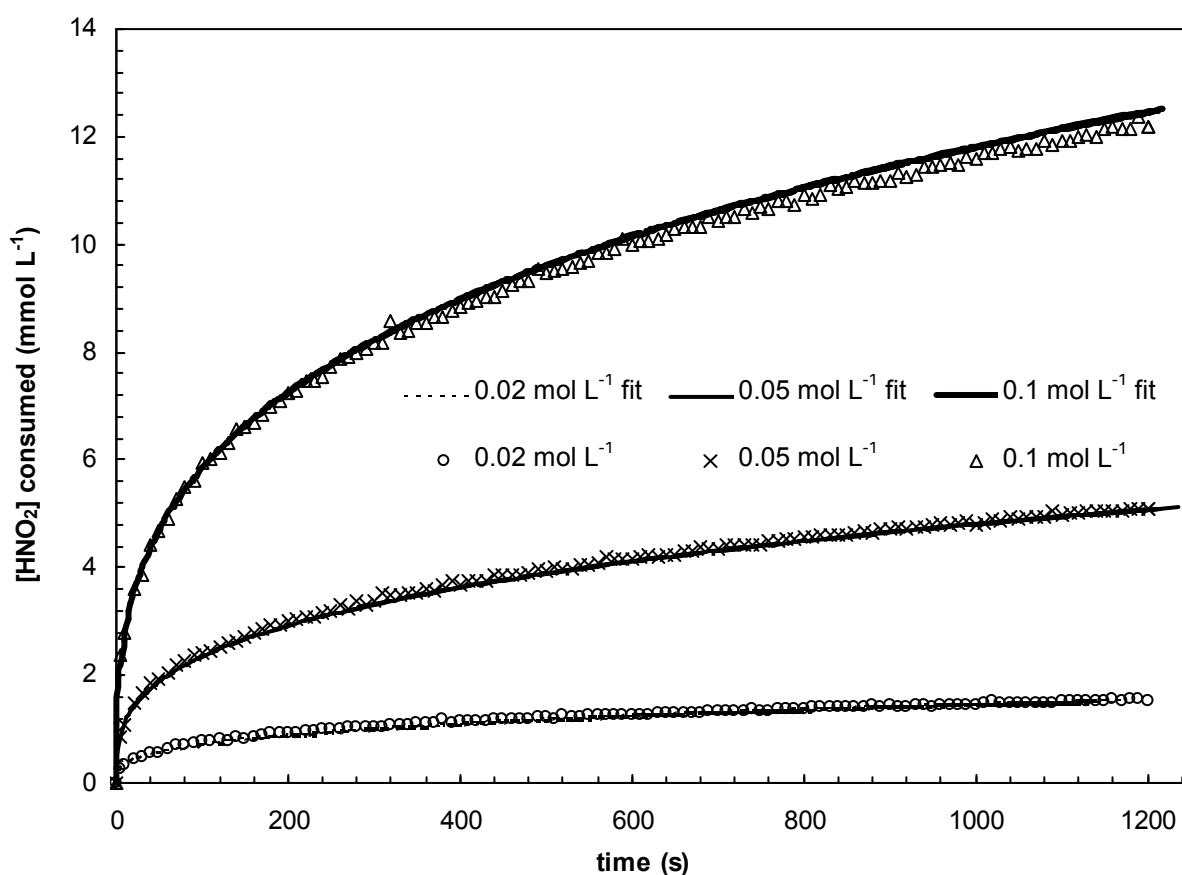


**Figure 3: Experimental and simulated nitrous acid decomposition results for 20-100 mmol L<sup>-1</sup> NaNO<sub>2</sub>. For simulations,  $K_4^2k_5$  remains constant at  $1.34 \times 10^{-6} \text{ mol L}^{-1} \text{ s}^{-1}$**

The value of  $K_4^2k_5$  presently deduced amounts to approximately half that recommended by Schwartz and White<sup>12</sup> and determined by Beake and Moodie<sup>16</sup>. It exceeds the largest value of Ram and Stanbury<sup>17</sup> by 30%, and surpasses the value of Park and Lee<sup>15</sup> by a similar margin, after correcting that result from 22 °C to 25 °C. The difference between the present result and that derived from the values recommended by Schwartz and White<sup>12</sup> most likely stems from the uncertainty in the individual constants  $k_4$ ,  $k_{-4}$  and  $k_5$  of that study, in particular  $k_{-4}$ , for which the upper and lower estimates span an order of magnitude. The study of Beake and Moodie employed a similar method to the present study (UV spectroscopy, but with stoppered cells rather than stopped flow) and recorded a significantly larger rate constant. That study concentrated on relatively low

HNO<sub>2</sub> concentrations (2-8 mmol L<sup>-1</sup>) and very long reaction times (> 3 hours), which could have allowed the measurements to be influenced by a slow rate of oxygen diffusion past the cell stopper. In contrast to the measurements of Beake and Moodie, the present result coincides relatively closely with the values of  $K_4^2k_5$  deduced from the measurements of Park and Lee and Ram and Stanbury, supporting the present determination.

### 1.3.2 Kinetics at 25 °C in the presence of oxygen

To extend the measurements to lower concentrations of nitrous acid (2.5 mmol L<sup>-1</sup>), experiments were performed with solutions initially saturated with atmospheric oxygen. This had the advantages of both increasing the change in absorbance and removing the error associated with the presence of a small amount of residual oxygen in the degassed solutions, which can have a significant effect on the kinetics at low concentrations of nitrous acid. It does, however, introduce some uncertainty owing to the fact that the oxidation of NO by O<sub>2</sub> could become at least partially rate limiting, and hence the values determined would depend on the rate constant assumed for that reaction. The oxidation of NO to NO<sub>2</sub> by O<sub>2</sub> is a third order reaction, second order in NO and first order in O<sub>2</sub> (Reaction 10)<sup>24</sup>. Rate constants for that reaction have been determined in a number of studies with estimates ranging from 1.6-2.9 × 10<sup>6</sup> L<sup>2</sup> mol<sup>-2</sup> s<sup>-1</sup>.<sup>25</sup> A value of  $k_{10} = 2.1 \times 10^6 \text{ L}^2 \text{ mol}^{-2} \text{ s}^{-1}$ , consistent with the results of Lewis and Dean<sup>24</sup>, provides an identical value of  $K_4^2k_5$  to that in the anaerobic experiments. Figure 4 compares the results for decomposition of 2.5 mmol L<sup>-1</sup> HNO<sub>2</sub> in air saturated solutions to simulations for different values of  $K_4^2k_5$ .



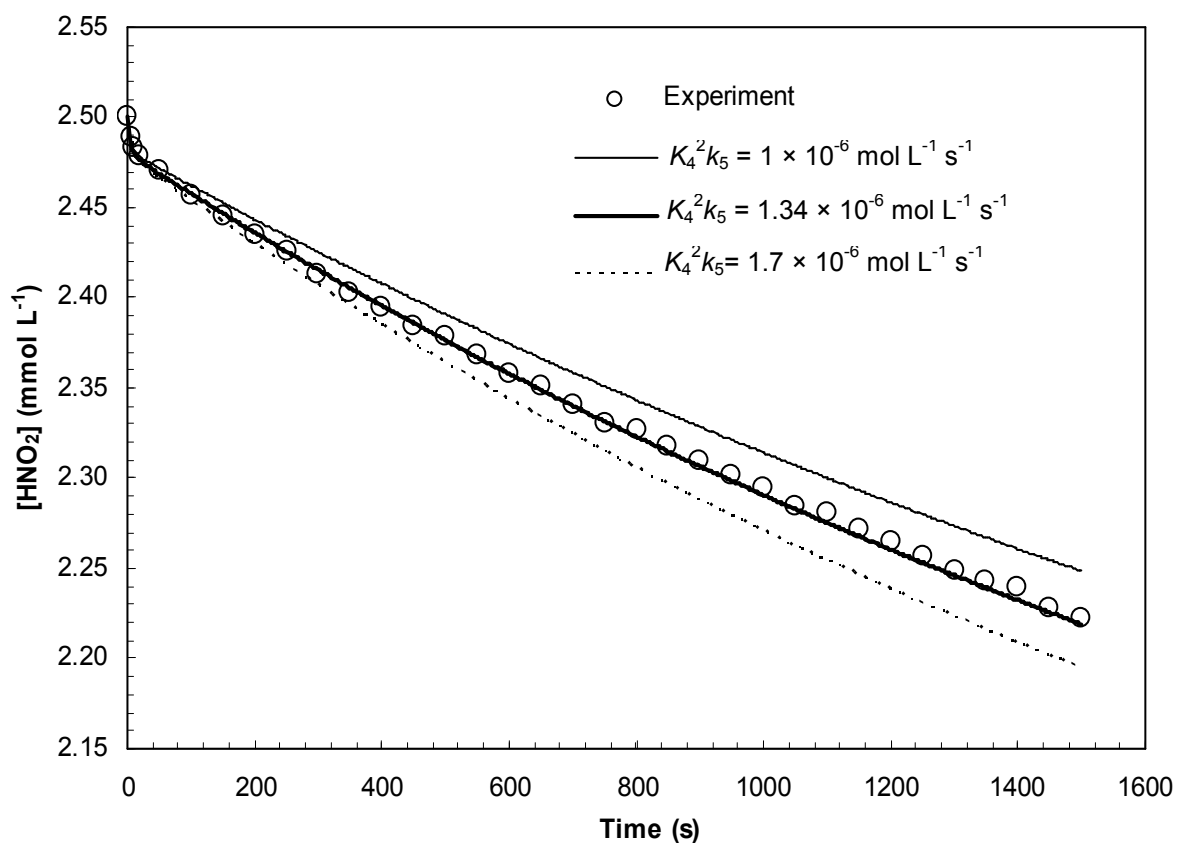


*Figure 4: Comparison of experimental result and simulations for decomposition of 2.5 mmol L<sup>-1</sup> HNO<sub>2</sub> in air-saturated solutions*

**Table 2: Rate constants at 298 K for  $\text{HNO}_2$  decomposition**

<i>Experiment</i>	<i><math>\text{NaNO}_2</math></i> (mol L <sup>-1</sup> )	<i><math>\text{HClO}_4</math></i> (mol L <sup>-1</sup> )	<i><math>\text{NaClO}_4</math></i> (mol L <sup>-1</sup> )	<i>T (K)</i>	<i><math>K_4^2 k_5</math></i> (L mol <sup>-1</sup> s <sup>-1</sup> )
1	0.02	0.04	0.04	298.15	$1.39 \times 10^{-6}$
2	0.02	0.1	0.08	298.15	$1.37 \times 10^{-6}$
3	0.02	0.1	0.08	298.15	$1.33 \times 10^{-6}$
4	0.02	0.1	0.08	298.15	$1.35 \times 10^{-6}$
5	0.05	0.1	0.05	298.15	$1.33 \times 10^{-6}$
6	0.05	0.1	0.05	298.15	$1.29 \times 10^{-6}$
7	0.05	0.1	0.05	298.15	$1.34 \times 10^{-6}$
8	0.05	0.1	0.05	298.15	$1.32 \times 10^{-6}$
9	0.1	0.15	0.05	298.15	$1.46 \times 10^{-6}$
10	0.1	0.15	0.05	298.15	$1.32 \times 10^{-6}$
11	0.1	0.15	0.05	298.15	$1.21 \times 10^{-6}$

### 4.3.3 Kinetics of reverse reaction

Under the conditions of the present study with relatively low nitrite and acid concentrations, nitrate ions are produced at sufficiently low concentrations that the hydrolysis of  $\text{NO}_2$  (Reaction 5) can be assumed to be irreversible. In the presence of added nitrate, or very high acid concentrations, the reverse of Reaction 5 results in the formation of  $\text{NO}_2$ , reducing the net rate of nitrous acid decomposition. This reaction exhibits first order dependencies on nitrous acid, hydrogen ion and nitrate ion concentrations<sup>26,27</sup>. Analogous rate laws are observed for the nitrosation of a range of species by nitrous acid<sup>4</sup>, suggesting that a similar mechanism operates for the reaction of nitrous acid and nitrate. The rate law for nitrous acid decomposition can be modified

to incorporate the effect of this reaction, by assuming that the rate of decomposition depends on the net rate of NO<sub>2</sub> hydrolysis; i.e., the net rate of Reaction 5a.



$$\frac{d[\text{HNO}_2]_T}{dt} = -\frac{3K_4^2 k_5 [\text{HNO}_2]^4}{[\text{NO}]^2} + 3k_{-5} [\text{HNO}_2] [\text{H}^+][\text{NO}_3^-] \quad (12)$$

Experiments with added nitrate ions showed a similar initial rate of decomposition, but did not proceed to as great an extent as the accumulation of NO eventually makes the two terms of Equation 12 equal. That is, the presence of nitrate causes the reactions to reach an equilibrium position. The constant  $k_{-5}$  was evaluated by performing a series of experiments with different hydrogen and nitrate ion concentrations and ascertained to be  $5.9 (\pm 0.6) \times 10^{-3} \text{ L}^2 \text{ mol}^{-2} \text{ s}^{-1}$  at an ionic strength of  $0.18 \text{ mol L}^{-1}$ . This result is 20-40% smaller compared to previous values reported in the literature at zero ionic strength<sup>12</sup>. This discrepancy arises as a result of non-unity activity coefficients of nitrate and hydrogen ions at  $0.18 \text{ mol L}^{-1}$  ionic strength, which reduce the observed rate of the reverse reaction. Our result lies in close agreement with the prior determination by Abel and Schmidt<sup>28</sup> and Jordan and Bonner<sup>26</sup>. This provides further support for the value of  $K_4^2 k_5$  ( $1.34 \times 10^{-6} \text{ L mol}^{-1} \text{ s}^{-1}$ ) determined in the present study, as employing this constant in Equation 12 results in the same value of  $k_{-5}$  determined independently in the literature. Had the value of  $K_4^2 k_5$  been in error, it would not have been possible to reproduce the correct value of  $k_{-5}$ . Figure 5 provides a comparison of a kinetic trace for  $0.1 \text{ mol L}^{-1} \text{ NO}_3^-$  to an equivalent experiment with no added nitrate, whilst Table 3 provides the experimental conditions and associated values of  $k_{-5}$ .

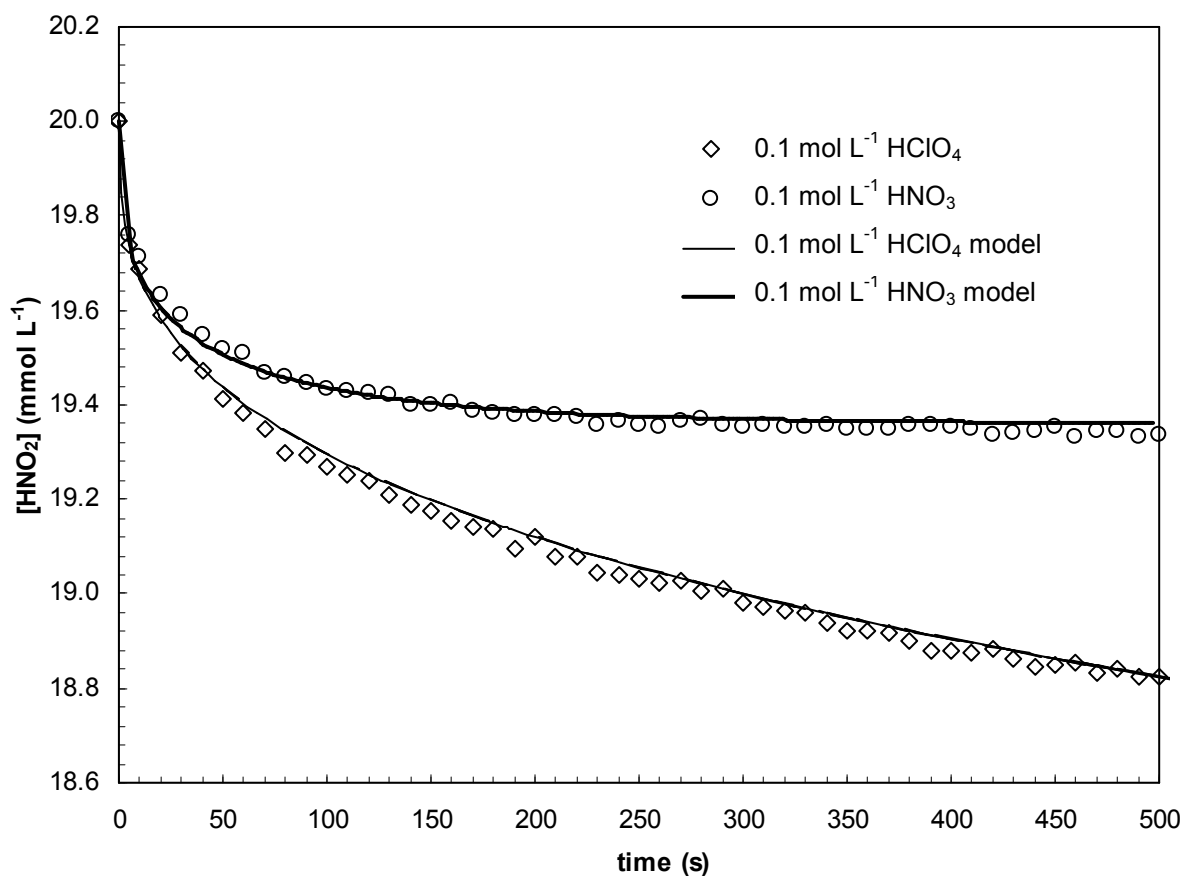


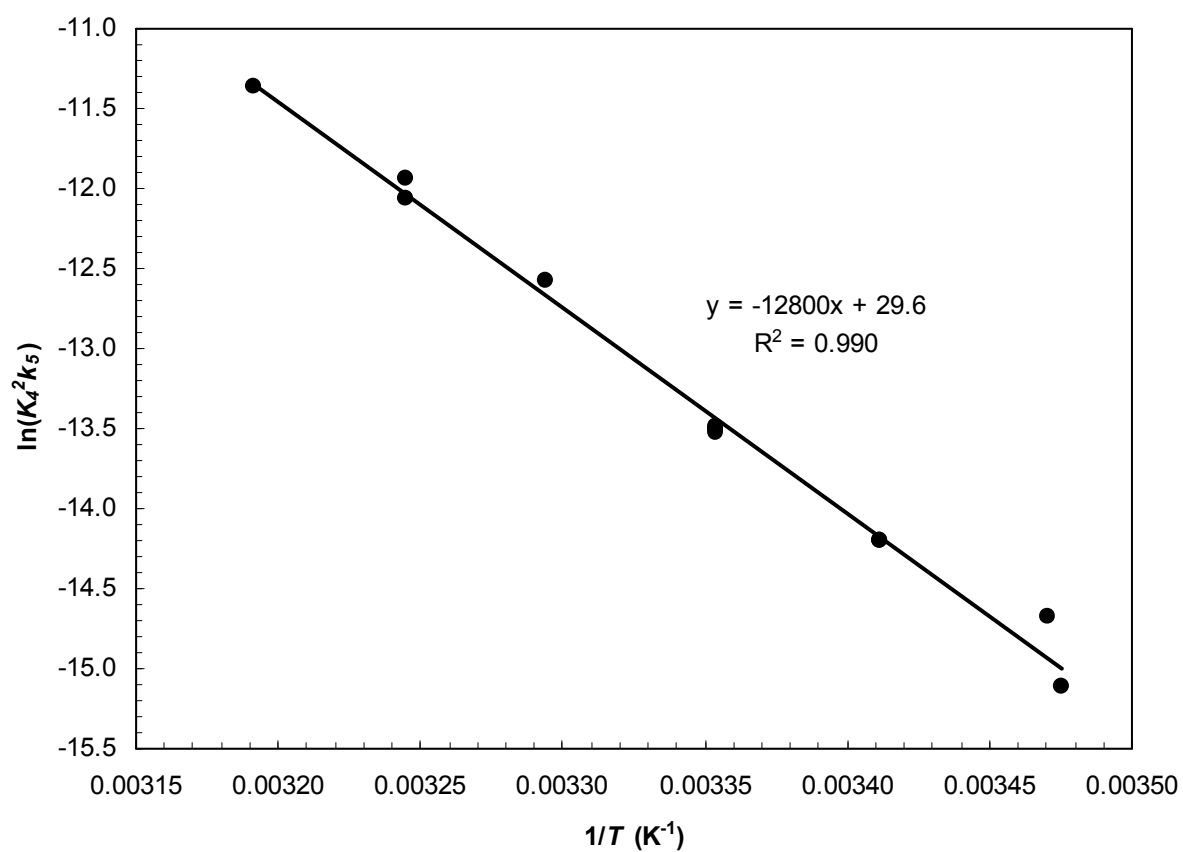
Figure 5. Experiment and model for decomposition of  $0.02 \text{ mol L}^{-1} \text{HNO}_2$  in  $0.1 \text{ mol L}^{-1} \text{HClO}_4$  and  $0.1 \text{ mol L}^{-1} \text{HNO}_3$

Table 3: Rate constants for reverse reaction at 298 K

Experiment	$\text{H}^+$ (mol $\text{L}^{-1}$ )	$\text{NO}_3^-$ (mol $\text{L}^{-1}$ )	$\text{NaNO}_2$ (mol $\text{L}^{-1}$ )	$k_{-5}$ ( $\text{L}^2 \text{ mol}^{-2} \text{ s}^{-1}$ )
21	0.05	0.05	0.02	$6.48 \times 10^{-3}$
22	0.05	0.05	0.02	$6.69 \times 10^{-3}$
23	0.1	0.05	0.02	$6.23 \times 10^{-3}$
24	0.1	0.05	0.02	$5.13 \times 10^{-3}$
25	0.1	0.15	0.02	$5.33 \times 10^{-3}$
26	0.1	0.15	0.02	$5.87 \times 10^{-3}$
27	0.1	0.1	0.02	$5.28 \times 10^{-3}$
28	0.1	0.1	0.02	$5.83 \times 10^{-3}$

### 1.3.1 Temperature dependence and thermochemical analysis of the elementary reaction mechanism

The temperature dependence of both the forward and reverse reactions was examined between 20 and 55 °C. The rate of nitrous acid decomposition increased markedly with increasing temperature, a plot of  $\ln(K_4^2 k_5)$  yielding an apparent activation energy of  $106.6 \pm 3 \text{ kJ mol}^{-1}$  (Figure 6). The uncertainty represents the standard error obtained from a plot of  $\ln(K_4^2 k_5)$  versus  $1/T$ , which was determined using a least-squares linear fitting routine. This large activation energy may have contributed to the considerable scatter in the literature data, with a temperature increase of just 1 °C resulting in an increase in  $K_4^2 k_5$  of approximately 20% at 25 °C. This underscores the importance of accurately maintaining the temperature when studying this reaction. The activation energy of the reverse reaction was determined to be  $76 \pm 4 \text{ kJ mol}^{-1}$  from a plot of  $\ln(k_{-5})$  versus  $1/T$  (Figure 7), in close agreement with the prior determination of  $74 \text{ kJ mol}^{-1}$  by Akhtar et al.<sup>27</sup>. Tabulations of the experimental conditions and individual results are provided in Appendix A.



*Figure 6: Plot of  $\ln(K_4^2 k_5)$  versus  $1/T$*

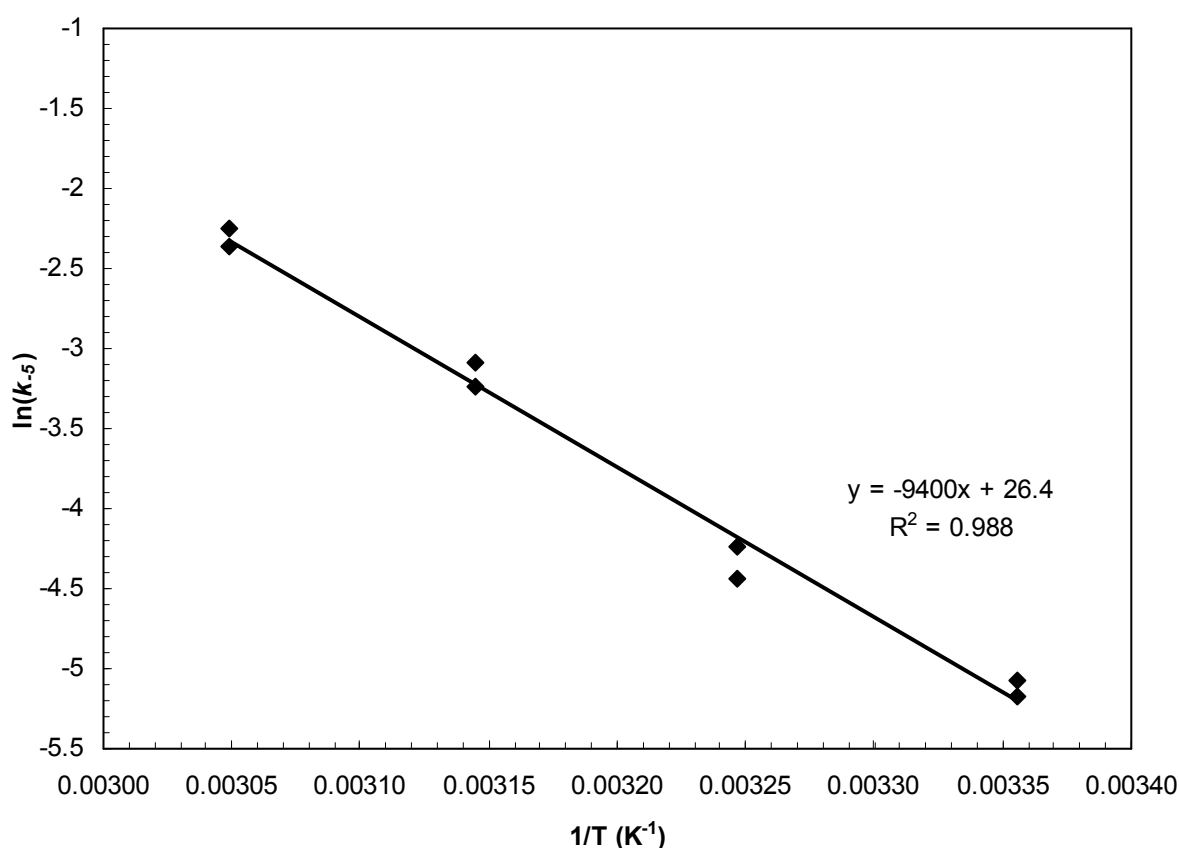


**Figure 7: Plot of  $\ln(k_{-5})$  versus  $1/T$**

A quantum chemistry study was undertaken to determine the origin of the high activation energy associated with  $K_4^2 k_5$ . The gas phase free energies and enthalpies of Reactions 6-9 were established using the average results of the CBS-QB3 and G3B3 methods. The gas phase free energy of the proton, -26.3 kJ/mol, was taken from the literature.<sup>29</sup> Nitrous acid exists in both the *cis* and *trans* conformations, with the energy of the *cis* isomer located 2.2 and 2.5 kJ higher than *trans* for CBS-QB3 and G3B3, respectively. Owing to the small difference in the calculated energy of HONO isomers, we use the average energy when determining all thermodynamic quantities, as previously reported<sup>30</sup>. The first reaction results in the formation of dinitrogen trioxide and involves the combination of two nitrous acid molecules with simultaneous elimination of H<sub>2</sub>O (Reaction 6). The transition states (TS) for the gas phase reaction

have previously been identified<sup>31,32</sup> and because this reaction has been demonstrated to be at equilibrium<sup>9</sup>, we do not investigate the TS further.  $\text{N}_2\text{O}_3$  undergoes homolytic fission producing NO and  $\text{NO}_2$ , followed by combination of two  $\text{NO}_2$  molecules forming  $\text{N}_2\text{O}_4$ . The final reaction involves the hydrolysis of  $\text{N}_2\text{O}_4$ , forming nitrous acid, nitrate and hydrogen ions. The calculated gas phase enthalpies and free energies of reaction are in good agreement with experimental values<sup>33</sup>, with mean absolute errors in the gas phase  $\Delta H_r$  and  $\Delta G_r$  of 1.9 kJ and 3.0 kJ/mol respectively, for Reactions 6-8. There was however a significant difference of 14 kJ/mol between the experimental results for Reaction 9 and those calculated with the CBS-QB3 method, inclusion of which increases the average error in  $\Delta H_r$  to 3.5 kJ/mol.

The aqueous phase enthalpies and free energies of reaction were determined by combining the solvation enthalpies and free energies determined with the PCM solvent model to the accurate gas-phase results in accordance with the thermochemical cycle depicted in Figure 2. In the case of water and the hydrogen cation, the experimental enthalpies and free energies of vaporisation were applied, as opposed to the calculated ones<sup>33,34</sup>. Table 4 presents the calculated aqueous enthalpies and free energies of reaction for Reactions 6-9, including the calculated equilibrium constants which are compared to experimental results. Note that the free energies include a correction for a change in standard state from 1 atm to 1 mol  $\text{L}^{-1}$ ,<sup>23</sup> and that the calculated equilibrium constants are derived based on the average of G3B3 and CBS-QB3 free energies of reaction.



**Table 4. Calculated aqueous enthalpies and free energies of reactions 6-9 and comparison of calculated and experimental equilibrium constants. All energies are in kJ.**

<b>Reaction</b>	$\Delta H_{298}$ <b>G3B3</b>	$\Delta H_{298}$ <b>CBS-QB3</b>	$\Delta G_{298}$ <b>G3B3</b>	$\Delta G_{298}$ <b>CBS-QB3</b>	$K_{calc}^a$	$K_{expt}$	<b>Unit</b>	<b>Source</b>
<b>6</b>	-4.0	-2.4	25.2	27.0	$2.65 \times 10^{-5}$	$3 \times 10^{-3}$	L mol <sup>-1</sup>	Ref. <sup>35</sup>
<b>7</b>	50.7	46.9	15.4	11.6	$4.30 \times 10^{-3}$	$3.3 \times 10^{-5}$	mol L <sup>-1</sup>	Ref. <sup>12</sup>
<b>8</b>	-69.3	-66.6	-19.4	-16.5	$1.39 \times 10^3$	$7 \times 10^4$	L mol <sup>-1</sup>	Ref. <sup>12</sup>
<b>9</b>	-18.5	-26.9	-24.3	-32.9	$1.04 \times 10^5$	$1.25 \times 10^5$	mol L <sup>-1</sup>	Ref. <sup>12</sup>
<b>4 (6 + 7)</b>	46.7	44.5	40.7	38.6	$1.14 \times 10^{-7}$	$1.87 \times 10^{-7}$		Ref. <sup>12</sup>

<sup>a</sup> Calculated equilibrium constants are based on the average of G3B3 and CBS-QB3 results

Table 4 shows that the predicted equilibrium constants for Reactions 6 and 7 deviate from the experimental values by two orders of magnitude, equivalent to a 12 kJ error in  $\Delta G_r$ . The predicted equilibrium constant for Reaction 8 is almost two orders of magnitude smaller than the experimental value. The higher error of the aqueous reaction free energies relative to the gas phase results arises due to inaccuracies in the prediction of solvation free energies, which are typically in the order of 4 kJ/mol for neutral species<sup>36</sup>. With regard to Reactions 7 and 8, the present method predicts that formation of the compound oxides N<sub>2</sub>O<sub>3</sub> and N<sub>2</sub>O<sub>4</sub> (from the simple oxides NO and NO<sub>2</sub>) is considerably less favorable than predicted from experiments. Considering that the calculated gas phase energies are in good agreement with experimental results, it appears that the PCM model underestimates the solvation free energies of N<sub>2</sub>O<sub>4</sub> and N<sub>2</sub>O<sub>3</sub> relative to the simple oxides NO and NO<sub>2</sub>. Despite the errors associated with  $K_6$  and  $K_7$ , combining Reactions 6 and 7 into the overall Reaction 4 provides close agreement between the calculated and experimental equilibrium constants. The results

for Reaction 9 with CBS-QB3 and G3B3 differ by 8.6 kJ/mol, however, the average is fortuitously in excellent agreement with experiments.

The calculated enthalpy of Reaction 4 can be employed to determine the contribution of this reaction to the activation energy of  $K_4^2 k_5$  by means of Equation (13). Provided that the enthalpy of reaction is independent of temperature, a plot of  $\ln(K)$  versus the reciprocal of temperature is linear with a slope equal to the negative of the enthalpy of reaction. Combining the expression for the equilibrium constant with the Arrhenius expression for the temperature dependence of the reaction rate of (5) yields Equation (13), as shown in the Appendix A. Thus, the apparent activation energy, determined from a plot of  $\ln(K_4^2 k_5)$  versus  $1/T$ , is equal to twice the enthalpy of reaction (4) summed with the activation energy of reaction (5).

$$\ln(K_4^2 k_5) = -\frac{(2\Delta H_{(4)} + E_{A(5)})}{RT} + 2\frac{\Delta S}{R} + \ln(A) \quad (13)$$

Reaction 4 is considerably endothermic, with gas phase enthalpies of reaction of 34.4 and 37.7 kJ at the G3B3 and CBS-QB3 levels respectively. The effect of solvation serves to make the reaction more endothermic, leading to an average value of 45 kJ for the aqueous enthalpy of Reaction 4. Thus, this reaction contributes approximately 90 kJ to the apparent activation energy of  $K_4^2 k_5$  due to the second order dependence on  $K_4$ . It can therefore be concluded that Reaction 5 has a small activation energy on the order of 17 kJ. Although the solvation energies introduce some uncertainty in the value of  $\Delta H_{(4)}$ , the contribution of  $K_4^2$  to the apparent activation energy is clearly much higher than the contribution of  $k_5$ . The close agreement between the experimental and calculated free energies for Reaction 4 provides support for the calculated enthalpy of reaction.

## 1.1 Conclusion

The decomposition of nitrous acid, including the reverse reaction between nitrous acid and nitrate ions has been studied by stopped flow spectrophotometry to resolve discrepancies in literature values of the rate constants. The value determined ( $K_4^2 k_5 = 1.34 \pm (0.06) \times 10^{-6} \text{ L mol}^{-1} \text{ s}^{-1}$ ), is of higher accuracy than those previously reported in the literature as it does not depend on the rate of parallel reaction pathways or on the rate of interphase mass transfer of gaseous reaction products. The activation energy associated with  $K_4^2 k_5$  is 107 kJ, the majority of this being attributable to the endothermic nature of the reaction  $2\text{HONO} \rightarrow \text{NO} + \text{NO}_2 + \text{H}_2\text{O}$ .

## 1.5 References

1. Patwardhan, J.; Joshi, J., Unified model for NO<sub>x</sub> absorption in aqueous alkaline and dilute acidic solutions. *AIChE J.* **2003**, *49* (11), 2728-2748.
2. Ingale, N. D.; Chatterjee, I. B.; Joshi, J. B., Role of nitrous acid decomposition in absorber and bleacher in nitric acid plant. *Chem. Eng. J. (Amsterdam, Neth.)* **2009**, *155* (3), 851-858.
3. Zollinger, H., *Azo and diazo chemistry: Aliphatic and aromatic compounds*. Interscience Publishers Inc.: New York, 1961.
4. Williams, D. L. H., *Nitrosation reactions and the chemistry of nitric oxide*. Elsevier B. V.: Amsterdam, 2004.
5. Finlayson-Pitts, B. J.; Pitts, J. N. J., *Atmospheric chemistry: Fundamentals and experimental techniques*. Wiley: New York, 1986.
6. Butler, A. R.; Ridd, J. H., Formation of nitric oxide from nitrous acid in ischemic tissue and skin. *Nitric Oxide* **2004**, *10* (1), 20-24.
7. Aga, R. G.; Hughes, M. N., The preparation and purification of NO gas and the use of NO releasers: The application of NO donors and other agents of nitrosative stress in biological systems. *Methods Enzymol.* **2008**, *436*, 35-48.
8. Klepper, L., Comparison between NO<sub>x</sub> evolution mechanisms of wild-type and nr1 mutant soybean leaves. *Plant Physiol.* **1990**, *93*, 26-32.
9. da Silva, G.; Dlugogorski, B. Z.; Kennedy, E. M., An experimental and theoretical study of the nitrosation of ammonia and thiourea. *Chem. Eng. Sci.* **2006**, *61* (10), 3186-3197.
10. Abel, E.; Schmid, H., The kinetics of nitrous acid. III. Kinetics of the decomposition of nitrous acid. *Z. physik. Chem.* **1928**, *134*, 279-300.

11. da Silva, G. R.; Dlugogorski, B. Z.; Kennedy, E. M., Elementary reaction step model of the N-nitrosation of ammonia. *Int. J. Chem. Kinet.* **2007**, *39* (12), 645-656.
12. Schwartz, S. E.; White, W. H., Kinetics of reactive dissolution of nitrogen oxides into aqueous solution. *Adv. Environ. Sci. Technol.* **1983**, *12*, 1-116.
13. Armor, J. N., Influence of pH and ionic strength upon solubility of NO in aqueous solution. *J. Chem. Eng. Data* **1974**, *19* (1), 82-84.
14. Becker, R. H.; Nicoson, J. S.; Margerum, D. W., Nucleophile assistance of electron-transfer reactions between nitrogen dioxide and chlorine dioxide concurrent with the nitrogen dioxide disproportionation. *Inorganic Chemistry* **2003**, *42* (24), 7938-7944.
15. Park, J. Y.; Lee, Y. N., Solubility and decomposition kinetics of nitrous acid in aqueous solution. *J. Phys. Chem.* **1988**, *92* (22), 6294-302.
16. Beake, B. D.; Moodie, R. B., Role of the reaction of nitric oxide with oxygen in the decomposition of nitrous acid in aqueous acid solution. *J. Chem. Soc., Perkin Trans. 2* **1995**, (6), 1045-8.
17. Ram, M. S.; Stanbury, D. M., Kinetics and equilibria for reactions of the hexachloroiridate redox couple in nitrous acid. *Inorg. Chem.* **1985**, *24* (19), 2954-62.
18. Frisch, M. J.; Trucks, G. W.; Schlegel, H. B.; Scuseria, G. E.; Robb, M. A.; Cheeseman, J. R.; Montgomery, J., J. A.; Vreven, T. K., K. N.; Burant, J. C.; Millam, J. M.; Iyengar, S. S.; Tomasi, J.; Barone, V.; Mennucci, B.; Cossi, M.; Scalmani, G.; Kudin, K. N.; Rega, N.; Petersson, G. A.; Nakatsuji, H.; Hada, M.; Ehara, M.; Toyota, K.; Fukuda, R.; Hasegawa, J.; Ishida, M.; Nakajima, T.; Honda, Y.; Kitao, O.; Nakai, H.; Klene, M.; Li, X. K., J. E.; Hratchian, H. P.;

- Cross, J. B.; Bakken, V.; Adamo, C.; Jaramillo, J.; Gomperts, R.; Stratmann, R. E.; Yazyev, O.; Austin, A. J.; Cammi, R.; Pomelli, C.; Ochterski, J. W.; Ayala, P. Y.; Morokuma, K.; Voth, G. A.; Salvador, P.; Dannenberg, J. J.; Zakrzewski, V. G.; Dapprich, S.; Daniels, A. D.; Strain, M. C.; Farkas, O.; Malick, D. K.; Rabuck, A. D.; Raghavachari, K.; Foresman, J. B.; Ortiz, J. V.; Cui, Q.; Baboul, A. G.; Clifford, S.; Cioslowski, J.; Stefanov, B. B.; Liu, G.; Liashenko, A.; Piskorz, P.; Komaromi, I.; Martin, R. L.; Fox, D. J.; Keith, T.; Al-Laham, M. A.; Peng, C. Y.; Nanayakkara, A.; Challacombe, M.; Gill, P. M. W.; Johnson, B.; Chen, W.; Wong, M. W.; Gonzalez, C.; Pople, J. A. *Gaussian 03, Revision B.05*, Gaussian Inc: Pittsburgh PA, 2003.
19. Baboul, A. G.; Curtiss, L. A.; Redfern, P. C.; Raghavachari, K., Gaussian-3 theory using density functional geometries and zero-point energies. *J. Chem. Phys.* **1999**, *110* (16), 7650-7657.
  20. Montgomery, J. A.; Ochterski, J. W.; Petersson, G. A., A complete basis set model chemistry. IV. An improved atomic pair natural orbital method. *J. Chem. Phys.* **1991**, *101* (7), 5900-5909.
  21. Becke, A. D., Density-functional thermochemistry. III. The role of exact exchange. *J. Chem. Phys.* **1993**, *98* (7), 5648-5652.
  22. Tomasi, J.; Mennucci, B.; Cances, E., The IEF version of the PCM solvation method: an overview of a new method addressed to study molecular solutes at the QM ab initio level. *J. Mol. Struct.: THEOCHEM* **1999**, *464* (1-3), 211-226.
  23. Bryantsev, V. S.; Diallo, M. S.; Goddard, W. A., III, Calculation of solvation free energies of charged solutes using mixed cluster/continuum models. *J. Phys. Chem. B* **2008**, *112* (32), 9709-9719.

24. Lewis, R. S.; Deen, W. M., Kinetics of the reaction of nitric oxide with oxygen in aqueous solutions. *Chem. Res. Toxicol.* **1991**, *7*, 568-574.
25. Goldstein, S.; Czapski, G., Kinetics of nitric oxide autooxidation in aqueous solution in the absence and presence of various reductants. The nature of the oxidizing intermediates. *J. Am. Chem. Soc.* **1995**, *117* (49), 12078-12084.
26. Jordan, S.; Bonner, F. T., Nitrogen and oxygen exchange between nitric oxide and aqueous solutions of nitric acid. *Inorg. Chem.* **1973**, *12* (6), 1369-1373.
27. Akhtar, M. J.; Axente, D.; Bonner, F. T., Nitrogen iostope exchange between nitric and nitrous acids. *J. Chem. Phys.* **1979**, *71* (9), 3570-3572.
28. Abel, E.; Schmid, H., Kinetics of nitrous acid. VI. Equilibrium of the nitrous acid-nitric acid-nitric oxide reaction together with its kinetics. *Z. physik. Chem.* **1928**, *136*, 430-6.
29. Liptak, M. D.; Shields, G. C., Accurate  $pK_a$  calculations for carboxylic acids using complete basis set and Gaussian-n models combined with CPCM continuum solvation methods. *J. Am. Chem. Soc.* **2001**, *123* (30), 7314-7319.
30. da Silva, G.; Kennedy, E. M.; Dlugogorski, B. Z., Ab Initio procedure for aqueous-phase  $pK_a$  calculation: The acidity of nitrous acid. *J. Phys. Chem. A* **2006**, *110*, 11371-11376.
31. Mebel, A. M.; Lin, M. C.; Melius, C. F., Rate constant of the  $\text{HONO} + \text{HONO} \rightleftharpoons \text{H}_2\text{O} + \text{NO} + \text{NO}_2$  reaction from ab Initio MO and TST calculations. *J. Phys. Chem. A* **1998**, *102* (10), 1803-1807.
32. Tantanak, D.; Hillier, I. H.; Vincent, M. A., A theoretical study of the formation of a nitrogen-nitrogen triple bond from  $\text{RNH}_2$  and NO species: implications for the selective catalytic reduction of nitrogen oxides. *J. Mol. Struct.: THEOCHEM* **2003**, *626*, 239-246.

33. Linstrom, P. J.; Mallard, W. G. NIST chemistry webbook, NIST standard reference database number 69. <http://webbook.nist.gov> (accessed September 12, 2011).
34. Tissandier, M. D.; Cowen, K. A.; Feng, W. Y.; Gundlach, E.; Cohen, M. H.; Earhart, A. D.; Coe, J. V.; Tuttle, T. R., The proton's absolute aqueous enthalpy and gibbs free energy of solvation from cluster-ion solvation data. *J. Phys. Chem. A* **1998**, *102* (40), 7787-7794.
35. Markovits, G. Y.; Schwartz, S. E.; Newman, L., Hydrolysis equilibrium of dinitrogen trioxide in dilute aqueous solution. *Inorg. Chem.* **1981**, *20*, 445-450.
36. Marenich, A. V.; Cramer, C. J.; Truhlar, D. G., Universal solvation model based on solute electron density and on a continuum model of the solvent defined by the bulk dielectric constant and atomic surface tensions. *J. Phys. Chem. B* **2009**, *113* (18), 6378-6396.



## **CHAPTER 5**

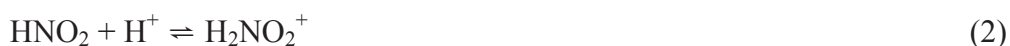
### **Experimental study of decomposition of aqueous nitrosyl thiocyanate**

**Table of Contents**

5.1	Introduction	103
5.2	Experimental	106
5.2.1	Reagents and solutions	106
5.2.2	Kinetics - Stopped flow UV-Vis	107
5.2.3	Analysis of gaseous products – FTIR and MIMS	107
5.2.4	Analysis of aqueous products	108
5.2.5	Data analysis	109
5.3	Results	111
5.3.1	Equilibrium constant for the formation of ONSCN	111
5.3.2	Reaction products	112
5.3.3	Spectrum of intermediate species	114
5.3.4	Effect of initial dissolved oxygen on reaction kinetics	118
5.3.5	Kinetics: Initial rates and effect of thiocyanate ion concentration	120
5.3.6	Kinetics: Effect of nitric oxide	121
5.3.7	Reaction mechanism – global kinetic fit	124
5.4	Discussion	134
5.5	Conclusions	142
5.6	References	143

## 5.1 Introduction

Nitrosation reactions, in which the nitroso ( $\text{NO}^+$ ) group transfers from a reactant to a substrate, are important in a diverse range of industrial, environmental and biological applications. Under acidic conditions, nitrosation reactions proceed via the nitrosating agents  $\text{N}_2\text{O}_3$  and  $\text{H}_2\text{NO}_2^+$ , derived from nitrous acid<sup>1</sup>.  $\text{N}_2\text{O}_3$  serves as the primary nitrosating agent under mildly acidic conditions ( $\text{pH} > 1$ ), whilst  $\text{H}_2\text{NO}_2^+$  dominates under highly acidic conditions.



In the presence of added nucleophiles, such as  $\text{Cl}^-$ ,  $\text{Br}^-$ ,  $\text{I}^-$  and  $\text{SCN}^-$ , a new nitrosation pathway operates as a consequence of the formation of nitrosyl halides, denoted ONX (where  $\text{X} = \text{Cl}, \text{Br}^-, \text{I}^-$  or  $\text{SCN}^-$ ). The formation of nitrosyl halides catalyses a wide range of nitrosation reactions, with elevated reaction rates induced by an increase in the concentration of nitrosating agents in the system. Thiocyanate ions, in particular, represent powerful catalysts owing to the large equilibrium constant for the formation of nitrosyl thiocyanate,  $\text{ONSCN}$ , and in many cases the catalysed rate of nitrosation can be many orders of magnitude faster than the uncatalysed rate<sup>2-6</sup>. For a wide variety of substrates, the formation of  $\text{ONSCN}$  is sufficiently fast for this species to reach its equilibrium concentration as shown below<sup>7</sup>.



$$K_{ONSCN} = \frac{[ONSCN]}{[H^+][HNO_2][SCN^-]} \quad (4)$$

The interest in nitrosyl thiocyanate in the present study stems from the potential for this species to produce nitric oxide as a side product during thiocyanate catalysed nitrosation reactions, in particular, the sensitization of emulsion explosives, wherein thiocyanate ions catalyse the nitrosation of ammonia (from ammonium nitrate) forming small bubbles of nitrogen gas within the explosive. Whilst the sensitization reaction produces primarily N<sub>2</sub>, a fraction of the gas generated consists of NO and NO<sub>2</sub>, which can pose a safety hazard to miners prior to explosive detonation, particularly when used in confined underground mines. It has been shown that the reaction between nitrosyl thiocyanate and ammonia is the primary pathway for nitrogen formation during explosive sensitisation<sup>8</sup>, and it is of interest to determine whether this species also contributes to the formation of unwanted nitric oxide under the conditions relevant to explosive sensitisation.

Pure nitrosyl thiocyanate is known to be highly unstable, decomposing readily even at temperatures approaching -60 °C to form nitric oxide and thiocyanogen<sup>9</sup>.



Dilute aqueous solutions of ONSCN are relatively stable, however, the red colour of the solutions fades over time with evolution of nitric oxide<sup>10</sup>. Despite its widespread applications as a catalyst for nitrosation reactions, the kinetics and mechanism of ONSCN decomposition have not been studied in detail. Thus, it is of interest to determine the kinetics and mechanism of ONSCN decomposition, allowing an

assessment of the contribution of ONSCN to the formation of  $\text{NO}_x$  during explosive sensitisation. In addition to its industrial applicability, ONSCN has the potential to function as a source of nitric oxide in living systems. Knowledge of the mechanism and rate of ONSCN decomposition will enable an assessment of its contribution to NO formation in biological systems. Further to its role as a catalyst for nitrosation reactions, ONSCN has been detected during the oxidation of thiocyanate ions by nitric acid,<sup>11, 12</sup> however, the role of ONSCN in the reaction mechanism is unclear. Knowledge of the rate and mechanism of ONSCN decomposition will also assist in elucidating this reaction pathway.

## 5.2 Experimental

### 5.2.1 Reagents and solutions

Sodium nitrite (>99.5%), sodium thiocyanate (>98%) and sodium perchlorate (ACS reagent, 98%) were obtained from Sigma Aldrich, whilst perchloric acid (analytical reagent grade) was purchased from Ajax. Reactant solutions were prepared by dissolving a known mass of solid in distilled deionised water. In the case of NaSCN, the solid was dried in an oven at 150 °C to constant weight before use<sup>13</sup>. Sodium perchlorate was stored in a desiccator to prevent moisture absorption. Solutions of perchloric acid of the desired concentration were produced by diluting 70% HClO<sub>4</sub> in distilled deionised water and were standardised by titrating against Na<sub>2</sub>CO<sub>3</sub>. The ionic strength of all reactant solutions was adjusted to 1 mol L<sup>-1</sup> using NaClO<sub>4</sub>, except for the initial rates study in which the ionic strength was 2 mol L<sup>-1</sup>.

Nitric oxide (NO) solutions were prepared by first degassing the target solution with N<sub>2</sub> to remove oxygen, prior to bubbling with NO generated via the reduction of nitrous acid by ascorbate<sup>14</sup>. Dissolved NO concentrations were determined by UV absorbance (as nitrite) subsequent to reaction of a small aliquot of NO solution with water containing dissolved oxygen. Results coincided with literature values<sup>15</sup> for NO saturation in water ( $1.9 \times 10^{-3}$  mol L<sup>-1</sup> atm<sup>-1</sup>), and in 1 mol L<sup>-1</sup> NaClO<sub>4</sub> ( $1.2 \times 10^{-3}$  mol L<sup>-1</sup> atm<sup>-1</sup>). Further details of this procedure are contained in Appendix B.

### 5.2.2 Kinetics - Stopped flow UV-Vis

An RX-2000 rapid mixing accessory from Applied Photophysics was coupled to a Varian Cary50 UV-Visible spectrometer, to study the decomposition kinetics of ONSCN. A constant-temperature circulating bath supplied the water to surround the drive syringes of the RX-2000 and maintain them at a preset temperature. A thermostatted cell holder, regulated by a Varian Cary single cell Peltier temperature controller, housed the observation cell. All experiments were performed at 298 K. De-oxygenation of reactant solutions was achieved by bubbling with nitrogen gas for at least 15 min, with longer degassing times yielding identical results. Prior to each experiment, the stopped flow apparatus was flushed with de-oxygenated water and a baseline absorbance reading acquired and stored in the Varian software to be automatically subtracted from subsequent measurements. ONSCN was produced in situ, by reacting a solution containing both  $\text{NaNO}_2$  and  $\text{NaSCN}$  with a solution of perchloric acid. The absorbance at 460 nm ( $\epsilon_{460} = 100 \text{ L mol}^{-1} \text{ cm}^{-1}$ ) served to determine the concentration of ONSCN.

### 5.2.3 Analysis of gaseous products – FTIR and MIMS

Fourier transform infrared spectroscopy (FTIR) of product gases was performed on a Varian IR-600 with  $0.5 \text{ cm}^{-1}$  resolution and 10 m path length cell (Infrared Analysis Inc.). Gas samples were generated in a sealed 50 mL glass reactor initially containing a deoxygenated solution of  $\text{SCN}^-$  and  $\text{NO}_2^-$  at  $\text{pH} > 7$ . Reaction was initiated by addition of a small volume of  $2 \text{ mol L}^{-1} \text{ HClO}_4$  through a septum side port in the reactor, forming ONSCN in-situ. The product gases were purged from the reactor with high purity

nitrogen gas, dried by passage over a column of silica gel and collected in a 3 L gas transfer bag for analysis. Separate experiments established that silica gel did not adsorb NO. Prior to recording a background spectrum, the gas cell was subjected to three cycles of evacuation and filling with high purity nitrogen. The cell was then loaded with the sample for scanning, with the background automatically subtracted from the sample spectrum by the Varian software. Gases were quantified using the QASoft program (Infrared Analysis Inc.) which applies a region integration and subtraction (RIAS) method to determine the concentrations based on standard spectra from the QASoft database.

The membrane inlet mass spectroscopy (MIMS)<sup>16</sup> experiments employed a Pfeifer Thermostar quadrupole mass spectrometer to detect the gases diffusing from the aqueous solution. A 1 cm length of semi-permeable silastic tubing housed the end of the MS capillary, allowing direct measurement of dissolved gases. In these experiments, the solution was degassed with high purity argon to remove oxygen and nitrogen present from air. The purge gas was turned off at the start of the experiment.

#### **5.2.4 Analysis of aqueous products**

Analysis of ionic products was performed on a Dionex DX-100 ion chromatograph with an eluent containing 8 mmol L<sup>-1</sup> Na<sub>2</sub>CO<sub>3</sub> and 1 mmol L<sup>-1</sup> NaHCO<sub>3</sub>, an Ionpac AS14A analytical column and AG14A guard column, with suppressed conductivity detection. The same reactor set up was employed for these experiments as was used for generating gases for the FTIR analysis. In these experiments, HCl functioned to acidify the solution rather than HClO<sub>4</sub> due to the incompatibility of ClO<sub>4</sub><sup>-</sup> with the IC column.



Samples were drawn from the reactor using a gas tight syringe via a septum side port and quenched with 0.1 mol L<sup>-1</sup> NaOH to cease the reaction, before being diluted between 20 and 50 times for analysis. Concentrations of NO<sub>2</sub><sup>-</sup>, NO<sub>3</sub><sup>-</sup> and SO<sub>4</sub><sup>2-</sup> were determined by comparing the peak area and retention time of the sample solution to a calibration plot generated using known standards. A Nico2000 cyanide ion selective electrode and double junction reference electrode, connected to a Hanna 213 pH/mV meter via a Nico2000 dual electrode head, determined the cyanide ion concentration after the sample was diluted in 0.1 mol L<sup>-1</sup> NaOH. The electrode system was calibrated with cyanide solutions prepared by dissolving solid NaCN in 0.1 mol L<sup>-1</sup> NaOH and diluting to the appropriate concentration.

### 5.2.5 Data analysis

We fitted the measurements for the first 5 min of experiments to potential reaction mechanisms using the DynaFit program<sup>17</sup>. The mechanism was written into a Dynafit script file, and rate constants included for all known reactions. In the case of protonation equilibria, we followed the same approach as da Silva et al.<sup>8</sup> whereby the association reaction between the hydrogen ion and a negatively charged base (i.e. reaction between NO<sub>2</sub><sup>-</sup> and H<sup>+</sup>) was assumed to occur with a rate of 10<sup>10</sup> L mol<sup>-1</sup> s<sup>-1</sup>, with the dissociation reaction rate constant determined from the equilibrium constant. The DynaFit program automatically generates a system of first order ordinary differential equations describing the reaction mechanism, and fits the rate constants in these equations to minimize the error between the model and the experimental data using a Levenberg–Marquardt algorithm. For each potential mechanism, several initial guesses were trialled to ensure the convergence of the program to a global minimum.

Under the experimental conditions of this study, conversion of  $\text{HNO}_2$  to  $\text{ONSCN}$  is incomplete, and absorbance readings must be corrected for this when determining the overall rate of nitrous acid consumption (or  $\text{NO}$  generation). Equation 6 relates the concentration of  $\text{ONSCN}$  to the total nitrous acid concentration:

$$[\text{ONSCN}] = \frac{K_{\text{ONSCN}}[\text{SCN}^-][\text{H}^+]}{1 + K_{\text{ONSCN}}[\text{SCN}^-][\text{H}^+]}[\text{HNO}_2]_{\text{Total}} \quad (6)$$

Under the conditions of the present study, with high  $\text{H}^+$  and relatively low nitrous acid concentrations, the concentrations of nitrite ion and dinitrogen trioxide are negligible, and the total nitrous acid concentration is defined according to (7).

$$[\text{HNO}_2]_{\text{Total}} = [\text{HNO}_2] + [\text{ONSCN}] \quad (7)$$

## 5.3 Results

### 5.3.1 Equilibrium constant for the formation of ONSCN

Applying the molar absorptivity of  $100 \text{ L mol}^{-1} \text{ cm}^{-1}$  for ONSCN reported by Stedman and Whincup<sup>18</sup>, we determined the equilibrium constant for the formation of nitrosyl thiocyanate at an ionic strength of  $1 \text{ mol L}^{-1}$  as  $22.1 \pm 0.7 \text{ L}^2 \text{ mol}^{-2}$ . This value agrees with those of Jones et al.<sup>11</sup> ( $K_{\text{ONSCN}} = 22 \text{ L}^2 \text{ mol}^{-2}$ ) and Bazsa and Epstein<sup>12</sup> ( $K_{\text{ONSCN}} = 20.4 \text{ L}^2 \text{ mol}^{-2}$ ), measured in  $1 \text{ mol L}^{-1}$  perchloric and nitric acids, respectively. Note that  $K_{\text{ONSCN}}$  constitutes an apparent equilibrium constant as it involves no correction for the effect of non-unity activity coefficients. The apparent molar absorptivity of nitrosyl thiocyanate increases at high thiocyanate ion concentrations. Doherty et al. investigated this increase in absorbance and found it to be consistent with formation of an adduct between  $\text{SCN}^-$  and ONSCN.



The absorbance of  $\text{ON}(\text{SCN})_2^-$  must be taken into account when determining the concentration of ONSCN, especially at higher  $\text{SCN}^-$  concentrations where reliance on the  $100 \text{ L mol}^{-1} \text{ cm}^{-1}$  extinction coefficient would result in considerable error. Appendix B provides further details of these experiments.

### 5.3.2 Reaction products

The decomposition of pure nitrosyl thiocyanate produces NO and (SCN)<sub>2</sub><sup>9</sup>. Aqueous solutions of (SCN)<sub>2</sub> are unstable<sup>19</sup>, decaying to form SCN<sup>-</sup>, SO<sub>4</sub><sup>2-</sup> and HCN (Reaction 9). Therefore, if ONSCN decomposition in aqueous solution proceeds with the stoichiometry of Reaction 5, the overall stoichiometry of ONSCN disappearance corresponds to that of Reaction 10. We therefore attempted to analyse both the aqueous and gaseous reaction products to determine if this is indeed the correct stoichiometry.



#### Analysis of gaseous reaction products using FTIR and MIMS:

As quantified by FTIR, nitric oxide accounted for 87% (245 ppm) of the detected gases. A considerable amount of NO<sub>2</sub> also formed, corresponding to 10% (27 ppm) of the products as a result of NO oxidation by a small volume of air contaminating the sample bag. Thus, in complete absence of oxygen, NO would constitute 97 % of the gaseous reaction products.

Unexpectedly, we observed a small amount of N<sub>2</sub>O, corresponding to 2.5% (7 ppm) of the gaseous products. This result indicates a side reaction leading to N<sub>2</sub>O rather than NO, as outlined in the Discussion. A small amount of CO<sub>2</sub> also appeared in the analysed mixture, corresponding to less than 1 % (1.5 ppm) of the gases detected. The

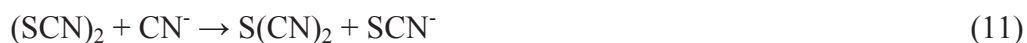
very low concentration of  $\text{CO}_2$  made it impossible to determine whether  $\text{CO}_2$  arises in a side reaction, or whether it results from the liberation of dissolved  $\text{CO}_2/\text{HCO}_3^-$  upon acidification of the reactant solution. The yields of  $\text{CO}_2$  and  $\text{N}_2\text{O}$  are sufficiently small that the reactions generating these species have a negligible impact on the overall kinetics of ONSCN decomposition.

The gases were also analysed by MIMS to determine if any  $\text{N}_2$  formed as a product of ONSCN decomposition. The reaction solution was degassed with argon prior to generation of ONSCN via the addition of a small volume of  $\text{HClO}_4$  to a sealed reactor housing the MIMS probe. The results showed a rapid increase in the ion current at  $m/z = 30$  corresponding to the production of  $\text{NO}$ . The signal at  $m/z = 28$  remained constant throughout the experiment, indicating that no  $\text{N}_2$  formed as a result of ONSCN decomposition.

#### Analysis of aqueous products:

Ion chromatography afforded the analysis of the ionic products, with the exception of  $\text{CN}^-$ , as quantified with an ion selective electrode. The nitrite concentration decreased with increasing decomposition time, owing to the decomposition of ONSCN. Nitrate was detected at concentrations corresponding to less than 1 % of the initial nitrite added, with the nitrate concentration initially increasing with time before decreasing slowly. This small amount of nitrate formed from the decomposition of nitrous acid. This process is reversible under the experimental conditions and explains why the concentration of nitrate displays non-monotonic concentrations during experiments<sup>20</sup>.

The concentration of sulfate increased with time, with the final yield enclosed between 75 and 90 % of the stoichiometric conversion according to Reaction 10, for acid concentrations ranging from 0.18 to 0.33 mol L<sup>-1</sup>. Under the same conditions, the final concentration of cyanide varied from 35 to 50 % of that expected for complete conversion according to Reaction 10. The results appear very similar to those of a prior study on the oxidation of SCN<sup>-</sup> by HNO<sub>3</sub>, which also proceeds via an (SCN)<sub>2</sub> intermediate.<sup>21</sup> In that study, Stedman and Wincup reported lower than expected yields of sulfate and HCN, findings consistent with a competing reaction between (SCN)<sub>2</sub> and CN<sup>-</sup> forming sulfur dicyanide, S(CN)<sub>2</sub>. More recently, sulfite and cyanate have been reported as products of the decomposition of (SCN)<sub>2</sub> at pH 4-7 which may account for the incomplete yields of sulphate and HCN<sup>22</sup>.

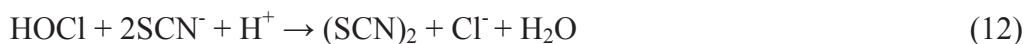


During the initial stages of reaction, when the concentration of HCN is low, the formation of HCN and sulfate advances in accordance with Reactions 9 and 10, which strongly suggests the intermediacy of (SCN)<sub>2</sub>.

### 5.3.3 Spectrum of intermediate species

The formation of sulfate and cyanide ions suggests that ONSCN decomposition proceeds through an (SCN)<sub>2</sub> intermediate. (SCN)<sub>2</sub> has been identified as a product of the oxidation of SCN<sup>-</sup> by a variety of oxidizing species, including H<sub>2</sub>O<sub>2</sub>,<sup>23</sup> HNO<sub>3</sub>,<sup>21</sup> ClO<sub>2</sub><sup>24</sup> and HOCl<sup>25</sup>, and has a UV spectrum with an absorption maximum near 290 nm. By following the procedure outlined by Barnett et al. (2004)<sup>19</sup>, we recorded the

spectrum of (SCN)<sub>2</sub> to confirm that it did not extend into the visible region where it might interfere with the absorbance of ONSCN, and to aid in identifying (SCN)<sub>2</sub> as a reaction intermediate. This involved the oxidation of a NaSCN solution by acidified NaOCl to generate (SCN)<sub>2</sub> as shown below:



The reaction was performed with 1 mol L<sup>-1</sup> HClO<sub>4</sub>, 0.9 mmol L<sup>-1</sup> NaOCl and SCN<sup>-</sup> concentrations of 0.1 and 0.2 mol L<sup>-1</sup>, conditions leading to reasonably stable solutions of (SCN)<sub>2</sub> and reliable measurements of its spectrum. Figure 1 confirms a negligible absorbance of (SCN)<sub>2</sub> above 420 nm that does not interfere with the measurements acquired at 460 nm, the absorbance maximum of ONSCN.

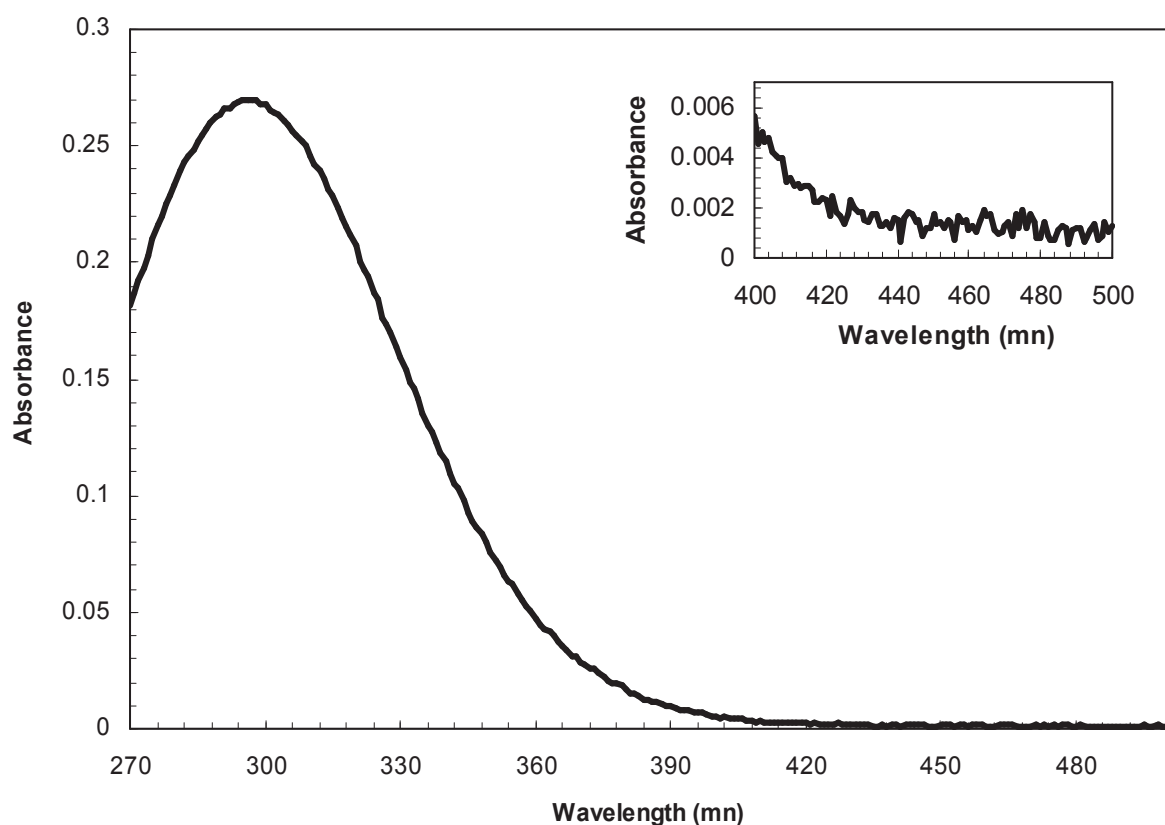


***Figure 1: Spectrum of  $(\text{SCN})_2$  generated from  $0.1 \text{ mol L}^{-1} \text{ SCN}^-$ ,  $1 \text{ mol L}^{-1} \text{ HClO}_4$  and  $0.9 \text{ mmol L}^{-1} \text{ NaClO}$ . The spectrum shown was calculated by subtracting the spectrum after 1 h (at which time  $(\text{SCN})_2$  had been almost completely hydrolysed) from the initial spectrum.***

Non-uniform changes to the spectra of decomposing ONSCN solutions indicated the formation of a UV absorbing species not present at the start of the experiments. To isolate the spectrum of the intermediate, we subtracted the spectrum of  $\text{SCN}^-$  and assumed that species in equilibrium with nitrous acid (e.g.  $\text{HNO}_2$ ,  $\text{ONSCN}$  and  $\text{ON}(\text{SCN})_2^-$ ) accounted exclusively for the initial absorbance. In the absence of additional absorbing species, the decomposition of ONSCN should therefore result in a consistent decrease in absorbance across all wavelengths. This was the case only for wavelengths above 400 nm, with absorbance at lower wavelengths decreasing at a



slower rate. Assuming that ONSCN was solely responsible for the absorption at 460 nm, the additional absorbance caused by the reaction intermediate at other wavelengths was calculated and compared to that of  $(\text{SCN})_2$  in Figure 2, after scaling the spectrum to a common absorbance. The spectrum of the intermediate concurs with the spectrum of  $(\text{SCN})_2$  generated in the independent experiment, indicating that  $(\text{SCN})_2$  indeed represents the observed intermediate. The absorbance of the intermediate below 310 nm exceeds that of  $(\text{SCN})_2$ , suggesting the presence of an additional species absorbing in this region. However, the data at these wavelengths display considerable scatter, induced by high absorbance of ONSCN, which confined the measurements to wavelengths longer than 300 nm.

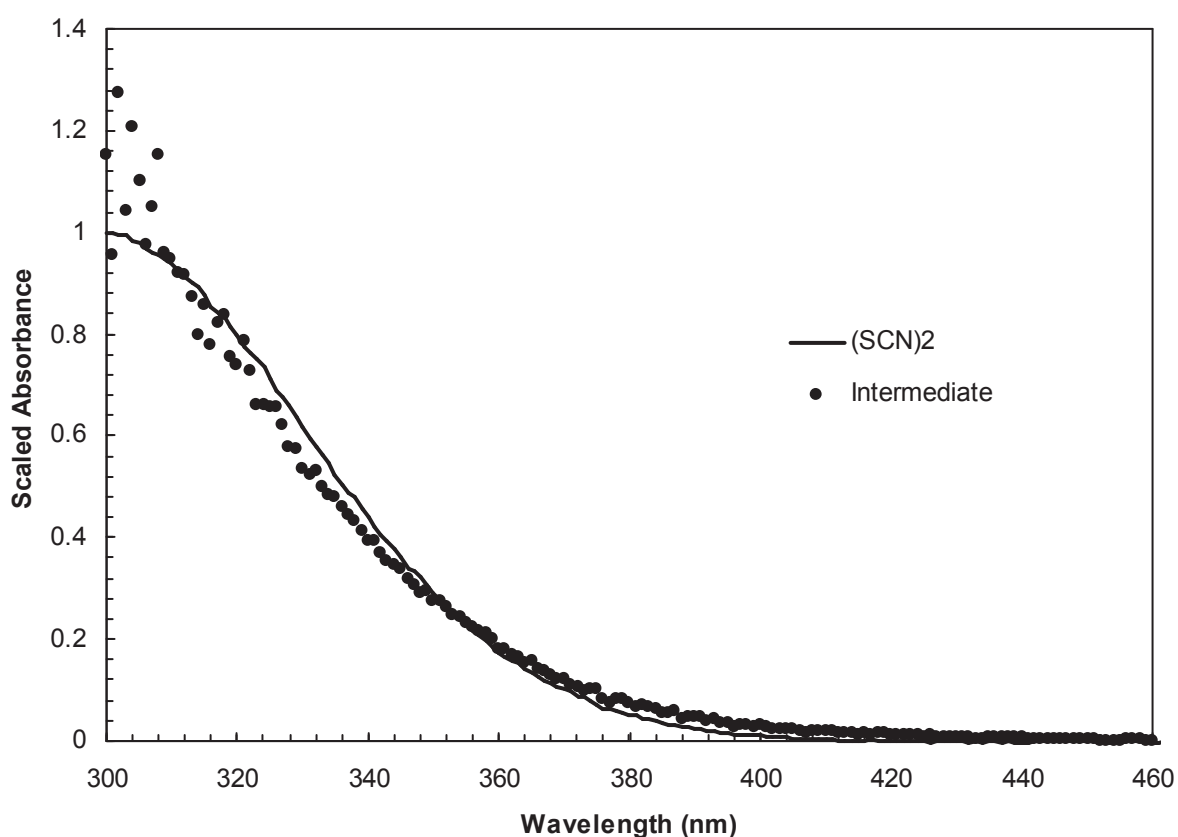


**Figure 2:** Comparison of spectrum of intermediate species and  $(\text{SCN})_2$ ; intermediate spectrum from experiment with  $3 \text{ mmol L}^{-1} \text{ NaNO}_2$ ,  $0.2 \text{ mol L}^{-1} \text{ HClO}_4$ ,  $0.2 \text{ mol L}^{-1} \text{ NaSCN}$ .

### 5.3.4 Effect of initial dissolved oxygen on reaction kinetics

Initial kinetic experiments with solutions that had not been degassed exhibited an induction period of slow decomposition during the early stages. Bubbling nitrogen gas through the reactant solutions for 15 min prior to starting the reaction removed the induction period, as demonstrated in Figure 3. The induction period arises as a consequence of dissolved oxygen, initially present in the solutions from the atmosphere, reacting with nitric oxide to form NO<sub>2</sub>. NO<sub>2</sub> combines with NO and water to regenerate nitrous acid, and as nitrous acid exists in equilibrium with ONSCN, the concentration of ONSCN remains unchanged, as illustrated in Scheme 1:

***Scheme 1: Regeneration of ONSCN via oxidation of NO by O<sub>2</sub>***



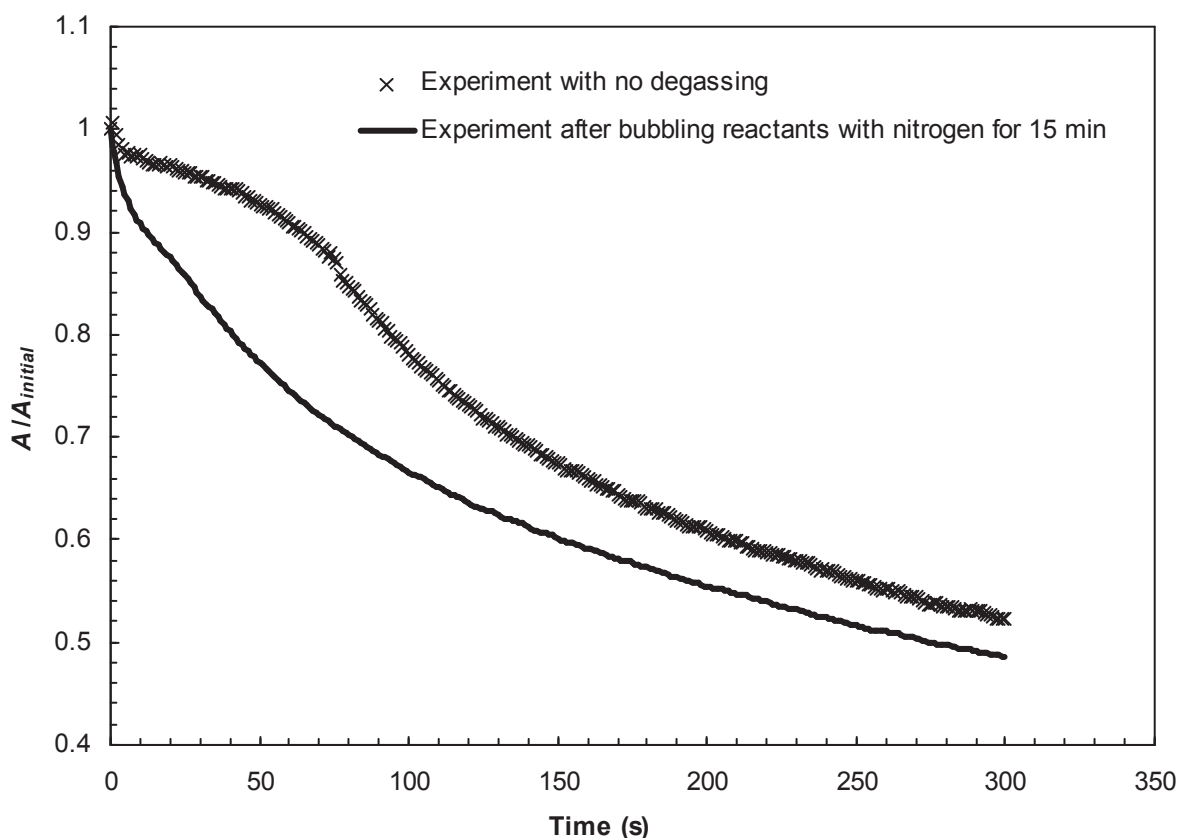


**Figure 3: Effect of oxygen on ONSCN decomposition,  $\lambda = 460$  nm. Both experiments started with  $1 \text{ mmol L}^{-1} \text{ NaNO}_2$ ,  $1 \text{ mol L}^{-1} \text{ HClO}_4$  and  $0.1 \text{ mol L}^{-1} \text{ NaSCN}$ .**

Therefore, to avoid complications owing to dissolved oxygen, we degassed all reactant solutions by bubbling high purity nitrogen for at least 15 min. This was sufficient to remove the induction period, however, some experiments showed a miniscule but noticeable rise in the curve suggesting a residual contamination of the solutions by a minute amount of oxygen. This rise, which was not reproducible and was not removed by degassing for longer time periods, arises because of diffusion of a small amount of  $\text{O}_2$  through the fluorinated ethylene propylene (FEP) tubing in the stopped flow device. This phenomenon appears to have no effect on the overall kinetics and was neglected in the kinetic analysis.

### 5.3.5 Kinetics: Initial rates and effect of thiocyanate ion concentration

ONSCN was generated in-situ via the reaction of  $\text{HClO}_4$ ,  $\text{SCN}^-$  and  $\text{NO}_2^-$  ions. To assist in the development of the mechanism, the initial rates of ONSCN decomposition were studied as a function of the concentrations of nitrous acid and thiocyanate ions. A number of issues complicated this part of the investigation, limiting the quality and usefulness of the initial rates measurements to identifying the early decomposition mechanism and the inhibitory effect of NO on the reaction (described in Section 6). For this reason, the measurements of initial rates did not serve to fit the kinetic parameters of the model. The first problem involved the absorbance increasing slightly over the first 200 ms of reaction, as opposed to an expected decrease. This increase was not reproducible, suggesting inefficient mixing in the hand-driven stopped flow device. The second problem comprised the rate remaining constant only for a very short period of time ( $< 1$  s) before commencing to decrease rapidly, leading to a small change in absorbance. The resulting initial rate measurements displayed a significant uncertainty, owing to the large noise in the measurements relative to the change in absorbance, and to the irreproducible nature of the early increase in absorbance.

In the first set of experiments (see Appendix B), the nitrous acid concentration was varied from 1 to 4  $\text{mmol L}^{-1}$  in increments of 1  $\text{mmol L}^{-1}$ , with concentrations of 1 and 0.1  $\text{mol L}^{-1}$   $\text{HClO}_4$  and NaSCN, respectively. Under these conditions, with a large excess of  $\text{SCN}^-$  and  $\text{H}^+$ , the concentration of ONSCN becomes directly proportional to the concentration of nitrous acid. Using higher concentrations of nitrous acid engendered interference from the decomposition of nitrous acid, which is initially very rapid. Plotting the log of the initial rate versus the log of the  $\text{HNO}_2$  concentration indicated a reaction order with respect to nitrous acid of  $1.07 \pm 0.09$ . In the second

series of experiments, the concentration of  $\text{SCN}^-$  was varied from 0.1 to 0.25 mol L<sup>-1</sup> in increments of 0.05 mol L<sup>-1</sup>, with constant concentrations of  $\text{HNO}_2$  and  $\text{HClO}_4$  of 2 mmol L<sup>-1</sup> and 1 mol L<sup>-1</sup> respectively. Under these conditions, the fraction of initial nitrous acid converted into ONSCN ranges from 0.77 to 0.9. The order with respect to  $\text{SCN}^-$  amounted to 1.2, however, the slight elevation in ONSCN concentration with increasing  $\text{SCN}^-$  concentration induced a portion of the rate increase. The initial rate was corrected for the effect of the increased ONSCN concentration, assuming that the initial rate was first order in ONSCN, resulting in an order in  $\text{SCN}^-$  of  $1.06 \pm 0.16$ . Thus, a process first order in nitrous acid and first order in  $\text{SCN}^-$  dominates the initial rate of decomposition of ONSCN, as described by Equation 13, assuming that ONSCN accounts for the term first order in nitrous acid, where  $k = 0.28 \text{ L mol}^{-1} \text{ s}^{-1}$  gives the best fit to the measurements.

$$-\frac{d[\text{HNO}_2]_{\text{Total}}}{dt} = k[\text{ONSCN}][\text{SCN}^-] \quad (13)$$

### 5.3.6 Kinetics: Effect of nitric oxide

The rate of ONSCN decomposition decreases rapidly with time, despite only relatively small changes in ONSCN concentration. This decrease resulted from the inhibition of the reaction by one of the reaction products, either  $(\text{SCN})_2$  or NO. It was impossible to test directly for inhibition of ONSCN decomposition by  $(\text{SCN})_2$ , owing to the instability of  $(\text{SCN})_2$  in aqueous solution. However, we readily generated stable NO solutions by passing NO gas through the solution of interest and ensuring that oxygen was strictly excluded during generation and transfer of the solution. Our approach involved

examining the effect of NO on the decomposition of ONSCN, by first saturating the reactant solution containing  $\text{SCN}^-$  and  $\text{NO}_2^-$  with NO before reacting it with  $\text{HClO}_4$  in the stopped flow apparatus. Figure 4 illustrates the results of a typical experiment, confirming that the solution initially saturated with NO exhibits significantly slower decomposition of ONSCN. Whereas the solution without NO exhibited a rapid decrease in the rate over time, the solution with NO decomposed at a much steadier and considerably slower rate. This result appears qualitatively very similar to decomposition of nitrosothiourea<sup>26, 27</sup>, which is also inhibited by NO.

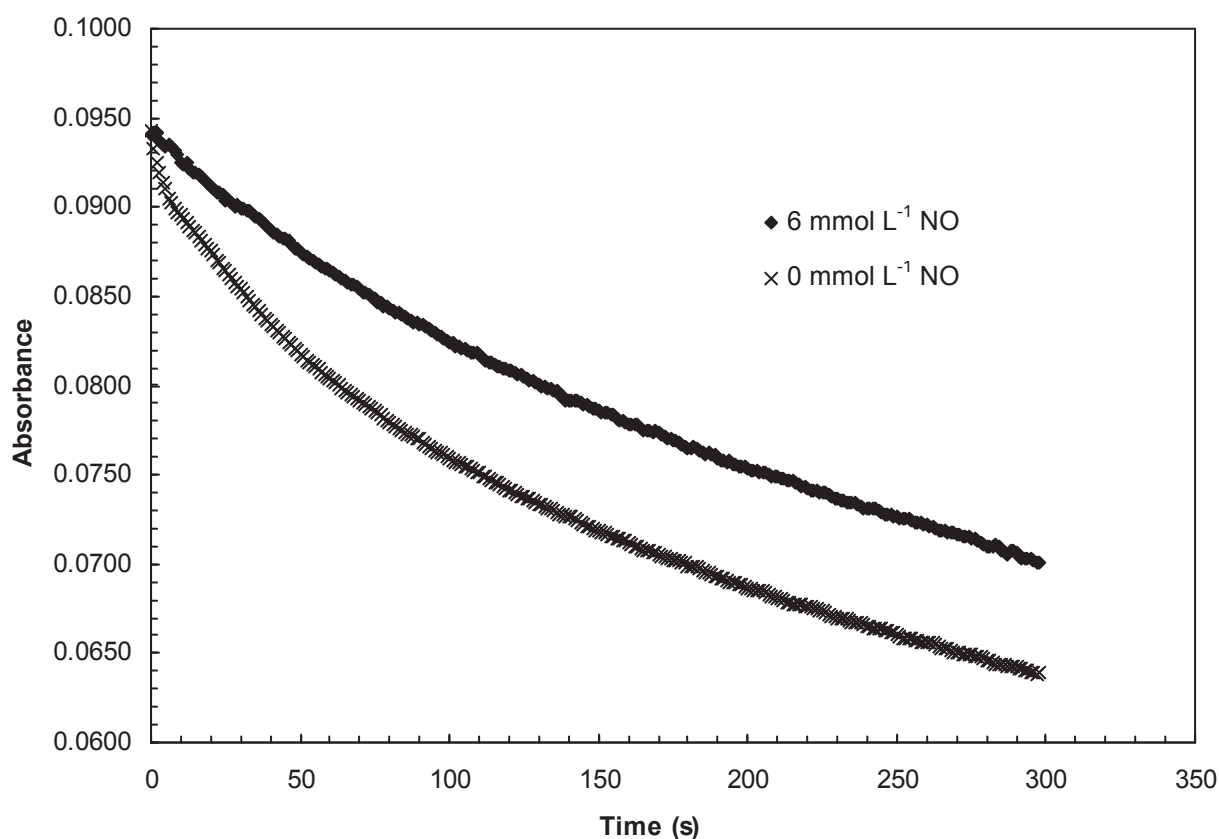


**Figure 4: Effect of nitric oxide on ONSCN decomposition,  $\lambda = 460 \text{ nm}$ . Both experiments contain  $3 \text{ mmol L}^{-1} \text{ NaNO}_2$ ,  $0.2 \text{ mol L}^{-1} \text{ HClO}_4$ ,  $0.1 \text{ mol L}^{-1} \text{ NaSCN}$ .**

The fact that NO suppresses the initially rapid decomposition of ONSCN, yet the slope decreases at a steady rate suggests a combination of reversible and irreversible reaction

steps in the mechanism. The presence of NO suppresses the reversible step, responsible for the initial rapid decrease in ONSCN concentration, whilst similar slopes of both curves at 300 s indicate other pathways, or subsequent reaction steps that remain unaffected by NO. Figure 5 illustrates plots of  $1/[\text{HNO}_2]_{\text{Total}}$  versus  $t$ , with their linearity after the first 350 s revealing a second order reaction in total nitrous acid concentration, largely independent of NO concentration.

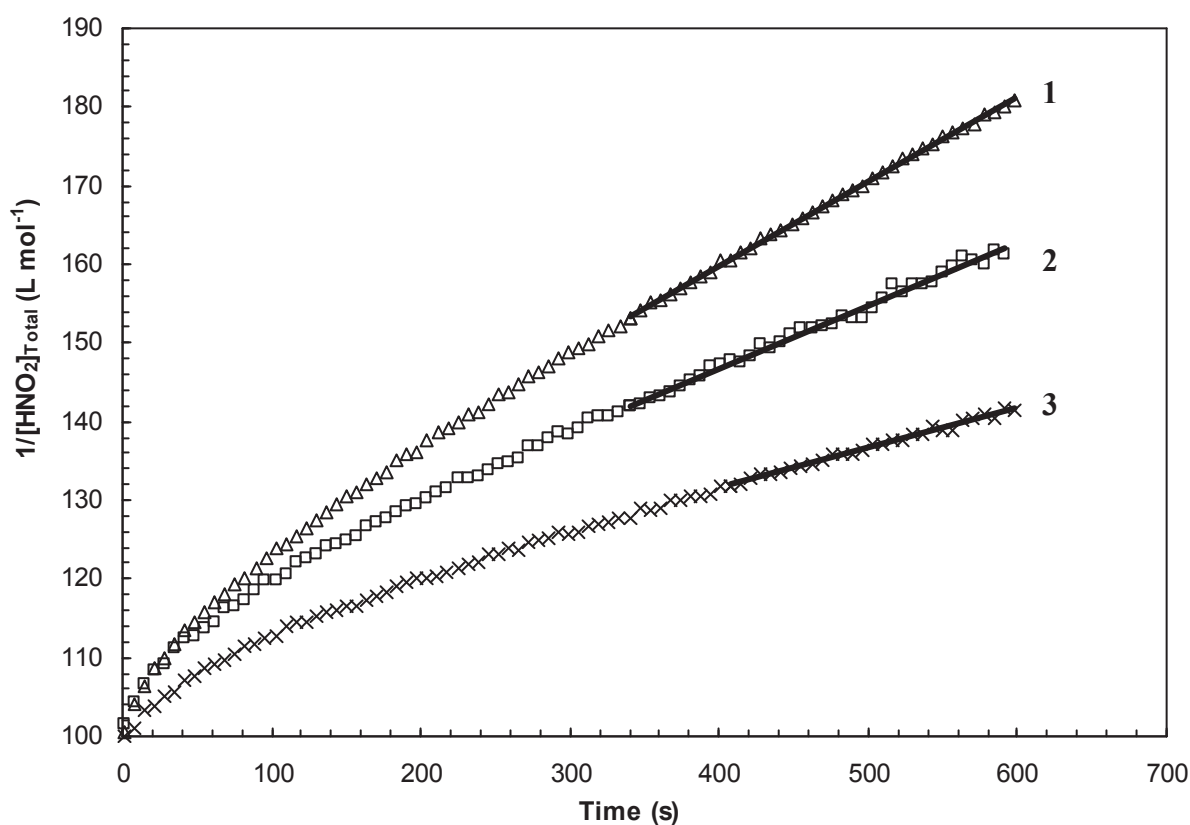


**Figure 5: Second order plots of ONSCN decomposition. All experiments contain initially  $0.01 \text{ mol L}^{-1} \text{ HNO}_2$  and  $0.05 \text{ mol L}^{-1} \text{ NaSCN}$ .  $\text{HClO}_4$  concentrations are 0.4, 0.3 and  $0.2 \text{ mol L}^{-1}$  for experiments 1, 2 and 3, respectively.**

### 5.3.7 Reaction mechanism – global kinetic fit

The initial rates study has identified the early decomposition of ONSCN to be first order in both ONSCN and  $\text{SCN}^-$  and has demonstrated the reaction to be inhibited by nitric oxide. As the starting rate remained valid only for the first second or so of reaction, we excluded the results of initial rates experiments when deriving the kinetic parameters. Potential models were fitted to a set of 20 experiments simultaneously, each executed for 300 s, with the experiments covering a reasonably wide range of  $\text{HNO}_2$ ,  $\text{SCN}^-$  and  $\text{H}^+$  concentrations including some with solutions initially saturated with nitric oxide. Thus,  $[\text{HNO}_2]_{\text{Total}}$  ranged from 2 to 10 mmol  $\text{L}^{-1}$ ,  $[\text{SCN}^-]$  from 0.05 to 0.5 mol  $\text{L}^{-1}$  and  $[\text{H}^+]$  from 0.02 to 0.5 mol  $\text{L}^{-1}$ . This approach allowed the inclusion of the decomposition of  $\text{HNO}_2$  in the model, by incorporating appropriate equations and rate constants from the literature (Table 1, Reactions 28-30). Table B3 in Appendix B provides the initial conditions of each experiment.

#### Kinetics at high $\text{SCN}^-$ concentration:

At thiocyanate concentrations of 200 mmol  $\text{L}^{-1}$  or higher, the kinetics of ONSCN decomposition comprises two parallel reaction pathways. Pathway 1, denoted as the thiocyanate dependent pathway, involves reaction between nitrosyl thiocyanate and thiocyanate ions producing nitric oxide and  $(\text{SCN})_2^-$  radicals (14), followed by rate limiting consumption of  $(\text{SCN})_2^-$  forming NO and thiocyanogen,  $(\text{SCN})_2$  (15). Pathway 2 consists of a second order reaction in nitrosyl thiocyanate, which produces two molecules of NO and one of thiocyanogen.



### Pathway 1



### Pathway 2



The principle of microscopic reversibility requires that  $K_{14}K_{15} = K_5$ . Simulations suggest both reactions 5 and 15 are irreversible, and as such, the principle is not violated. Provided that Reaction 14 governs the early rate, this mechanism is consistent with our initial rates study, which highlighted a reaction first order in both ONSCN and  $\text{SCN}^-$ . Reaction 14 might be expected to be rate limiting initially, when the concentration of NO remains low. Czapski et al.<sup>28</sup> studied the reverse of Reaction 14, the reaction between NO and  $(\text{SCN})_2^-$ , by monitoring the decay of  $(\text{SCN})_2^-$  produced via the pulse radiolysis of  $\text{SCN}^-$  solutions containing NO. They reported  $k_{-14}$  as  $4.3 \times 10^9 \text{ L mol}^{-1} \text{ s}^{-1}$ , and we have adopted this value in our simulations. We fitted the kinetic parameters of Reactions 5, 14 and 15 to the measurements at high  $[\text{SCN}^-]$ , in conjunction with relevant equations for formation of ONSCN, and for the protonation and decomposition of nitrous acid as outlined in Table 1. For values of  $10^5 < k_{15} < 10^8 \text{ L mol}^{-1} \text{ s}^{-1}$ , the simulations were insensitive to changes in  $k_{14}$  and  $k_{15}$  provided that the product  $K_{14}k_{15}$  remained constant. A value of  $K_{14}k_{15}$  of  $1.15 \times 10^{-2} \text{ L mol}^{-1} \text{ s}^{-1}$  in conjunction with  $k_{16} = 0.5 \text{ L mol}^{-1} \text{ s}^{-1}$  afforded a good match to the acquired

measurements. Figure 6 shows the best fit of Reactions 5, 14 and 15 to the results of selected experiments, characterised by initial concentrations of  $\text{SCN}^-$  in excess of 200  $\text{mmol L}^{-1}$ . Appendix B provides additional graphs for other high  $[\text{SCN}^-]$  experiments.

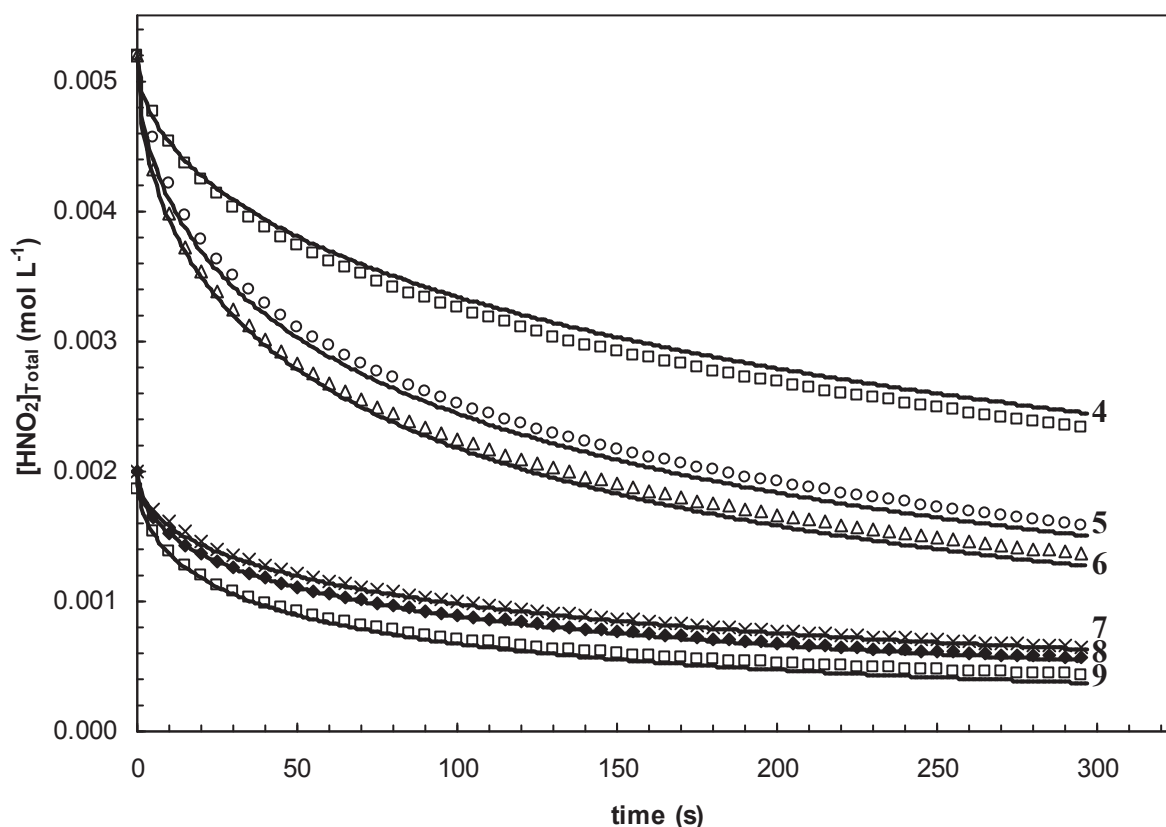


**Figure 6: Comparison of experimental data and kinetic model (Reactions 14-16) for selected experiments with high thiocyanate ion concentrations. Data points correspond to experimental measurements whilst solid curves correspond to the best fit of Pathways 1 and 2 to the dataset of 10 experiments with  $[\text{SCN}^-] \geq 0.2 \text{ mol L}^{-1}$ . Conditions are 4:  $[\text{SCN}^-] = 0.3 \text{ mol L}^{-1}$ ,  $[\text{H}^+] = 0.1 \text{ mol L}^{-1}$ , 5:  $[\text{SCN}^-] = 0.3 \text{ mol L}^{-1}$ ,  $[\text{H}^+] = 0.3 \text{ mol L}^{-1}$ , 6:  $[\text{SCN}^-] = 0.3 \text{ mol L}^{-1}$ ,  $[\text{H}^+] = 0.5 \text{ mol L}^{-1}$ , 7:  $[\text{SCN}^-] = 0.3 \text{ mol L}^{-1}$ ,  $[\text{H}^+] = 0.3 \text{ mol L}^{-1}$ , 8:  $[\text{SCN}^-] = 0.3 \text{ mol L}^{-1}$ ,  $[\text{H}^+] = 0.5 \text{ mol L}^{-1}$ , 9:  $[\text{SCN}^-] = 0.5 \text{ mol L}^{-1}$ ,  $[\text{H}^+] = 0.5 \text{ mol L}^{-1}$ .**

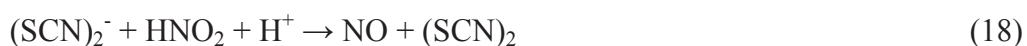
Kinetics at low SCN<sup>-</sup> concentrations:

At thiocyanate concentrations below 200 mmol L<sup>-1</sup>, the decomposition of ONSCN displayed faster kinetics than would be expected from Pathways 1 and 2, indicating the presence of an additional reaction pathway operating under these conditions. A variety of different reaction schemes were considered, with three potential mechanisms for ONSCN decomposition found to provide similarly good fits to the data. All three mechanisms contain Pathways 1 and 2 in conjunction with an additional reaction channel. These additional pathways include (i) the homolysis of ONSCN followed by rapid reaction of SCN radicals with SCN<sup>-</sup> forming (SCN)<sub>2</sub><sup>-</sup>, (ii) the nitrosation of (SCN)<sub>2</sub><sup>-</sup> by NO<sup>+</sup>/H<sub>2</sub>NO<sub>2</sub><sup>+</sup> forming NO and (SCN)<sub>2</sub> or (iii) the nitrosation of HOSCN (formed from (SCN)<sub>2</sub> hydrolysis) to produce ONOSCN, and subsequent decomposition of this species. These pathways are outlined below:

Pathway 3-(i)



Pathway 3-(ii)



Assuming that the rate limiting step in Pathways 3-(i) and 3-(ii) is the consumption of (SCN)<sub>2</sub><sup>-</sup>, the following simplified rate law can be derived for ONSCN decomposition, where  $k_a = k_{15}k_{16}/k_{-14}$  for pathway 3-(i) and  $k_{18}K_{14}/K_3$  for pathway 3-(ii) (derivation provided in Appendix B):

$$-\frac{d[HNO_2]_{Total}}{dt} = \frac{k_a[ONSCN]^2}{[NO]} + \frac{k_{15}K_{14}[SCN^-][ONSCN]^2}{[NO]} + k_5[ONSCN]^2 \quad (19)$$

SCN radicals are known to react at or near the diffusion controlled limit with  $SCN^-$  ions forming  $(SCN)_2^-$  radicals,<sup>29</sup> with an equilibrium constant of  $2 \times 10^5 \text{ L mol}^{-1}$ . Thus, in accordance with Hess' Law, the equilibrium constants for Reactions 14 and 16 must satisfy the relationship  $K_{14}/K_{16} = K_{17} = 2 \times 10^5 \text{ L mol}^{-1}$ . The best fit of Pathway 3-(i) (occurring in parallel with Pathways 1 and 2) to the data resulted in  $K_{14}/K_{16} = 10$ , a factor of  $10^4$  lower than required thermodynamically. Therefore, although this reaction model provides an excellent fit to the data, the required equilibrium parameters are not thermodynamically feasible and alternate mechanisms must be considered. As noted above, Pathway 3-(ii) simplifies to the same rate law as Pathway 3-(i), with the distinguishing feature of that mechanism being an acid catalysed reaction between  $(SCN)_2^-$  (generated via Reaction 14) and nitrous acid. Such a reaction would likely proceed via a  $H_2NO_2^+$  intermediate, making it possible to estimate an upper bound on this rate constant based on the observed rate of other acid catalysed nitrosation reactions involving negatively charged substrates. The rate constants of such reactions, including the nitrosation of  $SCN^-$  appear to approach a limiting value of  $12,000 \text{ L}^2 \text{ mol}^{-2} \text{ s}^{-1}$  with increasing substrate reactivity.<sup>7</sup> Hence, the rate of nitrosation of  $(SCN)_2^-$  is unlikely to exceed this value. The fact that similar rate constants are observed for a range of reactive substrates suggests that these reactions are encounter controlled, with  $H_2NO_2^+$  in equilibrium with  $HNO_2$  and  $H^+$ . In contrast, the minimum value of  $k_{18}$  required to fit the data for ONSCN decomposition at low  $SCN^-$  concentrations is  $6.5 \times 10^5 \text{ L}^2 \text{ mol}^{-2} \text{ s}^{-1}$ , which is significantly larger than that observed for other substrates. As a result,

Pathway 3-(ii), although providing a good fit to the data, is unlikely to represent the correct mechanism because the required rate constant for Reaction 18 is not feasible.

Pathway 3-(iii) involves formation of a previously unreported species, ONOSCN resulting from the nitrosation of HOSCN. HOSCN forms as a result of the hydrolysis of (SCN)<sub>2</sub> (Reaction 20)<sup>13</sup>, produced from Pathways 1-2. HOSCN can then either disproportionate via a second order reaction which results eventually in sulfate and cyanide (Reactions 24-26 in Table 1)<sup>19</sup>, or it can react with ONSCN, forming ONOSCN (Reaction 21). The decomposition of ONOSCN is proposed to form NO and OSCN radicals via Reaction 22. Two OSCN molecules then combine to form a dimer, which hydrolyses forming HOSCN and HO<sub>2</sub>SCN. This reaction scheme, combined with Pathways 1 and 2 operating in parallel, provides an excellent fit to the data over the complete range of reactant concentrations used in this study, as outlined in Figures 7-9. Table 1 summarizes the complete model and associated rate parameters.

#### Pathway 3-(iii)



**Table 1: Reaction mechanism for ONSCN decomposition**

Reaction	Equation Number	$k_f^*$	$k_b^*$	Source
$\text{HNO}_2 + \text{H}^+ + \text{NO}_2^- \rightleftharpoons \text{N}_2\text{O}_3 + \text{H}_2\text{O}$	1	$32,000 \text{ M}^{-2}\text{s}^{-1}$	$6400 \text{ s}^{-1}$	Ref. <sup>8</sup>
$\text{HNO}_2 + \text{H}^+ + \text{SCN}^- \rightleftharpoons \text{ONSCN} + \text{H}_2\text{O}$	3	$11900 \text{ M}^{-2}\text{s}^{-1}$	$530 \text{ s}^{-1}$	Ref. <sup>7</sup>
$2\text{ONSCN} \rightarrow 2\text{NO} + (\text{SCN})_2$	5	$0.57 \text{ M}^{-1}\text{s}^{-1}$	N/A	This study
$\text{SCN}^- + \text{ONSCN} \rightleftharpoons \text{NO}^+ + (\text{SCN})_2^-$	14	$2.3 \text{ M}^{-1}\text{s}^{-1}$	$4.3 \times 10^9 \text{ M}^{-1}\text{s}^{-1}$	This study, Ref <sup>28</sup>
$(\text{SCN})_2^- + \text{ONSCN} \rightarrow \text{NO} + (\text{SCN})_2 + \text{SCN}^-$	15	$1.9 \times 10^7 \text{ M}^{-1}\text{s}^{-1}$	N/A	This study, Ref <sup>28</sup>
$(\text{SCN})_2^- + \text{HNO}_2 + \text{H}^+ \rightarrow \text{NO} + (\text{SCN})_2 + \text{H}_2\text{O}$	18	$12,000 \text{ M}^{-2}\text{s}^{-1}$	N/A	This study
$(\text{SCN})_2 + \text{H}_2\text{O} \rightleftharpoons \text{HOSCN} + \text{SCN}^- + \text{H}^+$	20	$19.8 \text{ s}^{-1}$	$5140 \text{ M}^{-2}\text{s}^{-1}$	Ref. <sup>13</sup>
$\text{ONSCN} + \text{HOSCN} \rightleftharpoons \text{ONOSCN} + \text{H}^+ + \text{SCN}^-$	21	$260 \text{ M}^{-1}\text{s}^{-1}$	$980 \text{ M}^{-2}\text{s}^{-1}$	This study
$\text{ONOSCN} \rightleftharpoons \text{NO} + \text{OSCN}$	22	$1.3 \times 10^6 \text{ M}^{-1}\text{s}^{-1}$	$4.3 \times 10^9 \text{ M}^{-1}\text{s}^{-1}$	This study
$2\text{OSCN} + \text{H}_2\text{O} \rightarrow \text{HOSCN} + \text{HO}_2\text{SCN}$	23	$1.7 \times 10^7 \text{ M}^{-1}\text{s}^{-1}$	N/A	This study
$2\text{HOSCN} \rightarrow \text{HO}_2\text{SCN} + \text{SCN}^- + \text{H}^+$	24	$1600 \text{ M}^{-1}\text{s}^{-1}$	N/A	Ref. <sup>19**</sup>
$2\text{HO}_2\text{SCN} \rightarrow \text{HOSCN} + \text{HO}_3\text{SCN}$	25	$2 \times 10^8 \text{ M}^{-1}\text{s}^{-1}$	N/A	Ref. <sup>24</sup>
$\text{HO}_3\text{SCN} + \text{H}_2\text{O} \rightarrow \text{SO}_4^{2-} + \text{HCN} + 2\text{H}^+$	26	$5 \times 10^8 \text{ M}^{-1}\text{s}^{-1}$	N/A	Ref. <sup>24</sup>
$2(\text{SCN})_2^- \rightarrow (\text{SCN})_2 + 2\text{SCN}^-$	27	$1.3 \times 10^9 \text{ M}^{-1}\text{s}^{-1}$	N/A	Ref. <sup>30</sup>
$\text{NO}_2^- + \text{H}^+ \rightleftharpoons \text{HNO}_2$	28	$10^{10} \text{ M}^{-1}\text{s}^{-1}$	$6.76 \times 10^6 \text{ s}^{-1}$	Ref. <sup>8</sup>
$\text{N}_2\text{O}_3 \rightleftharpoons \text{NO} + \text{NO}_2$	29	$3941 \text{ s}^{-1}$	$1.0 \times 10^8 \text{ M}^{-1}\text{s}^{-1}$	Ref. <sup>31</sup> Ref. <sup>20***</sup>
$2\text{NO}_2 + \text{H}_2\text{O} \rightarrow \text{HNO}_2 + \text{NO}_3^- + \text{H}^+$	30	$8.4 \times 10^7 \text{ M}^{-1}\text{s}^{-1}$	$5 \times 10^{-3} \text{ M}^{-2}\text{s}^{-1}$	Ref. <sup>20</sup>
$(\text{SCN})_2^- + \text{NO}_2^- \rightarrow 2\text{SCN}^- + \text{NO}_2$	31	$2.2 \times 10^6 \text{ M}^{-1}\text{s}^{-1}$	N/A	Ref <sup>32</sup>

\* Units “M” denotes “mol L<sup>-1</sup>”

\*\* The value of  $K_{20}$  from Ref. <sup>13</sup> was used in conjunction with the value of  $K_{20}^2 k_{24}$  from Ref. <sup>19</sup> to determine  $k_{24}$ . The rate limiting step of  $(\text{SCN})_2/\text{HOSCN}$  decomposition may change at  $\text{pH} > 4$ , consult ref<sup>22</sup>

\*\*\* The value of  $k_{29}$  was determined from Ref. <sup>31</sup> in conjunction with the equilibrium constant for  $\text{N}_2\text{O}_3$  from Ref. <sup>8</sup>.  $k_{29}$  was taken as the average of values reported in Ref. <sup>31</sup> and Ref. <sup>20</sup>

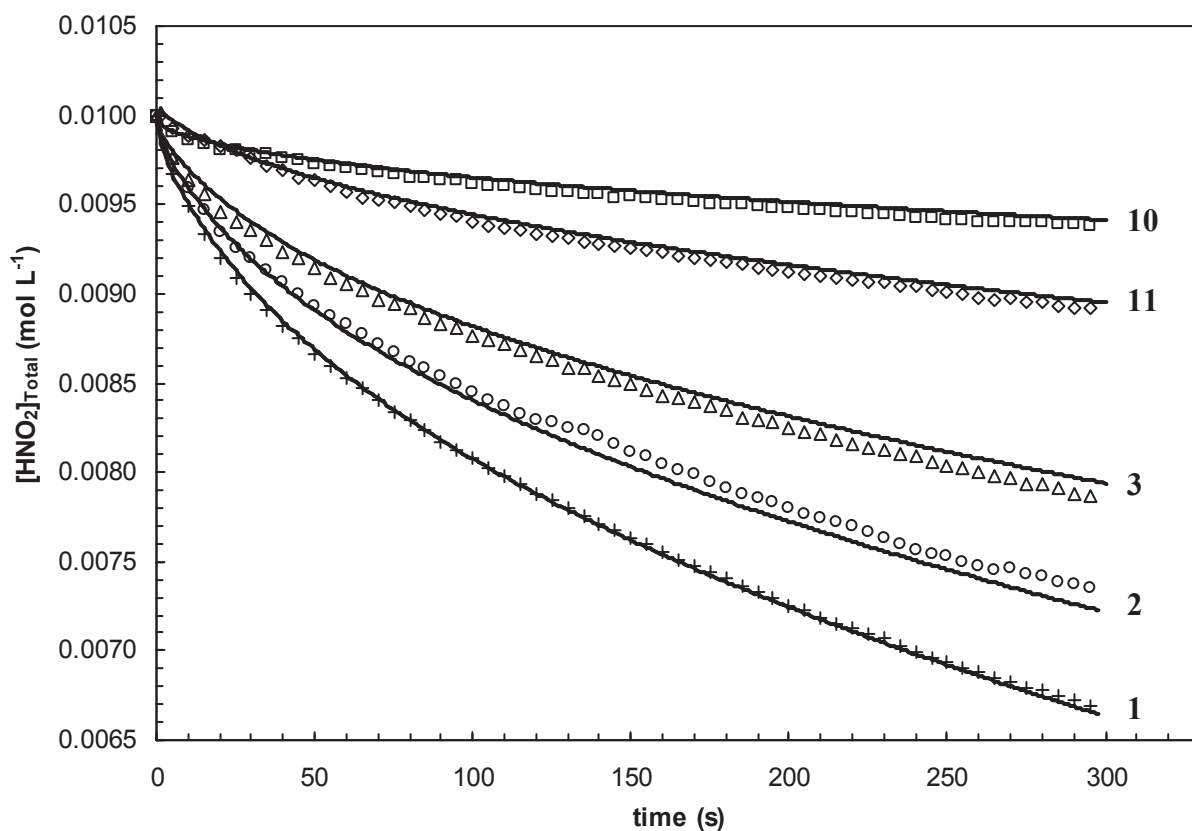


*Figure 7: Comparison of experimental and modelled decomposition of ONSCN for  $0.05 \text{ mmol L}^{-1} \text{ NaSCN}$ ,  $0.01 \text{ mol L}^{-1} \text{ NaNO}_2$  and increasing initial acid concentrations,  $0.05$ ,  $0.1$ ,  $0.2$ ,  $0.3$  and  $0.4 \text{ mol L}^{-1} \text{ HClO}_4$  for experiments 10, 11, 3, 2 and 1 respectively. Experiment numbers correspond to those tabulated in Appendix B.*

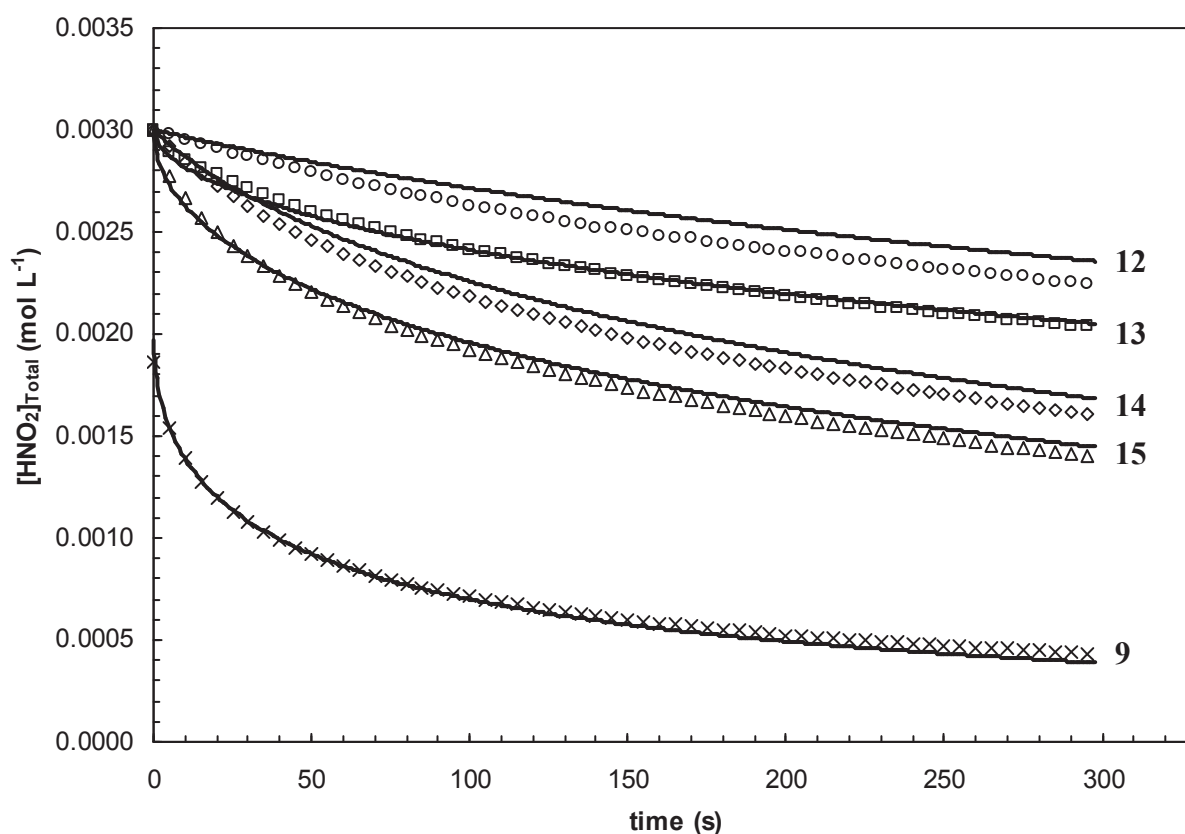


**Figure 8: Comparison of experimental and modelled decomposition of ONSCN at low  $\text{NaNO}_2$  concentrations. Concentrations are 9:  $[\text{SCN}^-] = 0.5 \text{ mol L}^{-1}$ ,  $[\text{H}^+] = 0.5 \text{ mol L}^{-1}$ , 12:  $[\text{SCN}^-] = 0.1 \text{ mol L}^{-1}$ ,  $[\text{H}^+] = 0.2 \text{ mol L}^{-1}$ ,  $[\text{NO}] = 0.62 \text{ mmol L}^{-1}$ , 13:  $[\text{SCN}^-] = 0.1 \text{ mol L}^{-1}$ ,  $[\text{H}^+] = 0.2 \text{ mol L}^{-1}$ , 14:  $[\text{SCN}^-] = 0.2 \text{ mol L}^{-1}$ ,  $[\text{H}^+] = 0.2 \text{ mol L}^{-1}$ ,  $[\text{NO}] = 0.62 \text{ mmol L}^{-1}$ , 15:  $[\text{SCN}^-] = 0.2 \text{ mol L}^{-1}$ ,  $[\text{H}^+] = 0.2 \text{ mol L}^{-1}$ .**



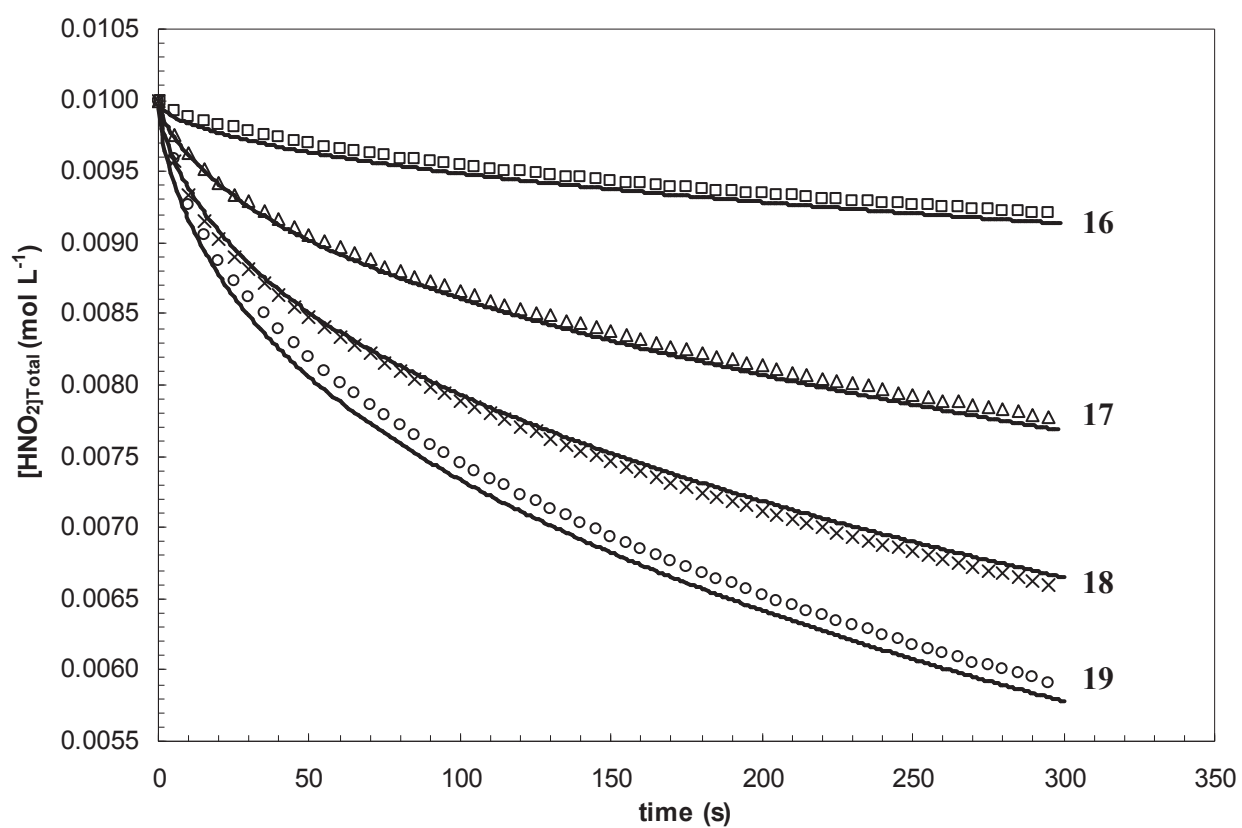


*Figure 9: Comparison of experimental and modelled decomposition of ONSCN for experiments 16:  $[H^+] = 0.02 \text{ mol L}^{-1}$ ,  $[SCN] = 0.2 \text{ mol L}^{-1}$ , and 17-19:  $[H^+] = 0.1 \text{ mol L}^{-1}$ ,  $[SCN] = 0.1, 0.15, 0.2 \text{ mol L}^{-1}$  respectively.*

## 5.4 Discussion

### Pathway 1 - Reactions 14 and 15

Pathway 1 involves a reaction between nitrosyl thiocyanate and thiocyanate ions generating  $(\text{SCN})_2^-$  radicals. This reaction is analogous to those reported for decomposition of other nitroso-species, including nitroso-thioureas<sup>27</sup> and nitrosyl iodide<sup>33</sup>, which feature a reaction between the nitroso compound and the relevant nucleophile. The fact that similar reactions operate for other nitroso species supports the proposed mechanism for ONSCN decomposition, and may indicate a general mechanism applicable for this class of compounds. With regard to the elementary mechanism of this reaction, our measurements and the results of studies published in the literature indicate that the reaction between ONSCN and  $\text{SCN}^-$  likely proceeds through an  $\text{ON}(\text{SCN})_2^-$  intermediate. A species of this stoichiometry formed as a result of pulse radiolysis of nitric oxide saturated thiocyanate solutions<sup>28</sup> (i.e. the reverse of Reaction 14). Doherty et al. proposed a species of the same stoichiometry, denoted  $\text{ON}(\text{SCN})_2^-$  to explain the visible spectrum of nitrosyl thiocyanate solutions containing very high thiocyanate ion concentrations<sup>10</sup>. These researchers claimed that this species differs from the species denoted  $\text{NO}(\text{SCN})_2^-$  observed in pulse radiolysis experiments, and that Czapski et al.<sup>28</sup> had observed a different form of ONSCN. This distinction results from the differences in the UV spectra of ONSCN and NOSCNCN, and the rapid rate of decay of  $\text{NO}(\text{SCN})_2^-$ , which, according to Doherty et al., would cause the species to “have completely decomposed long before our first measurements, even with stopped flow”. The latter point seems somewhat tenuous considering that Doherty et al. measured an equilibrium concentration of  $\text{ON}(\text{SCN})_2^-$ , thus despite having a rapid rate of decay,  $\text{ON}(\text{SCN})_2^-$  would still be observable provided the rate of its formation exhibited a

comparable magnitude to that of its consumption. The small equilibrium constant ( $\sim 0.036 \text{ L mol}^{-1}$ ) for formation of the  $\text{ON}(\text{SCN})_2^-$  adduct would mean that under the conditions of Czapski et al.'s experiments with  $0.1 \text{ mol L}^{-1} \text{ SCN}^-$ , the equilibrium concentration of  $\text{ON}(\text{SCN})_2^-$  would be very low and its absorbance indistinguishable from  $\text{ONSCN}$  considering their similar UV spectra. As such, one cannot conclude whether the species observed in these studies are indeed different. Provided that  $\text{ON}(\text{SCN})_2^-$  exists at equilibrium with  $\text{ONSCN}$  and  $\text{SCN}^-$ , the reaction proceeding via  $\text{ON}(\text{SCN})_2^-$  remains kinetically indistinguishable from that producing  $\text{NO}$  and  $(\text{SCN})_2^-$  from  $\text{ONSCN}$  and  $\text{SCN}^-$  in a single step. Doherty et al.<sup>10</sup> showed that  $\text{ON}(\text{SCN})_2^-$  formation reached equilibrium within the dead time of their stopped flow, thus, we have defined this rate constant in terms of  $\text{ONSCN}$  and  $\text{SCN}^-$ .

The simulations were insensitive to changes in  $k_{14}$  and  $k_{15}$  for  $10^5 < k_{15} < 10^8 \text{ L mol}^{-1} \text{ s}^{-1}$ , provided that the magnitude of  $K_{14}k_{15}$  remained constant. The constancy of this quantity can be readily explained by the fact that the rate of Reaction 14 is significantly faster than Reaction 15. As such,  $\text{NO}$  and  $(\text{SCN})_2^-$  exist in equilibrium with  $\text{ONSCN}$  and  $\text{SCN}^-$ , and the rate limiting reaction step is the consumption of  $(\text{SCN})_2^-$  via Reaction 15. Therefore, under conditions where Reaction 14 is at equilibrium, it is not possible to isolate the parameters  $k_{14}$  and  $k_{15}$ , only  $K_{14}k_{15}$  can be determined.

A key step in the proposed reaction mechanism is Reaction 15 between  $(\text{SCN})_2^-$  and  $\text{ONSCN}$ , for which the rate constant,  $k_{15}$ , could range from  $2 \times 10^5$  to  $5 \times 10^8 \text{ L mol}^{-1} \text{ s}^{-1}$  depending on the magnitude of  $K_{14}$ . This reaction could be interpreted as the S-nitrosation of  $(\text{SCN})_2^-$  by  $\text{ONSCN}$ , wherein  $\text{NO}^+$  transfers from  $\text{ONSCN}$  to one of the sulfur atoms of  $(\text{SCN})_2^-$ , presumably forming an unstable intermediate species

ON(SCN)<sub>2</sub> which rapidly decomposes to NO and (SCN)<sub>2</sub>. Alternatively, the reaction could be interpreted as a substitution of the (SCN)<sub>2</sub><sup>-</sup> radical for NO in ONSCN, releasing NO and forming (SCN)<sub>3</sub><sup>-</sup>, which is known to persist in equilibrium with (SCN)<sub>2</sub> and SCN<sup>-</sup>.<sup>25</sup> It is of interest to compare the magnitude of  $k_{15}$  suggested in this study to the rate constants of nitrosation reactions involving ONSCN to determine if the required values of  $k_{15}$  are plausible. In the case of S-nitrosation, the high reactivity of many substrates makes it impossible to determine the rate constant, as is the case for the reaction between ONSCN and a range of heterocyclic thiones<sup>3</sup>, whilst the reaction of ONSCN with mercapto-carboxylic acids occurs with a rate constant of  $\sim 1 \times 10^4 \text{ L mol}^{-1} \text{ s}^{-1}$ . In the case of N-nitrosation, the rate constant for the reaction between ONSCN and aniline and several primary amino acids<sup>34</sup> is  $\sim 1 \times 10^8 \text{ L mol}^{-1} \text{ s}^{-1}$ , whilst a range of aniline derivatives react with rate constants between  $1 \times 10^5$  and  $5 \times 10^8 \text{ L mol}^{-1} \text{ s}^{-1}$ . Thus, the rate constants required for Reaction 15 in the proposed mechanism lie within the range of values typically encountered for nitrosation reactions effected by ONSCN. In the case of the substitution of the (SCN)<sub>2</sub><sup>-</sup> radical for NO in ONSCN, the analogous reactions between thiyl radicals and thionitrites are reportedly barrierless<sup>35</sup>, suggesting a reaction rate close to the diffusion controlled limit. Reactions 18 and 27, which offer alternate pathways for the consumption of (SCN)<sub>2</sub><sup>-</sup>, do not have a significant impact on the kinetics. Although the rate constant for Reaction 27 is large, it is second order in (SCN)<sub>2</sub><sup>-</sup>, the concentration of which is low (i.e., due to the low value of  $K_{14}$ ) and as such the rate of this reaction remains insignificant compared with the rate of Reaction 15.

### Pathway 2 - Reaction 5

This pathway comprises a second order reaction in ONSCN, directly generating NO and (SCN)<sub>2</sub>. Evidence supporting this reaction includes the tendency of ONSCN decomposition kinetics to approach a second order reaction in the later stages (conditions whereby the accumulation of NO in the solution suppresses Reaction 14) and the fact that inclusion of this reaction in kinetic simulations leads to a substantially improved fit to the data. Other related systems, including the decomposition of nitrosothiourea<sup>26, 27</sup> and the oxidation of iodide ions by HNO<sub>2</sub><sup>33, 36</sup> (which likely proceeds through an ONI intermediate) contain a term in the initial rate that is second order in nitroso species. Hence, it stands to reason that a similar mechanism operates for ONSCN.

### Pathway 3 - (iii) Formation and decomposition of ONOSCN – Reactions 21-23

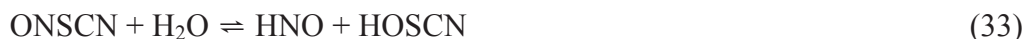
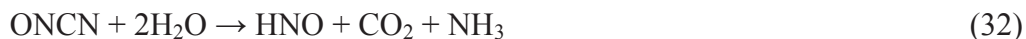
Pathways 1 and 2 proceed too slowly to account for the observed rate of decomposition at thiocyanate concentrations below 0.2 mol L<sup>-1</sup>, indicating that an additional reaction pathway must operate under these conditions. We propose the formation and decomposition of a new species, ONOSCN, to account for the kinetics of ONSCN decomposition under conditions of relatively low thiocyanate ion concentration. In the proposed mechanism, ONOSCN arises as a consequence of the reaction of ONSCN with HOSCN, and decomposes via homolysis forming nitric oxide and OSCN. The magnitude of  $K_{ONOSCN}$  indicates that only a small fraction of HOSCN converts into ONOSCN. The combination of OSCN and NO was assumed to occur rapidly with a rate constant of  $4.3 \times 10^9 \text{ L mol}^{-1} \text{ s}^{-1}$ , which falls in the range of rate constants reported in the literature for reactions between NO and a variety of radicals, including (SCN)<sub>2</sub><sup>-</sup>,

$(\text{Br})_2^-$ ,  $\text{CO}_3^-$ ,<sup>28</sup> organic peroxy radicals<sup>37</sup> and thiyl radicals<sup>38</sup> that all occur with rate in excess of  $10^9 \text{ L mol}^{-1} \text{ s}^{-1}$ . Formation of OSCN has previously been proposed to account for the complex kinetics associated with oxidation of  $\text{SCN}^-$  by  $\text{ClO}_2$ .<sup>24</sup> That study assumed that OSCN undergoes dimerisation and hydrolysis with a rate constant of  $1 \times 10^7 \text{ L mol}^{-1} \text{ s}^{-1}$  (i.e.  $k_{23}$ ), which coincides reasonably well with the value of  $1.7 \times 10^7 \text{ L mol}^{-1} \text{ s}^{-1}$  determined in the present study. Experimentation with different values of  $k_{23}$  in the simulations showed that the previously reported value could be accommodated by making appropriate changes to  $K_{21}$  and  $k_{22}$  with no reduction in the goodness of fit. Numerous intermediates contribute to the hydrolysis of  $(\text{SCN})_2$  and it is plausible that they too participate in reactions with nitrous acid or nitrosyl thiocyanate. However, owing to the large rate constants for their consumption<sup>24</sup>, the concentration of such intermediates (e.g.  $\text{HO}_2\text{SCN}$ ,  $\text{HO}_3\text{SCN}$ ) is predicted to be low, resulting in minimal contributions from these reactions.

### Formation of $\text{N}_2\text{O}$

Small amounts of  $\text{N}_2\text{O}$  arise in the product gases at levels of less than 3 %, as confirmed both by FTIR and MIMS. Because of its low abundance and subsequently insignificant impact on the overall decomposition kinetics, we did not attempt to model the formation of this species. A potential pathway for the formation of  $\text{N}_2\text{O}$  involves the decomposition of nitrosyl cyanide, ONCN, which reportedly hydrolyses to produce  $\text{N}_2\text{O}$  and  $\text{CO}_2$ .<sup>39</sup> Cyanide ions, formed via the hydrolysis of  $(\text{SCN})_2$  (generated from the decomposition of ONSCN) could react with nitrous acid to produce ONCN, in the same way as thiocyanate ions react with nitrous acid to form nitrosyl thiocyanate. An

alternative pathway may consist of ONSCN hydrolysing to form HNO, leading to formation of N<sub>2</sub>O (via combination of HNO<sup>40</sup>).



#### Comparison to HNO<sub>2</sub> decomposition kinetics

Simulations were performed based on the kinetic models developed for the decomposition of nitrous acid and nitrosyl thiocyanate to determine the dominant NO<sub>x</sub> formation pathway under conditions relevant to emulsion explosives. The simulations were executed for an initial nitrite concentration of 0.015 mol L<sup>-1</sup> and a thiocyanate ion concentration of 0.025 mol L<sup>-1</sup>, reflecting the concentrations of chemical used in the standard Dyno Nobel procedure for a target emulsion density of 1.00 g/cm<sup>3</sup>. The simulations were performed for pH values ranging from 1 to 4, and the NO concentration recorded after 5 min of reaction. The amount of NO increased with decreasing pH for both pathways. For nitrous acid decomposition, the rate of reaction increased with decreasing pH until pH 2, after which point the rate became independent of pH. This is because at pH 2 all nitrite is present as in the form of nitrous acid and reducing the pH further does not lead to an increase in the concentration of HNO<sub>2</sub>. The decomposition of nitrosyl thiocyanate on the other hand showed a rapid increase in

reaction rate at high acidities. Thus, at  $\text{pH} > 2.5$  the decomposition of nitrous acid was responsible for the majority of  $\text{NO}_x$  formation. Between  $\text{pH} 1$  and  $2.5$ ,  $\text{NO}_x$  formation from both nitrous acid and nitrosyl thiocyanate decomposition is significant, whilst at  $\text{pH}$  below  $1$  the decomposition of nitrosyl thiocyanate is the dominant  $\text{NO}_x$  formation pathway. The  $\text{pH}$  employed for gassing emulsion explosives typically ranges from  $3$  to  $4$  depending on the quantity of acetic acid added for  $\text{pH}$  reduction. Over this range the decomposition of nitrosyl thiocyanate is slow and as such the decomposition of nitrous acid is expected to be the dominant pathway for  $\text{NO}_x$  formation during explosive sensitisation. The decomposition of nitrosyl thiocyanate could be a significant  $\text{NO}_x$  source if a stronger acid is employed to lower the emulsion  $\text{pH}$ , or if thiocyanate ions are present in the gasser solutions. Figure 10 shows the  $\text{NO}$  concentration produced from each pathway after  $5$  min of reaction.



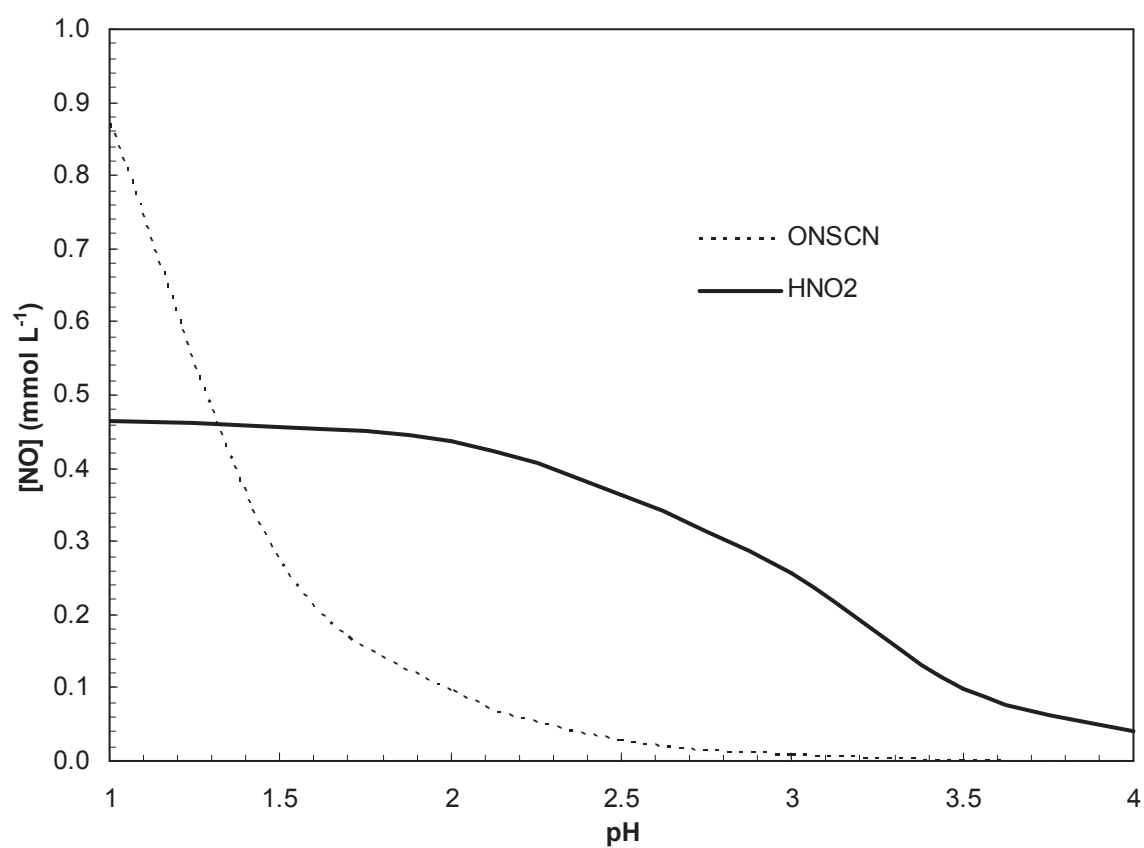


*Figure 10. NO formation from the decomposition of nitrous acid and nitrosyl thiocyanate at pH 1-4*

## 5.5 Conclusions

The mechanism of the decomposition of nitrosyl thiocyanate involves a complex system of reactions, with the rate suppressed by the accumulation of the product, nitric oxide, and catalysed by thiocyanate ions. Potential reaction mechanisms were examined by fitting the kinetic parameters to the experimental measurements, with kinetic parameters subjected to thermodynamic and kinetic scrutiny, to identify three parallel pathways for the decomposition of ONSCN. The first two pathways, which describe the kinetics at high thiocyanate ion concentrations comprise a reaction that is second order in ONSCN to generate NO and  $(\text{SCN})_2$  and a reaction between ONSCN and  $\text{SCN}^-$  to form NO and  $(\text{SCN})_2^-$ , with the latter pathway being reversible. The rate limiting step in the mechanism corresponds to the consumption of  $(\text{SCN})_2^-$  radicals by ONSCN, which could occur via either radical substitution or S-nitrosation. The third reaction pathway, which becomes significant at low thiocyanate concentrations, involves the formation of a previously unreported species, ONOSCN, via reaction between ONSCN and HOSCN, the latter being an intermediate in the hydrolysis of  $(\text{SCN})_2$ . ONOSCN contributes to NO formation via homolysis of the O-NO bond and subsequent dimerisation and hydrolysis of OSCN. The proposed kinetic mechanism provides an excellent fit to the experimental measurement, allowing the rate of NO formation from the decomposition of ONSCN to be modelled accurately. Comparison of the kinetics of nitrosyl thiocyanate and nitrous acid decomposition indicates that the decomposition of nitrous acid is the dominant  $\text{NO}_x$  formation pathway under conditions relevant to emulsion explosives.

## 5.6 References

1. Ridd, J. H., Nitrosation, diazotisation, and deamination. *Q. Rev., Chem. Soc.* **1961**, *15* (4), 418-441.
2. Meyer, T. A.; Williams, D. L. H., Nucleophilic catalysis in the nitrosation of sarcosine and proline. *J. Chem. Soc., Perkin Trans. 2* **1988**, (4), 517-521.
3. Amado, S.; Blakelock, L.; Holmes, A. J.; Williams, D. L. H., Kinetics and mechanism of the formation and reactions of S-nitroso derivatives of some heterocyclic thiones. *J. Chem. Soc., Perkin Trans. 2* **2001**, (4), 441-447.
4. Hughes, E. D.; Ridd, J. H., 17. Nitrosation, diazotisation, and deamination. Part V. Catalysis by anions of strong acids in the diazotisation of aniline and of o-chloroaniline in dilute perchloric acid. *J. Chem. Soc.* **1958**, 82-88.
5. Francisco, V.; Garcia-Rio, L.; Antonio Moreira, J.; Stedman, G., Kinetic study of an autocatalytic reaction: nitrosation of formamidine disulfide. *New J. Chem.* **2008**, *32* (12), 2292-2298.
6. Garley, M. S.; Stedman, G., An unusual reactivity pattern in the kinetics of nitrosyl halide catalysed nitrosation of thiourea and tetramethylthiourea. *J. Chem. Res.* **1996**, *9* (420-421).
7. Williams, D. L. H., *Nitrosation reactions and the chemistry of nitric oxide*. Elsevier B. V.: Amsterdam, 2004.
8. da Silva, G. R.; Dlugogorski, B. Z.; Kennedy, E. M., Elementary reaction step model of the N-nitrosation of ammonia. *Int. J. Chem. Kinet.* **2007**, *39* (12), 645-656.
9. Lecher, H.; Graf, F., Nitrosyl derivatives of bivalent sulfur. III. Nitrosyl thiocyanate. *Ber. Dtsch. Chem. Ges. B* **1926**, *59B*, 2601-2.

10. Doherty, A. M.; Garley, M. S.; Haine, N.; Stedman, G., Formation of an adduct between thiocyanate ion and nitrosyl thiocyanate. *J. Chem. Soc., Dalton Trans.* **1997**, 2163-2166.
11. Jones, E.; Munkley, C. G.; Phillips, E. D.; Stedman, G., Kinetics and equilibria in the nitric acid-nitrous acid-sodium thiocyanate system. *J. Chem. Soc., Dalton Trans.* **1996**, 1915-1920.
12. Bazsa, G.; Epstein, I. R., Autocatalysis and bistability in the reaction between nitric acid and thiocyanate. *Int. J. Chem. Kinet.* **1985**, *17*, 601-612.
13. Nagy, P.; Lemma, K.; Ashby, M. T., Kinetics and mechanism of the comproportionation of hypothiocyanous acid and thiocyanate to give thiocyanogen in acidic aqueous solution. *Inorg. Chem.* **2007**, *46* (1), 285-292.
14. Bunton, C. A.; Dahn, H.; Loewe, L., Oxidation of ascorbic acid and similar reductones by nitrous acid. *Nature* **1959**, *183* (4655), 163-165.
15. Armor, J. N., Influence of pH and ionic strength upon solubility of NO in aqueous solution. *J. Chem. Eng. Data* **1974**, *19* (1), 82-84.
16. Tu, C.; Swenson, E. R.; Silverman, D. N., Membrane inlet for mass spectrometric measurement of nitric oxide. *Free Radical Biol. Med.* **2007**, *43*, 1453-1457.
17. Kuzmic, P., Program DYNAFIT for the analysis of enzyme kinetic data: Application to HIV proteinase. *Anal. Biochem.* **1996**, *237*, 260-273.
18. Stedman, G.; Whincup, P. A. E., The equilibrium constant for the formation of nitrosyl thiocyanate in aqueous solution. *J. Chem. Soc.* **1963**, 5796-5799.
19. Barnett, J. J.; McKee, M. L.; Stanbury, D. M., Acidic aqueous decomposition of thiocyanogen. *Inorg. Chem.* **2004**, *43* (16), 5021-5033.

20. Schwartz, S. E.; White, W. H., Kinetics of reactive dissolution of nitrogen oxides into aqueous solution. *Adv. Environ. Sci. Technol.* **1983**, *12*, 1-116.
21. Stedman, G.; Whincup, P. A. E., Oxidation of metal thiocyanates by nitrous and nitric acids. Part I. Products. *J. Chem. Soc.* **1969**, 1945-1948.
22. Kalmar, J.; Woldegiorgis, K. L.; Biri, B.; Ashby, M. T., Mechanism of decomposition of the human defense factor hypothiocyanate near physiological pH. *Journal of the American Chemical Society* **2011**, *133* (49), 19911-19921.
23. Figlar, J. N.; Stanbury, D. M., Thiocyanogen as an intermediate in the oxidation of thiocyanate by hydrogen peroxide in acidic aqueous solution. *Inorg. Chem.* **2000**, *39* (22), 5089-5094.
24. Figlar, J. N.; Stanbury, D. M., Kinetics and a revised mechanism for the autocatalytic oxidation of SCN<sup>-</sup> by ClO<sub>2</sub>. *J. Phys. Chem. A* **1999**, *103* (29), 5732-5741.
25. Barnett, J. J.; Stanbury, D. M., Formation of trithiocyanate in the oxidation of aqueous thiocyanate. *Inorg. Chem.* **2002**, *41* (2), 164-166.
26. Collings, P.; Garley, M. S.; Stedman, G., Kinetics and mechanism of the decomposition of nitrosyl thiourea. *J. Chem. Soc., Dalton Trans.* **1981**, 331-335.
27. Garley, M. S.; Stedman, G.; Miller, H., Kinetics and mechanism of the decomposition of thionitrites derived from thioureas. *J. Chem. Soc., Dalton Trans.* **1984**, 1959-1963.
28. Czapski, G.; Holcman, J.; Bielski, B. H. J., Reactivity of nitric oxide with simple short-lived radicals in aqueous solution. *J. Am. Chem. Soc.* **1994**, *116*, 11465-11469.
29. Milosavljevic, B. H.; LaVerne, J. A., Pulse radiolysis of aqueous thiocyanate solution. *J. Phys. Chem. A* **2005**, *109* (1), 165-168.

30. Neta, P.; Huie, R. E.; Ross, A. B., Rate constants for reactions of inorganic radicals in aqueous solution. *J. Phys. Chem. Ref. Data* **1988**, *17* (3), 1027-1284.
31. Park, J. Y.; Lee, Y. N., Solubility and decomposition kinetics of nitrous acid in aqueous solution. *J. Phys. Chem.* **1988**, *92* (22), 6294-302.
32. Huie, R. E.; Neta, P., Kinetics of one-electron transfer reactions involving chlorine dioxide and nitrogen dioxide. *J. Phys. Chem.* **1986**, *90* (6), 1193-1198.
33. Dózsa, L.; Szilassy, I.; Beck, M. T., Mechanism of the nitrite-iodide reaction. *Inorg. Chim. Acta* **1976**, *17*, 147-153.
34. da Silva, G.; Kennedy, E. M.; Dlugogorski, B. Z., Effect of added nucleophilic species on the rate of primary amino acid nitrosation. *J. Am. Chem. Soc.* **2005**, *127* (11), 3664-3665.
35. Stamler, J. S.; Toone, E. J., The decomposition of thionitrites. *Curr. Opin. Chem. Biol.* **2002**, *6* (6), 779-785.
36. Ferranti, F.; Indelli, A., Kinetics and mechanism of the reaction of nitrous acid with iodide ion in acid medium at 25 C. *Gazz. Chim. Ital.* **1980**, *110*, 273-277.
37. Goldstein, S.; Lind, J.; Merenyi, G., Reaction of organic peroxy radicals with NO<sub>2</sub> and NO in aqueous solution: Intermediacy of organic peroxyxynitrate and peroxyxynitrite species. *J. Phys. Chem. A* **2004**, *108* (10), 1719-1725.
38. Madej, E.; Folkes, L. K.; Wardman, P.; Czapski, G.; Goldstein, S., Thiyl radicals react with nitric oxide to form S-nitrosothiols with rate constants near the diffusion-controlled limit. *Free Radical Biol. Med.* **2008**, *44*, 2013-2018.
39. Shiota, F. N.; Goon, D. J. W.; DeMaster, E. G.; Nagasawa, H. T., Nitrosyl cyanide, a putative metabolic oxidation product of the alcohol-deterrent agent cyanamide. *Biochem. Pharmacol.* **1996**, *52* (1), 141-147.

40. Bazylnski, D. A.; Hollocher, T. C., Evidence from the reaction between trioxodinitrate(II) and nitrogen-15-labeled nitric oxide that trioxodinitrate(II) decomposes into nitrosyl hydride and nitrite in neutral aqueous solution. *Inorg. Chem.* **1985**, 24 (25), 4285-4288.





## **CHAPTER 6**

### **Quantum chemistry study of nitrosyl thiocyanate decomposition mechanism**

**Table of Contents**

6.1	Introduction	151
6.2	Computational methods	153
6.2.1	Method development and validation	154
6.3	Results	164
6.3.1	Formation of nitrosyl thiocyanate	164
6.3.2	Decomposition Pathway 1	165
6.3.3	Decomposition Pathway 2	173
6.3.4	Decomposition Pathway 3	177
6.3.5	Formation of N <sub>2</sub> O	182
6.4	Conclusions	184
6.5	References	186

## 6.1 Introduction

Chapter 5 presents experimental results for the kinetics and mechanism for the decomposition of nitrosyl thiocyanate<sup>1</sup>. The reaction mechanism consists of three individual reaction pathways, each comprising a complex series of elementary reactions, containing numerous proposed intermediate species. Some of these intermediates, such as (SCN)<sub>2</sub>, have been identified experimentally, as have the primary reaction products, NO, SO<sub>4</sub><sup>2-</sup> and HCN. However, a number of the proposed intermediates, including the highly reactive (SCN)<sub>2</sub><sup>-</sup> radical anions, are predicted to exist at concentrations too low to be observed experimentally. Furthermore, owing to the broad nature of the UV-Vis spectra of nitrosyl compounds, it was not possible to confirm the existence of other nitrosyl compounds derived from HOSCN, such as ONOSCN, owing to the large absorbance of ONSCN. A quantum chemistry study has therefore been undertaken to examine the thermodynamic feasibility of the proposed reaction mechanism and to study the properties of the proposed intermediate species. For convenience, the experimentally proposed mechanism is summarised below:

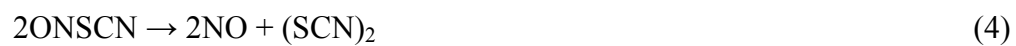
### ONSCN formation:



### Decomposition Pathway 1



Decomposition Pathway 2

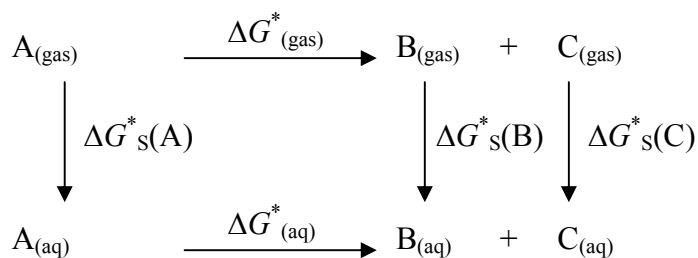


Decomposition Pathway 3



## 6.2 Computational methods

The computational methods are similar to those described in Chapter 4, for the study of nitrous acid decomposition. Gaussian03<sup>2</sup> was employed for all calculations, with the exception of SMD solvation free energies which were computed in Gaussian09<sup>3</sup>. The gas phase enthalpies and free energies of reaction were determined with the G3B3<sup>4</sup> and CBS-QB3<sup>5</sup> methods, and combined with solvation free energies calculated with continuum solvent models by means of the thermochemical cycle depicted in Figure 1<sup>6</sup>.



$$\Delta G^*_{(\text{gas})} = \Delta G^0_{(\text{gas}, 1 \text{ atm})} + \Delta n RT \ln(24.46)^a$$

$$\Delta G^*_{(\text{aq})} = \Delta G^*_{(\text{gas})} + \Delta G^*_s(B) + \Delta G^*_s(C) - \Delta G^*_s(A).$$

**Figure 1. Thermochemical cycle for determining aqueous free energy change of reaction, for reaction  $A \rightarrow B + C$ . <sup>a</sup>The value 24.46 reflects the ratio of the molar volume of a gas at 1 atm to that at 1 mol L<sup>-1</sup>**

where  $\Delta G^*_s$  is the free energy of solvation and  $\Delta n$  is the difference in the number of moles of products and reactants. Gas phase reaction free energies are typically calculated with a standard state of 1 atm or 1 bar, whilst aqueous free energies employ a 1 mol L<sup>-1</sup> standard state. As such, if the number of moles of species changes in the

course of a reaction, a correction must be applied to account for the difference in the entropy component of the free energy for the 1 mol L<sup>-1</sup> standard state compared to the 1 atm. This correction amounts to 7.92Δ*n* kJ at 298 K. In the case of H<sup>+</sup>, the experimental values for the solvation enthalpies and free energies were employed, corresponding to -1150 and -1104.5 kJ mol<sup>-1</sup>, respectively, as reported by Tissandier et al.<sup>7</sup>. Note that for H<sup>+</sup>, the free energy change reflects standard states of 1 atm and 1 mol L<sup>-1</sup> for the gas and liquid phases, respectively.<sup>8</sup> The standard state for water is the liquid state, equivalent to a concentration of 55.5 mol L<sup>-1</sup>. As such, an additional correction is required to convert the solvation of free energy of water to the correct standard state, comprising an additional 9.6 kJ mol<sup>-1</sup>.

### 6.2.1 Method development and validation

The polarisable continuum model (PCM) can be employed to calculate the free energy of solvation necessary to compute aqueous reaction free energies. However, numerous variations of the PCM model have been proposed, mostly differing in their definition of the solvent cavity. In Gaussian 03, the default solvation model is the IEFPCM model of Tomasi et al.<sup>9</sup>, in which the solvent cavity is defined by a series of overlapping spheres, with the default atomic radii defined according to the UFF force field<sup>10</sup>. However, the Gaussian 03 user guide recommends that UAHF radii<sup>11</sup> be employed for calculation of solvation free energies. In addition, the conductor-like polarisable continuum model has frequently been employed in the literature for calculation of solvation free energies<sup>6</sup>, whilst the Gaussian 09 program contains a new variation of the PCM method known as SMD, which reportedly exhibits smaller errors than the previous version<sup>12</sup>.

A series of calculations were performed for reactions with experimentally known free energies of reaction with a variety of solvent models to determine the most suitable solvation model for calculations on reactions where experimental data is unavailable. The experimental reaction free energies were determined from the reported equilibrium constants in accordance with Equation 9. The reactions employed in the benchmarking study, shown in Table 1, include the formation of ONSCN (Reaction 1), the hydrolysis of (SCN)<sub>2</sub> (Reaction 5), the protonation of SCN<sup>-</sup> (Reaction 10) and the equilibria for the formation of adducts between thiocyanate ions and (SCN)<sub>2</sub>, SCN radicals and ONSCN (Reactions 11, 12 and 13, respectively). These reactions are suitable for examining the accuracy of the solvent models for the present study as they contain a selection of the species participating in Reactions 2-8. Table 1 summarises the experimental equilibrium constants and reaction free energies.

$$\Delta G_{rxn}^o = -RT \ln(K_{eqm}) \quad (9)$$

**Table 1: Summary of experimental equilibrium constants and reaction free energies employed to test the accuracy of solvent models**

Rxn No	Stoichiometry	$K_{eqm}$	$\Delta G^{\circ}_{rxn}$ (kJ)	Source
1	$\text{HNO}_2 + \text{SCN}^- + \text{H}^+ \rightleftharpoons \text{ONSCN} + \text{H}_2\text{O}$	$29 \text{ L}^2 \text{ mol}^{-2}$	-8.3	Ref <sup>13</sup>
5	$(\text{SCN})_2 + \text{H}_2\text{O} \rightleftharpoons \text{HOSCN} + \text{SCN}^- + \text{H}^+$	$3.9 \times 10^{-3} \text{ mol}^2 \text{ L}^{-2}$	13.8	Ref <sup>14</sup>
10	$\text{HNCS} \rightleftharpoons \text{SCN}^- + \text{H}^+$	$100 \text{ mol L}^{-1}$	-11.4	Refs <sup>15,16</sup>
11	$(\text{SCN})_2 + \text{SCN}^- \rightleftharpoons (\text{SCN})_3^-$	$0.43 \text{ mol L}^{-1}$	2.1	Refs <sup>17,18</sup>
12	$\text{SCN} + \text{SCN}^- \rightleftharpoons (\text{SCN})_2^-$	$2 \times 10^5 \text{ mol L}^{-1}$	-30.2	Refs <sup>19,20</sup>
13	$\text{ONSCN} + \text{SCN}^- \rightleftharpoons \text{ON}(\text{SCN})_2^-$	$0.036 \text{ mol L}^{-1}$	10.7	Ref <sup>21</sup>

The equilibrium constant for Reaction 1 has been determined from measurements of the visible absorbance of nitrous acid solutions containing  $\text{SCN}^-$ , originally by Stedman et al.<sup>13</sup>, and later confirmed in several other studies<sup>22,23</sup>, including the present work (Chapter 5). The equilibrium constant for thiocyanogen hydrolysis ( $K_5$ ) is less well established, with reported values spanning an order of magnitude<sup>14,17</sup>. The most recent determination by Nagy et al.<sup>14</sup> has been employed in this study. Similarly, there is significant variation in the  $pK_a$  values reported for HNCS, with estimates ranging from -0.7 to -2.3.<sup>15,16,24,25</sup> The measurements by Morgan et al.<sup>15</sup> and Crowell & Hankins<sup>16</sup> are in reasonable agreement ( $-2.3 < pK_a < -1.84$ ), both of which attempt to account for the activity coefficients of the species in concentrated solution, and as such, a value of -2 for the  $pK_a$  of HNCS has been assumed. The equilibrium constants for the adducts between  $\text{SCN}^-$  and  $(\text{SCN})_2$  and ONSCN have both been established by examining the increase in UV-Visible absorbance of  $(\text{SCN})_2$  and ONSCN solutions with increasing



SCN<sup>-</sup> concentration<sup>17,18,21</sup>. In both cases, it is difficult to separate the effects of the equilibrium constant and extinction coefficient, leading to uncertainties on the order of  $\pm 50\%$  in the equilibrium constant.  $K_{12}$  has been determined in pulse radiolysis studies of thiocyanate solutions.<sup>19,20</sup>

The calculations utilised four different methods for the calculation of solvation free energies comprising the PCM model with UFF and UAHF radii, the SMD model, and the CPCM<sup>26</sup> model with UAHF radii. The CPCM model is a version of the PCM wherein the solvent is treated as a conductor rather than a dielectric. The PCM and CPCM results were computed with the B3LYP hybrid density functional<sup>27,28</sup>, with an additional Hartree Fock (HF) calculation performed with the UAHF radii. The SMD results were computed with both the B3LYP and M05-2X<sup>29</sup> density functional theory methods. Calculations were performed with the 6-31G+(d,p) basis set for all methods, with selected calculations repeated with the 6-31G(d,p) and 6-311++G(d,p) basis sets to examine the effect of diffuse functions and basis set size, respectively<sup>30,31</sup>. The solvation free energy was determined by comparing the energy of the species determined with the solvent model to that computed in the gas phase with the same method and basis set. The geometry was optimised in both the gas and solution calculations, to ensure that any effects of geometry relaxation upon solvation were accounted for. The gas phase reaction free energies were combined with the calculated solvation free energies to calculate the aqueous free energy changes of Reactions 1, 5 and 10-13. Table 2 reports the results for the gas phase free energies of reaction for the G3B3 and CBS-QB3 methods. Tables 3 and 4 illustrate the errors between the experimental results and those calculated based on G3B3 and CBS-QB3 results, respectively, for a variety of solvent models.

**Table 2: Gas phase reaction free energies calculated with the G3B3 and CBS-QB3 model chemistries at 298 K, 1 atm. All energies are in kJ**

<b>Reaction</b>	<b><math>\Delta G^0_{298}</math> - CBS-QB3</b>	<b><math>\Delta G^0_{298}</math> - G3B3</b>	<b>Difference</b>
1	-1336.9	-1341.8	4.9
5	1362.0	1364.3	-2.3
10	1319.4	1322.8	-3.4
11	-85.8	-77.1	-8.8
12	-99.1	-87.2	-11.9
13	-19.2	-17.2	-2.0

**Table 3: Difference between experimental and calculated aqueous free energies of reactions 1, 5 and 10-13 computed with gas phase CBS-QB3 energies and solvation free energies calculated with different models. All free energies were calculated at 298 K and employ the 1 mol L<sup>-1</sup> standard state. All energies are in kJ**

<b>Method<sup>a,b</sup></b>	<b>Reaction</b>						<b>MAD<sup>c</sup></b>
	<b>1</b>	<b>5</b>	<b>10</b>	<b>11</b>	<b>12</b>	<b>13</b>	
1. B3/6-311++G(d,p) UFF <sup>b,c</sup>	-1.5	17.2	-4.2	8.0	-6.6	-1.9	6.6
2. B3/6-31+G(d,p) UFF	-0.3	17.1	-3.0	5.6	-6.8	4.0	6.1
3. B3/6-31G(d,p) UAHF	21.5	-8.6	7.1	5.2	-12.5	14.9	11.6
4. B3/6-31+G(d,p) UAHF	8.7	-0.5	16.9	-2.6	-15.9	-0.9	7.6
5. HF/6-31+G(d,p) UAHF	15.8	-0.8	9.9	-46.4	-17.6	4.5	15.8
6. B3/6-31+G(d,p) CPCM UAHF	8.7	-0.8	17.1	-2.4	-15.8	3.4	8.0
7. B3/6-31+G(d,p) SMD	-18.6	15.5	11.5	-15.0	-19.4	0.8	13.5
8. M052X/6-31+G(d,p) SMD	-17.6	15.3	12.6	-16.4	-25.6	1.5	14.8

<sup>a</sup>Methods 1-5 employ the Gaussian 03 PCM model, Method 6 employs the CPCM model, and Methods 7-8 employ the Gaussian 09 SMD model. <sup>b</sup>B3 refers to the B3LYP DFT method. <sup>c</sup>Mean absolute deviation.

**Table 4: Difference between experimental and calculated aqueous free energies of reactions 1, 5 and 10-13 computed with gas phase G3B3 energies and solvation free energies calculated with different models. All free energies were calculated at 298 K and employ the 1 mol L<sup>-1</sup> standard state. All energies are in kJ**

	<i>Reaction</i>						
<i>Method</i> <sup>a,b</sup>	<i>1</i>	<i>5</i>	<i>10</i>	<i>11</i>	<i>12</i>	<i>13</i>	<b>MAD<sup>c</sup></b>
1. B3/6-311++G(d,p) UFF	-6.4	19.5	-0.9	16.8	5.3	0.1	8.2
2. B3/6-31+G(d,p) UFF	-5.2	19.4	0.4	14.3	5.2	6.0	8.4
3. B3/6-31G(d,p) UAHF	16.6	-6.3	10.5	14.0	-0.6	16.8	10.8
4. B3/6-31+G(d,p) UAHF	3.8	1.8	20.3	6.1	-4.0	1.1	6.2
5. HF/6-31+G(d,p) UAHF	10.9	1.4	13.3	-37.6	-5.6	6.5	12.6
6. B3/6-31+G(d,p) CPCM UAHF	3.7	1.5	20.5	6.4	-3.9	5.4	6.9
7. B3/6-31+G(d,p) SMD	-23.5	17.7	14.9	-6.2	-7.4	2.8	12.1
8. M05-2X/6-31+G(d,p) SMD	-22.5	17.6	15.9	-7.6	-13.7	3.4	13.5

<sup>a</sup>Methods 1-5 employ the Gaussian 03 PCM model, Method 6 employs the CPCM model, and Methods 7-8 employ the Gaussian 09 SMD model. <sup>b</sup>B3 refers to the B3LYP DFT method. <sup>c</sup>Mean absolute deviation.

As demonstrated in Table 2, the gas phase free energies of Reactions 1, 5, 10, and 13 calculated with the G3B3 and CBS-QB3 methods are in excellent agreement, with differences of less than 5 kJ. The discrepancies for Reactions 11 and 12 are slightly larger, with differences of 9 and 12 kJ, respectively. The mean absolute deviation (MAD) for all reactions is 5.5 kJ. This deviation is similar to the average errors exhibit by the CBS-QB3 and G3B3 methods relative to the G2 test set, which are on the order

of 4 kJ mol<sup>-14,5</sup>. It is therefore concluded that these methods perform satisfactorily for computation of gas phase reaction free energies.

For the aqueous reaction free energies based on the gas phase CBS-QB3 calculations, the MAD ranged from 6.1 kJ for the B3LYP/6-31+G(d,p) PCM method with UFF atomic radii, to 15.8 kJ for the HF/6-31+G(d,p) PCM method with UAHF radii. Increasing the basis set size from the double zeta 6-31+G(d,p) to the triple zeta 6-311++G(d,p) increased the error slightly, possibly owing to the fact that solvation models are typically optimised for use with smaller basis sets<sup>11,26</sup>. There was a relatively small difference of 1.5 kJ between the average results of B3LYP/6-31+G(d,p) calculations with the UFF and UAHF radii. Removing diffuse functions from the basis set produced a further increase in error of 5.5 kJ, most likely due to the presence of ionic species which require diffuse functions for accurate energy calculations. The results for calculations with the PCM and C-PCM model with the same method and basis set were almost identical and yielded similar MAD's. The error in the results computed with the SMD model were 7.3 kJ higher than the same method with the earlier PCM model, with the M05-2X results being 1 kJ worse than those of B3LYP. The solvation free energies of individual species were systematically more positive with the SMD compared to PCM model, with the exception of H<sub>2</sub>O, for which the SMD solvation free energies were the lowest. This results in large errors for the SMD model for Reactions 1 and 5 which involve H<sub>2</sub>O.

For gas phase calculations with the G3B3 method, the smallest MAD of 6.2 kJ was achieved with the B3LYP/6-31+G(d,p) PCM methods with UAHF radii. The CPCM results with the same method and basis set yielded a similar MAD of 6.9. The

B3LYP/6-31+G(d,p) PCM-UFF method, which produced the lowest errors when combined with CBS-QB3 gas phase energies, exhibited a slightly larger error of 8.4 kJ when combined with the G3B3 results. Overall, employing G3B3 for gas phase reaction energies yielded a slight improvement in the agreement between the calculated and experimental aqueous reaction free energies compared to CBS-QB3. The maximum error, however, was slightly higher for G3B3 compared to CBS-QB3.

The poor performance of the HF method was a somewhat surprising outcome, because the UAHF radii are optimised for  $\Delta G_S$  calculations with HF, and would be expected to produce reasonable results. The larger discrepancy for the HF results arise due to the very large errors of 38 to 46 kJ (depending on the method of gas phase free energy calculation) associated with the free energy change of Reaction 11. This error is a consequence of the high solvation free energy of  $(\text{SCN})_3^-$  predicted with HF, compared to other methods, with the HF method predicting a solvation free energy 40.5 kJ more negative than the nearest other method. This high solvation free energy results from an incorrect geometry of  $(\text{SCN})_3^-$  predicted by the HF method. The structure of  $(\text{SCN})_3^-$  optimised with HF resembles a weak complex between an  $\text{SCN}^-$  ion and the  $(\text{SCN})_2$  molecule, with an S-S separation distance of 3.55 Å between the  $\text{SCN}^-$  and  $(\text{SCN})_2$  moieties, and a 2.08 Å bond length in  $(\text{SCN})_2$ . In contrast, the B3LYP geometry exhibits even separation of the three SCN groups, with S-S bond lengths of 2.51 Å. The unsymmetrical HF structure results in a high charge density on the  $\text{SCN}^-$  group, which exhibits greater stabilisation upon solvation compared to the B3LYP geometry wherein the charge is distributed over the whole molecule.

The magnitude of error in the solvation free energies, which averages in the range of approximately 6-8 kJ for the Gaussian 03 PCM and CPCM models, is on the whole, quite pleasing, considering that solvation models typically exhibit average errors of around 20-30 kJ mol<sup>-1</sup> for ionic species<sup>12</sup>. Clearly, there is a degree of error cancellation occurring between the species on the left and right hand sides of Equations 1, 5 and 10-13 which reduces the overall error in the calculated reaction free energies. Because errors in individual reaction energies could be as high as 20 kJ mol<sup>-1</sup>, it is desirable to compute unknown reaction free energies with two different solvation models. The B3LYP/6-31+G(d,p) method has been selected for this purpose, with calculations to be performed at both the UFF and UAHF atomic radii for unknown reaction free energies. These solvent models are combined with both the G3B3 and CBS-QB3 gas phase reaction free energies, with the overall method denoted CBS-QB3//B3LYP/6-31+G(d,p)-PCM(UFF), CBS-QB3//B3LYP/6-31+G(d,p)-PCM(UAHF), G3B3//B3LYP/6-31+G(d,p)-PCM(UFF) and G3B3//B3LYP/6-31+G(d,p)-PCM(UAHF).

## 6.3 Results

### 6.3.1 Formation of nitrosyl thiocyanate

Nitrosyl thiocyanate forms as the result of an acid catalysed reaction between nitrous acid and thiocyanate ions<sup>13</sup>. Nitrosation of  $\text{SCN}^-$  could potentially occur at either the sulfur or nitrogen sites, forming nitrosyl thiocyanate (ONSCN) or nitrosyl isothiocyanate (ONNCS), respectively. Pasinszki & Westwood<sup>32</sup> previously examined a range of nitrosyl thiocyanate isomers in the gas phase at the MP2/6-31G(d) level of theory, demonstrating that formation of both ONSCN and ONNCS isomers is indeed possible. Additionally, both *cis* and *trans* conformers were identified, with the *cis* configuration exhibiting the lowest energy in both cases. In the gas phase, the energy of ONSCN is approximately  $26 \text{ kJ mol}^{-1}$  lower than ONNCS at the MP2/6-31G(d) level of theory<sup>32</sup>. Results have also been reported for single point CCSD(T)/aug-cc-PVQZ calculations based on B3LYP/6-311++G(3df,2dp) geometries, which predict an energy difference of  $31 \text{ kJ mol}^{-1}$  between ONSCN and ONNCS. However, the *trans* form of the ONNCS isomer has a slightly lower energy than the *cis* isomer at this level of theory.<sup>33</sup> Similar results were obtained in the present study, for gas phase calculations employing the G3B3 and CBS-QB3 methods, which predict free energies in the order of *cis* ONSCN < *trans* ONSCN < *trans* ONNCS < *cis* ONNCS. The results computed with inclusion of solvation effects indicate that the two ONSCN isomers lie close in energy, with the *trans* isomer exhibiting a free energy  $6 \text{ kJ mol}^{-1}$  greater than the *cis* isomer. Owing to this small energy difference, these isomers would be expected to co-exist in solution and could both potentially participate in the decomposition reactions. The *cis* and *trans* ONNCS isomers, on the other hand, exhibit free energies 53 and 46 kJ higher than *cis* ONSCN, indicating that the equilibrium concentration of the ONNCS isomers



will be negligible. As such, the ONNCS species are unlikely to participate in the decomposition process. Figure 2 illustrates the relative free energies and geometries of the ONSCN isomers.

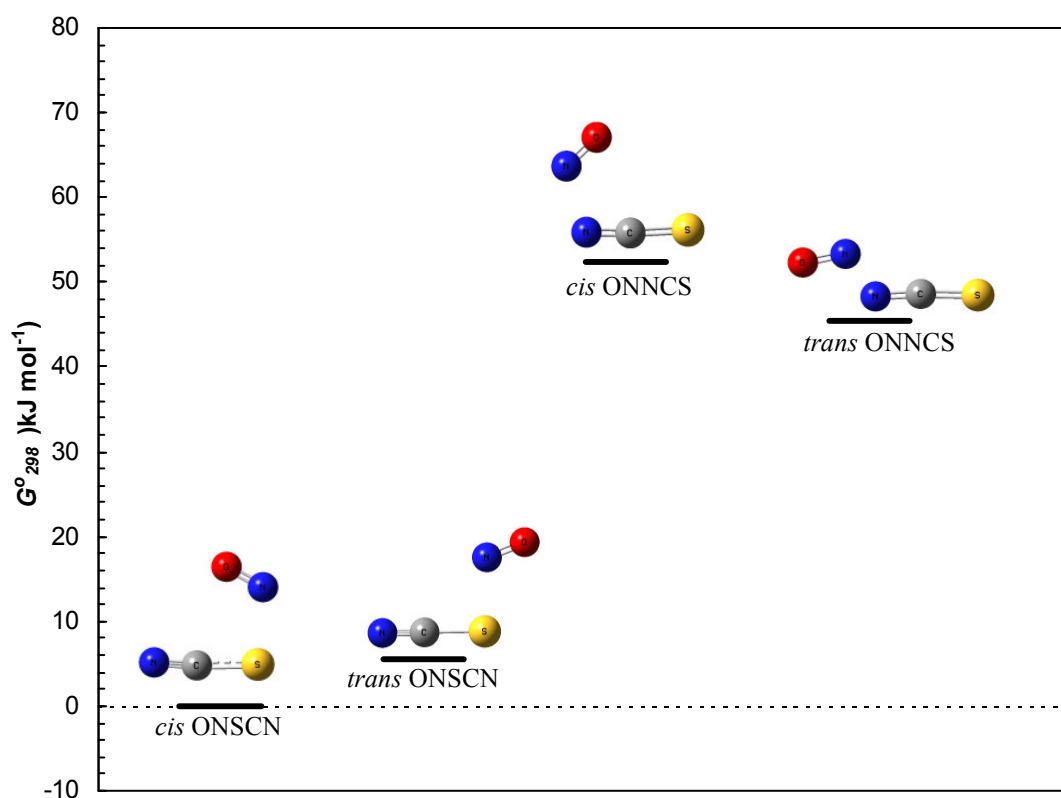


**Figure 2:** Free energies of ONSCN isomers relative to cis ONSCN, computed at the CBS-QB3//B3LYP/6-31+G(d,p)-PCM(UFF) level

### 6.3.2 Decomposition Pathway 1

The experimental kinetic study of ONSCN decomposition identified a reaction pathway second order in nitrosyl thiocyanate and first order in thiocyanate ions. Consistent with this rate law, Reactions 2 and 3 were proposed, in which a pre-equilibrium is established between thiocyanate ions, nitrosyl thiocyanate, nitric oxide and

thiocyanogen radical anions (i.e.,  $(\text{SCN})_2^-$ ), followed by rate limiting consumption of  $(\text{SCN})_2^-$  by reaction with a second ONSCN molecule. For  $10^5 < k_3 < 10^8 \text{ L mol}^{-1} \text{ s}^{-1}$ , different values of  $K_2$  and  $k_3$  can provide an equally good fit to the data, provided that the product of the rate and equilibrium constant,  $K_2 k_3$ , remains constant (note that  $K_2$  and  $k_3$  correspond to  $K_{14}$  and  $k_{15}$  in Chapter 5). It is also possible that the mechanism for Reaction 2 could proceed via initial dissociation of ONSCN into NO and SCN radicals (Reaction 14), and subsequent reaction between SCN and  $\text{SCN}^-$  forming  $(\text{SCN})_2^-$  (Reaction 12), provided that these reactions are fast enough to establish equilibrium concentrations of these species. In addition, the species  $\text{ON}(\text{SCN})_2^-$  has been proposed as a product of the reaction between NO and  $(\text{SCN})_2^-$ , and as a minor species in equilibrium with ONSCN and  $\text{SCN}^-$ . To distinguish between these competing reaction mechanisms, a thermodynamic analysis of the various elementary steps that could constitute Reaction 2 has been performed. In addition, the transition state for Reaction 3 has been located, and a rate constant calculated by means of transition state theory, for comparison with the experimental value.



The formation of  $(\text{SCN})_2^-$  and NO from ONSCN and  $\text{SCN}^-$  (Reaction 2) was established to be exothermic in the gas phase, with  $\Delta G_{rxn}$  of -35 and -20 kJ at the CBS-QB3 and G3B3 levels, respectively. As noted in Section 6.2, there is a considerable difference in the gas phase free energy of  $(\text{SCN})_2^-$  computed with the two methods. The reaction becomes considerably endothermic upon inclusion of solvation effects, with aqueous reaction free energies of 41 and 56 kJ with UFF radii at the CBS-QB3 and G3B3 levels, respectively. The results with UAHF radii are 7 kJ lower in free energy than those with

the UFF radii. The difference between the gas phase and aqueous phase reaction free energies arises due to the higher solvation free energy of  $\text{SCN}^-$  relative to  $(\text{SCN})_2^-$ . Based on the calculated aqueous reaction free energies, estimates for  $K_2$  range from  $2 \times 10^{-10}$  to  $1 \times 10^{-6}$ . The wide range in the estimate of  $K_3$  arises as a result of the large difference in the CBS-QB3 and G3B3 gas phase reaction free energies. Owing to the large difference between the gas phase reaction free energies calculated with CBS-QB3 and G3B3 for Reaction 2, an alternate method was sought to determine the free energy change of this reaction. It was noted that Reaction 2 can be written as the sum of Reactions 12 and 14, hence  $\Delta G_{(2)}^0 = \Delta G_{(12)}^0 + \Delta G_{(14)}^0$ . Calculated gas phase results for the free energy change for Reaction 14 with CBS-QB3 and G3B3 were in close agreement (within 3 kJ), whilst  $\Delta G_{(12)}^0$  can be computed from the experimentally determined equilibrium constant, which is well established<sup>19,20</sup>. Employing this scheme yields values for  $K_2$  ranging from  $4 \times 10^{-10}$  to  $5 \times 10^{-9}$ , comparing favourably with the experimental results, which range from  $1 \times 10^{-10}$  to  $8 \times 10^{-8}$  depending on the value of  $k_3$ .

An alternate reaction mechanism consists of the homolytic fission of ONSCN into NO and SCN radicals (Reaction 14), with a subsequent reaction between SCN and  $\text{SCN}^-$  (Reaction 12). The latter reaction has been observed to occur in the pulse radiolysis of  $\text{SCN}^-$  solutions, where equilibrium between  $(\text{SCN})_2^-$  and SCN and  $\text{SCN}^-$  is rapidly established.<sup>20,34</sup> Formation of SCN and NO from ONSCN, however, is considerably endothermic, with calculated aqueous reaction free energies ranging from 78 to 81 kJ, corresponding to an equilibrium constant on the order of  $10^{-14} \text{ mol L}^{-1}$ . If it is assumed that the reverse reaction occurs with a rate constant of  $5 \times 10^9 \text{ L mol}^{-1} \text{ s}^{-1}$ , typical for reactions between NO and other radicals<sup>34</sup>, an estimate for the forward rate constant of 5

$\times 10^{-5} \text{ s}^{-1}$  is obtained, a value too small to account for the experimentally observed reaction rate. As such, decomposition of ONSCN does not proceed via homolysis of ONSCN.

A transition state was identified for the reaction between ONSCN and  $(\text{SCN})_2^-$  (Reaction 3), yielding NO and  $(\text{SCN})_3^-$  as reaction products, corresponding to the substitution of the NO group in ONSCN with  $(\text{SCN})_2^-$ . Figure 3 shows the geometry of the transition state. The imaginary vibration mode shows shortening of the two S-S bonds, and lengthening of the S-NO bond. In the gas phase at the CBS-QB3 level, the free energy of the transition state lies just 15 kJ above the reactants, ONSCN and  $(\text{SCN})_2^-$ , whilst the TS free energies in solution were calculated as 36 and 37 kJ for the CBS-QB3 gas phase results combined with UAHF and UFF solvent calculations, respectively. Employing transition state theory (TST), the average reaction rate constant for the two solvation methods was calculated as  $2.8 \times 10^6 \text{ L mol}^{-1} \text{ s}^{-1}$ . As discussed earlier, it was only possible to determine  $K_2k_3$  experimentally, with the values of  $k_3$  ranging from  $10^5$  to  $10^8 \text{ L mol}^{-1} \text{ s}^{-1}$ , provided that the product  $K_2k_3$  remained constant. The value of  $k_3$  determined quantum chemically lies within the range of values predicted experimentally. The value of  $K_2k_3$  determined quantum chemically ranges from  $9.4 \times 10^{-4}$  to  $0.014 \text{ L mol}^{-1} \text{ s}^{-1}$ , which compares favourably to the experimental value of  $0.011 \text{ L mol}^{-1} \text{ s}^{-1}$ . Owing to the large number of atoms in the transition state, it was not feasible to perform the G3B3 calculation.

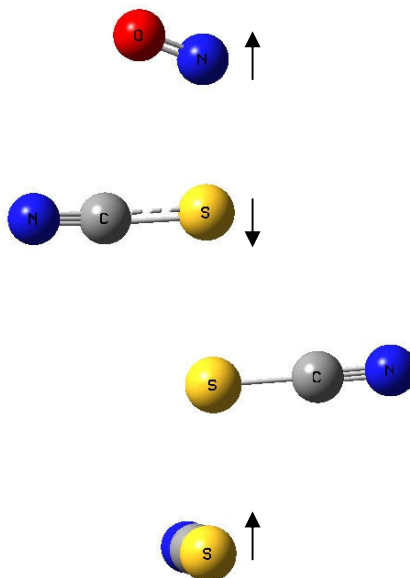


***Figure 3: Transition state geometry for Reaction 3 computed with B3LYP/6-31+G(d,p) and PCM solvent model with UFF radii. Arrows indicate the direction of atom movements along the reaction coordinate.***

Regarding the intermediacy of  $\text{ON}(\text{SCN})_2^-$ , two different stationary points of this stoichiometry were identified quantum chemically. The first contains a long S-S bond between SCN and ONSCN of 3.07 Å in the gas phase. This bond is elongated to 3.84 Å when the PCM(UAHF) model is employed. The second structure contains an S-N-S linkage, with one SCN group in plane with the NO group, and the second SCN group rotated by approximately 70 degrees. Figure 4 shows the structure of the two isomers computed at the B3LYP/6-31+G(d,p) PCM(UAHF) level. In the gas phase, formation of the S-N-S isomer is more energetically favourable, with the average of the CBS-QB3 and G3B3 free energy changes for Reaction 13 being -77 and -50 kJ mol<sup>-1</sup> for the S-N-S and S-S isomers, respectively.

Upon solvation, formation of both isomers exhibit positive Gibbs free energy changes, and the S-S isomer becomes energetically more favourable than the S-N-S variant. The

reason for the large difference between the gas and aqueous phase reaction free energies is the high solvation free energy of  $\text{SCN}^-$  compared to  $\text{ON}(\text{SCN})_2^-$ . The preference for the S-S isomer in solution results from the relatively large solvation free energy of this species compared to the S-N-S isomer. The larger solvation free energy of S-S  $\text{ON}(\text{SCN})_2^-$  likely arises due to a high negative charge held on the SCN group, owing to the longer distance between ONSCN and  $\text{SCN}^-$  in this isomer. The S-N-S isomer would be expected to exhibit a much more uniform charge distribution, and correspondingly lower free energy of solvation. The predicted equilibrium constant for the S-S isomer, which ranges from  $1.1 \times 10^{-3}$  to  $1.9 \times 10^{-2} \text{ L mol}^{-1}$  depending on the solvent model employed, is in reasonable agreement with that estimated experimentally by Doherty et al ( $0.013 < K < 0.036$ ). The presence of two different isomers of  $\text{ON}(\text{SCN})_2^-$  may account for some of the discrepancies between the work of Czapski et al<sup>34</sup> and Doherty et al<sup>21</sup>. At equilibrium, the S-S isomer would be the dominant species, however, this does not preclude the formation of transient  $\text{ON}(\text{SCN})_2^-$  in the reaction between NO and  $(\text{SCN})_2^-$  (i.e. in the experiments of Czapski et al<sup>34</sup>), which could explain the different  $\text{ON}(\text{SCN})_2^-$  stabilities reported in the two literature studies.

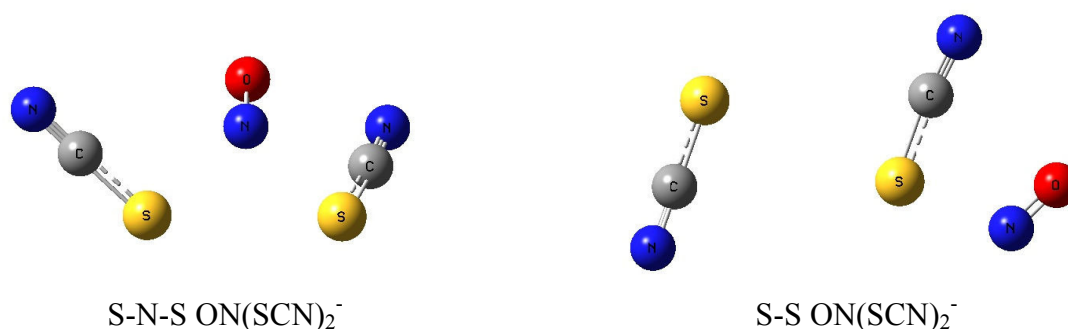


**Figure 4: Geometries of S-S and S-N-S isomers of  $\text{ON}(\text{SCN})_2^-$  optimised at B3LYP/6-31+G(d,p) with PCM model and UAHF radii**

Provided that formation of  $\text{ON}(\text{SCN})_2^-$  is sufficiently rapid that Reaction 13 is at equilibrium, formation of  $(\text{SCN})_2^-$  directly via Reaction 2 and via  $\text{ON}(\text{SCN})_2^-$  is kinetically indistinguishable. The formation of NO and  $(\text{SCN})_2^-$  from  $\text{ON}(\text{SCN})_2^-$  involves a crossing from the singlet to the triplet potential energy surface, and it is therefore not possible to isolate a transition structure for this reaction with the software employed in the present study. Consequently, the intermediacy of  $\text{ON}(\text{SCN})_2^-$  cannot be conclusively proven quantum chemically. However, it has been shown experimentally that the reverse reaction between NO and  $(\text{SCN})_2^-$  produces  $\text{ON}(\text{SCN})_2^-$  and that equilibrium between  $\text{ONSCN}$ ,  $\text{SCN}^-$  and  $\text{ON}(\text{SCN})_2^-$  is rapidly established. As such, it is likely that Reaction 2 indeed proceeds via an  $\text{ON}(\text{SCN})_2^-$  intermediate. Table 5 summarises the results of the calculations for Pathway 1.

**Table 5: Calculated Gibbs free energies of reaction for Pathway 1 and comparison of calculated and experimentally determined equilibrium constants. All energies in kJ**

	Reaction			
Method <sup>a</sup>	1	2	2a <sup>b</sup>	3
$\Delta G_{298}^o$ CBS-QB3 (UFF)	-8.6	40.7	47.4	-47.1
$\Delta G_{298}^o$ G3B3 (UFF)	-13.5	56.0	50.9	-45.7
$\Delta G_{298}^o$ CBS-QB3 (UAHF)	0.4	34.1	52.0	-44.0
$\Delta G_{298}^o$ G3B3 (UAHF)	-4.6	49.5	55.5	-42.6
$K_{\text{calc}}$ (lower)	$0.86 \text{ L}^2 \text{ mol}^{-2}$	$1.5 \times 10^{-10}$	$1.9 \times 10^{-10}$	$3.0 \times 10^{-7}$
$K_{\text{calc}}$ (upper)	$236 \text{ L}^2 \text{ mol}^{-2}$	$1.0 \times 10^{-6}$	$4.9 \times 10^{-9}$	$1.8 \times 10^8$
$K_{\text{expt}}$	$29 \text{ L}^2 \text{ mol}^{-2}$	$1 \times 10^{-10} < K < 8 \times 10^{-8}$		irreversible
Method	12	14	13 (S-S)	13 (S-N-S)
$\Delta G_{298}^o$ CBS-QB3 (UFF)	-37.0	77.7	14.8	27.7
$\Delta G_{298}^o$ G3B3 (UFF)	-25.1	81.1	16.7	24.0
$\Delta G_{298}^o$ CBS-QB3 (UAHF)	-46.2	82.2	9.8	24.4
$\Delta G_{298}^o$ G3B3 (UAHF)	-34.2	85.7	11.8	20.8
$K_{\text{calc}}$ (lower)	$2.5 \times 10^4$	$9.4 \times 10^{-16}$	$1.2 \times 10^{-3}$	$1.4 \times 10^{-5}$
	$\text{L mol}^{-1}$	$\text{mol L}^{-1}$	$\text{L mol}^{-1}$	$\text{L mol}^{-1}$
$K_{\text{calc}}$ (upper)	$1.2 \times 10^8$	$2.4 \times 10^{-14}$	$1.9 \times 10^{-2}$	$2.3 \times 10^{-4}$
	$\text{L mol}^{-1}$	$\text{mol L}^{-1}$	$\text{L mol}^{-1}$	$\text{L mol}^{-1}$
$K_{\text{expt}}$	$2 \times 10^5 \text{ L mol}^{-1}$	N/A	$0.013 < K < 0.036$	

<sup>a</sup>Solvation energies computed at the B3LYP/6-31+G(d,p) with the PCM solvent model

implemented in Gaussian03



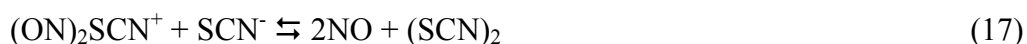
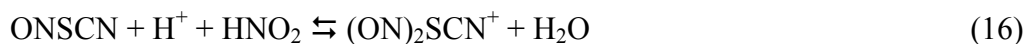
<sup>b</sup>Free energy of reaction computed by combining the experimental free energy change of Reaction 12 with that calculated for Reaction 14, i.e.  $\Delta G^0_{(2a)} = \Delta G^0_{(12)} + \Delta G^0_{(14)}$ .

### 6.3.3 Decomposition Pathway 2

The second pathway for nitrosyl thiocyanate decomposition determined experimentally involves an irreversible reaction second order in nitrosyl thiocyanate (Reaction 4). The calculated free energy change of reaction ranged from just -1.3 kJ, computed with G3B3 in combination with PCM model and UAHF radii, to -14 kJ for CBS-QB3 combined with the PCM-UFF solvent calculation. The difference between the gas phase reaction free energies calculated with G3B3 and CBS-QB3 is 8 kJ, whilst the results with solvation included were 5 kJ more negative for the UFF compared to the UAHF radii. The resulting equilibrium constants for the reaction range from 1.7 to 295 mol L<sup>-1</sup>. Although the lower end of the range for the calculated equilibrium constant is quite small for a reaction that was experimentally found to be irreversible, the reverse process comprises an overall third order reaction, second order in NO, which makes the reaction essentially irreversible at low NO concentrations. Furthermore, the reverse reaction rate also depends on the concentration of (SCN)<sub>2</sub>, a species which readily hydrolyses in aqueous solution, accounting for the experimental observation that the reaction is irreversible.

The rate equation second order in ONSCN could arise from several possible elementary reaction mechanisms. Firstly, the reaction could indeed involve a bimolecular interaction between two nitrosyl thiocyanate molecules, as written in Equation 4. Alternatively, the reaction could involve initial formation of either an ON(SCN)<sub>2</sub><sup>-</sup> or (ON)<sub>2</sub>SCN<sup>+</sup> intermediates, followed by their reaction with H<sub>2</sub>NO<sub>2</sub><sup>+</sup> and SCN<sup>-</sup>,

respectively, to produce NO and (SCN)<sub>2</sub>. Both alternate pathways, described in Equations 15-17 below, yield equivalent rate laws to Reaction 4.



$$r_4 = k_4 K_1^2 [\text{HNO}_2]^2 [\text{H}^+]^2 [\text{SCN}^-]^2 \quad (18)$$

$$r_{15} = k_{15} K_1 K_{13} [\text{HNO}_2]^2 [\text{H}^+]^2 [\text{SCN}^-]^2 \quad (19)$$

$$r_{17} = k_{17} K_1 K_{16} [\text{HNO}_2]^2 [\text{H}^+]^2 [\text{SCN}^-]^2 \quad (20)$$

The predicted equilibrium constant for ON(SCN)<sub>2</sub><sup>-</sup> ranges from 10<sup>-3</sup>-10<sup>-2</sup> L mol<sup>-1</sup> for the S-S isomer, to approximately 10<sup>-4</sup>-10<sup>-5</sup> L mol<sup>-1</sup> for the S-N-S geometry. Employing these values for *K*<sub>13</sub> necessitates that *k*<sub>15</sub> lie in the range of 10<sup>3</sup>-10<sup>6</sup> L<sup>2</sup> mol<sup>-2</sup> s<sup>-1</sup>. Nitrosation reactions similar to Reaction 15 typically exhibit rate constants with an upper limit of ~10<sup>4</sup> L<sup>2</sup> mol<sup>-2</sup> s<sup>-1</sup>, suggesting that Reaction 15 is a plausible mechanism for Pathway 2. However, it should be noted that nitrosation of ON(SCN)<sub>2</sub><sup>-</sup> could also result in formation of two ONSCN molecules, instead of NO and (SCN)<sub>2</sub>. Because Reaction 15 involves a crossing from the singlet to the triplet potential energy surface, the transition structure for this reaction cannot be investigated, and consequently, it is not possible to conclusively establish Reaction 15 as the mechanism for Pathway 2.

The same problem is encountered for the transition state for Reaction 4 proceeding directly through two ONSCN molecules. However, a transition state was identified for the reaction producing (SCN)<sub>2</sub> and the NO dimer, ONNO, for which the free energy was 156 kJ higher than the reactants, resulting in a negligible rate of this reaction. Formation of ONNO is highly unfavourable in both the gas and liquid phase, with the free energy change of Reaction 20 being on the order of 90 kJ in solution and 110 kJ in the gas phase. As such, the TS free energy for formation of ONNO from ONSCN is likely to be significantly higher than the minimum energy crossing point that connects singlet ONSCN and the reaction products.



Two isomers were identified for (ON)<sub>2</sub>SCN<sup>+</sup>, the first containing both ON groups bonded to the sulfur atom and the second containing one ON group bonded to sulfur and a second ON group bonded to nitrogen, hereafter denoted ONSCNNO<sup>+</sup>. In the gas phase, formation of ONSCNNO<sup>+</sup> is favoured over (ON)<sub>2</sub>SCN<sup>+</sup> by 32 kJ mol<sup>-1</sup>, however, (ON)<sub>2</sub>SCN<sup>+</sup> exhibits a higher solvation free energy, yielding similar aqueous reaction free energies for both species. In solution, formation of both (ON)<sub>2</sub>SCN<sup>+</sup> and ONSCNNO<sup>+</sup> is highly energetically unfavourable, with the predicted equilibrium constant for Reaction 16 ranging from 10<sup>-16</sup> to 10<sup>-23</sup> L<sup>2</sup> mol<sup>-2</sup> depending on the choice of solvent model. The large variation in the estimates for *K*<sub>16</sub> results from the differences in the solvation free energies computed with the UFF and UAHF radii, with UFF calculations yielding a solvation free energy for (ON)<sub>2</sub>SCN<sup>+</sup> which is 28 kJ mol<sup>-1</sup> more negative than those with the UAHF radii. Comparing Equations 18 and 20, it can be seen that to yield the same rate of reaction, the product *k*<sub>17</sub>*K*<sub>1</sub>*K*<sub>16</sub> must be equal to the

observed value of  $k_4 K_I^2$ . Employing the largest value of  $K_{16}$  computed quantum chemically, the value of  $k_{17}$  required to yield the overall rate constant determined experimentally is  $\sim 10^{16} \text{ L mol}^{-1} \text{ s}^{-1}$ . This rate constant is six orders of magnitude greater than the diffusion controlled limit for bimolecular reactions in aqueous media (approx  $10^{10} \text{ L mol}^{-1} \text{ s}^{-1}$ )<sup>35</sup>, and it is therefore concluded that the second order pathway does not involve an  $(\text{ON})_2\text{SCN}^+$  intermediate. Table 6 summarises the results for Pathway 2 (note that the results for Reaction 13 have been presented in Table 5 above).

**Table 6: Calculated Gibbs free energies and equilibrium constants of Reactions 4 and**

**16**

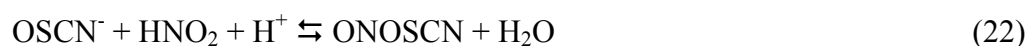
	<b>Reaction</b>	
<b>Method<sup>a</sup></b>	<b>4</b>	<b>16</b>
$\Delta G_{298}^\circ$ CBS-QB3 (UFF)	-14.1	96.7
$\Delta G_{298}^\circ$ G3B3 (UFF)	-6.1	87.4
$\Delta G_{298}^\circ$ CBS-QB3 (UAHF)	-9.4	128.3
$\Delta G_{298}^\circ$ G3B3 (UAHF)	-1.3	119.1
$K_{\text{calc}}$ (lower)	$1.72 \text{ mol L}^{-1}$	$3.2 \times 10^{-23} \text{ L}^2 \text{ mol}^{-2}$
$K_{\text{calc}}$ (upper)	$296 \text{ mol L}^{-1}$	$4.7 \times 10^{-16} \text{ L}^2 \text{ mol}^{-2}$
$K_{\text{expt}}$	irreversible	N/A

### 6.3.4 Decomposition Pathway 3

The third decomposition pathway for ONSCN involves reactions between ONSCN and the hydrolysis products of (SCN)<sub>2</sub>, itself formed as a product of ONSCN decomposition according to Reactions 1-4. (SCN)<sub>2</sub> hydrolyses to produce HOSCN according to Reaction 5, with experimentally determined equilibrium constants reported in the range of  $6 \times 10^{-4} - 4 \times 10^{-3} \text{ M}^2$ .<sup>14,17</sup> HOSCN is proposed to undergo subsequent nitrosation via ONSCN, producing ONOSCN (Reaction 6), with an experimental equilibrium constant of  $0.25 \text{ mol L}^{-1}$ . This equilibrium constant was estimated during the kinetic fitting process, and as such, exhibits large uncertainty, because changes to this value could potentially be offset by variations in other model parameters (i.e.  $K_7$ ). The computed equilibrium constants for ONOSCN formation range from  $3 \times 10^{-4} \text{ mol L}^{-1}$  at the G3B3//B3LYP/6-31+G(d,p)-PCM(UAHF) level, to  $0.8 \text{ mol L}^{-1}$  at the CBS-QB3//B3LYP/6-31+G(d,p)-PCM(UFF) level. This large discrepancy arises as a result of the difference in the solvation free energies of the species in the reaction computed with the different solvent models. The higher of the calculated values is in close agreement with that determined experimentally, suggesting that formation of ONOSCN is indeed plausible.

The next proposed step in Pathway 3 involves the homolysis of ONOSCN, producing nitric oxide and OSCN radicals (Reaction 7). Compared to the homolytic fission of ONSCN, which exhibits a free energy change of approximately 80 kJ, formation of NO and OSCN from ONOSCN is much more favourable, with a computed free energy change between 5 and 14 kJ, depending on the choice of solvent model. This corresponds to values of  $K_7$  ranging from  $3 \times 10^{-3}$  to  $0.15 \text{ mol L}^{-1}$ , which is slightly larger than that predicted experimentally ( $K_{7, \text{expt}} = 3 \times 10^{-4} \text{ mol L}^{-1}$ ). The formation and

decomposition of ONOSCN may also contribute to nitric oxide formation in biological systems. HOSCN, produced via the oxidation of thiocyanate ions by a variety of oxidants<sup>36</sup>, is a weak acid ( $pK_a = 4.85$ )<sup>37</sup>, and as such, at physiological pH will convert almost exclusively to OSCN<sup>-</sup> ions. Nitrosation of OSCN<sup>-</sup> is highly favourable (Reaction 22) with a calculated equilibrium constant ranging from  $6 \times 10^5$  to  $9 \times 10^7 \text{ L}^2 \text{ mol}^{-2}$ , many orders of magnitude higher than the corresponding value for ONSCN ( $29 \text{ L}^2 \text{ mol}^{-2}$ ).



In the experimental study (Chapter 5) OSCN radicals were proposed to undergo dimerisation and hydrolysis, forming HOSCN and HO<sub>2</sub>SCN respectively. This reaction was previously proposed to occur during the oxidation of SCN<sup>-</sup> by ClO<sub>2</sub><sup>38</sup>. Reaction 8 comprises a third order process, and is hence unlikely to constitute the elementary reaction mechanism. Rather, OSCN could be expected to dimerise, with subsequent hydrolysis of the OSCN dimer. Three different dimer structures were considered, one containing an S-S bond, the second containing an S-O-S linkage and the third comprising an S-O-O-S structure, as shown in Figure 5:

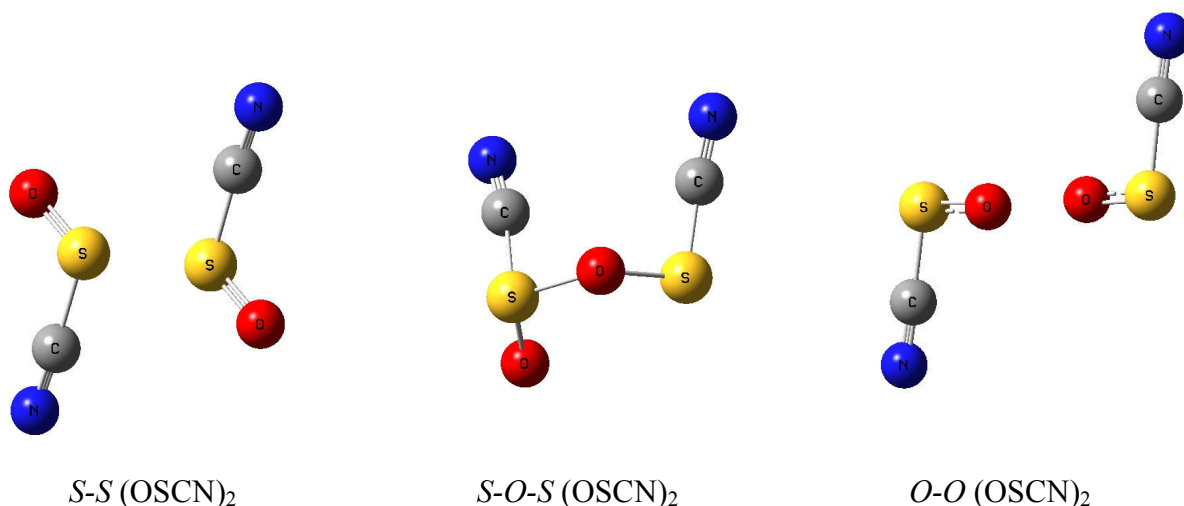


**Figure 5: Geometries of different OSCN dimers optimised at the B3LYP/6-31+G(d,p)-PCM(UFF) level**

The *S-O-S* isomer (denoted  $NCS(=O)OSCN$ ) exhibits the lowest free energy of the  $(OSCN)_2$  isomers, with formation of this species from OSCN according to Reaction 23 having a free energy change of -30 to -37 kJ depending on the calculation method. Similar results were obtained with both solvent models, however, the gas phase G3B3 reaction free energy is approximately 7 kJ more negative than that computed using CBS-QB3. The corresponding equilibrium constant ranged from  $2 \times 10^5$  to  $3 \times 10^6$  L mol<sup>-1</sup>, indicating that the formation of the dimer is essentially irreversible.



Hydrolysis of  $NCS(=O)OSCN$  constitutes the final reaction step in Pathway 3 and produces HOSCN and HO<sub>2</sub>SCN. The latter is expected to undergo further hydrolysis

and disproportionation reactions to ultimately yield  $\text{SO}_4^{2-}$  and  $\text{HCN}^{17,38-41}$ . Reaction 24 also exhibits a favourable Gibbs free energy change, ranging from -20 to -30 kJ depending on the choice of solvent model. As such, formation and subsequent decomposition of ONOSCN represents a thermodynamically feasible reaction pathway, contributing to the formation of NO during ONSCN decomposition. Table 7 summarises the results for Pathway 3.



**Table 7: Calculated Gibbs free energies and equilibrium constants for Pathway 3. All energies in kJ**

	<i>Reaction</i>		
<i>Method</i>	<i>5</i>	<i>6</i>	<i>7</i>
$\Delta G_{298}^{\circ}$ CBS-QB3 (UFF)	31.9	0.6	4.7
$\Delta G_{298}^{\circ}$ G3B3 (UFF)	34.2	6.1	9.2
$\Delta G_{298}^{\circ}$ CBS-QB3 (UAHF)	20.7	14.8	9.6
$\Delta G_{298}^{\circ}$ G3B3 (UAHF)	23.0	20.2	14.1
$K_{\text{calc}}$ (lower)	$1.0 \times 10^{-6}$ $\text{mol}^2 \text{L}^{-2}$	$2.8 \times 10^{-4}$ $\text{mol L}^{-1}$	$3.4 \times 10^{-3}$ $\text{mol L}^{-1}$
$K_{\text{calc}}$ (upper)	$2.4 \times 10^{-4}$ $\text{mol}^2 \text{L}^{-2}$	0.77 $\text{mol L}^{-1}$	0.15 $\text{mol L}^{-1}$
$K_{\text{expt}}$	$6 \times 10^{-4} - 4 \times 10^{-3}$ $\text{mol}^2 \text{L}^{-2}$	0.25 $\text{mol L}^{-1}$	$3 \times 10^{-4}$ $\text{mol L}^{-1}$
<i>Method</i>	<i>22</i>	<i>23</i>	<i>24</i>
$\Delta G_{298}^{\circ}$ CBS-QB3 (UFF)	-43.3	-29.7	-21.9
$\Delta G_{298}^{\circ}$ G3B3 (UFF)	-45.2	-36.2	-20.3
$\Delta G_{298}^{\circ}$ CBS-QB3 (UAHF)	-33.0	-30.7	-31.1
$\Delta G_{298}^{\circ}$ G3B3 (UAHF)	-35.0	-37.2	-29.4
$K_{\text{calc}}$ (lower)	$6.1 \times 10^5$ $\text{L}^2 \text{mol}^{-2}$	$1.6 \times 10^5$ $\text{L mol}^{-1}$	$3.6 \times 10^3$ $\text{mol L}^{-1}$
$K_{\text{calc}}$ (upper)	$8.5 \times 10^7$ $\text{L}^2 \text{mol}^{-2}$	$3.3 \times 10^6$ $\text{L mol}^{-1}$	$2.8 \times 10^5 \text{ mol}$ $\text{L}^{-1}$
$K_{\text{expt}}$	N/A	irreversible	irreversible

### 6.3.5 Formation of N<sub>2</sub>O

Traces of N<sub>2</sub>O were observed during the decomposition of ONSCN. It was hypothesised that the N<sub>2</sub>O could originate from the hydrolysis of either ONSCN or ONCN to produce ONH, which yields N<sub>2</sub>O upon dimerisation and water elimination<sup>42</sup> (Reactions 25-28).



Formation of ONCN according to Reaction 25 was calculated to be energetically unfavourable, with a predicted equilibrium constant ranging from  $2 \times 10^{-5}$  to  $1 \times 10^{-4}$  mol L<sup>-1</sup>, indicating that only a small fraction of HCN will be converted into ONCN. The hydrolysis of ONCN to produce ONH, however, exhibits a large equilibrium constant, which ranges from 400 to  $3 \times 10^7$  depending on the calculation method employed. The large discrepancy arises as a result of the difference in the calculated solvation free energy of HOCN and ONH with the UAHF and UFF radii. Owing to the large equilibrium constant for Reaction 26, it is possible that this reaction could contribute to N<sub>2</sub>O formation. Hydrolysis of ONSCN, however, was calculated to be highly energetically unfavourable, with the calculated Gibbs free energy change for

Reaction 27 ranging from 97 to 120 kJ. As such, Reaction 27 does not contribute to ONH formation. Table 8 summarises the thermochemistry of Reactions 25-27:

**Table 8: Calculated Gibbs free energies and equilibrium constants for Reactions 23-**

**25**

<i>Method</i>	<i>Reaction</i>		
	<i>25</i>	<i>26</i>	<i>27</i>
$\Delta G_{298}^{\circ}$ CBS-QB3 (UFF)	22.8	-16.9	116.5
$\Delta G_{298}^{\circ}$ G3B3 (UFF)	27.5	-15.1	119.9
$\Delta G_{298}^{\circ}$ CBS-QB3 (UAHF)	25.1	-43.0	97.2
$\Delta G_{298}^{\circ}$ G3B3 (UAHF)	29.8	-41.3	100.6
$K_{\text{calc}}$ (lower)	$5.9 \times 10^{-6} \text{ mol L}^{-1}$	$4.5 \times 10^2 \text{ mol L}^{-1}$	$9.6 \times 10^{-22} \text{ mol L}^{-1}$
$K_{\text{calc}}$ (upper)	$1.0 \times 10^{-4} \text{ mol L}^{-1}$	$3.5 \times 10^7 \text{ mol L}^{-1}$	$9.3 \times 10^{-18} \text{ mol L}^{-1}$

## 6.4 Conclusions

Quantum chemistry calculations were performed to investigate the thermodynamic feasibility of the ONSCN decomposition mechanism proposed on the basis of kinetic experiments. The calculation procedure involved computing the gas phase reaction free energy with the CBS-QB3 and G3B3 compound methods, and combining this result with solvation free energies calculated using DFT methods by means of a thermochemical cycle. To ascertain the accuracy of the calculations, the performance of a variety of solvation models was evaluated by comparing the computed reaction free energies to experimental results for six reactions with experimentally established equilibrium constants. The PCM model yielded the best agreement with the experimental data set, with a mean absolute deviation ranging from 6-8 kJ, depending on the choice of atomic radii and the method employed for computing the gas phase reaction free energies. The calculations confirmed that the first decomposition pathway for ONSCN proceeds via the reaction between  $\text{SCN}^-$  and ONSCN, yielding  $(\text{SCN})_2^-$ , with subsequent oxidation of this species by ONSCN. The formation of SCN radicals from ONSCN homolysis was shown to be energetically unfeasible, and does not contribute to ONSCN decomposition. The decomposition pathway second order in ONSCN could proceed via reaction of two ONSCN molecules, or, alternatively, could involve initial formation of  $\text{ON}(\text{SCN})_2^-$  and its subsequent nitrosation. Formation of ONOSCN was demonstrated to be plausible, with dissociation of this species into NO and OSCN radicals exhibiting a low free energy change relative to the homolysis of ONSCN. The ensuing dimerisation and hydrolysis of OSCN was shown to be thermodynamically favourable. Production of  $\text{N}_2\text{O}$  via hydrolysis of ONCN appears to

be feasible, however, the corresponding reaction of ONSCN is highly energetically unfavourable.

## 6.5 References

1. Rayson, M. S.; Mackie, J. C.; Kennedy, E. M.; Dlugogorski, B. Z., Experimental study of decomposition of aqueous nitrosyl thiocyanate. *Inorg. Chem.* **2011**, *50* (16), 7440-7452.
2. Frisch, M. J.; Trucks, G. W.; Schlegel, H. B.; Scuseria, G. E.; Robb, M. A.; Cheeseman, J. R.; Montgomery, J., J. A.; Vreven, T. K., K. N.; Burant, J. C.; Millam, J. M.; Iyengar, S. S.; Tomasi, J.; Barone, V.; Mennucci, B.; Cossi, M.; Scalmani, G.; Kudin, K. N.; Rega, N.; Petersson, G. A.; Nakatsuji, H.; Hada, M.; Ehara, M.; Toyota, K.; Fukuda, R.; Hasegawa, J.; Ishida, M.; Nakajima, T.; Honda, Y.; Kitao, O.; Nakai, H.; Klene, M.; Li, X. K., J. E; Hratchian, H. P.; Cross, J. B.; Bakken, V.; Adamo, C.; Jaramillo, J.; Gomperts, R.; Stratmann, R. E.; Yazyev, O.; Austin, A. J.; Cammi, R.; Pomelli, C.; Ochterski, J. W.; Ayala, P. Y.; Morokuma, K.; Voth, G. A.; Salvador, P.; Dannenberg, J. J.; Zakrzewski, V. G.; Dapprich, S.; Daniels, A. D.; Strain, M. C.; Farkas, O.; Malick, D. K.; Rabuck, A. D.; Raghavachari, K.; Foresman, J. B.; Ortiz, J. V.; Cui, Q.; Baboul, A. G.; Clifford, S.; Cioslowski, J.; Stefanov, B. B.; Liu, G.; Liashenko, A.; Piskorz, P.; Komaromi, I.; Martin, R. L.; Fox, D. J.; Keith, T.; Al-Laham, M. A.; Peng, C. Y.; Nanayakkara, A.; Challacombe, M.; Gill, P. M. W.; Johnson, B.; Chen, W.; Wong, M. W.; Gonzalez, C.; Pople, J. A. *Gaussian 03, Revision B.05*, Gaussian Inc: Pittsburgh PA, 2003.
3. Frisch, M. J. T., G. W.; Schlegel, H. B.; Scuseria, G. E.; Robb, M. A.; Cheeseman, J. R.; Scalmani, G.; Barone, V.; Mennucci, B.; Petersson, G. A.; Nakatsuji, H.; Caricato, M.; Li, X.; Hratchian, H. P.; Izmaylov, A. F.; Bloino,

- J.; Zheng, G.; Sonnenberg, J. L.; Hada, M.; Ehara, M.; Toyota, K.; Fukuda, R.; Hasegawa, J.; Ishida, M.; Nakajima, T.; Honda, Y.; Kitao, O.; Nakai, H.; Vreven, T.; Montgomery, Jr., J. A.; Peralta, J. E.; Ogliaro, F.; Bearpark, M.; Heyd, J. J.; Brothers, E.; Kudin, K. N.; Staroverov, V. N.; Kobayashi, R.; Normand, J.; Raghavachari, K.; Rendell, A.; Burant, J. C.; Iyengar, S. S.; Tomasi, J.; Cossi, M.; Rega, N.; Millam, N. J.; Klene, M.; Knox, J. E.; Cross, J. B.; Bakken, V.; Adamo, C.; Jaramillo, J.; Gomperts, R.; Stratmann, R. E.; Yazyev, O.; Austin, A. J.; Cammi, R.; Pomelli, C.; Ochterski, J. W.; Martin, R. L.; Morokuma, K.; Zakrzewski, V. G.; Voth, G. A.; Salvador, P.; Dannenberg, J. J.; Dapprich, S.; Daniels, A. D.; Farkas, Ö.; Foresman, J. B.; Ortiz, J. V.; Cioslowski, J.; Fox, D. J. *Gaussian09, Revision C.01*, Gaussian, Inc.: Wallingford CT, 2009.
4. Baboul, A. G.; Curtiss, L. A.; Redfern, P. C.; Raghavachari, K., Gaussian-3 theory using density functional geometries and zero-point energies. *J. Chem. Phys.* **1999**, *110* (16), 7650-7657.
  5. Montgomery, J. J. A.; Frisch, M. J.; Ochterski, J. W.; Petersson, G. A., A complete basis set model chemistry. VI. Use of density functional geometries and frequencies. *J. Chem. Phys.* **1999**, *110* (6), 2822-2827.
  6. Ho, J.; Coote, M., A universal approach for continuum solvent  $pK_a$  calculations - are we there yet? *Theor. Chem. Acc.* **2010**, *125* (1), 3-21.
  7. Tissandier, M. D.; Cowen, K. A.; Feng, W. Y.; Gundlach, E.; Cohen, M. H.; Earhart, A. D.; Coe, J. V.; Tuttle, T. R., The proton's absolute aqueous enthalpy and gibbs free energy of solvation from cluster-ion solvation data. *J. Phys. Chem. A* **1998**, *102* (40), 7787-7794.

8. Camaioni, D. M.; Schwerdtfeger, C. A., Comment on accurate experimental values for the free energies of hydration of  $H^+$ ,  $OH^-$ , and  $H_3O^+$ . *J. Phys. Chem. A* **2005**, *109* (47), 10795-10797.
9. Tomasi, J.; Mennucci, B.; Cances, E., The IEF version of the PCM solvation method: an overview of a new method addressed to study molecular solutes at the QM ab initio level. *J. Mol. Struct.: THEOCHEM* **1999**, *464* (1-3), 211-226.
10. Rappe, A. K.; Casewit, C. J.; Colwell, K. S.; Goddard, W. A.; Skiff, W. M., UFF, a full periodic table force field for molecular mechanics and molecular dynamics simulations. *J. Am. Chem. Soc.* **1992**, *114* (25), 10024-10035.
11. Barone, V.; Cossi, M.; Tomasi, J., A new definition of cavities for the computation of solvation free energies by the polarizable continuum model. *J. Chem. Phys.* **1997**, *107* (8), 3210-3221.
12. Marenich, A. V.; Cramer, C. J.; Truhlar, D. G., Universal solvation model based on solute electron density and on a continuum model of the solvent defined by the bulk dielectric constant and atomic surface tensions. *J. Phys. Chem. B* **2009**, *113* (18), 6378-6396.
13. Stedman, G.; Whincup, P. A. E., The equilibrium constant for the formation of nitrosyl thiocyanate in aqueous solution. *J. Chem. Soc.* **1963**, 5796-5799.
14. Nagy, P.; Lemma, K.; Ashby, M. T., Kinetics and mechanism of the comproportionation of hypothiocyanous acid and thiocyanate to give thiocyanogen in acidic aqueous solution. *Inorg. Chem.* **2007**, *46* (1), 285-292.
15. Morgan, T. D. B.; Stedman, G.; Whincup, P. A. E., The ionization constant of thiocyanic acid. *J. Chem. Soc.* **1965**, 4813-22.
16. Crowell, T. I.; Hankins, M. G., Hydrolysis of thiocyanic acid. I. Dependence of rate on acidity function. *J. Phys. Chem.* **1969**, *73* (5), 1380-3.



17. Barnett, J. J.; McKee, M. L.; Stanbury, D. M., Acidic aqueous decomposition of thiocyanogen. *Inorg. Chem.* **2004**, *43* (16), 5021-5033.
18. Barnett, J. J.; Stanbury, D. M., Formation of trithiocyanate in the oxidation of aqueous thiocyanate. *Inorg. Chem.* **2002**, *41* (2), 164-166.
19. Elliot, A. J.; Sopchyshyn, F. C., A pulse radiolysis study of iodide radical ion ( $I_2^-$ ) and thiocyanate radical ion ( $(SCN)_2^-$ ) in aqueous solutions over the temperature range 15-90 °C. *Int. J. Chem. Kinet.* **1984**, *16* (10), 1247-56.
20. Milosavljevic, B. H.; LaVerne, J. A., Pulse radiolysis of aqueous thiocyanate solution. *J. Phys. Chem. A* **2005**, *109* (1), 165-168.
21. Doherty, A. M.; Garley, M. S.; Haine, N.; Stedman, G., Formation of an adduct between thiocyanate ion and nitrosyl thiocyanate. *J. Chem. Soc., Dalton Trans.* **1997**, 2163-2166.
22. Bazsa, G.; Epstein, I. R., Autocatalysis and bistability in the reaction between nitric acid and thiocyanate. *Int. J. Chem. Kinet.* **1985**, *17*, 601-612.
23. Jones, E.; Munkley, C. G.; Phillips, E. D.; Stedman, G., Kinetics and equilibria in the nitric acid-nitrous acid-sodium thiocyanate system. *J. Chem. Soc., Dalton Trans.* **1996**, 1915-1920.
24. Covington, A. K.; Matheson, R. A., A Raman study of the ionization of thiocyanic acid. *J. Solution Chem.* **1976**, *5* (11), 781-6.
25. Tribalat, S.; Caldero, J. M., Dissociation constant of thiocyanic acid in water. *Bull. Soc. Chim. Fr.* **1966**, (2), 774-5.
26. Cossi, M.; Rega, N.; Scalmani, G.; Barone, V., Energies, structures, and electronic properties of molecules in solution with the C-PCM solvation model. *J. Comput. Chem.* **2003**, *24* (6), 669-681.

27. Becke, A. D., Density-functional thermochemistry. III. The role of exact exchange. *J. Chem. Phys.* **1993**, 98 (7), 5648-5652.
28. Lee, C.; Yang, W.; Parr, R. G., Development of the Colle-Salvetti correlation-energy formula into a functional of the electron density. *Phys. Rev. B.* **1988**, 37 (2), 785-789.
29. Zhao, Y.; Schultz, N. E.; Truhlar, D. G., Design of density functionals by combining the method of constraint satisfaction with parametrization for thermochemistry, thermochemical kinetics, and noncovalent interactions. *J. Chem. Theory Comput.* **2006**, 2 (2), 364-382.
30. Clark, T.; Chandrasekhar, J.; Spitznagel, G. W.; Schleyer, P. V. R., Efficient diffuse function-augmented basis sets for anion calculations. III. The 3-21+G basis set for first-row elements, Li-F. *J. Comput. Chem.* **1983**, 4 (3), 294-301.
31. Ditchfield, R.; Hehre, W. J.; Pople, J. A., Self-consistent molecular-orbital methods. IX. An extended gaussian-type basis for molecular-orbital studies of organic molecules. *J. Chem. Phys.* **1971**, 54 (2), 724-728.
32. Pasinszki, T.; Westwood, N. P. C., Open-chain and ring isomers of CN<sub>2</sub>OS: ab initio study of structures and stabilities. *J. Chem. Soc., Faraday Trans.* **1996**, 92 (3), 333-41.
33. Chen, H.-L.; Zhu, R.; Chen, H.-T.; Li, H.-J.; Ju, S.-P., Ab Initio study on mechanisms and kinetics for reaction of NCS with NO. *J. Phys. Chem. A* **2008**, 112 (24), 5495-5501.
34. Czapski, G.; Holcman, J.; Bielski, B. H. J., Reactivity of nitric oxide with simple short-lived radicals in aqueous solution. *J. Am. Chem. Soc.* **1994**, 116, 11465-11469.

35. Atkins, P.; de Paula, J., *Elements of Physical Chemistry (5ed)*. Oxford University Press: New York, 2009.
36. Ashby, M. T.; Carlson, A. C.; Scott, M. J., Redox buffering of hypochlorous acid by thiocyanate in physiologic fluids. *J. Am. Chem. Soc.* **2004**, *126* (49), 15976-15977.
37. Nagy, P.; Jameson, G. N. L.; Winterbourn, C. C., Kinetics and mechanisms of the reaction of hypothiocyanous acid with 5-thio-2-nitrobenzoic acid and reduced glutathione. *Chem. Res. Toxicol.* **2009**, *22* (11), 1833-1840.
38. Figlar, J. N.; Stanbury, D. M., Kinetics and a revised mechanism for the autocatalytic oxidation of SCN<sup>-</sup> by ClO<sub>2</sub>. *J. Phys. Chem. A* **1999**, *103* (29), 5732-5741.
39. Chinake, C. R.; Mambo, E.; Simoyi, R. H., Complex oligooscillatory behavior in the reaction of chlorite with thiocyanate. *J. Phys. Chem.* **1994**, *98* (11), 2908-2916.
40. Figlar, J. N.; Stanbury, D. M., Thiocyanogen as an intermediate in the oxidation of thiocyanate by hydrogen peroxide in acidic aqueous solution. *Inorg. Chem.* **2000**, *39* (22), 5089-5094.
41. Stedman, G.; Whincup, P. A. E., Oxidation of metal thiocyanates by nitrous and nitric acids. Part I. Products. *J. Chem. Soc.* **1969**, 1945-1948.
42. Fehling, C.; Friedrichs, G., Dimerization of HNO in aqueous solution: An interplay of solvation effects, fast acid-base equilibria, and intramolecular hydrogen bonding? *J. Am. Chem. Soc.* **2011**, *133* (44), 17912-17922.



## **CHAPTER 7**

**Solubility of nitric oxide in concentrated solutions of ammonium and sodium nitrates**

## Table of Contents

7.1	Introduction	195
7.2	Experimental	199
7.3	Results and discussion	201
7.4	Conclusions	214
7.5	References	215

## 7.1 Introduction

The decomposition of nitrous acid to produce nitric oxide is an unwanted side reaction accompanying the nitrosation of ammonia, which is employed in the sensitisation of emulsion explosives in a process known as chemical gassing<sup>1</sup>.  $\text{NO}_x$  fumes originating from the chemical gassing process pose a hazard to explosive users, with inhalation of these gases resulting in serious respiratory problems. To determine the contribution of nitrous acid decomposition to  $\text{NO}_x$  formation during the explosive sensitisation process, it is necessary to relate the aqueous nitric oxide concentration predicted in kinetic models to an observable gas phase concentration (or partial pressure). For this purpose, it is essential to know or be able to predict the solubility of NO under conditions of practical interest, specifically, in ammonium nitrate solutions of various concentrations at temperatures up to 50 °C.

The solubility of gasses in salt solutions can vary significantly in comparison to their solubility in pure water, typically decreasing with increasing salt concentration<sup>2</sup>. The effect of electrolyte concentration on gas solubility, known as the salting out effect, is empirically described by the Sechenov equation<sup>3,4</sup>:

$$\log\left(\frac{k_{H,o}}{k_H}\right) = k_s C_s \quad (1)$$

$$k_H = \frac{P_{(g)}}{C_{(aq)}} \quad (2)$$

where  $k_{H,o}$  is the Henry's constant of the gas in pure water ( $\text{mol L}^{-1} \text{ bar}^{-1}$ )<sup>5</sup>,  $k_H$  is the solubility of the gas in the electrolyte ( $\text{mol L}^{-1} \text{ bar}^{-1}$ ),  $k_s$  ( $\text{L mol}^{-1}$ ) is known as the salting out parameter,  $C_s$  is the concentration of salt ( $\text{mol L}^{-1}$ ),  $P_{(g)}$  is the partial pressure of the gas (bar) and  $C_{(aq)}$  is the equilibrium concentration of gas in the aqueous phase ( $\text{mol L}^{-1}$ ). The constant  $k_s$  depends on the identity of the electrolyte and the dissolved gas, and is slightly affected by temperature<sup>6</sup>. The partitioning of a species between the gas and aqueous phases is related to the Gibbs free energy of solvation according to Equation 3<sup>7-11</sup>.

$$\Delta G_S = -R_g T \ln(k_H) \quad (3)$$

where  $R_g$  is the gas constant ( $\text{J mol}^{-1} \text{ K}^{-1}$ ),  $T$  is the absolute temperature (K),  $k_H$  is the Henry's constant ( $\text{mol L}^{-1} \text{ bar}^{-1}$ ) and  $\Delta G_S$  is the Gibbs free energy of solvation employing standard states of 1 bar for the gas phase and 1  $\text{mol L}^{-1}$  for the aqueous phase. Henry's constant is related to the enthalpy and entropy of solvation according to Equation 4.

$$\ln(k_H) = -\frac{\Delta H_S}{R_g T} + \frac{\Delta S_S}{R_g} \quad (4)$$

As can be seen in Equation 4, plotting the natural logarithm of the Henry's constant yields a slope equal to  $-\Delta H_S/R_g$  and an intercept equal to  $-\Delta S_S/R_g$ .

For equilibrium to exist, the chemical potential of a dissolved species is equal to the chemical potential of that species in the gas phase. As such, for a fixed gas phase



partial pressure, the chemical potential of the equilibrium concentration of gas dissolved in a salt solution is equal to the chemical potential of the gas at its equilibrium concentration in pure water. Equation 5 expresses this situation in terms of the activities<sup>3</sup>:

$$a_i = a_i^o \quad (5)$$

where  $a_i$  is the activity of species  $i$  in a multicomponent solution and  $a_i^o$  is the activity of the species dissolved in pure water (i.e. a binary solution). The activity can be expressed in terms of the product of an activity coefficient and a species concentration. If the gas phase partial pressure is assumed to be 1 bar, then the dissolved gas concentration is equal to the Henry's constant, yielding Equation 6:

$$y_i k_H = y_i^o k_{H,o} \quad (6)$$

where  $y_i$  is the activity coefficient of the dissolved gas in salt solution and  $y_i^o$  is the activity coefficient in pure water. The solubility of dissolved gases is typically very low, and as such, the activity coefficient  $y_i^o$  is assumed to be 1 (the activity coefficient approaches unity as the species concentration approaches zero). Equation 1 can then be written in terms of the activity coefficient:

$$\log\left(\frac{k_{H,o}}{k_H}\right) = \log(y_i) = k_s C_s \quad (7)$$

As demonstrated in Equation 7, the activity coefficient of a dissolved gas in a salt solution can be determined by examining the ratio of the gaseous solubility in the salt solution to that in pure water, and plotting the log of this ratio yields a straight line with a slope equal to  $k_s$ . Knowledge of the activity coefficient of NO is crucial for the prediction of the apparent equilibrium constant for the decomposition of nitrous acid in concentrated salt solutions, which forms the subject of the following chapter.

The solubility of NO in relatively dilute (up to  $1 \text{ mol L}^{-1}$ ) NaCl and  $\text{HClO}_4$  has been previously determined by Armor (1974)<sup>12</sup> and found to be significantly lower than in water, however, no data exist in the literature for the solubility of NO in concentrated  $\text{NH}_4\text{NO}_3$  solutions. In addition to the effect of salt concentration, the solubility of gases in solution is highly temperature dependent. Whilst the temperature dependence of NO solubility in water appears to be reasonably well established<sup>13</sup>, the effect of salt concentration on the temperature dependence is unclear. As such, the aim of this chapter is to quantify the effect of temperature and concentration of ammonium nitrate salt on the solubility of nitric oxide. A limited number of experiments were also performed with  $\text{NaNO}_3$  solutions to provide data on the activity coefficient required for Chapter 8.

## 7.2 Experimental

Saturated solutions of nitric oxide (NO) were generated by first degassing the target solution with  $\text{N}_2$  to remove oxygen, prior to bubbling with NO generated via the reduction of nitrous acid by ascorbate<sup>14</sup>. The apparatus employed to generate the NO solutions consisted of a 50 mL reaction flask, with the inlet connected to a supply of high purity nitrogen. The reactor was filled with 40 mL of a solution containing approximately  $0.35 \text{ mol L}^{-1}$  ascorbic acid (Sigma Aldrich) and  $0.7 \text{ mol L}^{-1}$   $\text{HClO}_4$ , prior to purging the system of air using  $\text{N}_2$ . A steady flow of NO was initiated by adding a 25 % solution of sodium nitrite dropwise to the reactor containing ascorbic acid, via a syringe inserted through a rubber stopper. The NO flowed through a scrubber containing a  $0.1 \text{ mol L}^{-1}$  NaOH solution to trap any traces of  $\text{NO}_2$  formed in the first reactor, before bubbling through the target solution contained within a 10 mL reaction flask with a septum side port. The reaction flask containing the salt solution was placed in a water bath at the desired reaction temperature, and the NO allowed to bubble through the solution for a period of approximately 20 min. Over this time, 0.7 L of NO was produced, corresponding to an average flow rate of  $35 \text{ cm}^3 \text{ min}^{-1}$ .

After half of the NO had been produced (i.e., 10 min), a 0.5 mL sample of NO saturated solution was withdrawn from the reactor by means of a gas tight syringe. The NO solution was injected into a second reactor that was continually purged with nitrogen gas, with the outlet connected to the Thermo 42i-HL nitric oxide analyser. This enabled the total amount of NO contained in the solution to be determined, allowing calculation of the NO solubility at a particular ammonium nitrate concentration. A second sample of solution was taken and analysed with the same method just before the production of

NO ceased. Comparison of the concentration determined in the two samples taken after different exposure times provided confirmation that the solutions were indeed saturated with NO, as identical concentrations were determined. Calibration of the nitric oxide analyzer was achieved with a 1000 ppm calibration gas obtained from Coregas Pty Ltd.

Figure 1 plots the output from the  $\text{NO}_x$  analyser for a typical experiment.

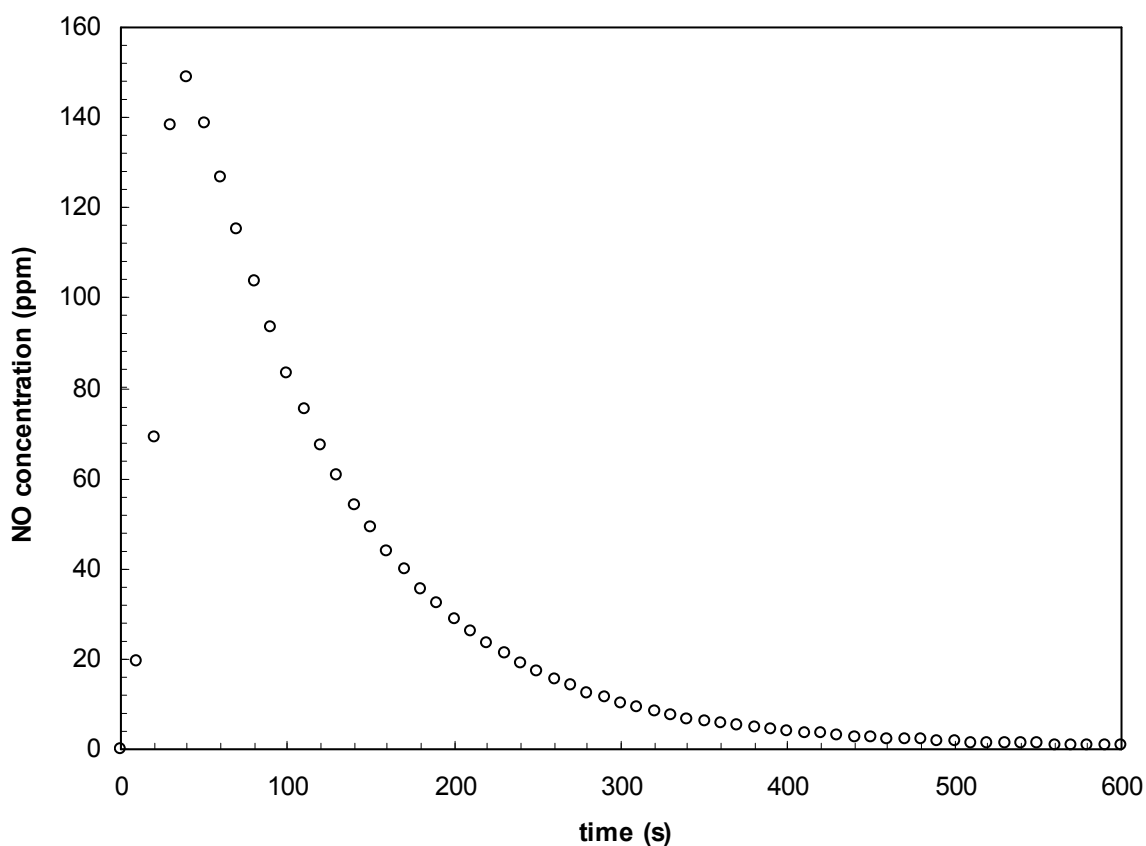


***Figure 1:  $\text{NO}_x$  analyser output for typical experiment***

### 7.3 Results and discussion

In order to relate the gas phase NO concentration observed during nitrous acid decomposition in sodium and ammonium nitrate solutions to the aqueous NO concentration, it was first necessary to determine the effect of the salt concentration on the NO solubility. The solubility of NO in salt solutions was determined at concentrations ranging from 0 to 10 mol L<sup>-1</sup> and from 0 to 7.5 mol L<sup>-1</sup> for ammonium and sodium nitrate, respectively. The upper limits of these ranges are approaching the saturation concentrations for solubility of ammonium nitrate and sodium nitrate in water at 25 °C, and as such, it was not possible to extend the measurements to higher concentrations.

The solubility of NO in water at 25 °C was ascertained to be  $1.93 \pm 0.05$  mol L<sup>-1</sup> bar<sup>-1</sup>, in excellent agreement with the prior determinations of  $1.92 \pm 0.03$  mol L<sup>-1</sup> bar<sup>-1</sup> by Zacharia and Deen (2005)<sup>15</sup> and  $1.93 \pm 0.06$  mol L<sup>-1</sup> bar<sup>-1</sup> by Armor (1974)<sup>12</sup>. As predicted from Equation 1, the solubility of nitric oxide was observed to decrease significantly with increasing concentrations of sodium and ammonium nitrate. Plots of  $\log(k_{H,o}/k_H)$  versus salt concentration were observed to be linear, with salting out parameters  $k_{\text{NH}_4\text{NO}_3}$  and  $k_{\text{NaNO}_3}$  determined to be 0.052 L mol<sup>-1</sup> and 0.104 L mol<sup>-1</sup> respectively, at 25 °C. The larger slope for  $\text{NaNO}_3$  indicates that the effect of  $\text{NaNO}_3$  on the NO solubility is significantly more pronounced than that of  $\text{NH}_4\text{NO}_3$ . Similar trends have been observed for a variety of other gases, for which in the presence of a common anion, the sodium salt exhibits a significantly larger effect on the gas solubility compared to that of the ammonium salt<sup>16,17</sup>. The ratio  $k_{H,o}/k_H$  is equal to the activity coefficient, and as such, the model for the solubility can be employed to determine the

activity coefficient of NO at different salt concentrations. Figure 2 plots  $\log(k_{H,o}/k_H)$  versus salt concentration, for both  $\text{NaNO}_3$  and  $\text{NH}_4\text{NO}_3$  at 25 °C.

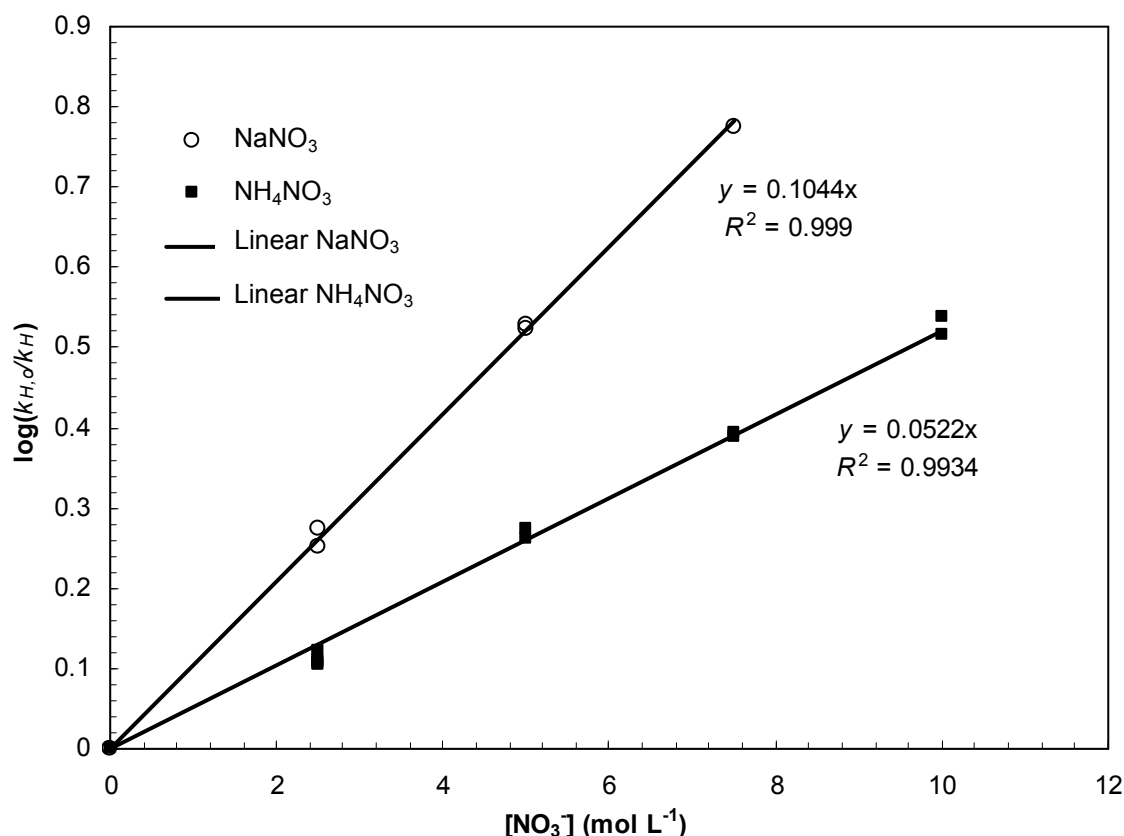


**Figure 2: Plot of  $\log(k_{H,o}/k_H)$  versus salt concentration for nitric oxide in sodium and ammonium nitrate solutions at 25 °C**

The effect of temperature on the solubility of NO in water, 5 and 10 mol L<sup>-1</sup>  $\text{NH}_4\text{NO}_3$ , and 5 mol L<sup>-1</sup>  $\text{NaNO}_3$  was determined at temperatures ranging from 25 to 55 °C. As expected, the solubility of NO in water decreased significantly with increasing temperature. The natural logarithm of the Henry's constant was plotted against the reciprocal of absolute temperature and found to be linear, as shown in Figure 3. The slope of this curve, which is equal to the enthalpy of solvation divided by the gas constant (slope =  $-\Delta H_{\text{solv}}/R_g$ )<sup>8</sup> was determined to be 1600 K in water, and agrees

favourably with previous literature data, which range from 1400 to 1700 K, as reported in the compilation of Sander (1999)<sup>13</sup>. The solubility of NO in 5 and 10 mol L<sup>-1</sup>  $\text{NH}_4\text{NO}_3$  was also observed to decrease with increasing temperature, however, the magnitude of the decrease was much smaller compared to that in water. The plot of  $\ln(k_H)$  versus  $1/T$  for 5 mol L<sup>-1</sup>  $\text{NH}_4\text{NO}_3$  is linear, with a slope of 1100 K. This is significantly smaller than the value in water (1600 K), and indicates that the dissolution of NO in 5 mol L<sup>-1</sup>  $\text{NH}_4\text{NO}_3$  is less exothermic than in water. The plot for 10 mol L<sup>-1</sup>  $\text{NH}_4\text{NO}_3$  was not linear, with the slope decreasing at higher temperatures. Table 1 summarises the results for the Henry's constant in water, 5 and 10 mol L<sup>-1</sup>  $\text{NH}_4\text{NO}_3$  for different temperatures. The results of all experiments in 10 mol L<sup>-1</sup>  $\text{NH}_4\text{NO}_3$  are plotted in Figure 4, wherein the solid circles represent the average result at each temperature and the error bars represent twice the standard deviation of the experiments at 25 °C.

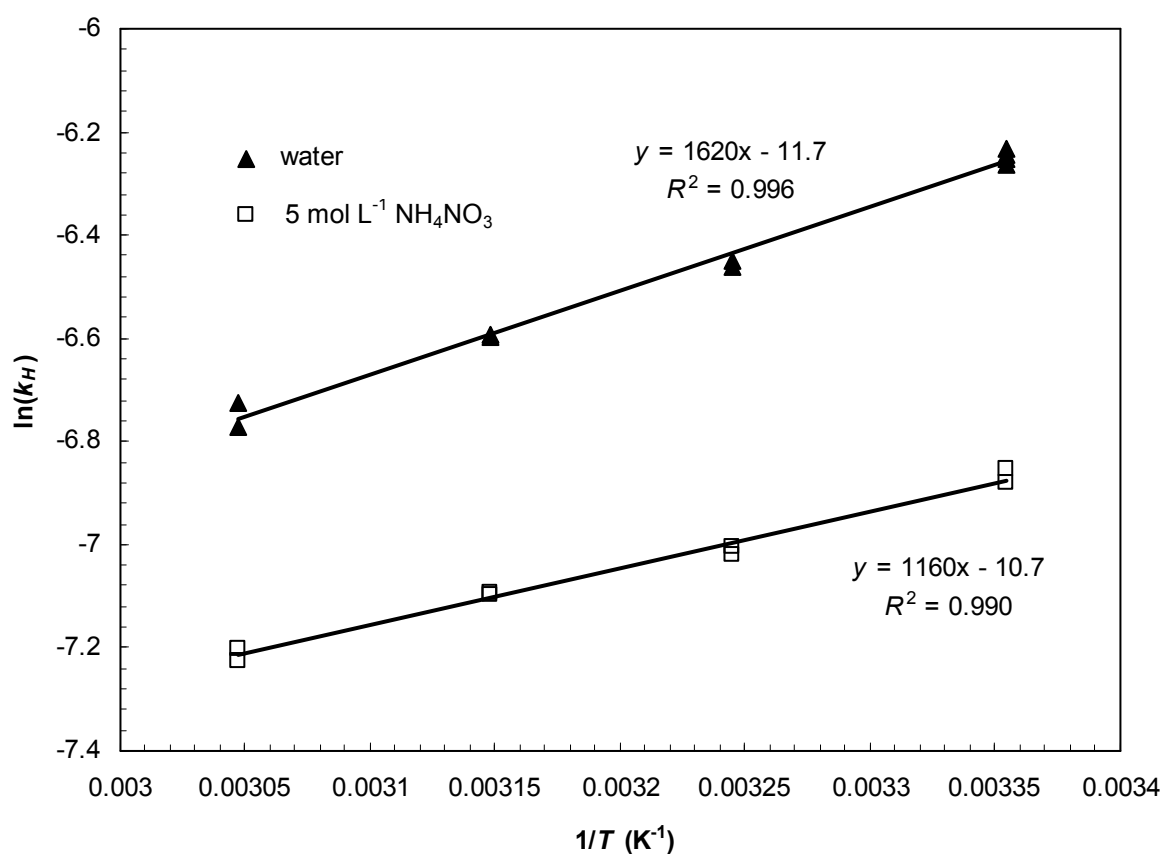
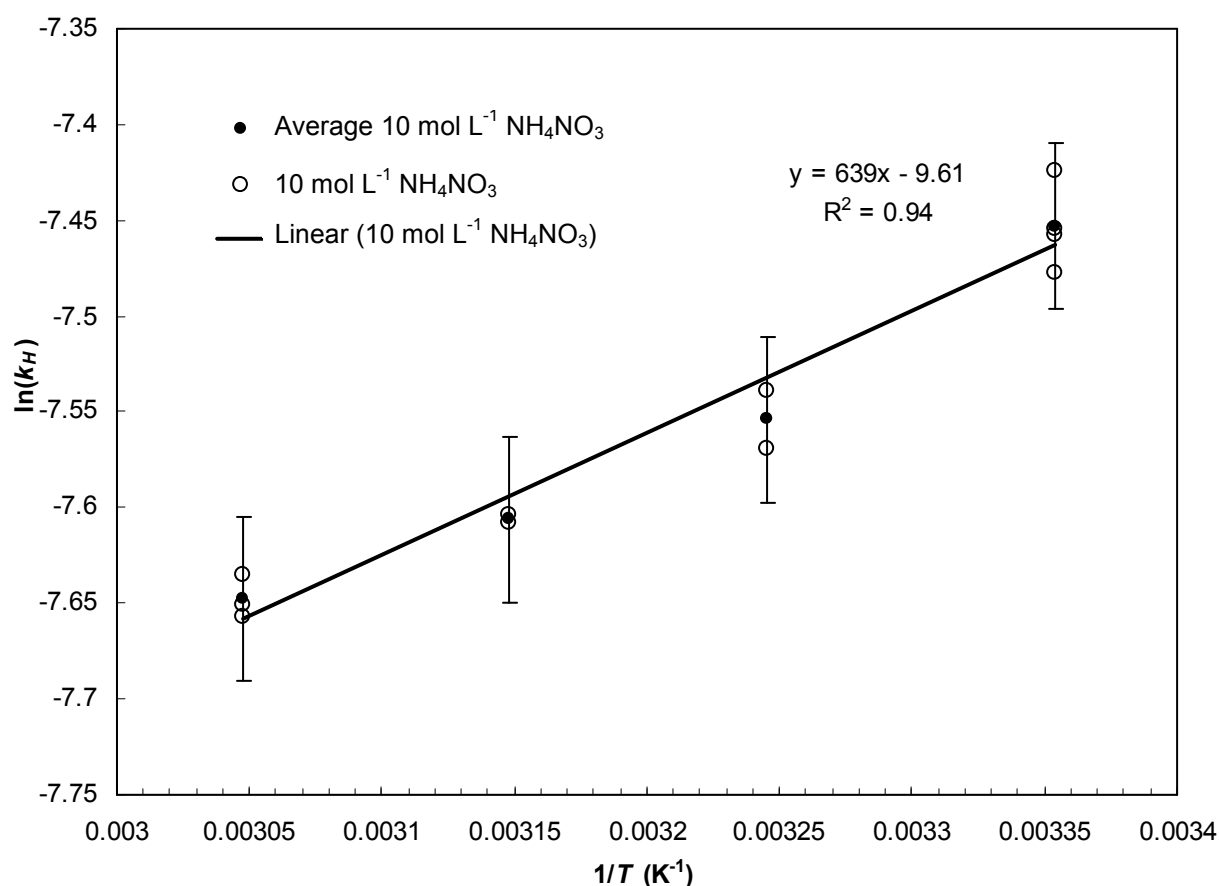


Figure 3: Plot of  $\ln(k_H)$  versus  $1/T$  for nitric oxide in water and 5 mol L<sup>-1</sup>  $\text{NH}_4\text{NO}_3$



**Table 1: Summary of Henry's constants at different temperatures for water, 5 and 10** **$\text{mol L}^{-1} \text{NH}_4\text{NO}_3$  and  $5 \text{ mol L}^{-1} \text{NaNO}_3$** 

<i>Solution</i>	<i>T (K)</i>	<i>k<sub>H</sub> (mol L<sup>-1</sup> bar<sup>-1</sup>)</i>
Water	298	0.00193
	308	0.00157
	318	0.00137
	328	0.00117
5 mol L <sup>-1</sup> $\text{NH}_4\text{NO}_3$	298	0.00104
	308	0.00090
	318	0.00083
	328	0.00074
10 mol L <sup>-1</sup> $\text{NH}_4\text{NO}_3$	298	0.00057
	308	0.00052
	318	0.00049
	328	0.00047
5 mol L <sup>-1</sup> $\text{NaNO}_3$	298	0.00058
	308	0.00053
	318	0.00050
	328	0.00045



**Figure 4:** Plot of  $\ln(k_H)$  versus  $1/T$  for nitric oxide in  $10 \text{ mol L}^{-1} \text{NH}_4\text{NO}_3$

As can be seen in Figure 4, the plot of  $\ln(k_H)$  versus  $1/T$  was somewhat non-linear, with the slope increasing with increasing  $1/T$ . However, the overall effect of temperature on the solubility at this concentration was very small, with a difference in solubility between 25 and 55 °C of only  $1.0 \times 10^{-4} \text{ mol L}^{-1} \text{ bar}^{-1}$ . The uncertainty in the measurements is large compared to the difference in the solubility over this temperature range. This uncertainty represents the statistical variation ( $2\sigma$ ) of the data at 25 °C and does not include estimation of any potential systematic errors, although the latter are expected to be small as supported by the excellent agreement between the present results and literature data for NO solubility in water. It is therefore impossible to

determine whether the non-linear plot is a real effect or whether it is an artefact of the experimental scatter.

Equations 8-10 were developed to quantify the effects of temperature and ammonium nitrate concentration on the solubility of NO, for temperature ranging from 298 – 328 K,  $\text{NH}_4\text{NO}_3$  concentrations from 0-10 mol L<sup>-1</sup> and  $\text{NaNO}_3$  concentrations from 0-5 mol L<sup>-1</sup>:

$$\log\left(\frac{k_{H,o}(T)}{k_H}\right) = k_S(T)[S] \quad (8)$$

$$k_S = -a_S T + b_S \quad (9)$$

$$k_{H,o} = 0.00193 \exp\left(-1615\left(\frac{1}{298.15} - \frac{1}{T}\right)\right) \quad (10)$$

where  $k_{H,o}$  is the Henry's constant of NO in water (mol L<sup>-1</sup> bar<sup>-1</sup>) at temperature  $T$  (K),  $k_H$  is the Henry's constant of NO in a salt solution with concentration  $[S]$  (mol L<sup>-1</sup>),  $k_S$  is the salting out parameter of species S (L mol<sup>-1</sup>) and  $a_S$  and  $b_S$  are salt specific parameters describing the temperature dependence of  $k_S$  and are provided in Table 2.

**Table 2: Temperature dependence parameters  $a_S$  and  $b_S$  for  $\text{NH}_4\text{NO}_3$  and  $\text{NaNO}_3$**

Salt	$a_S$ (L mol <sup>-1</sup> K <sup>-1</sup> )	$b_S$ (L mol <sup>-1</sup> )
$\text{NH}_4\text{NO}_3$	$4.27 \times 10^{-4}$	0.180
$\text{NaNO}_3$	$6.93 \times 10^{-4}$	0.309

The enthalpy and entropy of solvation,  $\Delta H_S$  and  $\Delta S_S$ , were computed from the temperature dependence of the Henry's constant in accordance with Equation 4, and are displayed in Table 3. The enthalpy of solvation was observed to become less negative with increasing ammonium nitrate concentration, ranging from  $-13.4 \text{ kJ mol}^{-1}$  in water to  $-5.3 \text{ kJ mol}^{-1}$  in  $10 \text{ mol L}^{-1} \text{ NH}_4\text{NO}_3$ . A similar trend was observed for  $\Delta S_S$ , which increased from  $-97 \text{ J mol}^{-1}$  to  $-80 \text{ J mol}^{-1}$  upon moving from water to  $10 \text{ mol L}^{-1} \text{ NH}_4\text{NO}_3$ . The enthalpy of solvation corresponds to the net amount of energy released from breaking solvent-solvent bonds and making new bonds between the solvent (i.e., the ammonium nitrate solution) and the solute (i.e., NO). As such, a reduction in the enthalpy of solvation could arise due to an increase in the strength of the solvent-solvent interactions or a decrease in the solvent-solute interaction with increasing salt concentration. The increase in the solvation entropy indicates that NO solvated by ammonium nitrate is less ordered relative to the starting solution than the corresponding process involving NO solvation by water.

**Table 3: Gibbs free energy (25 °C), enthalpy and entropy (25 – 55 °C) of solvation of NO in water, 5 and 10 mol L<sup>-1</sup> NH<sub>4</sub>NO<sub>3</sub> and 5 mol L<sup>-1</sup> NaNO<sub>3</sub>, with standard states of 1 bar in the gas phase and 1 mol L<sup>-1</sup> in aqueous phase**

Solution	$\Delta G_S \text{ (kJ mol}^{-1}\text{)}$	$\Delta H_S \text{ (kJ mol}^{-1}\text{)}$	$\Delta S_S \text{ (J mol}^{-1}\text{)}$
Water	15.5	-13.4	-97.1
5 mol L <sup>-1</sup> NH <sub>4</sub> NO <sub>3</sub>	17.0	-9.2	-88.2
10 mol L <sup>-1</sup> NH <sub>4</sub> NO <sub>3</sub>	18.5	-5.3	-79.8
5 mol L <sup>-1</sup> NaNO <sub>3</sub>	18.5	-6.6	-83.9

The effect of temperature can also be demonstrated in the plots of  $\log(k_{H,o}/k_H)$  versus  $\text{NH}_4\text{NO}_3$  concentration (Figure 5). The plots remain linear as the temperature increases, however, the magnitude of the slope decreases significantly with increasing temperature. This indicates that the effect of ammonium nitrate concentration on the solubility of NO decreases with increasing temperature, for example, at 25 °C the solubility of NO in 10 mol L<sup>-1</sup>  $\text{NH}_4\text{NO}_3$  is 30 % of the solubility in water, compared to 40 % at 55 °C. The linear relationship between  $\log(k_{H,o}/k_H)$  and salt concentration enabled prediction of the NO solubility in super-saturated ammonium nitrate solutions, which find relevance in emulsion explosives, where the ammonium nitrate concentration is on the order of 13 mol L<sup>-1</sup>.<sup>18</sup> Figure 6 plots the predicted NO solubility in 13 mol L<sup>-1</sup>  $\text{NH}_4\text{NO}_3$  at temperatures ranging from 25 to 55 °C. Over this temperature range, the predicted NO solubility is practically independent of temperature ranging from only 4.1 to  $3.6 \times 10^{-4}$  mol L<sup>-1</sup> bar<sup>-1</sup>.

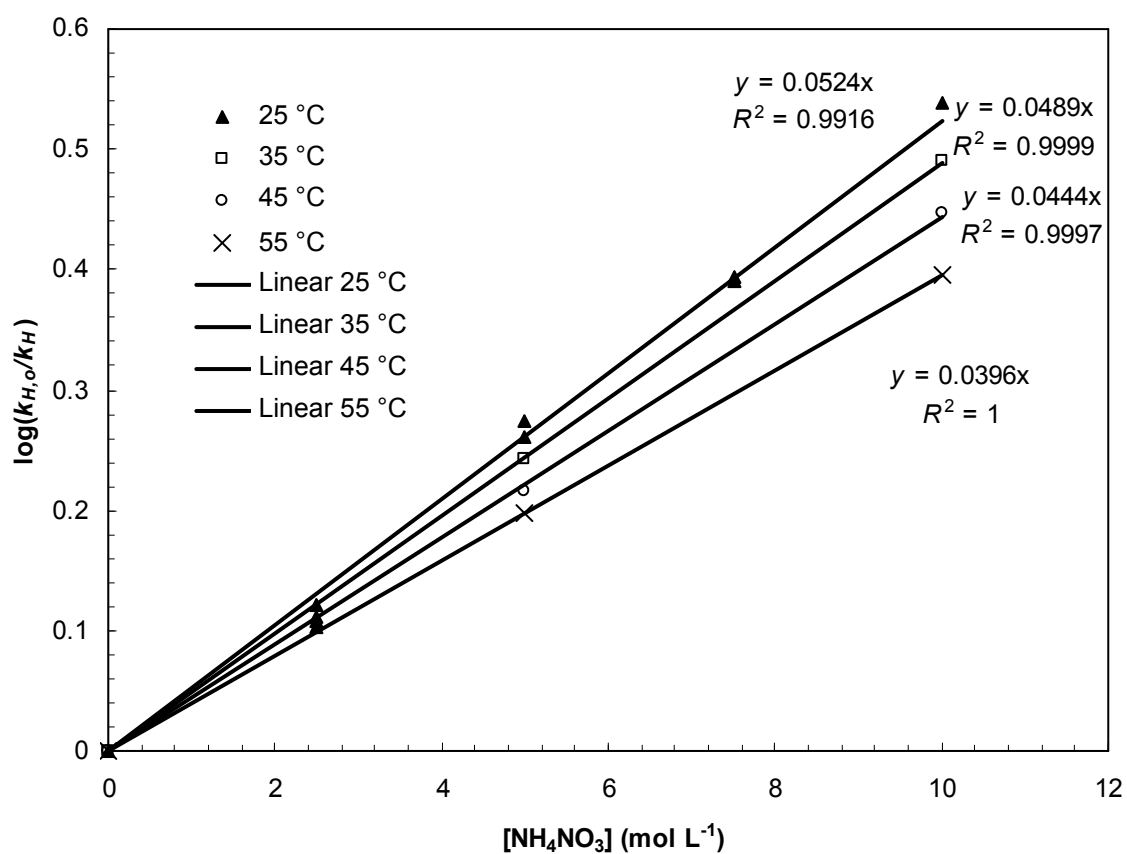
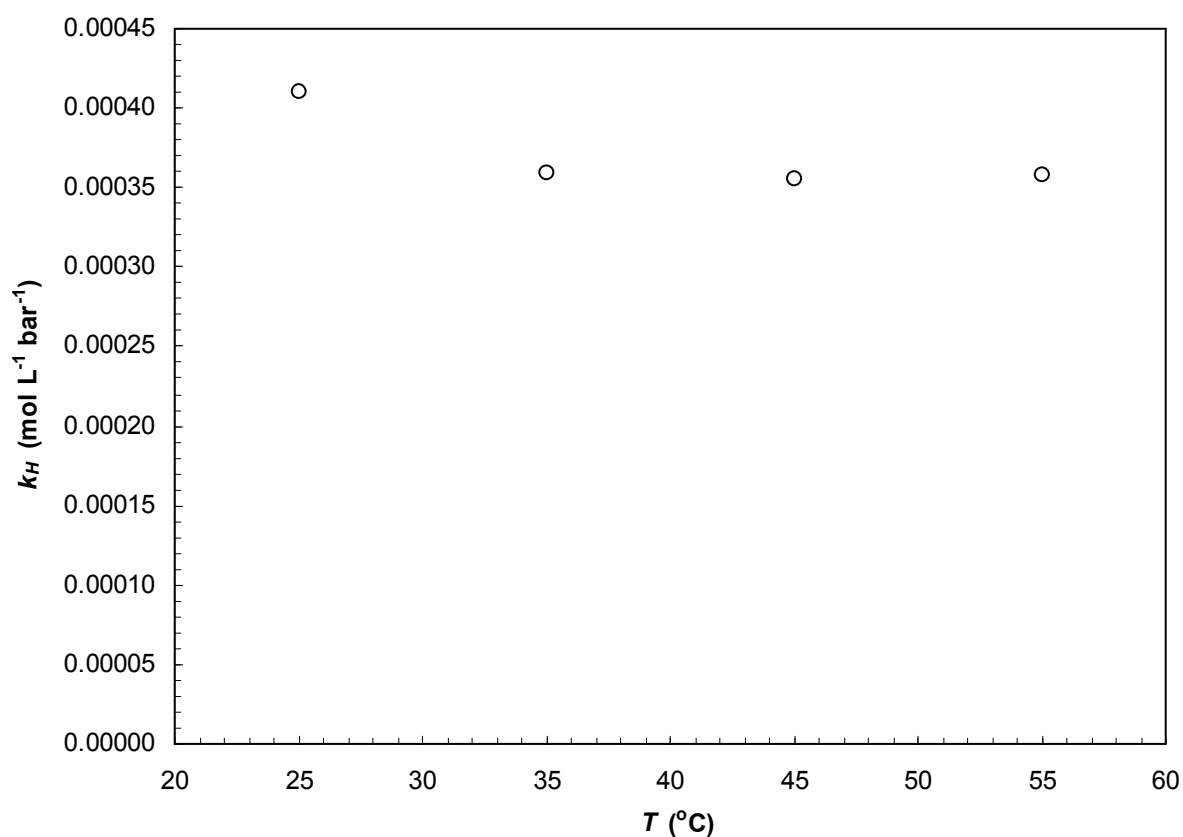


Figure 5: Plot of  $\log(k_{H,o}/k_H)$  versus  $[\text{NH}_4\text{NO}_3]$  at 25-55 °C



**Figure 6: Predicted Henry's constant for NO solubility in 13 mol L<sup>-1</sup>  $\text{NH}_4\text{NO}_3$  at temperatures ranging from 25-55 °C**

A more generalised model based on Equation 1 has been proposed by Schumpe (1993)<sup>19</sup>, which separates  $k_s$  into ion specific and gas specific salting out parameters,  $h_i$  and  $h_g$  respectively, to afford estimation of the salting out effect in multi-electrolyte solutions. Ion specific salting out parameters are tabulated for both anions and cations. It should be noted that the model is equivalent to Equation 1 in the case of a single-salt solution. The effect of temperature on  $h_g$  can also be modelled based on a temperature dependence parameter  $h_T$ . The parameters for Schumpe's model are provided in Table 4:

$$\log\left(\frac{k_{H,o}}{k_H}\right) = \sum (h_i + h_g) c_i \quad (11)$$

$$h_g = h_{g,o} + h_T(T - 298.15) \quad (12)$$

**Table 4: Salting out parameters for Schumpe's model**

<i>Parameter</i>	<i>Value (<math>\text{L mol}^{-1}</math>)</i>
$h_{\text{NO}}$	0.0060
$h_{\text{NH}_4^+}$	0.0556
$h_{\text{Na}^+}$	0.1143
$h_{\text{NO}_3^-}$	0.0128
$h_T$	N/A

For nitric oxide solubility in salt solutions, the only previously available literature data pertains to relatively dilute NaCl and  $\text{NaClO}_4$ <sup>12</sup> at 25 °C, and the values of  $h_g$  are based only on the data for NaCl. It is therefore possible to compare the model predictions to the present experimental results, however it should be noted that there is considerable uncertainty as the value of  $h_g$  which is based upon data of only one salt. Figure 7 compares the predicted solubility of nitric oxide in  $\text{NaNO}_3$  and  $\text{NH}_4\text{NO}_3$  to the present experimental results. Whilst there is relatively poor agreement between the present findings and the predictions of Schumpe's model, the model correctly predicts the trend that the solubility of NO in sodium nitrate will be significantly lower than the ammonium salt. As previously mentioned, the larger impact of  $\text{Na}^+$  on gas solubility compared to  $\text{NH}_4^+$  appears to be a general trend which has previously been observed for



the solubility of a wide range of gases in  $\text{NaCl}$  and  $\text{NH}_4\text{Cl}$  solutions.<sup>16</sup> The lack of quantitative agreement likely reflects that the model parameters for NO are based on results of a single experiment. As such, the  $h_g$  parameter was optimised for the nitrate salts, yielding a value of  $-0.0081 \text{ L mol}^{-1}$  compared to  $0.006 \text{ L mol}^{-1}$  recommended by Schumpe. The revised value of  $h_g$  resulted in an excellent fit between the model and the experimental data.

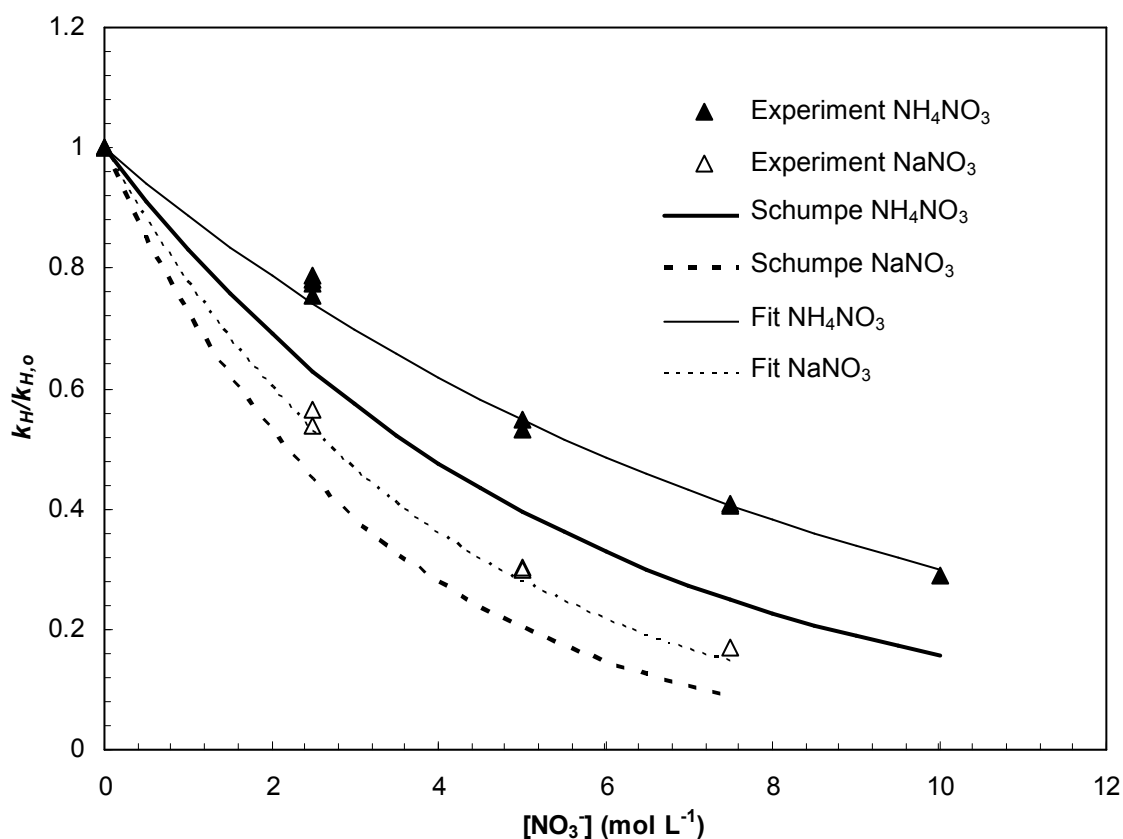


**Figure 7: Comparison of experimental NO solubilities in  $\text{NaNO}_3$  and  $\text{NH}_4\text{NO}_3$  compared to the model of Schumpe (1996)<sup>19</sup> and for fitted  $h_g$  parameter**

## 7.4 Conclusions

The solubility of nitric oxide in solutions of sodium and ammonium nitrate was examined for salt concentrations ranging up to the saturation limit at 25 °C. The Henry's constant decreased considerably with increasing salt concentration, as predicted from the Sechenov equation. The enthalpy of solvation of NO decreased considerably with increasing salt concentration, indicating that the effect temperature on the solubility diminishes with increasing salt concentration. The effect of sodium nitrate on NO solubility was significantly greater than that of ammonium nitrate, in agreement with previous literature results, which show that sodium ions have a much greater effect on gas solubility than ammonium ions. The solubility data yielded the activity coefficients of NO, which were observed to increase exponentially with increasing salt concentration. The model was employed to predict the solubility of NO in 13 mol L<sup>-1</sup>  $\text{NH}_4\text{NO}_3$ , as found in emulsion explosives, and shown to be independent of temperature, at that supersaturated concentration of  $\text{NH}_4\text{NO}_3$ .

## 7.5 References

1. da Silva, G.; Dlugogorski, B. Z.; Kennedy, E. M., An experimental and theoretical study of the nitrosation of ammonia and thiourea. *Chem. Eng. Sci.* **2006**, *61* (10), 3186-3197.
2. Hermann, C.; Dewes, I.; Schumpe, A., The estimation of gas solubilities in salt solutions. *Chem. Eng. Sci.* **1995**, *50* (10), 1673-1675.
3. Zemaitis, J. F. J.; Clark, D. M.; Rafal, M.; Scrivner, N. D., *Handbook of Aqueous Electrolyte Thermodynamics*. American Institute of Chemical Engineers, New York, NY: 1986.
4. Clever, H. L., Setchenov salt-effect parameter. *J. Chem. Eng. Data* **1983**, *28* (3), 340-3.
5. Smith, J. M.; Van Ness, H. C.; Abbott, M. M., *Introduction to Chemical Engineering Thermodynamics, Seventh Edition*. McGraw-Hill: New York, 2005.
6. Weisenberger, S.; Schumpe, A., Estimation of gas solubilities in salt solutions at temperatures from 273 K to 363 K. *AIChE J.* **1996**, *42* (1), 298-300.
7. Becker, K. H.; Kleffmann, J.; Negri, R. M.; Wiesen, P., Solubility of nitrous acid (HONO) in ammonium sulfate solutions. *J. Chem. Soc., Faraday Trans.* **1998**, *94* (11), 1583-1586.
8. Becker, K. H.; Kleffmann, J. R.; Kurtenbach, R.; Wiesen, P., Solubility of nitrous acid (HONO) in sulfuric acid solutions. *J. Phys. Chem.* **1996**, *100* (36), 14984-14990.
9. Delgado, E. J.; Alderete, J., On the calculation of Henry's law constants of chlorinated benzenes in water from semiempirical quantum chemical methods. *J. Chem. Inf. Comput. Sci.* **2002**, *42* (3), 559-563.

10. Heron, G.; Christensen, T. H.; Enfield, C. G., Henry's law constant for trichloroethylene between 10 and 95 °C. *Environ. Sci. Technol.* **1998**, 32 (10), 1433-1437.
11. Joensson, J. A.; Vejrosta, J.; Novak, J., Air/water partition coefficients for normal alkanes (n-pentane to n-nonane). *Fluid Phase Equilib.* **1982**, 9 (3), 279-86.
12. Armor, J. N., Influence of pH and ionic strength upon solubility of NO in aqueous solution. *J. Chem. Eng. Data* **1974**, 19 (1), 82-84.
13. Sander, R. Compilation of Henry's law constants for inorganic and organic species of potential importance in environmental chemistry (Version 3). <http://www.henrys-law.org> (accessed Accessed 18 Jan 2012).
14. Bunton, C. A.; Dahn, H.; Loewe, L., Oxidation of ascorbic acid and similar reductones by nitrous acid. *Nature* **1959**, 183 (4655), 163-165.
15. Zacharia, I.; Deen, W., Diffusivity and solubility of nitric oxide in water and saline. *Ann. Biomed. Eng.* **2005**, 33 (2), 214-222.
16. Millero, F., The activity coefficients of non-electrolytes in seawater. *Mar. Chem.* **2000**, 70 (1-3), 5-22.
17. Millero, F. J.; Huang, F.; Laferiere, A. L., Solubility of oxygen in the major sea salts as a function of concentration and temperature. *Mar. Chem.* **2002**, 78 (4), 217-230.
18. da Silva, G.; Dlugogorski, B. Z.; Kennedy, E. M., Water-in-oil emulsion foaming by thiourea nitrosation: Reaction and mass transfer. *AIChE J.* **2006**, 52 (4), 1558-1565.
19. Schumpe, A., The estimation of gas solubilities in salt solutions. *Chem. Eng. Sci.* **1993**, 48 (1), 153-158.

## **CHAPTER 8**

**Decomposition of nitrous acid in solutions of sodium and ammonium  
nitrates**

## **Table of Contents**

8.1	Introduction	219
8.2	Experimental	223
8.3	Results and discussion	227
8.4	Modelling of the effects of salt concentration on $K_{5, \text{observed}}$	234
8.5	Conclusions	239
8.6	References	240

## 8.1 Introduction

The mechanism for the decomposition of nitrous acid comprises a complex sequence of reaction steps as outlined in Reactions (1-4)<sup>1,2</sup>, with the net reaction resulting in production of nitric oxide and nitric acid (Reaction 5).

### *Elementary Reactions*



### *Overall Reaction*



The decomposition of nitrous acid is relevant to many industrial systems, including the absorption of  $\text{NO}_x$  in water for the production of nitric acid<sup>3,4</sup>, and as an undesired side reaction during synthesis reactions involving  $\text{HNO}_2$ .<sup>5</sup> The present study is motivated by the application of nitrous acid to sensitise emulsion blasting agents, which consist of a highly concentrated solution of ammonium nitrate dispersed within a continuous

hydrocarbon fuel phase, typically diesel. This type of explosive is widely used in mining, quarrying and construction applications owing to their excellent safety properties, low cost and superior water resistance<sup>6</sup>. As a consequence of their stability, emulsion blasting agents must be sensitised prior to detonation, by introduction of small voids within the emulsion matrix which act as hot spots to propagate the explosive front through the bulk emulsion<sup>7</sup>. A popular method of achieving sensitisation is the generation of nitrogen gas bubbles in the explosive via the reaction between a nitrite salt and ammonia (from ammonium nitrate)<sup>8</sup>. Whilst the desired product of the reaction is harmless N<sub>2</sub>, significant quantities of toxic nitrogen oxides (NO<sub>x</sub>) can be produced via Reactions 1-4 occurring in parallel.



Under conditions of practical interest where the removal of NO<sub>x</sub> species from solution is relatively slow, Reactions (1-3) are sufficiently rapid to establish equilibrium, with the rate of reaction being governed by the net rate of Reaction 4 (as demonstrated in Chapter 4). The kinetics of the reaction in dilute acid solution have been accurately determined and obey the rate law displayed in Equation 7. Under conditions of high nitrate ion concentrations or acidity, the rate of the reverse reaction becomes significant and an equilibrium is established according to Equation 8.<sup>9</sup>

$$\frac{d[\text{HNO}_2]}{dt} = -\frac{3K_4^2 k_5 [\text{HNO}_2]^4}{[\text{NO}]^2} + 3k_{-5} [\text{HNO}_2] [\text{H}^+] [\text{NO}_3^-] \quad (7)$$



$$K_5 = \frac{a_{NO}^2 a_{H^+} a_{NO_3^-} a_{H_2O}}{a_{HNO_2}^3} \quad (8)$$

$$a_i = \gamma_i [i] \quad (9)$$

where  $a$  is activity,  $\gamma$  is the molar activity coefficient,  $[i]$  is the concentration in mol L<sup>-1</sup> and the subscript  $i$  refers to species  $i$ . The activity is a measure of the difference between the chemical potential of a species at the state of interest and at its standard state<sup>10</sup>, and is related to the concentration by the activity coefficient. At very low electrolyte concentrations, the activities of the species are essentially the same as the species concentrations, that is,  $\gamma_i = 1$ . However, as the electrolyte concentration increases, the activities and concentrations diverge, requiring knowledge of the activity coefficients in order to predict the species concentrations at equilibrium. Typical concentrations of ammonium nitrate in emulsion explosives are on the order of 13 mol L<sup>-1</sup>. At such concentrations of NH<sub>4</sub>NO<sub>3</sub>, the activity coefficients of the species in Equation 5 could be expected to differ widely from unity.

The aim of this study is therefore to determine the effect of the ammonium nitrate concentration on the quantity of NO produced from decomposition of nitrous acid. To assist in quantifying the effect of salt concentration on the reaction equilibrium, we define the apparent equilibrium constant,  $K_{5,observed}$ , as the equilibrium constant measured in terms of concentrations. This is convenient because the concentrations of HNO<sub>2</sub>, H<sup>+</sup> and NO<sub>3</sub><sup>-</sup> can be easily determined from the known amount of each species added to a solution. The ratio of the apparent equilibrium constant to the ideal equilibrium constant depends on the activity coefficients of the relevant species, and, as

such, knowledge of the activity coefficients under a given set of conditions allows prediction of the observed equilibrium constant.

$$K_{5,observed} = \frac{[NO]^2[H^+][NO_3^-]}{[HNO_2]^3} \quad (10)$$

$$\frac{K_{5,observed}}{K_5} = \frac{y_{HNO_2}^3}{y_{NO}^2 y_{H^+} y_{NO_3^-} a_{H_2O}} \quad (11)$$

Experimental measurements are available for the mean ionic activity coefficients of ammonium nitrate and the water activity at various ammonium nitrate concentrations<sup>11</sup>. However, experimental data for the activity coefficients of  $H^+$  and  $HNO_2$  in ammonium nitrate solutions is unavailable, whilst the activity coefficients of  $NO$  have only recently been determined (Chapter 7). The purpose of this work was to establish the effect of ammonium and sodium nitrate concentration on the observed equilibrium constant for decomposition of nitrous acid and to quantify these effects in terms of the activity coefficients of the species involved in the reaction.

## 8.2 Experimental

A novel membrane inlet analysis method was employed to determine the observed equilibrium constant,  $K_{5,observed}$ , for nitrous acid decomposition in concentrated salt solutions. The apparatus, shown in Figure 1, consisting of a 125 cm<sup>3</sup> round bottomed flask with septum side port containing a magnetic stirrer, was mounted in a water bath to maintain a temperature of 25 °C in all experiments. Measurements of nitric oxide in the reactor were performed using a membrane inlet NO probe. A similar system has previously been employed for the measurement of nitric oxide by mass spectrometry<sup>12,13</sup>. The reactor was partially filled with liquid, and the probe positioned in the centre of the vessel such that the membrane section was exposed to the gas phase. The probe comprised a 5 cm section of Dow Corning Laboratory silastic tubing (catalogue number 508-006) mounted on 1/16" (1.59 mm) stainless steel tubing. The stainless steel tubes pierced a rubber stopper inserted in the top of the reactor. The silastic tubing acts as a selective membrane that allows passage of nitric oxide whilst being relatively impermeable to water. Nitric oxide diffusing through the membrane was collected by a flowing stream of nitrogen gas for analysis using a Thermo 42i-HL chemiluminescence NO<sub>x</sub> analyser.

The advantage of the membrane inlet setup over direct gas phase measurements of NO was that it enabled the concentration of NO in the gas phase of the reactor to be established without the need for a purge gas to pass through the headspace. This permitted the accumulation of NO in the gas phase over time to a point where the concentrations of gas and aqueous phase NO reached equilibrium. To maintain a constant pressure in the reactor, a syringe was mounted in the rubber stopper at the top

of the reactor, and the plunger allowed to expand with the increase in the gas volume (due to the production of gaseous NO, and N<sub>2</sub>, in the case of NH<sub>4</sub>NO<sub>3</sub> experiments). The reactor-probe setup was calibrated by generating a known partial pressure of nitric oxide in the reactor via the reaction between nitrous and ascorbic acids<sup>14</sup>.

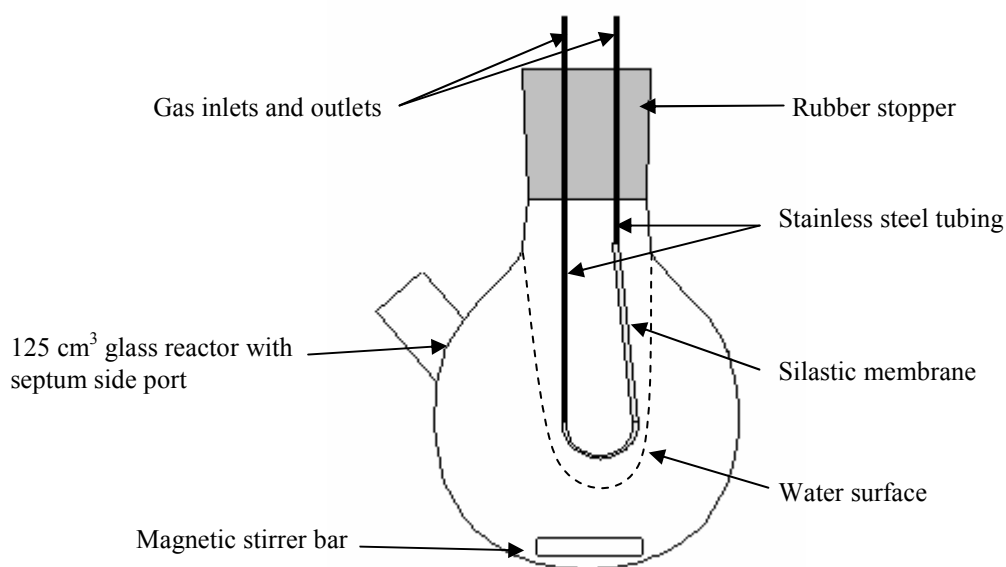


**Figure 1: Diagram of membrane inlet reactor apparatus for measurement of  $K_{5,observed}$**

Prior to each experiment, the reactor was partially filled with 90 cm<sup>3</sup> of ammonium nitrate solution and the H<sup>+</sup> concentration adjusted with 2 M HNO<sub>3</sub>. The motion of the magnetic stirrer created a vortex inside the reactor, with the probe in the centre, as shown in Figure 1. The reactor was purged for 30 min with nitrogen gas at a flow rate of 0.67 cm<sup>3</sup> s<sup>-1</sup> to eliminate oxygen from the reactor prior to each experiment, whilst a water bath surrounding the reactor maintained the temperature at 25 °C in all experiments. Reaction was initiated by injecting 1 cm<sup>3</sup> of a concentrated solution of

sodium nitrite through a needle inserted through the septum side port of the reactor. The nitric oxide concentration was monitored until a stable reading was obtained, indicating that the system had reached equilibrium. To determine the equilibrium constant it was essential to know precisely the final  $\text{HNO}_2$  concentration, and as such, a small sample of solution was withdrawn at the conclusion of the experiment and the final nitrous acid concentration determined using UV-vis<sup>15</sup>. This was necessary owing to the significant fraction of the initial nitrous acid converted into  $\text{NO}$ , and in the case of the  $\text{NH}_4\text{NO}_3$  experiments, the concurrent consumption of  $\text{HNO}_2$  via reaction with ammonia according to Reaction 6.

Measurements of pH were performed with a Hanna HI 1330 pH probe connected to a Hanna 213 pH meter. The activity coefficient of hydrogen ions in solutions of ammonium or sodium nitrate was determined by measuring the pH of a sample of a salt solution containing a known  $\text{H}^+$  concentration. The ratio of the  $\text{H}^+$  activity to the known  $\text{H}^+$  concentration yielded the activity coefficient according to Equation 9. The experiments employed initial nitrite concentrations of  $0.02 \text{ mol L}^{-1}$  and initial hydrogen ion concentrations of  $0.09 \text{ mol L}^{-1}$ , with the excess of hydrogen ions over nitrite ensuring near complete conversion of nitrite into nitrous acid. It should be noted that even at the moderately low acidities employed in the present study ( $[\text{H}^+] < 0.1 \text{ mol L}^{-1}$ ), the high concentration of nitrate ions could lead to conversion of a small proportion of  $\text{H}^+$  into  $\text{HNO}_3$  ( $\text{p}K_a$  of  $-1.2$ <sup>16</sup>). As such, the activity coefficients of  $\text{H}^+$  determined with the present method are likely to be slightly lower than the true activity coefficient at high  $\text{NO}_3^-$  concentrations. Consequently, the reported values of  $K_{5, \text{observed}}$  do not account for the protonation of  $\text{NO}_3^-$ . This approximation, however, will not adversely

affect subsequent calculations of  $y_{HNO_2}$ , because the errors in  $y_{H^+}$  and the assumed  $H^+$  concentration cancel out to yield the correct value of  $a_{H^+}$ .

The activity coefficients of ionic species in  $NaNO_3$  and  $NH_4NO_3$  were also predicted using the OLI Analyser Studio 3.0 software package. Appendix D provides further details of the calculation procedure and equations employed by OLI. The molal activity coefficients were predicted using the mixed solvent electrolyte framework,<sup>17,18</sup> and converted to molar activity coefficients as outlined in Zemaitis et al.,<sup>10</sup> employing the solution density predicted by OLI.

### 8.3 Results and discussion

As indicated by Equation 11, the observed equilibrium constant will increase with increase in the activity coefficient of  $\text{HNO}_2$ , decrease with increases in the activity coefficients of  $\text{NO}$ ,  $\text{H}^+$  and  $\text{NO}_3^-$ , and increase with decreasing water activity. The effects of  $\text{NH}_4\text{NO}_3$  and  $\text{NaNO}_3$  on the individual activity coefficients were examined in order to elucidate the contributions of the individual species activity coefficients on  $K_5$ , *observed*.

Experimental data have been reported for the mean ionic activity coefficient of ammonium nitrate and the water activity in concentrated ammonium nitrate solutions<sup>11</sup>. The activity coefficients of hydrogen ions in  $\text{NH}_4\text{NO}_3$  and  $\text{NaNO}_3$  solutions were established in the present work by measuring the pH of solutions of these salts acidified with known concentrations of  $\text{HNO}_3$ , whilst the effects of nitrate salt concentration on the activity coefficients of  $\text{NO}$  were determined from the solubility measurements in accordance with Equation 12 (See Chapter 7 for further details on  $\text{NO}$  activity coefficients). Simulations were performed in OLI Analyser Studio 3.0 to determine the activity coefficient of  $\text{NO}_3^-$  and the water activity in sodium nitrate solutions. Appendix D provides details of the Equations employed by OLI. The calculations were executed under the mixed solvent electrolyte framework. To ascertain the accuracy of the activity coefficients computed by the OLI software, the predicted nitrate activity coefficient and water activity in ammonium nitrate are compared to the experiments of Wishaw and Stokes<sup>11</sup> in Figure 2.

$$\log\left(\frac{k_{H,o}}{k_H}\right) = \log(y_i) = k_s C_s \quad (12)$$

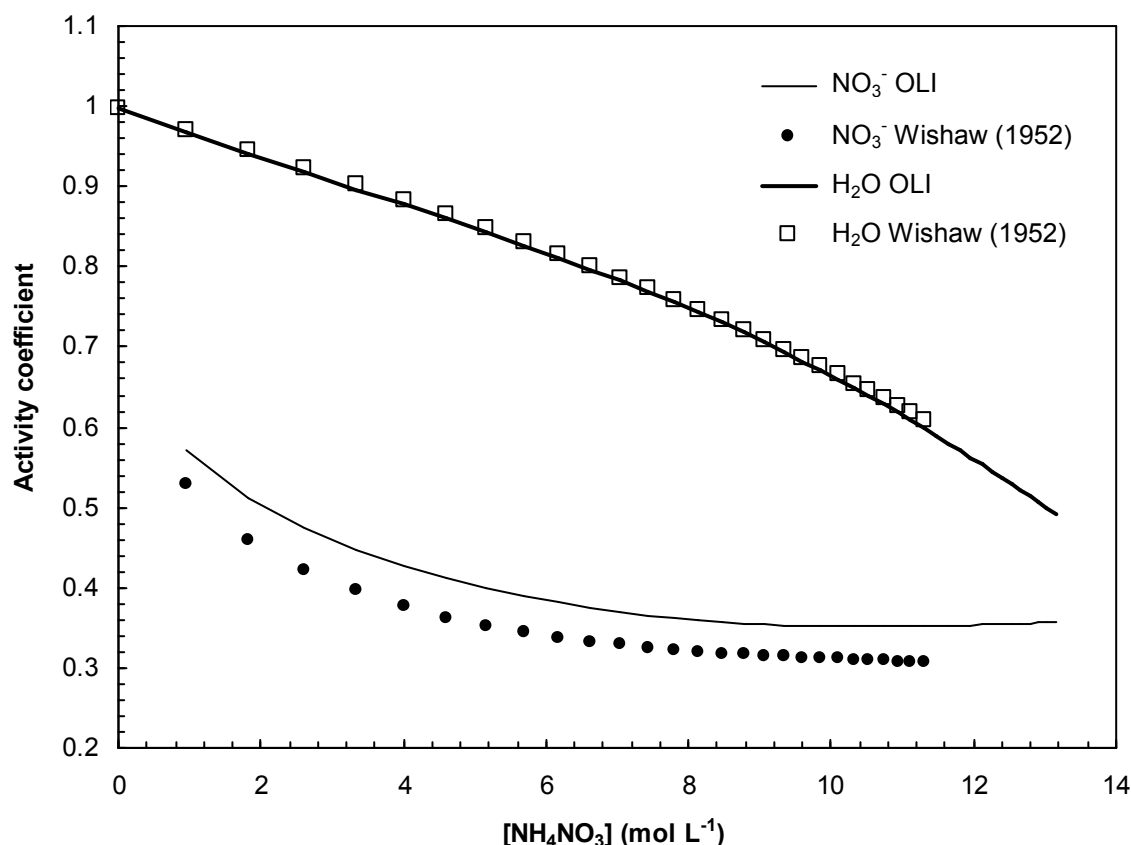


**Figure 2: Comparison of  $\text{NO}_3^-$  activity coefficients and water activities calculated with OLI to those reported by Wishaw & Stokes (1952) at 25 °C**

The activity coefficient for  $\text{NO}_3^-$  declines rapidly at low concentrations, with the rate of decrease diminishing with increasing  $\text{NH}_4\text{NO}_3$  concentration, eventually stabilising at around 9 M  $\text{NH}_4\text{NO}_3$ . Both the experimental data and that calculated by OLI show the same trend, however, the experimental data lie slightly lower than the OLI prediction. It should be noted that the experimental measurements constitute the mean activity coefficient of ammonium nitrate,  $\gamma_{+/-} = (\gamma_{\text{NO}_3^-} \gamma_{\text{NH}_4^+})^{0.5}$ . The mean activity coefficient is not necessarily the same as the nitrate activity coefficient, which could explain this discrepancy, if the  $\text{NH}_4^+$  activity coefficient is lower than that of  $\text{NO}_3^-$ . However, it



should be noted that OLI predicts near identical activity coefficients for  $\text{NH}_4^+$  and  $\text{NO}_3^-$ . The experimental data and the OLI prediction of the water activity are practically identical. Both show an approximate linear decrease at low concentrations and an accelerating decline at high concentrations.

The activity coefficients of  $\text{H}^+$  were measured using a pH probe, by making up known concentrations of  $\text{HNO}_3$  in  $\text{NH}_4\text{NO}_3$  and comparing the measured pH of a sample to the actual  $\text{H}^+$  concentration. Figure 3 compares the experimentally determined  $\text{H}^+$  activity coefficients to those predicted by OLI. The experimental measurements in  $\text{NH}_4\text{NO}_3$  show slightly higher  $\text{H}^+$  activity coefficients than predicted by OLI, however, both sets of data exhibit the same trend with an exponential increase in  $\gamma_{\text{H}^+}$ , with increasing  $\text{NH}_4\text{NO}_3$  concentration. The predicted and measured activity coefficients of  $\text{H}^+$  in  $\text{NaNO}_3$  are in reasonable agreement. Owing to the close similarity between OLI and experimental results for activity coefficients of  $\text{H}^+$  and  $\text{NO}_3^-$ , it was concluded that OLI provides acceptable estimates of ionic activity coefficients.

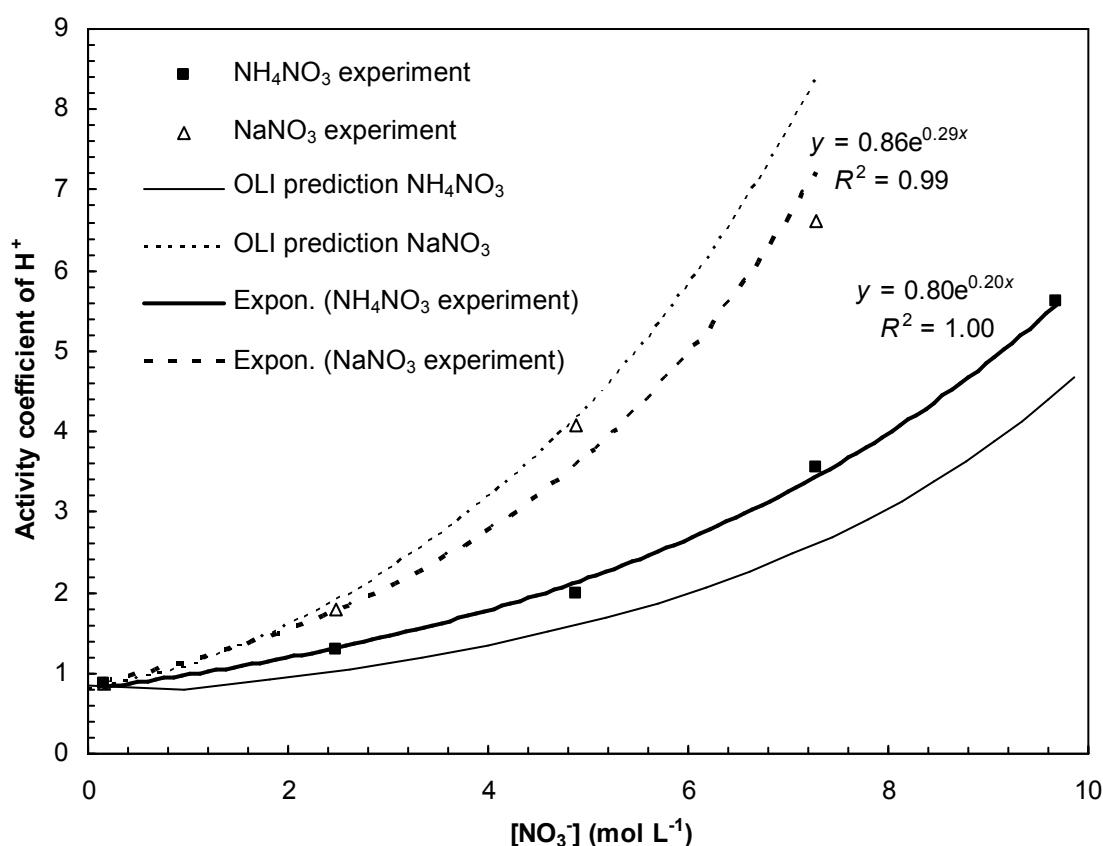


**Figure 3: Activity coefficients of  $H^+$  determined experimentally and by OLI at 25 °C**

Figure 4 shows the observed equilibrium constant for nitrous acid decomposition in  $NH_4NO_3$  and  $NaNO_3$  solutions ranging from 0-10 and 0-7.5 mol  $L^{-1}$ , respectively. At low salt concentrations, the observed equilibrium constant increases considerably with increasing salt concentrations in both  $NaNO_3$  and  $NH_4NO_3$ . From the maximum around 1 M, the observed equilibrium constant in  $NH_4NO_3$  decreases steadily with increasing salt concentration. A decrease of the observed equilibrium constant at high salt concentrations was also noted in  $NaNO_3$ ; however, the decrease in the equilibrium constant is significantly smaller than is observed in  $NH_4NO_3$ . The trend in  $K_{5,observed}$  is related to the changes in the values of the activity coefficients of  $NO$ ,  $H^+$ ,  $NO_3^-$  and  $HNO_2$ , and the water activity, with increasing salt concentration. At low salt concentrations, a large decrease in the nitrate activity coefficient occurs (Fig. 2), whilst

there are only smaller changes to the activity coefficients of  $H^+$  (Figure 3) and NO (Chapter 7), and the water activity (Figure 2). As such, the increase in  $K_{5,observed}$  at low salt concentrations is caused by the large decrease in the  $NO_3^-$  activity coefficient relative to the smaller increases in the NO and  $H^+$  activity coefficients.

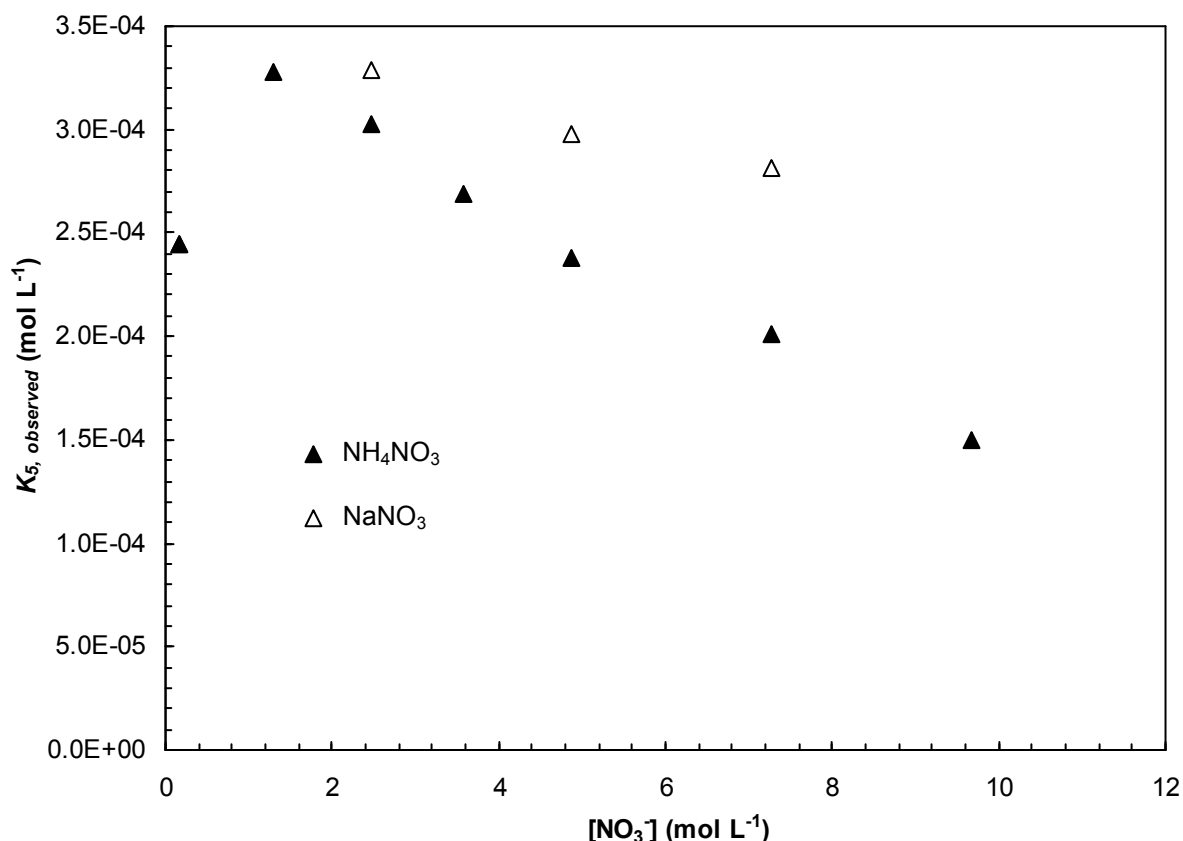


**Figure 4: Observed equilibrium constant for nitrous acid decomposition in solutions of ammonium and sodium nitrates**

The  $H^+$  and NO activity coefficients increase exponentially with increasing salt concentration, whilst the effect of salt concentration on the  $NO_3^-$  activity diminishes with increasing concentration. As the salt concentration increases, the activity coefficients of NO and  $H^+$  become important, and are balanced by increases in the  $HNO_2$  activity coefficient and decreases to the water activity. In  $NH_4NO_3$ ,  $K_{5,observed}$

decreases steadily with increasing concentration, indicating that the effects of  $y_{\text{NO}}$  and  $y_{\text{H}^+}$  outweigh those of  $y_{\text{HNO}_2}$  and  $a_{\text{H}_2\text{O}}$ . In  $\text{NaNO}_3$ ,  $K_{5,\text{observed}}$  decreases only slightly at higher salt concentrations, indicating that the effects of increasing  $y_{\text{NO}}$  and  $y_{\text{H}^+}$  are almost balanced by the corresponding changes to  $y_{\text{HNO}_2}$  and  $a_{\text{H}_2\text{O}}$ . Overall, there are minimal changes to  $K_{5,\text{observed}}$ , despite significant changes to the activity coefficients of the species involved, for example, the nitric oxide activity increases to 5.6 in 7.5 M  $\text{NaNO}_3$ , whilst  $K_{5,\text{observed}}$  remains practically unchanged owing the cancellation effects described above.

The nitrous acid activity coefficient was estimated based on the value of  $K_{5,\text{observed}}$ , nitrate activity coefficients and water activities from OLI and experimentally determined NO and  $\text{H}^+$  activity coefficients. The nitrous acid activity coefficient increased exponentially with increasing  $\text{NH}_4\text{NO}_3$  concentration, following the same trend as nitric oxide (and as predicted from Equation 12). Similar trends have been reported for the effect of  $\text{Na}_2\text{SO}_4$  and  $\text{H}_2\text{SO}_4$  concentration on the nitrous acid activity coefficient<sup>19,20</sup>. Plotting the logarithm of the activity coefficient versus the  $\text{NaNO}_3$  and  $\text{NH}_4\text{NO}_3$  concentration yielded a straight line as shown in Figure 5. The salting out parameters,  $k_s$ , for  $\text{HNO}_2$  in  $\text{NaNO}_3$  and  $\text{NH}_4\text{NO}_3$  solutions can be compared to those determined in Chapter 7 for NO under the same conditions. In the case of  $\text{NaNO}_3$ , similar salting out parameters were observed for  $\text{HNO}_2$  and NO, with  $k_s$  for  $\text{HNO}_2$  being approximately 7 % smaller than that for NO. However, in the case of  $\text{NH}_4\text{NO}_3$ , the derived value of  $k_s$  for  $\text{HNO}_2$  is 30 % smaller than that of NO. As such, the activity coefficient of nitric oxide is affected to a greater extent by ammonium nitrate than that of nitrous acid. The increase in the  $\text{HNO}_2$  activity coefficient is insufficient to

counteract the increases in the activity coefficients of  $H^+$  and  $NO$  resulting in a decrease in  $K_{5, observed}$  at high  $NH_4NO_3$  concentrations.

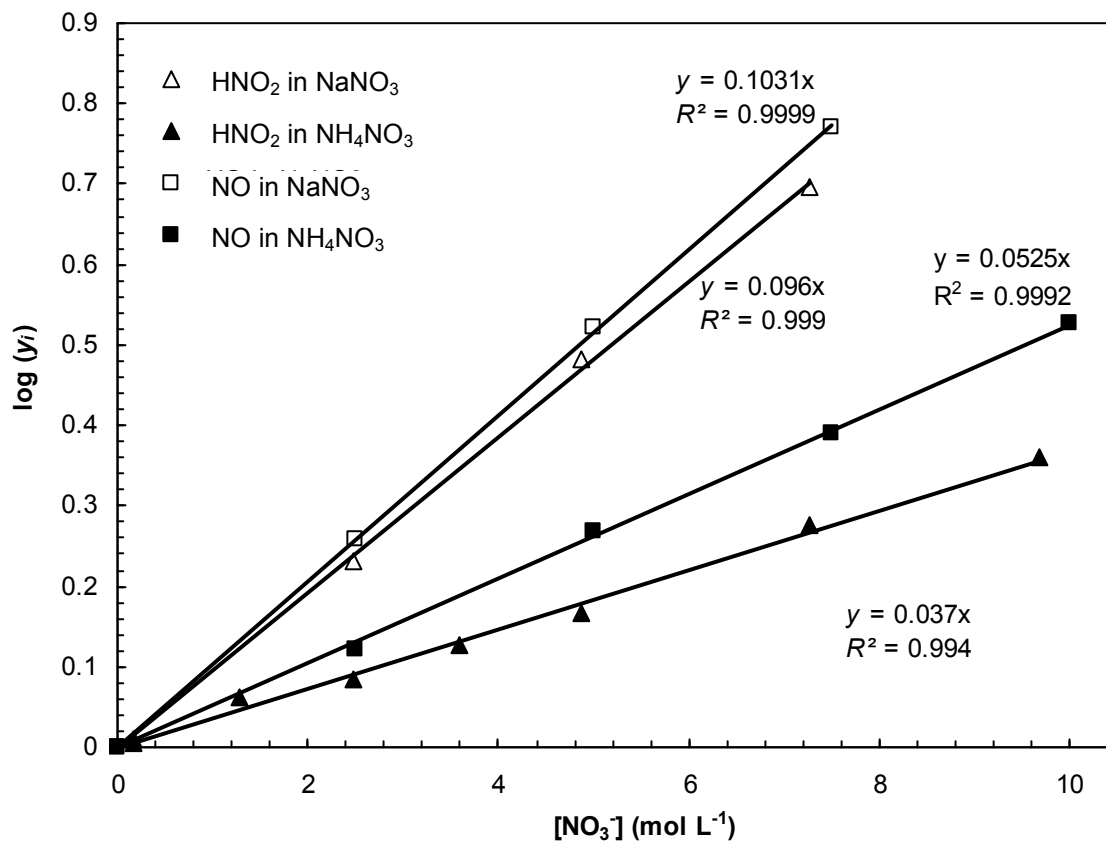


**Figure 5: Effect of  $NH_4NO_3$  and  $NaNO_3$  concentration on nitrous acid and nitric oxide activity coefficient**

#### 8.4 Modelling of the effects of salt concentration on $K_{5, \text{observed}}$

A model was developed to predict the effect of ammonium nitrate concentration on  $K_{5, \text{observed}}$ , based on the activity coefficients of the species involved in the reaction. In particular, the present work was motivated by the safety implications of Reaction 5 to the sensitisation of emulsion explosives. These emulsions are capable of maintaining a supersaturated concentration of ammonium nitrate (typically about 13 mol L<sup>-1</sup>) and it is of interest to predict the value of  $K_{5, \text{observed}}$  under these conditions, where direct measurements are impossible. Equations 16-18 were employed to predict the activity coefficients of H<sup>+</sup>, NO and HNO<sub>2</sub> in order to model the equilibrium constant for HNO<sub>2</sub> decomposition in NH<sub>4</sub>NO<sub>3</sub>. OLI predictions were employed to estimate the activity coefficients of NO<sub>3</sub><sup>-</sup> and the water activity. Figure 6 shows the excellent agreement between the model and experimental data. The model predicts a continued decline in  $K_{5, \text{observed}}$  at higher NH<sub>4</sub>NO<sub>3</sub> concentrations, with the rate of decrease beginning to decline at the highest concentrations, owing to the significant decrease in the water activity.

$$y_{H^+} = 0.80 \times 10^{0.0869[NH_4NO_3]} \quad (16)$$

$$y_{NO} = 10^{0.0525[NH_4NO_3]} \quad (17)$$

$$y_{HNO_2} = 10^{0.037[NH_4NO_3]} \quad (18)$$

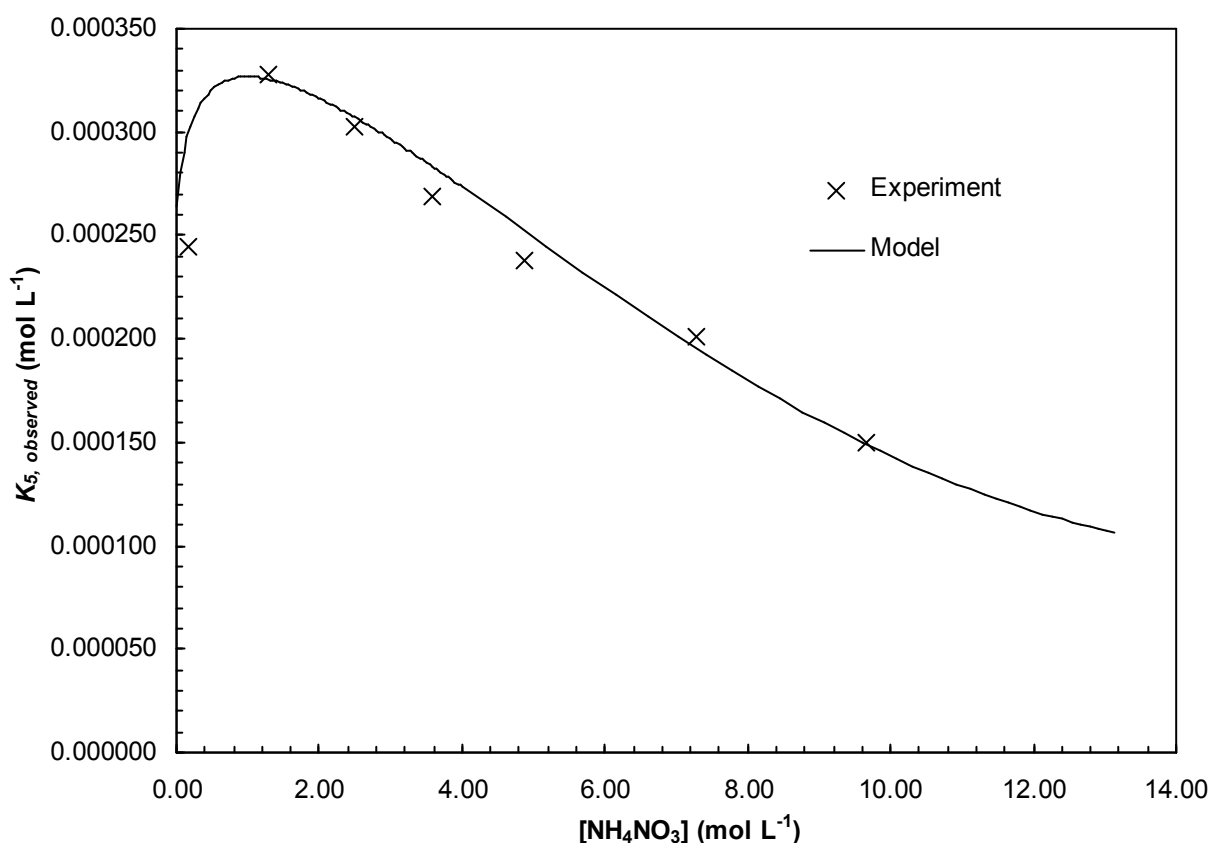


**Figure 6: Comparison of fitted and experimental data for nitrous acid decomposition equilibrium constant**

The model, comprising Equations 16-18 and OLI predictions for  $\text{NO}_3^-$  activity coefficients and the water activity, was also employed to predict both the equilibrium aqueous concentration and equilibrium partial pressure of NO that would exist in a system with 0.02 M  $\text{HNO}_2$  and 0.06 M  $\text{H}^+$  for  $\text{NH}_4\text{NO}_3$  ranging from 0-13 mol L<sup>-1</sup>. The Henry's constant for NO in the salt solution was determined by combining Equations 12 and 17. These results are compared in Figures 7 and 8 to those predicted for the same set of concentrations but neglecting the activity coefficients and reduced NO solubility, denoted as the ideal solution model. The models with and without activity coefficients predicted similar concentrations of aqueous NO, with the effect of activity coefficients

leading to slightly higher NO levels at low  $\text{NH}_4\text{NO}_3$  concentrations and slightly lower NO levels at high  $[\text{NH}_4\text{NO}_3]$ . This result reflects the minor effect of salt concentration on  $K_{5, \text{observed}}$ , with the increased activity coefficients of NO and  $\text{H}^+$  being almost entirely cancelled out by the increase in  $\text{HNO}_2$  activity coefficient and the decrease in water activity.

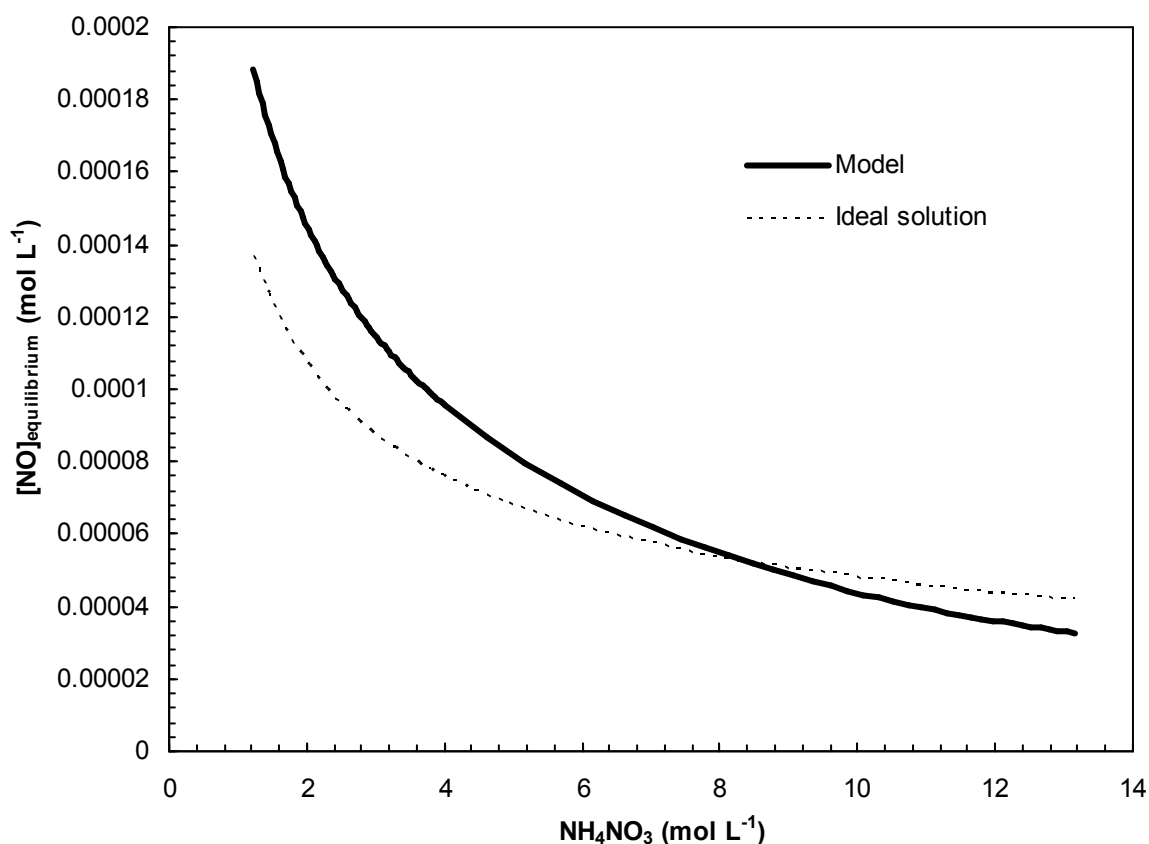


**Figure 7: Comparison of equilibrium aqueous NO concentration for 0.02 M  $\text{HNO}_2$  and 0.06 M  $\text{H}^+$  in  $\text{NH}_4\text{NO}_3$  predicted with activity coefficient and ideal solution (i.e., all  $y_i=1$ ) models**

Although the effect of non unity activity coefficients has little effect on the concentration of aqueous NO at equilibrium, there is a large difference in the equilibrium partial pressure of NO. This difference arises as a result of the increase in



the activity coefficient of NO with increasing  $\text{NH}_4\text{NO}_3$  concentration, corresponding to a large reduction in the NO solubility. Consequently, for a given aqueous concentration of NO, the equilibrium partial pressure will be significantly higher in an  $\text{NH}_4\text{NO}_3$  solution compared to the same NO concentration in pure water (i.e. the Henry's constant for NO in the salt solution is lower than in water). In  $13 \text{ mol L}^{-1}$   $\text{NH}_4\text{NO}_3$  (as found in emulsion explosives), the equilibrium NO partial pressure is approximately four times higher than that predicted when the effects of activity coefficients and reduced NO solubility are neglected. This observation is of practical significance, as it explains that the formation of  $\text{NO}_x$  cannot be avoided by the presently used nitrosation technology for sensitising emulsion explosives.

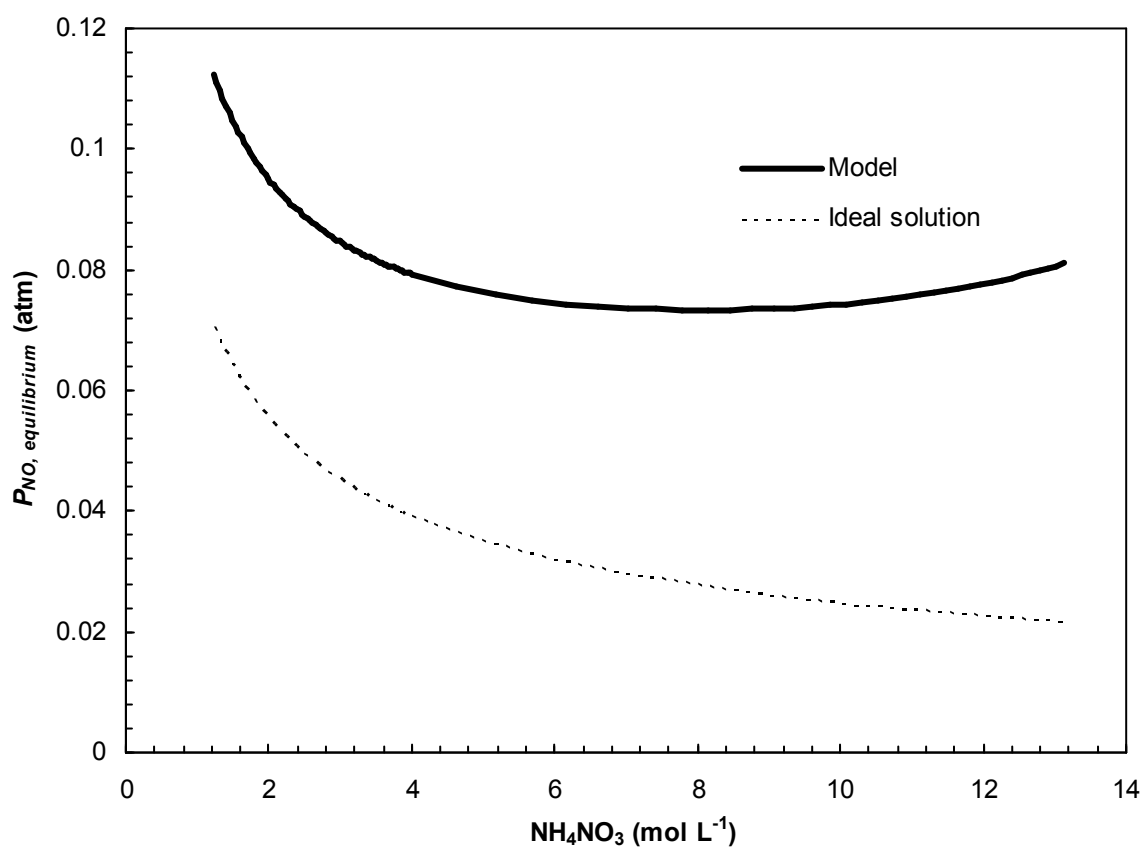


**Figure 8: Comparison of equilibrium NO partial pressures for 0.02 M  $\text{HNO}_2$  and 0.06 M  $\text{H}^+$  in  $\text{NH}_4\text{NO}_3$  predicted with activity coefficient and ideal solution (i.e., all  $y_i=1$ ) models**

## **8.5 Conclusions**

Experiments were conducted to determine the observed equilibrium constant for decomposition of nitrous acid in ammonium and sodium nitrate solutions, and the results interpreted in terms of the activity coefficients of the species involved. An initial increase in the observed equilibrium constant was caused by a decline in the activity coefficient of nitrate ions, whilst a decrease at higher concentrations arose as a result of increases in the activity coefficients of NO and  $\text{H}^+$  relative to that of  $\text{HNO}_2$ . Models were developed to describe the effect of  $\text{NH}_4\text{NO}_3$  concentration on the  $\text{HNO}_2$ , NO and  $\text{H}^+$  activity coefficients, permitting extrapolation of the results to solutions of supersaturated ammonium nitrate relevant to emulsion explosives, where direct measurements are not possible. It was shown that the effect of the activity coefficients on the equilibrium concentration of aqueous NO is small, however, the reduced solubility of NO in  $13 \text{ mol L}^{-1}$  ammonium nitrate results in a nitric oxide concentration four times larger than would be predicted without accounting for the effects of non-unity activity coefficients.

## 8.6 References

1. Park, J. Y.; Lee, Y. N., Solubility and decomposition kinetics of nitrous acid in aqueous solution. *J. Phys. Chem.* **1988**, *92* (22), 6294-302.
2. Schwartz, S. E.; White, W. H., Kinetics of reactive dissolution of nitrogen oxides into aqueous solution. *Adv. Environ. Sci. Technol.* **1983**, *12*, 1-116.
3. Patwardhan, J.; Joshi, J., Unified model for NO<sub>x</sub> absorption in aqueous alkaline and dilute acidic solutions. *AIChE J.* **2003**, *49* (11), 2728-2748.
4. Ingale, N. D.; Chatterjee, I. B.; Joshi, J. B., Role of nitrous acid decomposition in absorber and bleacher in nitric acid plant. *Chem. Eng. J. (Amsterdam, Neth.)* **2009**, *155* (3), 851-858.
5. Zollinger, H., *Azo and Diazo Chemistry: Aliphatic and Aromatic Compounds*. Interscience Publishers Inc.: New York, 1961.
6. Sudweeks, W. B., Physical and chemical properties of industrial slurry explosives. *Ind. Eng. Chem. Prod. Res. Dev.* **1985**, *24* (3), 432-6.
7. Bourne, N. K.; Field, J. E., Bubble collapse and the initiation of explosion. *Proc. R. Soc. London, Ser. A* **1991**, *435* (1894), 423-435.
8. da Silva, G.; Dlugogorski, B. Z.; Kennedy, E. M., An experimental and theoretical study of the nitrosation of ammonia and thiourea. *Chem. Eng. Sci.* **2006**, *61* (10), 3186-3197.
9. Abel, E.; Schmid, H., Kinetics of nitrous acid. VI. Equilibrium of the nitrous acid-nitric acid-nitric oxide reaction together with its kinetics. *Z. physik. Chem.* **1928**, *136*, 430-6.

10. Zemaitis, J. F. J.; Clark, D. M.; Rafal, M.; Scrivner, N. D., *Handbook of Aqueous Electrolyte Thermodynamics*. American Institute of Chemical Engineers, New York, NY: 1986.
11. Wishaw, B. F.; Stokes, R. H., The osmotic and activity coefficients of aqueous solutions of ammonium chloride and ammonium nitrate at 25 °C. *Trans. Faraday Soc.* **1953**, *49*, 27-31.
12. Tu, C.; Swenson, E. R.; Silverman, D. N., Membrane inlet for mass spectrometric measurement of nitric oxide. *Free Radical Biol. Med.* **2007**, *43*, 1453-1457.
13. Davey, N. G.; Krogh, E. T.; Gill, C. G., Membrane-introduction mass spectrometry (MIMS). *TrAC, Trends Anal. Chem.* **2011**, *30* (9), 1477-1485.
14. Williams, D. L. H., *Nitrosation Reactions and the Chemistry of Nitric Oxide*. Elsevier B. V.: Amsterdam, 2004.
15. da Silva, G.; Kennedy, E. M.; Dlugogorski, B. Z., Ab Initio procedure for aqueous-phase pKa calculation: The acidity of nitrous acid. *J. Phys. Chem. A* **2006**, *110*, 11371-11376.
16. Davis, W.; De Bruin, H. J., New activity coefficients of 0-100 per cent aqueous nitric acid. *J. Inorg. Nucl. Chem.* **1964**, *26* (6), 1069-1083.
17. Wang, P.; Anderko, A.; Young, R. D., A speciation-based model for mixed-solvent electrolyte systems. *Fluid Phase Equilib.* **2002**, *203* (1-2), 141-176.
18. Wang, P.; Springer, R. D.; Anderko, A.; Young, R. D., Modeling phase equilibria and speciation in mixed-solvent electrolyte systems. *Fluid Phase Equilib.* **2004**, *222-223* (0), 11-17.

19. Becker, K. H.; Kleffmann, J.; Negri, R. M.; Wiesen, P., Solubility of nitrous acid (HONO) in ammonium sulfate solutions. *J. Chem. Soc., Faraday Trans.* **1998**, *94* (11), 1583-1586.
20. Becker, K. H.; Kleffmann, J. r.; Kurtenbach, R.; Wiesen, P., Solubility of nitrous acid (HONO) in sulfuric acid solutions. *J. Phys. Chem.* **1996**, *100* (36), 14984-14990.

## **CHAPTER 9**

**Kinetic model of NO<sub>x</sub> and N<sub>2</sub> formation reactions and comparison to  
observed NO<sub>x</sub> formation during chemical gassing of emulsion explosives**

## Table of Contents

9.1	Introduction	245
9.2	Experimental	247
9.2.1	NO measurements during gassing of ammonium nitrate solutions	247
9.2.2	Generation of ammonium nitrate emulsions	247
9.2.3	NO <sub>x</sub> measurements during gassing of ammonium nitrate emulsions	248
9.3	Development of kinetic model	250
9.3.1	Model validation	261
9.3.2	Sensitivity analysis – NO <sub>x</sub> formation during emulsion gassing	265
9.4	Results for NO <sub>x</sub> formation in emulsion gassing	271
9.4.1	Effect of acetic acid concentration on NO <sub>x</sub> formation	271
9.4.2	Effect of added substrates	276
9.4.3	Effect of temperature	278
9.5	NO <sub>x</sub> formation from direct mixing of acid and nitrite gasser solutions	283
9.6	Conclusion	289
9.6	References	291



## 9.1 Introduction

The decomposition of nitrous acid has been identified as a possible source of NO<sub>x</sub> during the chemical gassing of emulsion explosives. Chapter 4 examined the kinetics of nitrous acid decomposition in dilute acid solution, whilst Chapters 7 and 8 discuss the effect of ammonium nitrate concentration on the solubility of nitric oxide and nitrous acid decomposition equilibrium, respectively. During the gassing of an emulsion explosive, nitrous acid can undergo decomposition, forming nitric oxide<sup>1</sup>, or can give rise to N<sub>2</sub> via reaction with ammonia<sup>2</sup>. The rates of these competing reaction pathways are interrelated, because they both depend on the concentration of nitrous acid<sup>3,4</sup>. As such, both reaction pathways must be taken into account when attempting to predict the quantity of NO<sub>x</sub> formed during the sensitisation process. A model for the nitrosation of ammonia, including the effect of added nucleophile catalysts, has previously been developed by da Silva et al. (2007)<sup>5</sup>. In this chapter, a kinetic model is developed to predict the rate of NO formation during the chemical gassing of emulsion explosives. The model incorporates the previous work of da Silva et al. (2007)<sup>5</sup>, in addition to new equations to simulate the decomposition of nitrous acid, the temperature dependence of the rate constants, and the rate of transfer of nitric oxide from the aqueous phase to the gas bubbles in an emulsion. In addition, the reactions between nitrous acid and additional reaction substrates were included to evaluate the impact of the substrate on NO formation.

To validate the model, experiments were performed to investigate the formation of both NO and N<sub>2</sub> resulting from the gassing of ammonium nitrate solutions with NaNO<sub>2</sub>. Additional experiments were then carried out to quantify the amount of NO<sub>x</sub> produced from gassing actual emulsion explosives. The procedure involved gassing the emulsion

inside a sealed glove box, liberating the gas trapped within the emulsion, and determining the NO<sub>x</sub> concentration. The aims of these experiments were:

- To determine the amount of NO<sub>x</sub> formed during gassing of emulsion explosives under laboratory conditions, and to examine the effect of acid concentration.
- To compare experimentally determined NO<sub>x</sub> levels to those predicted from kinetic models of known NO<sub>x</sub> formation reactions to establish conclusively if nitrous acid decomposition is the source of NO<sub>x</sub> during explosive sensitisation.

In addition, it was hypothesised that extremely rapid NO formation could result from direct contact between the concentrated acetic acid and sodium nitrite solutions which are employed for chemical gassing. Experiments were performed to quantify the amount of NO produced under this scenario, and to determine whether inclusion of additional reaction substrates in the gassing solutions could reduce NO formation.

## 9.2 Experimental

### 9.2.1 NO measurements during gassing of ammonium nitrate solutions

NO measurements in ammonium nitrate solutions were performed in a gas-liquid reactor with membrane inlet mounted in the gas phase, as described in Chapter 8. The reactor was loaded with 74 cm<sup>3</sup> of freshly prepared ammonium nitrate solution containing the desired concentration of nitrite ions. Oxygen was purged from the reactor with a stream of nitrogen gas, which flowed at a rate of 1.2 cm<sup>3</sup> s<sup>-1</sup> for 20 min prior to the start of the experiment. The nitrogen for the purging process was introduced via a section of ¼ inch (6.35 mm) stainless steel tubing inserted through a septum side port, and exited the vessel through a needle inserted through the rubber stopper at the top of the reactor. Upon completion of the purging process, the needle was plugged by inserting a 25 cm<sup>3</sup> syringe, and the stainless steel tubing removed. The nitrogen flow was then connected to the membrane inlet line, and adjusted to 0.67 cm<sup>3</sup> s<sup>-1</sup>. Reaction was initiated by injection of 1 cm<sup>3</sup> of acetic acid solution to the reaction vessel via the septum side port. The pressure inside the reactor was maintained at atmospheric by allowing expansion of the syringe plunger to accommodate N<sub>2</sub> produced in the course of the reaction. The rate of N<sub>2</sub> formation was determined from the rate of increase in the gas volume contained within the syringe.

### 9.2.2 Generation of ammonium nitrate emulsions

Emulsion explosives consist of a concentrated ammonium nitrate solution dispersed within a continuous hydrocarbon phase. The oxidiser phase of the emulsion (discontinuous phase) typically constitutes approximately 94 % of the emulsion mass

and comprises a 75 % w/w ammonium nitrate solution. To accelerate the gassing reaction, sodium thiocyanate can be incorporated into the ammonium nitrate solution. The continuous phase (fuel phase) constitutes the remaining 6% of the emulsion mass and typically contains a mixture of diesel fuel and a polyisobutylene succinic anhydride (PIBSA) based emulsifier<sup>6</sup>. To prepare the emulsion, the oxidiser phase components were weighed into a stainless steel jug, and heated to 80 °C with continuous stirring to dissolve all of the ammonium nitrate. Once the ammonium nitrate was dissolved, the pH of the solution was adjusted to 5 by addition of concentrated sodium hydroxide solution. The fuel phase was weighed out in a separate stainless steel container and heated to 60 °C. The emulsion was formed by slowly pouring the oxidiser phase solution into the fuel phase with continual stirring by an overhead mixer, over a period of 60 s. The speed of the mixer was increased gradually from 600 to 1700 rpm over a further 120 s, or until the viscosity had reached between 22 – 28 Pa s. Viscosity measurements were performed on a Brookfield RVDVII+ viscometer with no. 7 spindle at 20 rpm.

### **9.2.3 NO<sub>x</sub> measurements during gassing of ammonium nitrate emulsions**

The standard process for gassing an emulsion explosive in the laboratory involves consecutive addition of concentrated acetic acid (45 % w/w solution in water) and sodium nitrate solutions (25 % w/w solution in water) to the emulsion, mixing each solution for a period of 30 s. The emulsion is then weighed into a stainless steel cup of known mass and volume. A spatula is used to scrape the emulsion from the top of the cup, such that the emulsion is levelled with the rim of the cup, and the initial mass recorded. As gas is produced, the emulsion expands over the rim of the cup, and the

excess emulsion is removed with a spatula and the cup re-weighed. The density change of the gassed emulsion can then be determined from the change in the mass of emulsion held within the cup of known volume. This type of experiment enabled determination of the time taken for complete gassing to occur.

A similar procedure was employed to determine the level of NO<sub>x</sub> produced during gassing, except that in this case the gassing process occurred within a sealed glove box. The apparatus consisted of the Thermo 42i-HL NO<sub>x</sub> analyser connected to a plastic glove box with a volume of 50 L, similar to the apparatus described by Vestre (2003)<sup>7</sup>. A cylinder of nitrogen gas and a flow meter enabled the box to be purged with nitrogen prior to the start of experiments. A container holding a known mass of emulsion, along with syringes holding the gassing chemicals were loaded into the glove box. The box was then sealed to the atmosphere, and flushed with nitrogen for at least 15 min at a flow of 10 L min<sup>-1</sup>. After this time, the gas flow was reduced to 25 cm<sup>3</sup> min<sup>-1</sup>, and the gassing chemicals were mixed sequentially into the emulsion. The concentration of nitrogen oxides in the box was continually monitored using the NO<sub>x</sub> analyser. After gassing was substantially complete (typically around 90 min), the gas was stirred out of the emulsion using a spatula, liberating any NO<sub>x</sub> contained within the emulsion gas bubbles, and a final NO<sub>x</sub> reading taken.

### 9.3 Development of kinetic model

Table 1 summarises the chemical reactions constituting the kinetic model. Reactions M1-M8 describe the various nitrosation pathways and are as shown in da Silva et al. (2007)<sup>5</sup>, whilst reactions M9-M11 describe the formation of NO<sub>x</sub> from the decomposition of nitrous acid. The rate constants for Reaction M9 have been selected to yield the correct value of  $K_9^2 k_{10}$  as determined in Chapter 4 ( $k = 1.35 \times 10^{-6} \text{ L mol}^{-1} \text{ s}^{-1}$ ), whilst the reverse rate constant for Reaction M10 has been modified to yield the correct value of  $K_9^2 K_{10}$  in  $13 \text{ mol L}^{-1} \text{ NH}_4\text{NO}_3$  as determined in Chapter 8. Reaction M12 has been included so that the effect of the acetic acid concentration is accounted for, whilst Reactions M13-M14 describe the nitrosation of sulfamate ions and urea, respectively. It has been assumed that these substrates do not give rise to additional NO<sub>x</sub> formation reactions. It may be noted that the rate constant for reaction M6 estimated in Ref 5, somewhat exceeds the limit for diffusion control. The apparent rate of nitrosation depends on both the equilibrium constant for formation of ON<sup>+</sup> and the rate of reaction between the ON<sup>+</sup> and NH<sub>3</sub>. As such, it is likely that the high value of the rate constant arises due to uncertainty in the value of the equilibrium constant (i.e. M4), which is difficult to accurately measure. The model will predict the correct rate of the nitrosation reaction provided that the product of the rate and the equilibrium constant is correct. The model consists of a series of ordinary differential equations (ODEs) describing the reaction system summarised in Table 1. Appendix E provides a complete description of the equations comprising the model..

In the case of protonation equilibria, the rate constant of the association reaction between the hydrogen ion and the base was assumed to occur at the diffusion controlled limit ( $10^{10} \text{ L mol}^{-1} \text{ s}^{-1}$  at 298 K)<sup>8</sup> with the dissociation reaction rate constant determined

from the equilibrium constant. The stiff ODE solver in Polymath 5.0 was employed to solve the system of equations for a given set of initial conditions (i.e. species concentrations). Because the concentrations of gassing chemicals are low, and the rate of reaction is slow, the effect of heat released from the chemical reaction on the emulsion temperature is negligible. As such, the system is treated as isothermal, i.e. the temperature remains constant throughout the reaction. Incorporation of appropriate equations to describe the heat transfer between the emulsion and surroundings could potentially be included to allow modelling of transient temperatures. The effect of temperature on the reaction rate constants was determined using Equation 1

$$k = k_o \exp\left(\frac{E_A}{R} \left(\frac{1}{T_o} - \frac{1}{T}\right)\right) \quad (1)$$

where  $k$  is the reaction rate constant at temperature  $T$  (K),  $k_o$  is the rate constant at a reference temperature  $T_o$ ,  $E_A$  is the activation energy of the reaction (J mol<sup>-1</sup>) and  $R$  is the gas constant (J mol<sup>-1</sup> K<sup>-1</sup>). In some cases only the enthalpy of reaction was known, which allowed the changes to the equilibrium constant to be determined, but not the changes to the individual rates of reaction. In these cases, estimates were made for the activation energies such that they produced the correct value of the enthalpy of reaction. Reactions occurring at the diffusion controlled limit were assumed to have activation energies of 20 kJ mol<sup>-1</sup>.

It was noted that the activation energies for ammonia nitrosation reported by da Silva et al. (2006)<sup>9</sup> did not account for the effect of temperature on the equilibrium constants for N<sub>2</sub>O<sub>3</sub> and ONSCN formation and for dissociation of HNO<sub>2</sub> and NH<sub>4</sub><sup>+</sup>. That is, the effect of temperature on these equilibrium constants is included in the reported

activation energy. While the impact of temperature on  $K_{HNO_2}$ ,  $K_{N_2O_3}$  and  $K_{ONSCN}$  are reasonably small, the dissociation of  $NH_4^+$  exhibits a significant enthalpy of reaction of 52 kJ. As such, it was essential to correct the observed activation energies reported by da Silva et al. for the effect of temperature on these dissociation equilibria. Expressions for the observed rate constant (for which activation energies were reported by da Silva et al.) are shown in Equations 2 and 3 for ammonia nitrosation by  $N_2O_3$  and  $ONSCN$ , respectively.

$$k_{obs} = \frac{k_{M5} K_{N_2O_3} K_{NH_3} [H^+] [NH_4^+]}{(K_{HNO_2} + [H^+])^2} \quad (N_2O_3 \text{ pathway}) \quad (2)$$

$$k_{obs} = \frac{k_{M8} K_{ONSCN} K_{NH_3} [H^+] [NH_4^+]}{(K_{HNO_2} + [H^+])} \quad (ONSCN \text{ pathway}) \quad (3)$$

where  $k_N$  is the rate constant for the reaction of the nucleophile with  $NH_3$ . The following expressions were derived to determine the activation energy of  $k_N$ .

$$E_a(k_N) = E_a(k_{obs}) + 2\Delta H_{HNO_2} - \Delta H_{N_2O_3} - \Delta H_{NH_3} \quad (4)$$

$$E_a(k_N) = E_a(k_{obs}) + \Delta H_{HNO_2} - \Delta H_{ONSCN} - \Delta H_{NH_3} \quad (5)$$



**Table 1. Chemical reactions and rate constants employed in the model**

Eqn	Reaction	$k_f$	$k_b$	Ref
M1	$\text{NO}_2^- + \text{H}^+ \rightleftharpoons \text{HONO}$	$1 \times 10^{10} \text{ M}^{-1} \text{ s}^{-1}$	$6.93 \times 10^6 \text{ s}^{-1}$	Ref <sup>5</sup>
M2	$\text{NH}_4^+ \rightleftharpoons \text{NH}_3 + \text{H}^+$	$21.5 \text{ s}^{-1}$	$4.3 \times 10^{10} \text{ M}^{-1} \text{ s}^{-1}$	Ref <sup>5</sup>
M3	$\text{HONO} + \text{NO}_2^- + \text{H}^+ \rightleftharpoons \text{N}_2\text{O}_3 + \text{H}_2\text{O}$	$32,000 \text{ M}^{-2} \text{ s}^{-1}$	$6400 \text{ s}^{-1}$	Ref <sup>5</sup>
M4	$\text{HONO} + \text{H}^+ \rightleftharpoons \text{ON}^+ + \text{H}_2\text{O}$	$12,000 \text{ M}^{-1} \text{ s}^{-1}$	$1.0 \times 10^{12} \text{ s}^{-1}$	Ref <sup>5</sup>
M5	$\text{N}_2\text{O}_3 + \text{NH}_3 \rightarrow \text{N}_2 + \text{NO}_2^- + \text{H}^+ + \text{H}_2\text{O}$	$4.3 \times 10^6 \text{ M}^{-1} \text{ s}^{-1}$	N/A	Ref <sup>5</sup>
M6	$\text{ON}^+ + \text{NH}_3 \rightarrow \text{N}_2 + \text{H}^+ + \text{H}_2\text{O}$	$3.8 \times 10^{11} \text{ M}^{-1} \text{ s}^{-1}$	N/A	Ref <sup>5</sup>
M7	$\text{HONO} + \text{SCN}^- + \text{H}^+ \rightleftharpoons \text{ONSCN} + \text{H}_2\text{O}$	$11700 \text{ M}^{-2} \text{ s}^{-1}$	$366 \text{ s}^{-1}$	Ref <sup>5</sup>
M8	$\text{ONSCN} + \text{NH}_3 \rightarrow \text{N}_2 + \text{SCN}^- + \text{H}^+ + \text{H}_2\text{O}$	$8.4 \times 10^5 \text{ M}^{-1} \text{ s}^{-1}$	N/A	Ref <sup>5</sup>
M9	$2\text{HONO} \rightleftharpoons \text{NO} + \text{NO}_2 + \text{H}_2\text{O}$	11.6	$1 \times 10^8 \text{ M}^{-1} \text{ s}^{-1}$	Ref <sup>10</sup> , present study
M10	$2\text{NO}_2 + \text{H}_2\text{O} \rightleftharpoons \text{HNO}_2 + \text{NO}_3^- + \text{H}^+$	$1 \times 10^8 \text{ M}^{-1} \text{ s}^{-1}$	$0.0127 \text{ M}^{-2} \text{ s}^{-1}$	Ref <sup>10</sup> , present study
M11	$2\text{NO}_{(\text{Aq})} + \text{O}_{2(\text{Aq})} \rightarrow 2\text{NO}_{2(\text{Aq})}$	$2.1 \times 10^6 \text{ M}^{-2} \text{ s}^{-2}$	N/A	Ref <sup>11</sup>
M12	$\text{CH}_3\text{COO}^- + \text{H}^+ \rightleftharpoons \text{CH}_3\text{COOH}$	$1 \times 10^{10} \text{ M}^{-1} \text{ s}^{-1}$	$1.738 \times 10^5 \text{ s}^{-1}$	Ref <sup>12</sup>
M13	$\text{SO}_3\text{NH}_2^- + \text{NO}^+ \rightarrow \text{N}_2 + \text{HSO}_4^- + \text{H}^+$	$1.5 \times 10^{11} \text{ M}^{-1} \text{ s}^{-1}$	N/A	Refs <sup>13,14</sup>
M14	$\text{CO}(\text{NH}_2)_2 + \text{NO}^+ \rightarrow \text{N}_2 + \text{CO}_2 + \text{NH}_4^+$	$4.8 \times 10^7 \text{ M}^{-1} \text{ s}^{-1}$	N/A	Refs <sup>15,16</sup>
M15	$\text{HSO}_4^- \rightleftharpoons \text{H}^+ + \text{SO}_4^{2-}$	$1.1 \times 10^8 \text{ s}^{-1}$	$1 \times 10^{10} \text{ M}^{-1} \text{ s}^{-1}$	Ref <sup>17</sup>

**Table 2. Activation energies for forward and reverse reactions**

<b>Eqn</b>	<b><math>E_{a, forward}</math> (kJ/mol)</b>	<b><math>E_{a, backward}</math> (kJ/mol)</b>	<b>Ref</b>
M1	20	26.7	Ref <sup>18</sup>
M2	72	20	Ref <sup>19</sup>
M3	20	29.9	This study <sup>a</sup>
M4	65.2	20	Ref <sup>5</sup>
M5	30	N/A	Ref <sup>9</sup>
M6	20	N/A	Estimate
M7	20	32	This study <sup>b</sup>
M8	36	N/A	Ref <sup>9</sup>
M9	65	22	Ref <sup>20</sup>
M10	20	75	This study
M11	9.6	N/A	Ref <sup>21</sup>
M12	0	0	Ref <sup>12</sup>
M13	9.2	N/A	Refs <sup>13,14</sup>
M14	17	N/A	Refs <sup>15,16</sup>
M15	1.5	20	Ref <sup>17</sup>

<sup>a</sup> Values estimated based on the enthalpy of reaction determined quantum chemically.

<sup>b</sup> Estimated based on the enthalpy of reaction reported by Stedman & Whincup<sup>22</sup>

The rate of decomposition of nitrous acid depends on the concentration of aqueous nitric oxide (Reaction M9) and as such, accurate prediction of aqueous NO and NO<sub>2</sub> concentrations is essential for modelling the overall rate of NO<sub>x</sub> formation. Appropriate equations have been included in the model to account for the transfer of aqueous NO<sub>x</sub> to the gas phase. The precise formulation of these equations depends on the method employed to study the reactions (i.e. gas-liquid reactor or emulsion). Henry's law

states that the equilibrium concentration of dissolved gas is proportional to the partial pressure of the species in the gas phase.

$$[G]_{Eqm} = k_H P_G \quad (6)$$

where  $[G]_{Eqm}$  is the aqueous phase concentration of species  $G$  (mol L<sup>-1</sup>) at equilibrium with a gas phase partial pressure of  $P_G$  (bar), and  $k_H$  is the Henry's constant for that species (mol L<sup>-1</sup> bar), which is temperature dependent. The Henry's constants for nitric oxide in ammonium nitrate solutions were determined in Chapter 7. Extrapolation of these results to 13 mol L<sup>-1</sup> NH<sub>4</sub>NO<sub>3</sub> yields a Henry's constant for NO of  $4.1 \times 10^{-4}$  mol L<sup>-1</sup> bar<sup>-1</sup> at 25 °C. The solubility of NO<sub>2</sub> was estimated assuming that the ratio of the gas solubility in water to that in an ammonium nitrate solution was the same for NO and NO<sub>2</sub>. Equations 7-9 were employed to quantify the effects of temperature and ammonium nitrate concentration on the solubility of NO:

$$\log\left(\frac{k_{H,o}(T)}{k_H}\right) = k_s(T)[S] \quad (7)$$

$$k_s = -0.00043T + 0.18039 \quad (8)$$

$$k_{H,o} = 0.00193 \exp\left(-1615\left(\frac{1}{298.15} - \frac{1}{T}\right)\right) \quad (9)$$

where  $k_{H,o}$  is the Henry's constant of NO in water at temperature  $T$  (K),  $k_H$  is the Henry's constant of NO in a salt solution with concentration  $[S]$  (mol L<sup>-1</sup>) and  $k_s$  is the

salting out parameter (L mol<sup>-1</sup>). The rate of mass transfer of NO<sub>x</sub> from the aqueous phase to the gas phase has been modelled using Whitman's two film theory (as described by McCabe et al. 2005)<sup>23</sup>, in which the gas and liquid concentrations are assumed to be in equilibrium at the interface and the resistance to mass transfer in each phase is added to find the overall resistance, i.e.

$$R_{MT} = K_{MT} A ([G] - [G]_{Eqm}) \quad (10)$$

where  $R_{MT}$  is the rate of mass transfer (mol s<sup>-1</sup>),  $K_{MT}$  is the overall mass transfer coefficient (mm s<sup>-1</sup>),  $A$  is the interfacial area (m<sup>2</sup>),  $[G]$  is the concentration of species  $G$  (mol L<sup>-1</sup>) and  $[G]_{Eqm}$  is the liquid phase concentration of species  $G$  if it were in equilibrium with the gas phase.  $[G]_{Eqm}$  was calculated using Henry's law based on the bulk gas phase partial pressure of the species of interest.

In the case of the gas liquid reactor, Equation 10 was incorporated into the mass balance equations for NO in the gas and aqueous phases, as shown in Equations (11) and (12). For the gas liquid reactor, the interfacial area is unknown, and the parameters  $K_{MT}$  and  $A$  are lumped together and denoted  $K_{MT}^*$  (i.e.  $K_{MT}^* = K_{MT}A$ ).

$$\frac{d[NO]}{dt} = -\frac{K_{MT}^* ([NO] - k_{NO} RTC_{NO})}{V_{aq}} + r_{NO} \quad (11)$$

$$\frac{dC_{NO}}{dt} = \frac{K_{MT}^* ([NO] - k_{NO} RTC_{NO})}{V_{gas}} - \frac{v}{V_{gas}} C_{NO} \quad (12)$$

where  $V_{aq}$  is the volume of solution in the reactor (L),  $r_{NO}$  is the rate of nitric oxide generation by chemical reaction ( $\text{mol L}^{-1} \text{s}^{-1}$ ),  $V_{gas}$  is the volume of gas in the reactor (L) and  $v$  is the volumetric gas flowrate into the reactor ( $\text{L s}^{-1}$ ). Equations 7 and 8 consist of a coupled set of ordinary differential equations and were solved numerically using the Polymath 5.0 stiff ordinary differential equation solver. The complete model is provided in Appendix E. In the absence of chemical reaction,  $K_{MT}^*$  represents the only unknown term in Equations 11 and 12. As such, the mass transfer coefficient was determined in separate experiments by rapidly generating NO in the reactor via the reduction of nitrous acid by ascorbate. The parameter  $K_{MT}^*$  was determined by adjusting this variable in the Polymath simulations to provide the best fit to the experimental data. To confirm that the correct value of  $K_{MT}^*$  had been determined, and to verify that the gas-liquid membrane inlet setup was suitable for kinetic analysis, an experiment was performed to generate NO via the decomposition of  $0.015 \text{ mol L}^{-1}$  sodium nitrite in  $0.03 \text{ mol L}^{-1}$  acetic acid, and the results compared to the model predictions (Figure 1). The model predictions coincided closely with the experimental data, confirming the mass transfer coefficient ( $K_{MT}^*$ ) of the reactor setup to be  $0.003 \text{ L s}^{-1}$ .

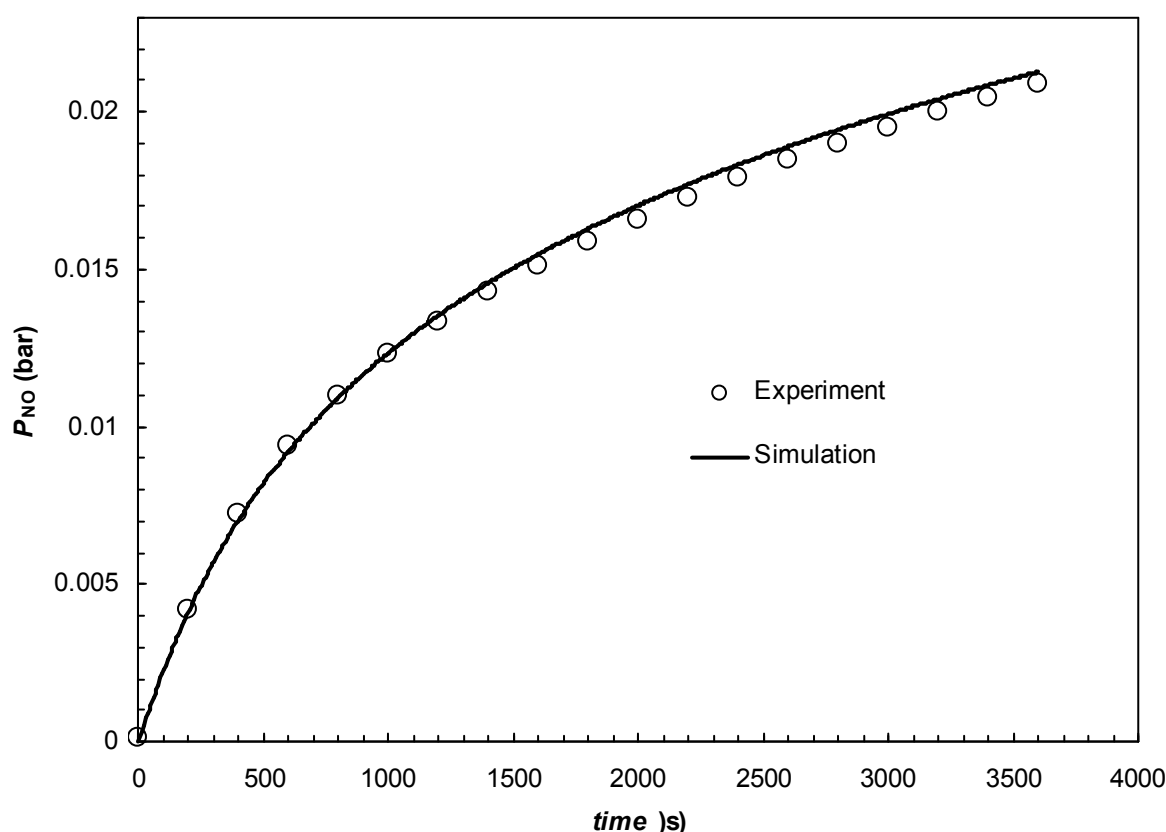


**Figure 1: Comparison of measured and simulated NO partial pressure for decomposition of  $0.015 \text{ mol L}^{-1} \text{ NaNO}_2$  in  $0.03 \text{ mol L}^{-1} \text{ CH}_3\text{COOH}$  in gas-liquid membrane reactor at  $25^\circ\text{C}$**

In the case of the emulsion experiments it was not possible to experimentally determine the mass transfer coefficient. Furthermore, the interfacial area would be expected to increase with time as the volume of gas bubbles in the emulsion increased. Consequently, the mass transfer coefficient and area must be treated explicitly. The overall mass transfer coefficient,  $K_{MT}$ , is made up of the coefficients of the individual phases, which depend on the diffusivity of the species and the film thickness over which mass transfer is occurring. Because the diffusivity of molecules through a gas is much higher than through liquids, the gas phase mass transfer resistance has been neglected

and the overall mass transfer coefficient approximated by the liquid phase coefficient,  $k_x$ :

$$k_x = \frac{D_{AB}}{\delta_T} \quad (13)$$

where  $D_{AB}$  is the diffusivity of species  $A$  through species  $B$  ( $\text{m}^2 \text{s}^{-1}$ ), and  $\delta_T$  is the thickness of the film (m) over which the change in  $C_A$  occurs (i.e. the distance from the interface to where local concentration of species  $A$  is the same as that of the bulk). The diffusivity of NO through water was taken as  $2.1 \times 10^{-9} \text{ m}^2 \text{s}^{-1}$  (Zacharia et al. 2005) and the film thickness assumed to be the maximum distance of an oxidiser phase emulsion droplet to a gas bubble, yielding an estimate value of  $k_x = 0.011 \text{ mm s}^{-1}$  for NO. The same value of the mass transfer coefficient was employed for NO<sub>2</sub>. The mass transfer film thickness should not be confused with the thickness of fuel films/lamellae in the emulsion. Selection of the mass transfer coefficient is explained in more detail on pages 266-267.

The interfacial area between the gas and aqueous phases, over which mass transfer occurs, increases as the gas bubbles grow. The mass transfer area was modelled assuming that the number of bubbles was constant throughout the simulation. The number of bubbles was estimated assuming a final bubble size of 400  $\mu\text{m}$ , and a final emulsion density of  $1.0 \text{ g cm}^{-3}$ . The gas bubbles were assumed to be of uniform size. In practice, a range of bubble sizes would be present, with coarsening occurring (i.e. shrinking of small bubbles and growth of larger ones) due to Ostwald ripening<sup>24</sup>. The bubbles start with negligible size and grow throughout the gassing process, allowing their area to be determined for the mass transfer rate calculation. For this purpose, an

additional ODE is included in the model to account for the increase in gas volume with time.

$$\frac{dV_{gas}}{dt} = \frac{8.314T}{101.325} (V_{aq}r_{N2} + R_{MT(NO)} + R_{MT(NO2)}) \quad (10)$$

where  $T$  is temperature (K),  $r_{N2}$  is the rate of nitrogen formation via chemical reaction ( $\text{mol L}^{-1} \text{s}^{-1}$ ),  $V_{aq}$  is the volume of the aqueous phase (L) and  $R_{MT(NO)}$  and  $R_{MT(NO2)}$  are the rates of mass transfer of NO and NO<sub>2</sub> from the aqueous to the gas phase ( $\text{mol s}^{-1}$ ).



### 9.3.1 Model validation

Experiments were performed in the gas liquid reactor with 2.5 mol L<sup>-1</sup> ammonium nitrate solutions to validate the kinetic model. Two experiments were conducted, both with 0.015 mol L<sup>-1</sup> NaNO<sub>2</sub> and 0.03 mol L<sup>-1</sup> CH<sub>3</sub>COOH, one of which also included 0.05 mol L<sup>-1</sup> NaSCN, which acts as a catalyst for N<sub>2</sub> production through formation of the nitrosating agent nitrosyl thiocyanate (ONSCN). At the conclusion of the run, the spectrum of the reactant solution was taken with the UV-vis. It was noted that the proportion of nitrite in the form of nitrous acid was significantly smaller than would be expected from the p*K<sub>a</sub>*'s of HONO and CH<sub>3</sub>COOH observed in water, precipitating a separate study to determine the effect of ammonium nitrate concentration on the protonation of NO<sub>2</sub><sup>-</sup> by CH<sub>3</sub>COOH. Experiments were performed to determine the fraction of nitrite (initially 0.015 mol L<sup>-1</sup>) converted into nitrous acid by 0.03 mol L<sup>-1</sup> CH<sub>3</sub>COOH in 2.5, 5, 7.5 and 10 mol L<sup>-1</sup> NH<sub>4</sub>NO<sub>3</sub>, the results of which are summarised in Table 3. Further details about these experiments are provided in Appendix E.

**Table 3: Fraction of total nitrite converted to nitrous acid at different ammonium nitrate concentrations for initial NaNO<sub>2</sub> and CH<sub>3</sub>COOH concentrations of 0.015 and 0.03 mol L<sup>-1</sup>, respectively**

[NH <sub>4</sub> NO <sub>3</sub> ] (mol L <sup>-1</sup> )	[HNO <sub>2</sub> ]/[NaNO <sub>2</sub> ] <sub>Total</sub>
0	0.192
2.5	0.159
5	0.136
7.5	0.112
10	0.128

The  $pK_a$  of nitrous acid was adjusted in the model to yield the same nitrous acid concentration determined experimentally. Figure 2 compares the predicted and experimentally determined NO partial pressure in the absence of SCN<sup>-</sup>, whilst Figures 3 and 4 compare the predicted and experimentally determined NO partial pressure and N<sub>2</sub> volumes, respectively, for the experiment with 0.05 mol L<sup>-1</sup> SCN<sup>-</sup>. In the absence of SCN<sup>-</sup>, the model predicts near identical NO partial pressures over time to those observed experimentally. A significantly lower NO partial pressure was observed in the presence of SCN<sup>-</sup>, owing to the increased rate of N<sub>2</sub> formation due to ONSCN. The NO partial pressure increased to a maximum after 1500 s, before decreasing slowly. Similar results were predicted by the model, which showed a slightly higher peak NO partial pressure than the experiment. The predicted and observed rates of N<sub>2</sub> formation were in excellent agreement. This shows that the model can successfully predict both the rates of NO and N<sub>2</sub> formation, including the effect of the nitrosation catalyst SCN<sup>-</sup>.

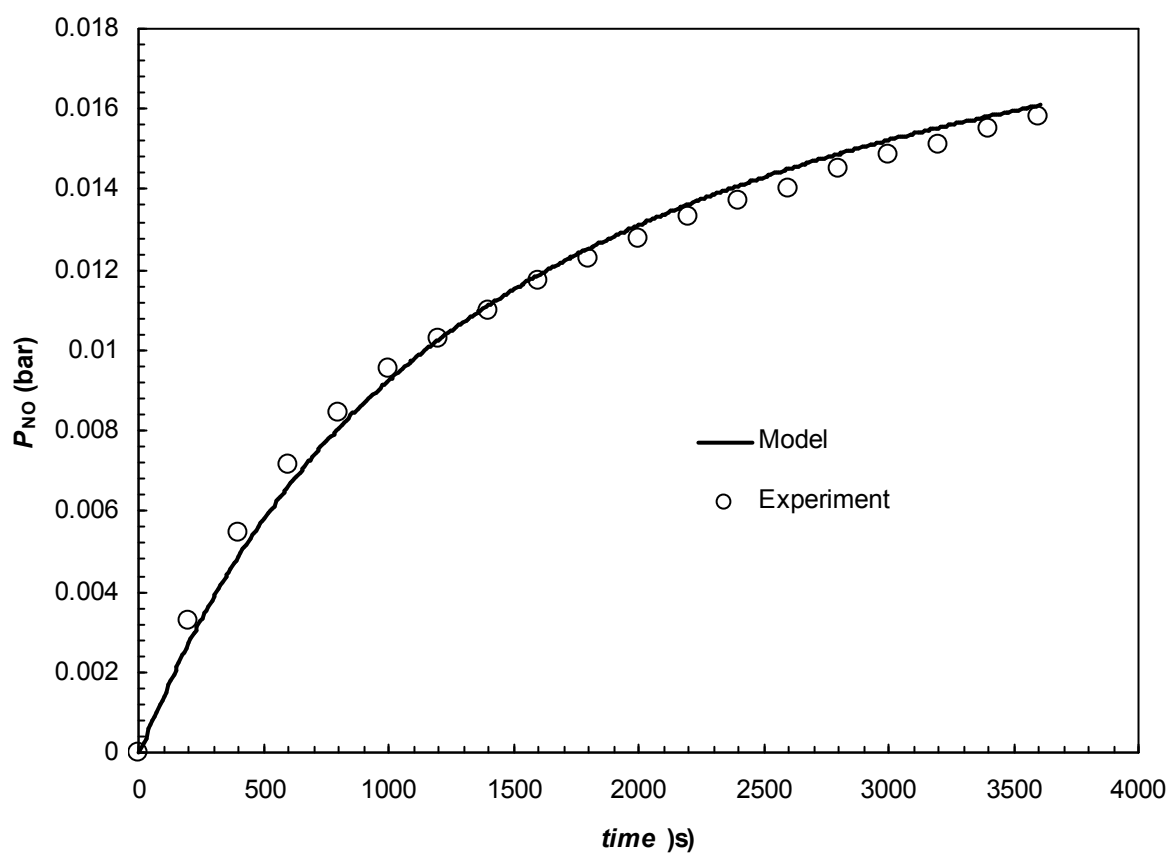


*Figure 2: Comparison of measured and simulated NO partial pressure for decomposition of  $0.015 \text{ mol L}^{-1} \text{ NaNO}_2$  with  $0.03 \text{ mol L}^{-1} \text{ CH}_3\text{COOH}$  in  $2.5 \text{ mol L}^{-1} \text{ NH}_4\text{NO}_3$  in gas-liquid membrane reactor at  $25^\circ\text{C}$*

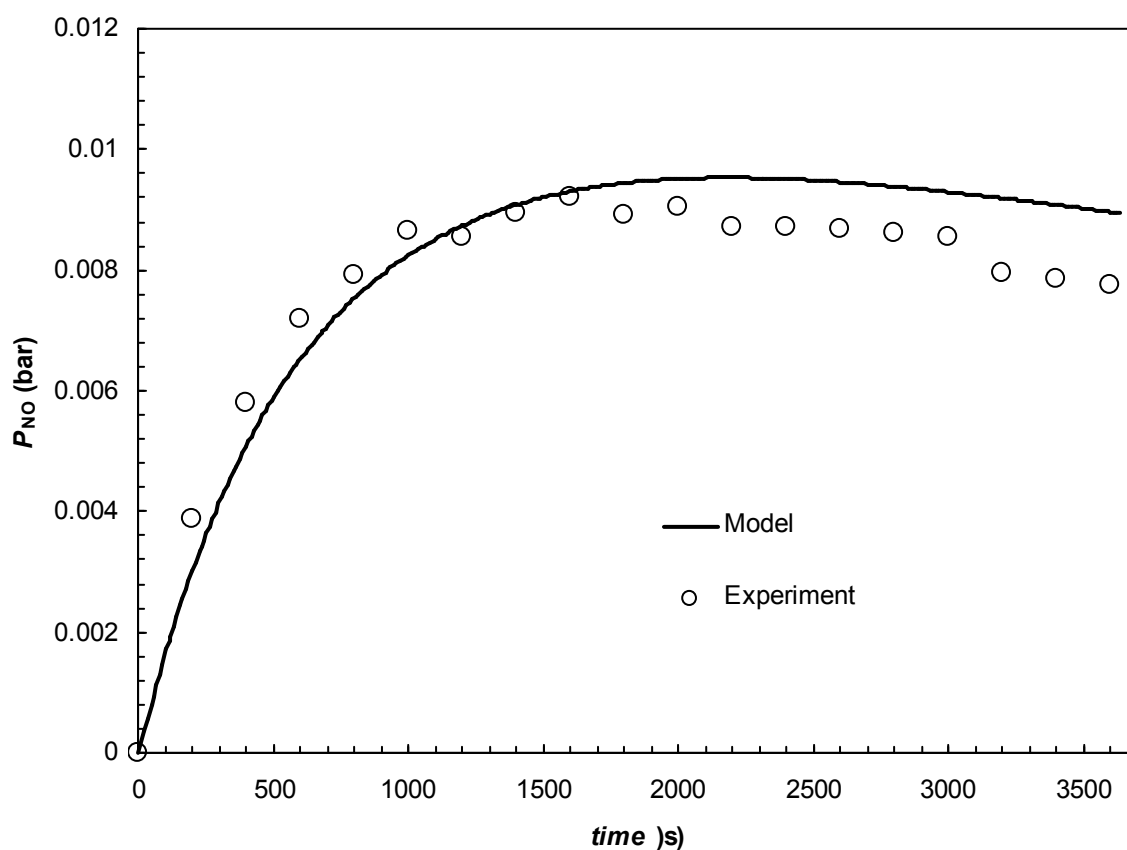


**Figure 3: Comparison of measured and simulated NO partial pressure for decomposition of  $0.015 \text{ mol L}^{-1} \text{ NaNO}_2$  with  $0.03 \text{ mol L}^{-1} \text{ CH}_3\text{COOH}$  and  $0.05 \text{ mol L}^{-1} \text{ NaSCN}$  in  $2.5 \text{ mol L}^{-1} \text{ NH}_4\text{NO}_3$  in gas-liquid membrane reactor at  $25^\circ\text{C}$**

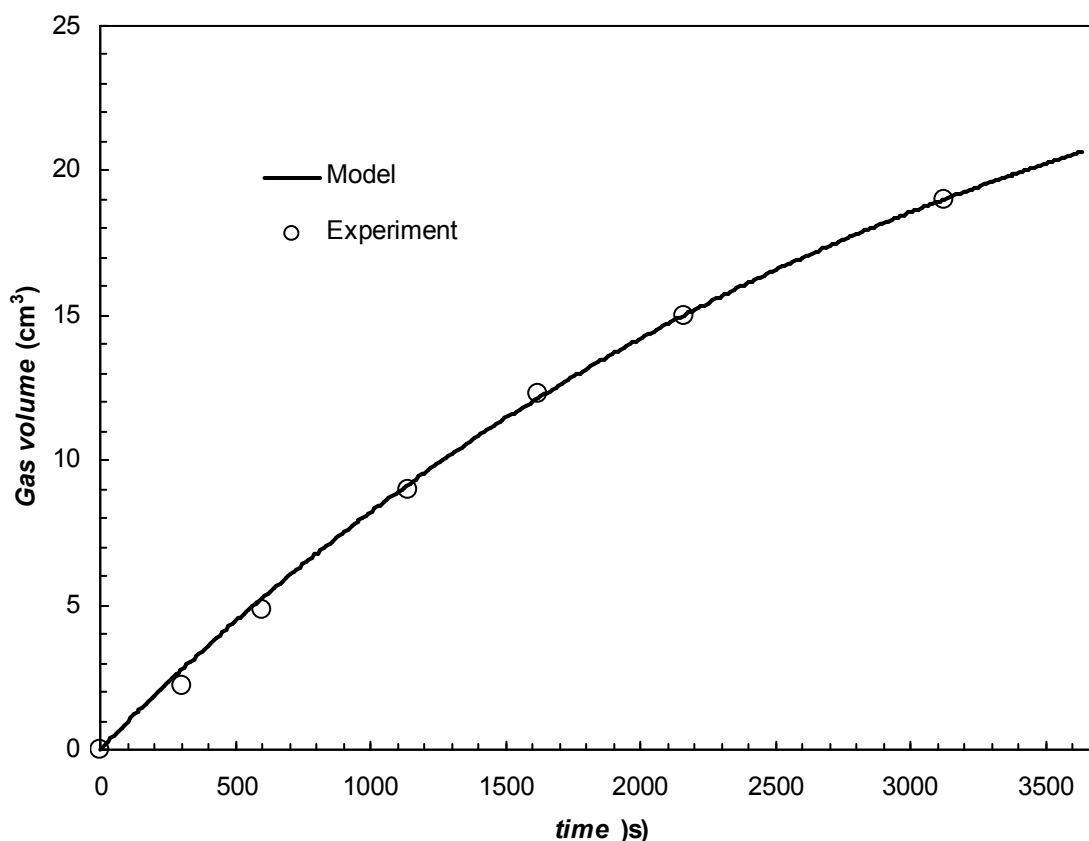


**Figure 4: Comparison of measured and simulated gas production for decomposition of 0.015 mol L<sup>-1</sup> NaNO<sub>2</sub> with 0.03 mol L<sup>-1</sup> CH<sub>3</sub>COOH and 0.05 mol L<sup>-1</sup> NaSCN in 2.5 mol L<sup>-1</sup> NH<sub>4</sub>NO<sub>3</sub> in gas-liquid membrane reactor at 25 °C**

### 9.3.2 Sensitivity analysis – NO<sub>x</sub> formation during emulsion gassing

A series of simulations were performed to ascertain the sensitivity of the model results to changes in a selection of key model parameters. In particular, certain parameters in the model could not be measured experimentally under the conditions present in an emulsion explosive (i.e. 13 mol L<sup>-1</sup> ammonium nitrate) and must therefore be estimated, resulting in a significant degree of uncertainty. These parameters include the mass transfer coefficient, which determines the rate at which NO is transferred from the

aqueous to gas phase, the values of  $K_9^2 k_{10}$  and  $k_{-10}$ , and dissociation constants of CH<sub>3</sub>COOH and HNO<sub>2</sub> in 13 mol L<sup>-1</sup> ammonium nitrate, which could not be measured under these conditions. However, the equilibrium constant,  $K_9^2 K_{10}$  can be estimated in 13 mol L<sup>-1</sup> NH<sub>4</sub>NO<sub>3</sub> based on the results in ammonium nitrate solution, and the individual rate constants  $K_9^2 k_{10}$  and  $k_{-10}$  must be chosen such as to reproduce the correct equilibrium constant. Simulations were therefore performed to determine how the predicted amount of NO<sub>x</sub> formation depends on the values of  $K_{MT}$ ,  $K_9^2 k_{10}$ ,  $k_{-10}$  and the dissociation constants of acetic and nitrous acids. In these simulations, the initial species concentrations were 13, 0.03, 0.024 and 0.015 mol L<sup>-1</sup> for NH<sub>4</sub>NO<sub>3</sub>, CH<sub>3</sub>COOH, NaSCN and NaNO<sub>2</sub>, respectively. Figures 4 and 5 show the effect of varying  $K_{MT}$  and  $K_9^2 k_{10}$  on the final NO<sub>x</sub> concentration within the gas bubbles.

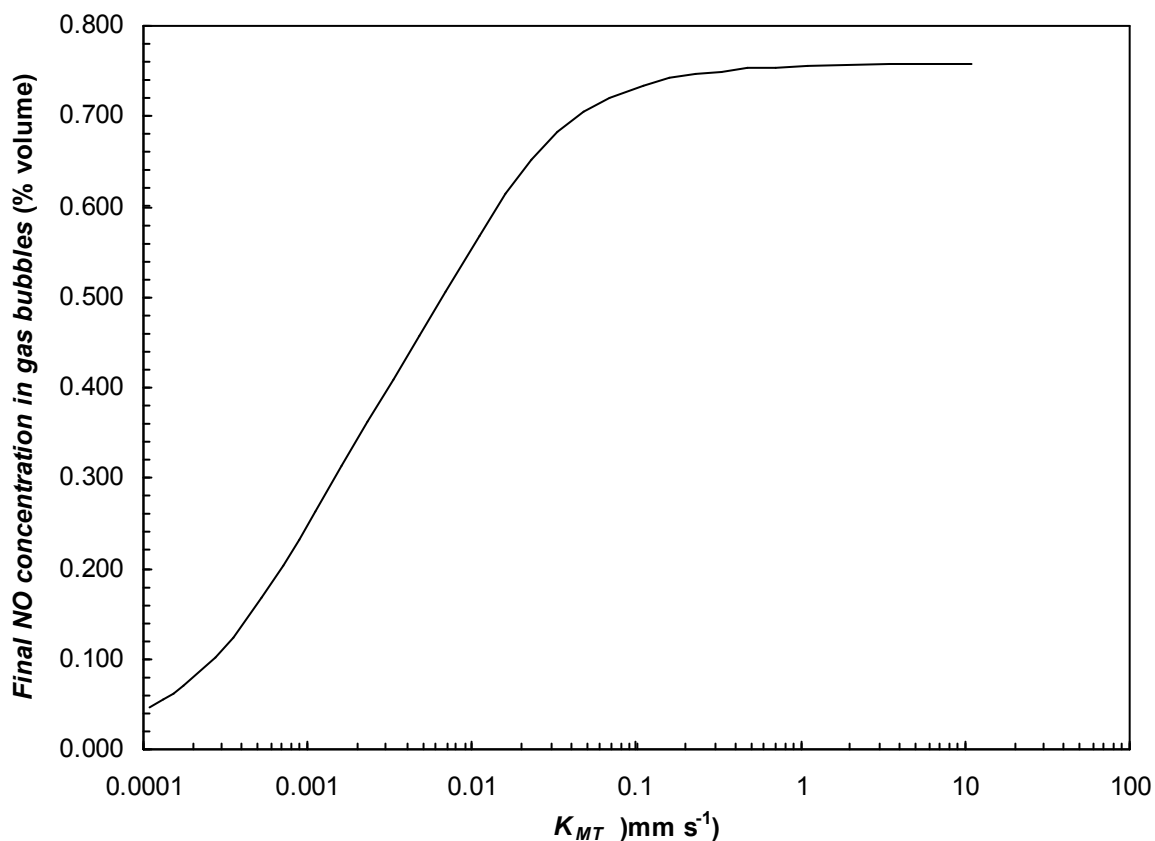


**Figure 4: Effect of  $K_{MT}$  on final NO<sub>x</sub> concentration with  $K_9^2 k_{10} = 1.35 \times 10^{-6} \text{ L mol}^{-1} \text{ s}^{-1}$ ,  $pK_a$ 's of  $\text{HNO}_2$  and  $\text{CH}_3\text{COOH}$  of 3.17 and 4.75, respectively and initial  $0.03 \text{ mol L}^{-1}$   $\text{CH}_3\text{COOH}$  and  $0.015 \text{ mol L}^{-1}$   $\text{NaNO}_2$  at  $25^\circ\text{C}$ .**

The final NO<sub>x</sub> concentration in the gas bubbles increases with increasing  $K_{MT}$ , for values of  $K_{MT}$  less than 0.1 mm/s. This indicates that over this range, the mass transfer of NO from the aqueous to gas phase is at least partially rate limiting. For values of  $K_{MT}$  greater than 0.1 mm s<sup>-1</sup>, the final NO<sub>x</sub> concentration was independent of the mass transfer coefficient, indicating that the mass transfer coefficient is sufficiently large for the aqueous and gas phases to be in equilibrium with respect to the nitric oxide concentration. For the purpose of simulations, an intermediate value of  $K_{MT} = 0.011 \text{ mm s}^{-1}$  was chosen.

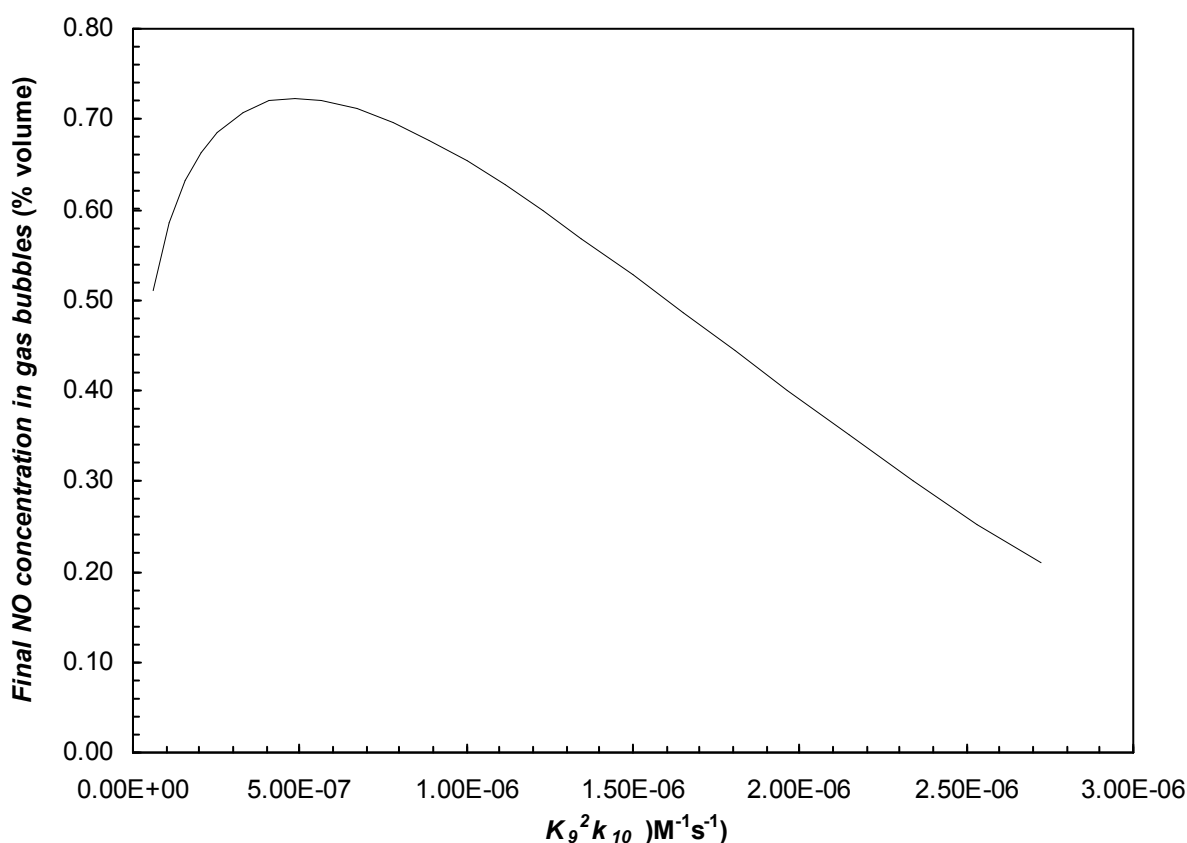


**Figure 5: Effect of  $K_9^2k_{10}$  on final NO<sub>x</sub> concentration, determined with  $K_{MT} = 0.011 \text{ mm s}^{-1}$  and  $pK_a$ s of  $\text{HNO}_2$  and  $\text{CH}_3\text{COOH}$  of 3.17 and 4.75, respectively**

As demonstrated in Figure 5, the effect of  $K_9^2k_{10}$  on the final NO<sub>x</sub> concentration is complex. The predicted NO<sub>x</sub> concentration increases at low values of  $K_9^2k_{10}$ , reaches a maximum at  $K_9^2k_{10} = 5.6 \times 10^{-7} \text{ L mol}^{-1} \text{ s}^{-1}$ , and decreases for larger values of the rate constant. The effect can be explained by examining the effect of changing  $K_9^2k_{10}$  on the value of  $k_{-10}$ , as the overall value of  $K_9^2K_{10}$  remains constant for all simulations. At small values of  $K_9^2k_{10}$ ,  $k_{-10}$  is very small, which causes the amount of NO<sub>x</sub> formation to increase with increases to the forward rate constant. However, at larger values of  $K_9^2k_{10}$ , the reverse rate constant becomes more significant and the overall amount of NO<sub>x</sub> produced declines. The value of  $K_9^2k_{10}$  determined in dilute acid solution yields final NO concentrations near the maximum.



Simulations were also performed to determine the effect of varying the dissociation constants of nitrous and acetic acids on the level of NO<sub>x</sub> formation. In concentrated ammonium nitrate, the activity coefficients of H<sup>+</sup>, HNO<sub>2</sub>, CH<sub>3</sub>COOH, NO<sub>2</sub><sup>-</sup> and CH<sub>3</sub>COO<sup>-</sup> differ widely from unity, causing changes to the apparent dissociation constants of the acids. This can alter the proportion of nitrite converted into nitrous acid, affecting the rate of NO formation. As shown in Table 3, the proportion of nitrite converted to nitrous acid by 0.03 mol L<sup>-1</sup> CH<sub>3</sub>COOH was observed to decrease from around 0.19 in water to 0.11 in 7.5 mol L<sup>-1</sup> NH<sub>4</sub>NO<sub>3</sub>, before increasing slightly to 0.13 in 10 mol L<sup>-1</sup> NH<sub>4</sub>NO<sub>3</sub>. Thus, the corresponding value in 13 mol L<sup>-1</sup> is somewhat uncertain and probably lies in the range between 0.1 and 0.2. This amounts to a difference in the p*K<sub>a</sub>*'s of the two acids ranging from 1.5 to 2.15 units (in water, the p*K<sub>a</sub>*'s are 3.17 and 4.75 for HNO<sub>2</sub> and CH<sub>3</sub>COOH, respectively). It should be noted that the aqueous phase of the emulsion is super-saturated with respect to ammonium nitrate, with the saturation concentration being approximately 10 mol L<sup>-1</sup> at 298 K. As such, it is impossible to directly measure the proportion of nitrite converted to nitrous acid under the conditions present in the emulsion. Two series of simulations were performed; the first in which the p*K<sub>a</sub>* of acetic acid was kept constant, and the nitrous acid p*K<sub>a</sub>* varied, and the second wherein the acetic acid p*K<sub>a</sub>* was adjusted with the p*K<sub>a</sub>* of nitrous acid remaining fixed. Figure 6 plots the results of the two series of simulations. When the nitrous acid p*K<sub>a</sub>* is kept constant, altering the acetic acid p*K<sub>a</sub>* has little effect on NO formation, with only a slight decrease in the final NO concentration predicted. This results in a higher pH, causing a decrease in the rate of the reverse of reaction M10 and the rate of N<sub>2</sub> formation, which offset the decrease in the rate of NO formation via the forward reaction. In contrast, a large decrease in the NO level is predicted when the p*K<sub>a</sub>* of nitrous acid is decreased. Decreasing the p*K<sub>a</sub>* of HNO<sub>2</sub>

results in a lower pH and a relative increase in the rate of the reverse of M10, reducing the net rate of NO formation.

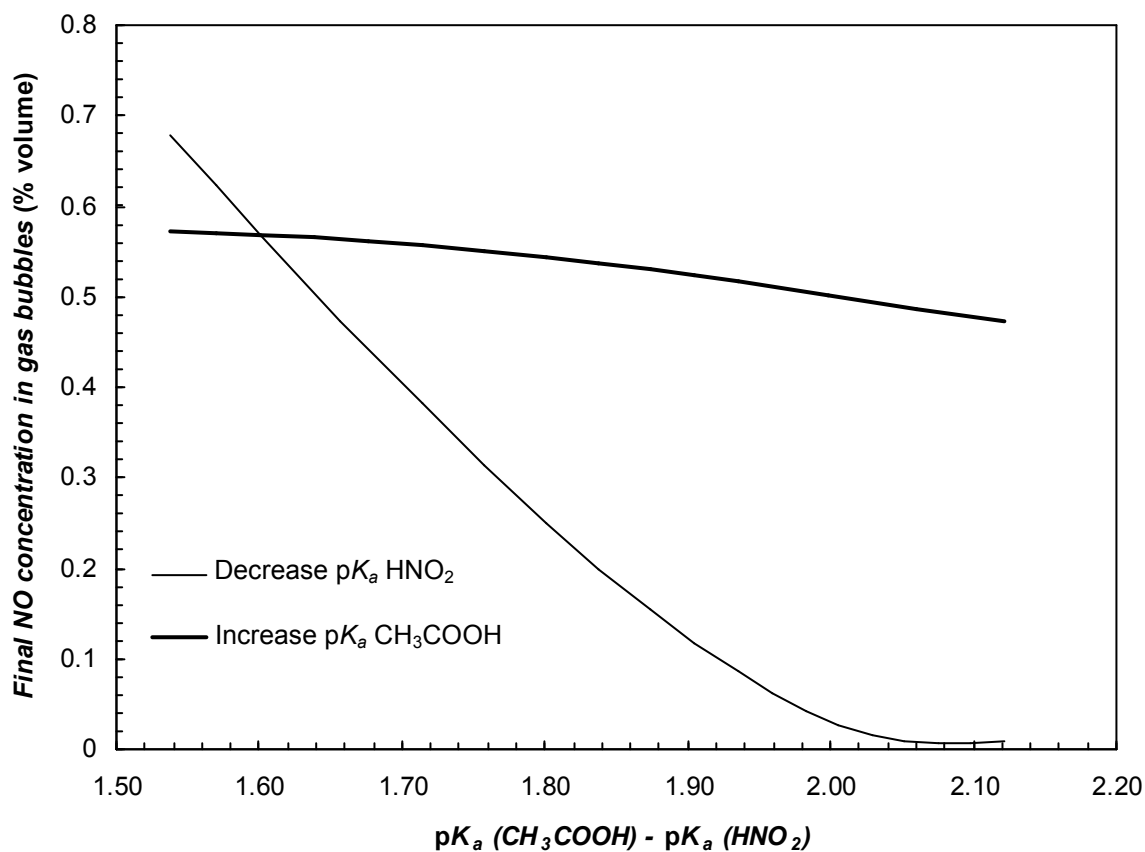


**Figure 6:** *Effect of varying the relative  $\text{p}K_a$ 's of nitrous and acetic acids on NO formation*

## 9.4 Results for NO<sub>x</sub> formation in emulsion gassing

### 9.4.1 Effect of acetic acid concentration on NO<sub>x</sub> formation

Experiments were performed to determine the effect of the acetic acid concentration on the amount of NO<sub>x</sub> produced. All experiments employed an initial nitrite and thiocyanate concentrations of 0.015 mol L<sup>-1</sup>, with the acetic acid concentration varied from 0.03 to 0.09 mol L<sup>-1</sup>. The experiments were performed at room temperature (25 ± 1 °C), with an emulsion containing 0.024 mol L<sup>-1</sup> sodium thiocyanate dissolved in the oxidiser phase.

The NO<sub>x</sub> concentration inside the glove box was observed to increase gradually after the gassers were mixed into the emulsion. The rate of increase in the NO<sub>x</sub> concentration decayed with time, with minimal changes to the NO<sub>x</sub> concentration occurring after 4000 – 5000 s, depending on the amount of acid employed. After this time, the emulsion was stirred to liberate any NO<sub>x</sub> trapped within the gas bubbles in the emulsion. This resulted in a sharp increase in the NO<sub>x</sub> concentration within the box. This increase was almost entirely caused by the elevated NO concentration, with only small increases in NO<sub>2</sub> concentration being observed. Figure 7 demonstrates the effect of acid concentration on the amount of NO<sub>x</sub> formed. Note that the sharp increase in concentration occurring between 4000 and 7500 s results from NO<sub>x</sub> liberated upon stirring the emulsion.

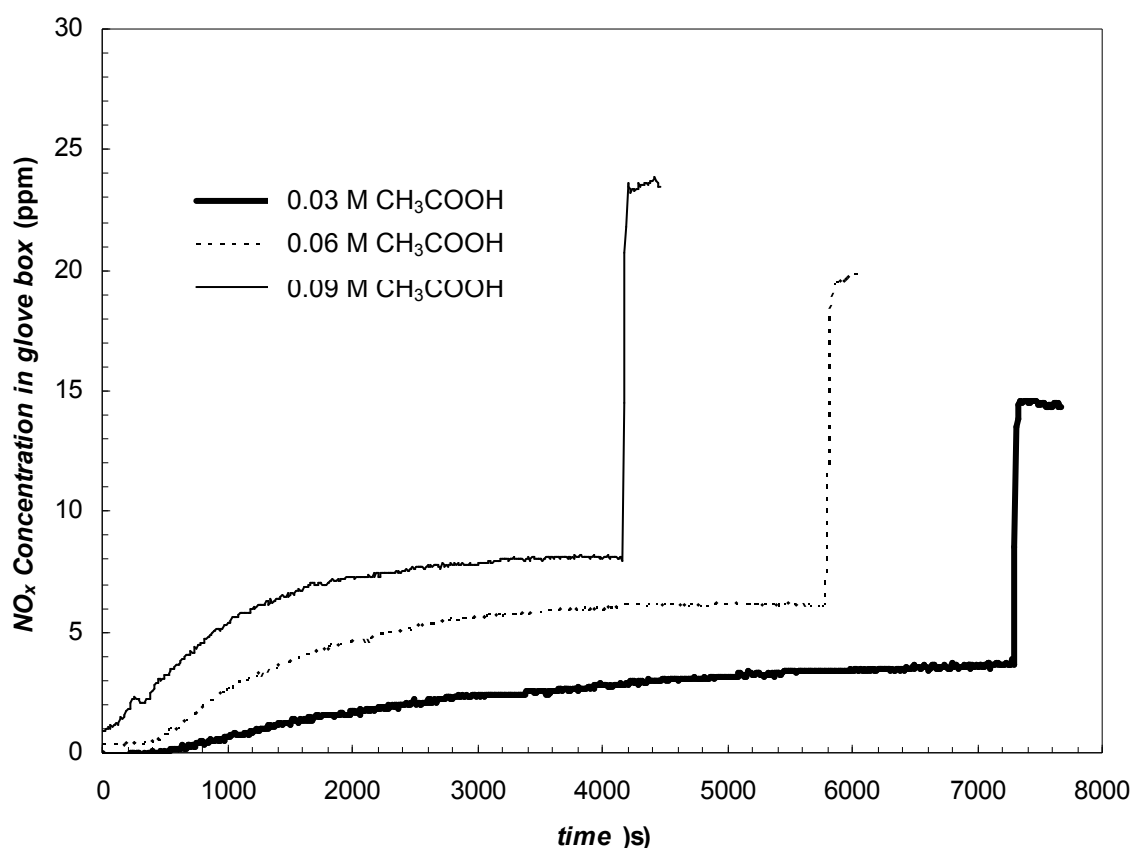


**Figure 7:**  $\text{NO}_x$  formation with increasing acetic acid concentration with  $0.015 \text{ mol L}^{-1} \text{ NaNO}_2$  at  $25^\circ\text{C}$

There was a slight increase in the quantity of  $\text{NO}_x$  liberated from the emulsion with increasing acetic acid concentration, with final  $\text{NO}_x$  readings of 14, 20 and 24 ppm for 0.03, 0.06 and  $0.09 \text{ mol L}^{-1}$  acetic acid, respectively. The elevation in  $\text{NO}_x$  observed upon stirring the emulsion corresponded to between 0.7 and 1.0 % of the initial nitrite being converted into NO. In addition to  $\text{NO}_x$  trapped in gas bubbles, the  $\text{NO}_x$  evolved from the emulsion before stirring also rose with increasing acid concentration, from 4 to 8 ppm. Thus, approximately 30% of the total  $\text{NO}_x$  was evolved from the emulsion within the first hour of gassing. The rate of diffusion of  $\text{NO}_x$  from the emulsion is likely related to the exposed surface area of the emulsion. In the present experiments, the ratio of the emulsions surface area to its mass is significantly higher than that of

large scale emulsion use. It is therefore likely that the rate of diffusion of NO<sub>x</sub> from emulsions gassed on a larger scale will be less significant, due to the lower exposed surface area per volume of emulsion. It was assumed that the NO<sub>x</sub> diffusing from the emulsion was produced as a result of enhanced nitrous acid decomposition occurring near the gas-liquid interface. This is supported by the observation that the rate of NO<sub>x</sub> diffusion decreases with time, and eventually ceases, despite an increase in NO concentration in the emulsion gas bubbles. Because the NO<sub>x</sub> diffusing from the emulsion is produced in the gas-liquid film, NO<sub>x</sub> diffusion is expected to have minimal effect on the bulk NO concentration in the emulsion, and has therefore been neglected in the simulations.

Simulations were performed to predict the effect of increasing acetic acid concentration on the quantity of NO<sub>x</sub> formed when gassing an emulsion explosive for comparison to the experimental results. The simulations employed a mass transfer coefficient of 0.011 mm s<sup>-1</sup> and a forward rate constant for nitrous acid decomposition,  $K_9^2 k_{10}$ , of  $1.35 \times 10^{-6}$  mol L<sup>-1</sup>. The dissociation constant for acetic acid was decreased slightly compared to water (pK<sub>a</sub> shifted from 4.76 to 4.96), resulting in initial conversion of 15 % of total nitrite into nitrous acid. Figure 8 compares the predicted NO<sub>x</sub> concentrations to those observed experimentally. The final concentration of NO in the gas bubbles was predicted to increase slightly upon increasing the acetic acid concentration from 0.03 to 0.06 mol L<sup>-1</sup>, and decreased slightly upon further increases in the acid concentration. Figure 9 shows the volume of NO produced versus time for the simulation with 0.03 mol L<sup>-1</sup> CH<sub>3</sub>COOH.

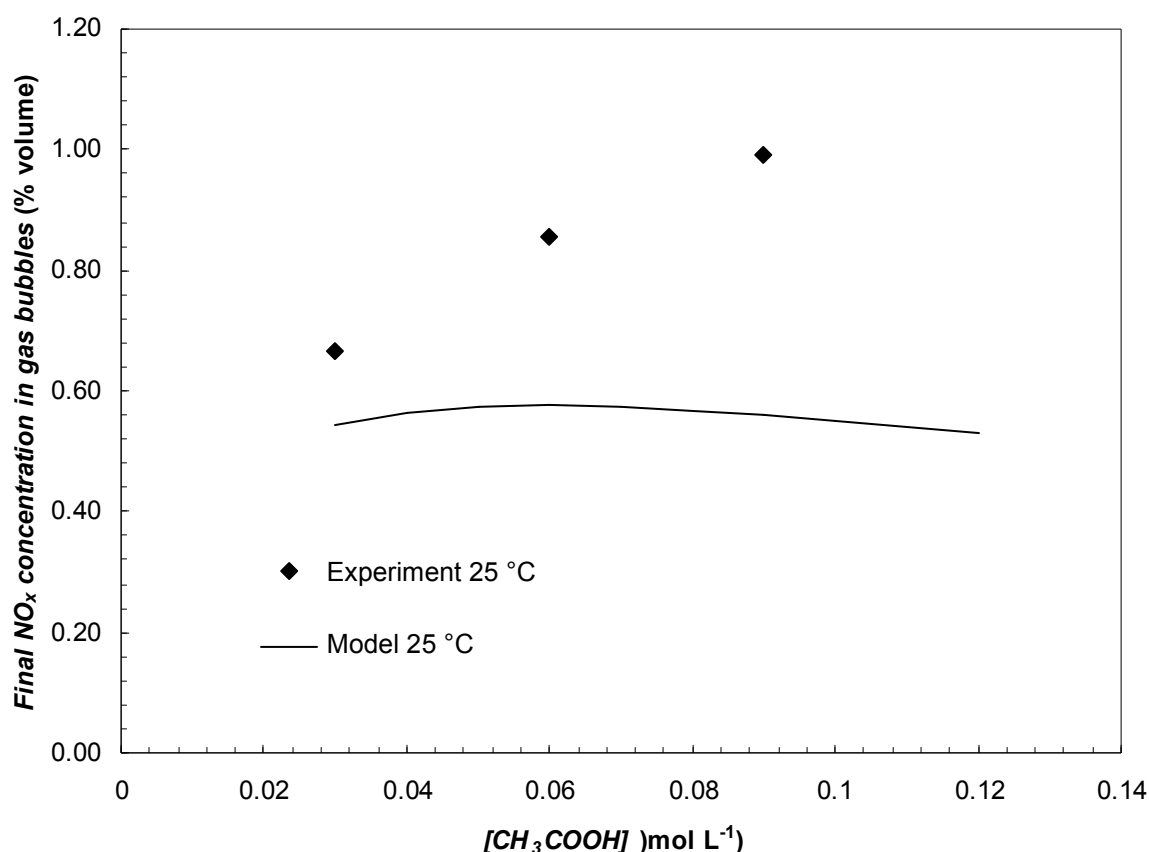


**Figure 8: Comparison of predicted and observed effect of acetic acid concentration on NO formation at 25 °C**

The initial increase in the predicted amount of NO results from an increase in the concentration of nitrous acid with increasing acetic acid concentration. However, the increase in acid concentration also increases the rate of both N<sub>2</sub> formation and the reverse of reaction M10, with the net effect resulting in a predicted reduction in the NO level at higher acid concentrations. The concentrations of NO predicted in the simulations correspond to approximately 0.5 % of the initial nitrite being converted into NO, indicating that the vast majority of nitrite is converted into the desired product, N<sub>2</sub>. This result is in reasonable agreement with experiment at low acid concentration, wherein approximately 0.7 % of initial nitrite is converted into NO<sub>x</sub>. The concentration

of NO<sub>2</sub> was predicted to be negligible, owing to its low equilibrium concentration (Reaction M9), in agreement with experimental observations.

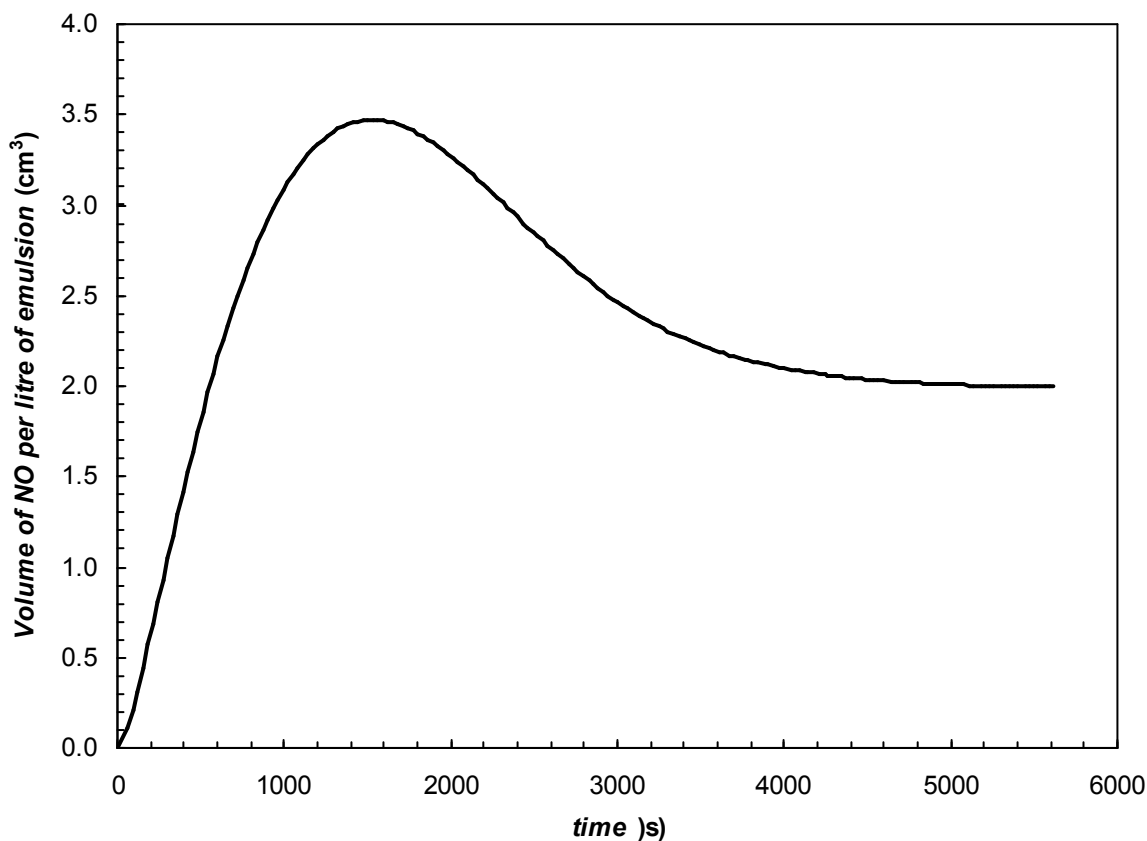


**Figure 9: Predicted volume of NO per litre of emulsion for initial acetic acid concentration of 0.03 mol L<sup>-1</sup>**

As shown in Figure 9, the volume of NO is predicted to increase rapidly over the first 1500 s to a maximum, before declining over the next 3000 s to the final value. Initially, the concentration of nitrous acid is high, which results in production of NO. However, as the reaction between HNO<sub>2</sub> and NH<sub>3</sub> progresses, the concentration of nitrous acid declines, and eventually the reverse rate of Reaction M10 exceeds the forward rate, resulting in the consumption of nitric oxide. Whilst the concentration of NO<sub>x</sub> within the bubbles is significant, these concentrations are not likely to result in visible NO<sub>x</sub>.

emissions, unless large quantities of emulsion are subjected to stirring after gassing to liberate the NO<sub>x</sub> trapped in the bubbles.

#### 9.4.2 Effect of added substrates

Simulations were performed to determine if inclusion of additional reaction substrates in the emulsion could reduce the amount of NO formed. It was hypothesised that inclusion of a substrate capable of rapidly converting HNO<sub>2</sub> into N<sub>2</sub> could reduce the amount of NO formed by increasing the rate of HNO<sub>2</sub> consumption, hence limiting its decomposition. The substrates selected for study include urea and sulfamate (the conjugate base of sulfamic acid), which have both been reported to react with nitrous acid to yield N<sub>2</sub><sup>14,16,25</sup>. Simulations were performed with initial acetic acid, nitrite and thiocyanate concentrations of 0.03, 0.015 and 0.024 mol L<sup>-1</sup>, respectively, for substrate concentrations up to 1 mol L<sup>-1</sup>, the results of which are plotted in Figure 10.



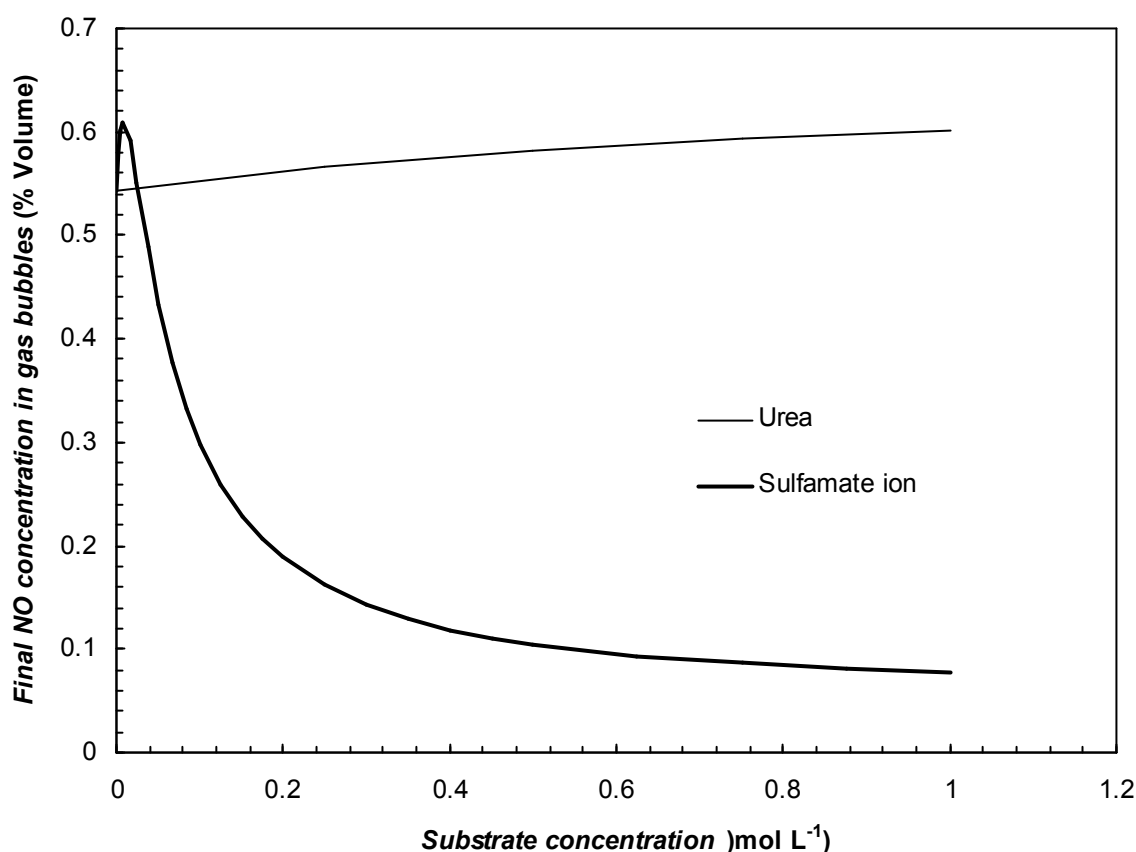


**Figure 10: Effect of urea and sulfamate ion on NO formation for nitrite and acetic acid concentrations of 0.015 and 0.03 mol L<sup>-1</sup>, respectively, at 25 °C**

The simulations showed that inclusion of sulfamate ions in the emulsion could provide a significant reduction in the formation of NO, with a three fold reduction achieved with 0.2 mol L<sup>-1</sup> SO<sub>3</sub>NH<sub>2</sub><sup>-</sup>. The nitrosation of sulfamate is rapid, and even at the lowest concentration simulated (0.025 mol L<sup>-1</sup>), the majority of N<sub>2</sub> is formed via this reaction pathway. Although sulfamate is quite reactive towards nitrous acid, a large excess of this species is required to produce a large reduction in NO. Urea, on the other hand, exhibits poor reactivity toward nitrous acid, with only 2 % of total N<sub>2</sub> produced via urea nitrosation even with 1 mol L<sup>-1</sup> urea. The simulations predict a slight increase in the NO concentration with increasing urea concentration. This strange result arises due to

the reversible nature of NO formation. As shown in Figure 9, the volume of NO produced in the course of the reaction goes through a maximum, before decreasing to a stable level. Inclusion of urea reduces the maximum concentration, however, the slightly faster rate of HNO<sub>2</sub> consumption reduces the extent of the reverse reaction (M10) in the final stages of gas production, leading to a marginally higher final NO concentration.

### 9.4.3 Effect of temperature

Simulations were performed to determine the effect of temperature on NO<sub>x</sub> formation, the results of which are provided in Figure 11. The amount of NO<sub>x</sub> predicted increased slightly between 273 and 298 K, and decreased at higher temperatures. This effect can be explained by considering the relative rates of the forward and reverse reactions of the NO formation pathways and those of N<sub>2</sub> production. At low temperatures, the reverse rate of Reaction M10 is less significant, and the amount of NO increases due to the increase in  $K_9^2 k_{10}$  relative to the nitrogen formation pathways. At temperatures of 298 K and greater, however, the rate of the reverse of Reaction M10 becomes much more significant, resulting in a decline in the amount of NO produced. Overall, the effect of temperature is minimal, as there is only a small difference between the activation energies of the N<sub>2</sub> and NO<sub>x</sub> producing pathways. For example, the apparent activation energy associated with  $K_9^2 k_{10}$  is 106 kJ mol<sup>-1</sup>, whilst the activation energy for  $k_{10}$  is 75 kJ mol<sup>-1</sup>. Thus, the value of  $K_9^2 K_{10}$  increases only slightly with increasing temperature, as there is a relatively small difference between the activation energies of the forward and reverse reaction for HNO<sub>2</sub> decomposition of only 30 kJ mol<sup>-1</sup>. Thus, whilst the rate of the forward reaction increases, this is partially offset by the increase in the reverse

reaction. The rate of N<sub>2</sub> formation via the thiocyanate catalysed reaction increases to a greater extent, owing to the overall 68 kJ mol<sup>-1</sup> activation energy (including the effect of related equilibrium constants, as discussed on page 251) associated with that pathway.

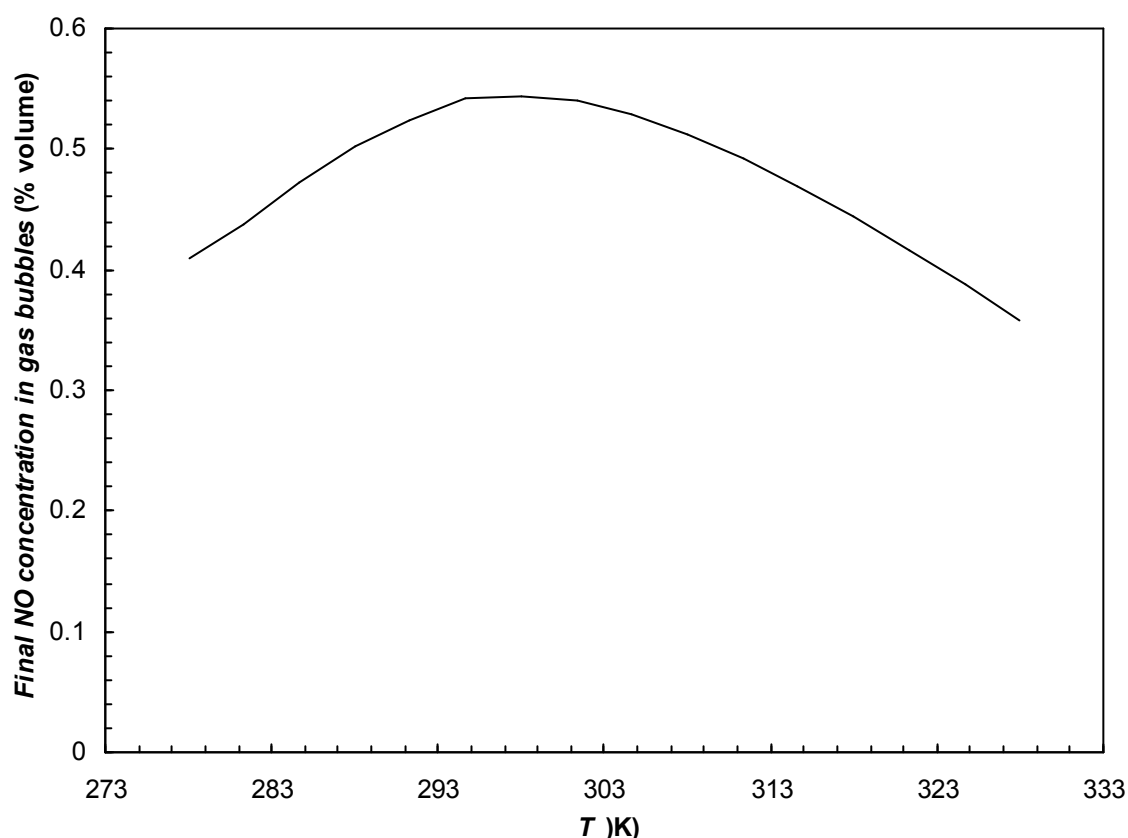


**Figure 11: Effect of temperature on final NO concentration for 0.015 mol L<sup>-1</sup> NaNO<sub>2</sub> and 0.03 mol L<sup>-1</sup> CH<sub>3</sub>COOH**

Experiments were also performed with acetic acid concentrations ranging from 0.03 to 0.09 mol L<sup>-1</sup> at a temperature of 15 °C, and are compared to the simulations in Figure 12. Owing to the slow gassing rate at this temperature, it was impractical to follow the reaction to completion. Instead, the gas was mixed from the emulsion after 60-75 min had elapsed, corresponding to about 85 % of reaction, and the simulations performed over the same time period. Note that because the reaction is incomplete, a higher final

NO concentration is predicted than would exist after all HNO<sub>2</sub> was consumed (due to NO consumption in the final stages of reaction, as shown in Figure 9). The experimental results at 15 °C show a significant increase in NO formation with increasing acid concentration, with between 1.1 and 1.9 % of initial nitrite being converted into NO. In 0.03 mol L<sup>-1</sup> CH<sub>3</sub>COOH, the predicted NO concentration is in close agreement with the experiment, however, the simulations predict a smaller increase in the amount of NO produced at higher acid concentrations.

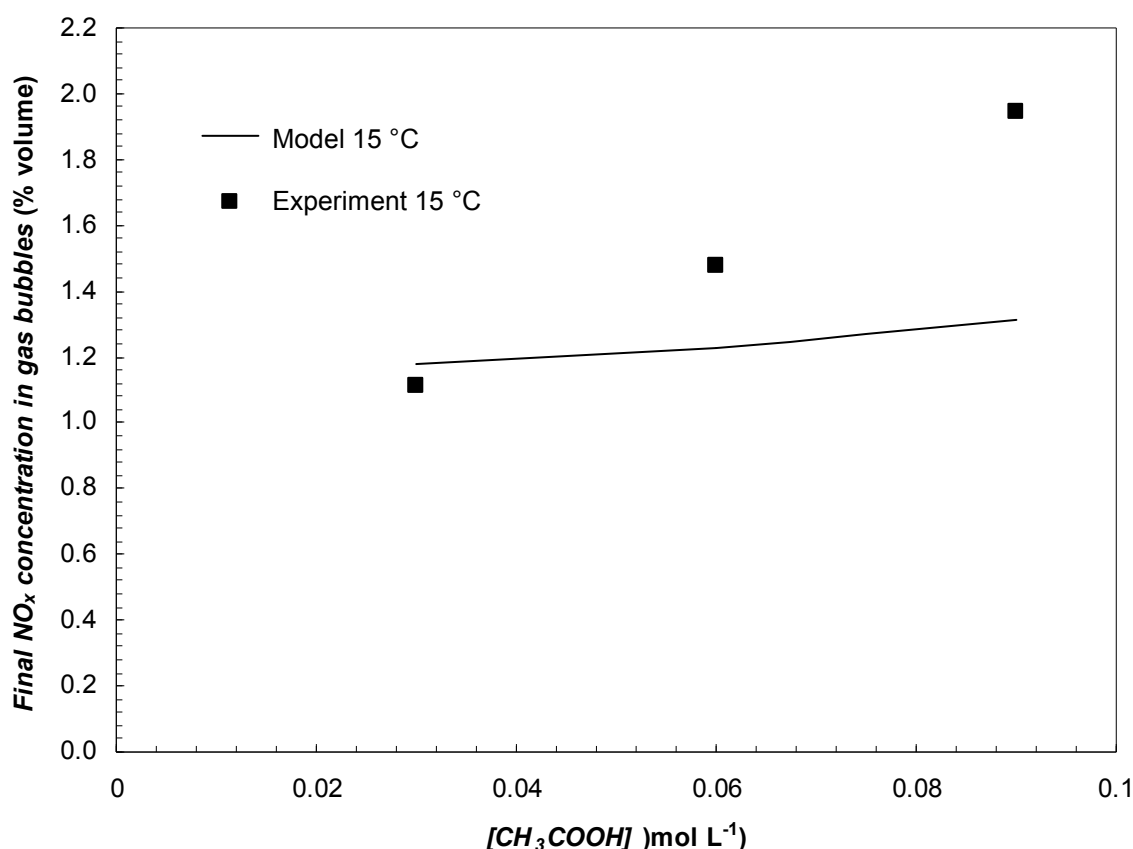


**Figure 12: Comparison of predicted and observed effect of acetic acid concentration on NO formation at 25 °C with 0.015 mol L<sup>-1</sup> NaNO<sub>2</sub>**

The discrepancies between the simulations and experimental results most likely result from the assumptions that the gassing chemicals were rapidly and homogeneously

dispersed throughout the emulsion, and that the mass transfer coefficient remained constant throughout the reaction. In reality, the gassing chemicals would be expected to form discrete droplets in the emulsion, and as such, the regions surrounding the droplets would experience elevated concentrations of the gassing chemicals. Owing to the fourth order dependence on the nitrous acid concentration, this situation would result in an increased level of NO<sub>x</sub> compared to the assumption that the species were homogeneously distributed throughout the emulsion. In addition, the rate of NO formation is inversely proportional to the square of the nitric oxide concentration. Near the interface between the gas bubbles and the emulsion, the concentration of dissolved NO would be lower than the bulk owing to its diffusion into the gas phase. The lower concentration of NO would give rise to an increase in the reaction rate near the interface, resulting in a steeper concentration gradient of NO, and a consequently faster rate of mass transfer than would occur in the absence of chemical reaction. This phenomenon, known as mass transfer enhancement by chemical reaction has been widely observed<sup>26-28</sup>. Changes in the concentrations of NO and HNO<sub>2</sub> throughout the course of reaction would change the rate of NO formation at the interface, in turn causing changes to the effective mass transfer coefficient. Considering these assumptions, the agreement between the simulations and experiments is quite satisfactory.

Overall, the experimentally observed NO<sub>x</sub> concentrations are of the same magnitude as those predicted from the kinetic model, confirming that the decomposition of nitrous acid is the primary source of NO<sub>x</sub> formation during chemical gassing. At 25 °C, the final NO<sub>x</sub> concentrations correspond to conversion of less than 1 % of the initial nitrite into NO. As the majority of NO<sub>x</sub> remains trapped within the gas bubbles in the

emulsion, it is unlikely that visible  $\text{NO}_x$  fumes would be observed. However, when gassing emulsions on an industrial scale, it is possible that mixing of the gasser solutions into the emulsion will be less effective than in the laboratory. As such, there is the possibility that droplets of the concentrated nitrite and acetic acid gasser solutions could come into direct contact leading to additional  $\text{NO}_x$  production. Section 9.5 examines the potential for  $\text{NO}_x$  formation from this pathway.

### 9.5 NO<sub>x</sub> formation from direct mixing of acid and nitrite gasser solutions

Laboratory emulsion gassing experiments have shown that only a small fraction of the initial nitrite present in the gassing solution is converted into NO<sub>x</sub>. In addition, the majority of this NO<sub>x</sub> remains trapped within the gas bubbles of the emulsion, and is unlikely to be released unless the emulsion is stirred or disturbed in some other way. In the laboratory experiments, the volume of emulsion used is small, which allows the gasser solutions to be mixed thoroughly into the emulsion. On a larger scale, mixing may be less effective, and it is possible that direct contact between the acid and nitrite solutions could occur, particularly if the proportion of acetic acid solution is increased. As such, a series of experiments were performed to determine the rate and quantity of NO<sub>x</sub> produced when mixing a solution containing 25 % NaNO<sub>2</sub> with a second solution containing 45 % by mass of acetic acid.

The experiments were performed with the gas phase membrane inlet reactor, as the concentrations of NO<sub>x</sub> produced were predicted to greatly exceed the maximum 5000 ppm concentration that can be directly measured by the analyser. In the first experiment, 0.25 mL of a 25 % NaNO<sub>2</sub> and 0.28 mL of a 45% CH<sub>3</sub>COOH solution were added to the 125 mL reactor containing the gas phase membrane, with a magnetic stirrer included in the reactor to agitate the solution. The second experiment was identical except that the magnetic stirrer was switched off after 5 seconds (enough just to mix the two solutions). Figure 13 plots the results of both experiments.

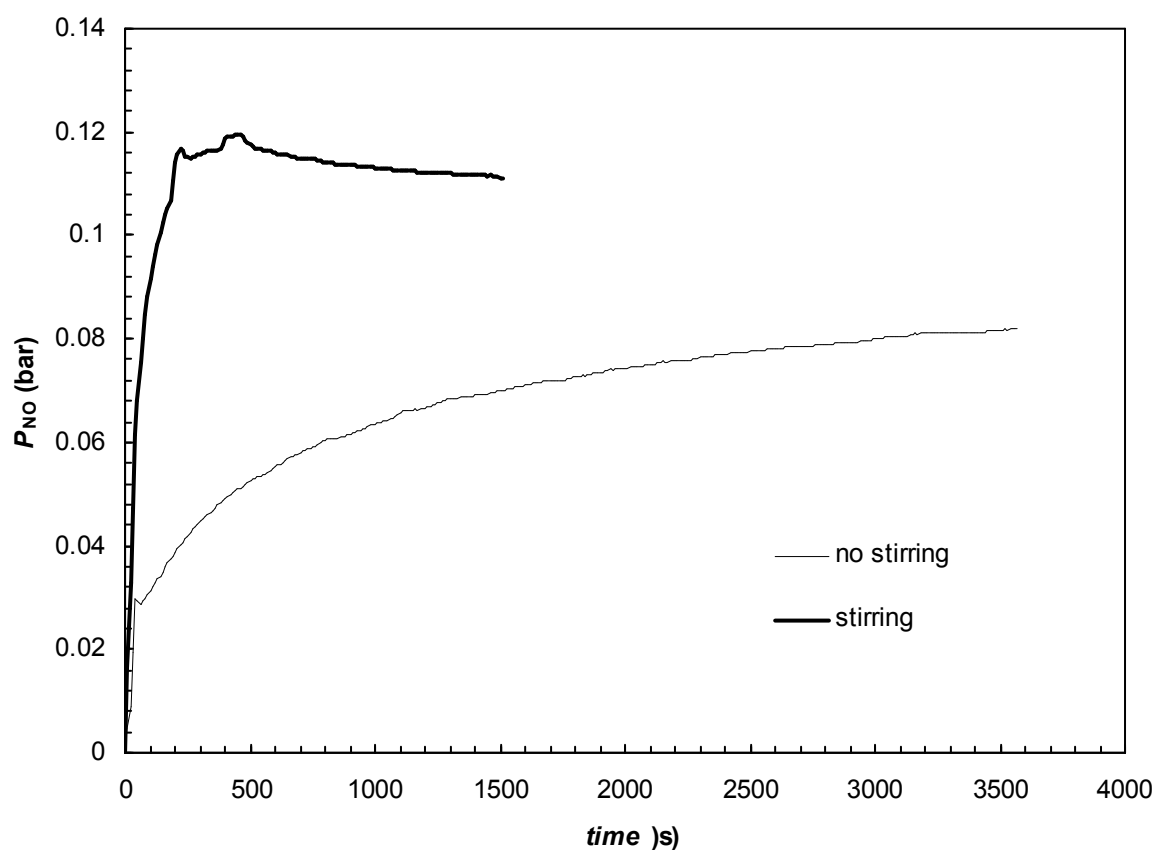


**Figure 13: NO production from mixing 25 % NaNO<sub>2</sub> and 45 % CH<sub>3</sub>COOH solutions with and without stirring**

As can be seen in Figure 13, mixing the two gasser solutions produces significant amounts of NO. With stirring, NO formation is complete within 500 s, at which point 63 % of the initial nitrite had been converted into NO. This is close to the stoichiometry expected from Reaction 9 (which would have been 66.6% of initial nitrite converted into NO):





The gas produced exhibited a light brown colour initially which faded over time, and NO<sub>2</sub> was observed by the analyser. However, the membrane setup had not been calibrated for NO<sub>2</sub> so it was not possible to quantify the amount of NO<sub>2</sub> produced. In contrast, when the solution was not mixed the formation of NO was quite slow, and had not reached the stoichiometric amount even after 1 hour. This is because stirring accelerates the transfer of NO from the liquid to the gas phase, reducing the concentration of aqueous NO and increasing the rate of HNO<sub>2</sub> decomposition. Without stirring, the concentration of NO in the solution is higher and the rate of nitrous acid decomposition is slower. The remaining experiments were all performed without mixing, as this is expected to more closely reflect the conditions in practical gassing situations. The third experiment was performed with double the volume of acetic acid solution. The initial rate of NO formation was similar for both acid concentrations; however, the experiment with the larger quantity of acid solution proceeded to produce a higher amount of NO over time. Figure 14 compares the results of experiments with different amounts of acetic acid.

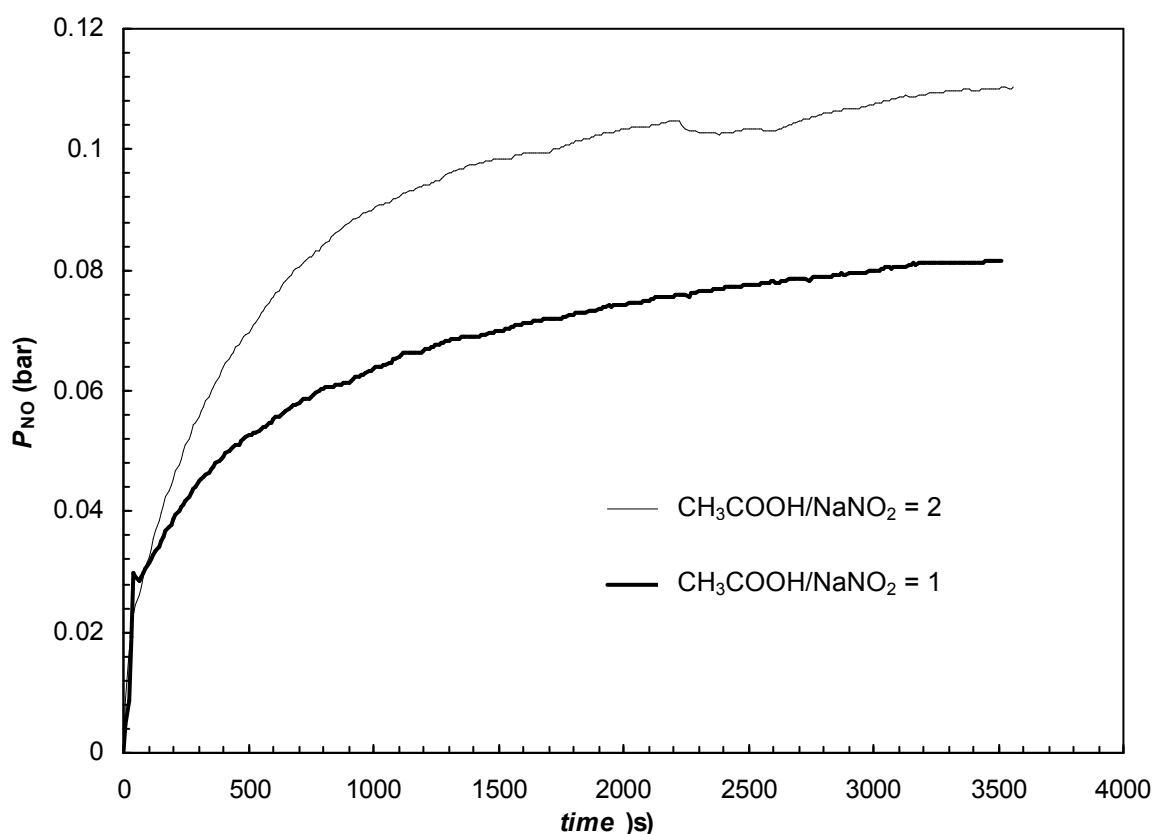


**Figure 14: NO production from mixing 25 %  $\text{NaNO}_2$  and 45 %  $\text{CH}_3\text{COOH}$  solutions without stirring for different quantities of  $\text{CH}_3\text{COOH}$  solution**

Addition of an excess of acetic acid solution relative to the nitrite solution results in a lower concentration of nitrite ions. However, the acetic acid concentration is higher, resulting in a larger proportion of nitrite being converted into reactive nitrous acid. In addition, the excess of acid acts to prevent the pH from rising with the progress of the reaction, further promoting the reaction rate. Therefore, although the concentration of nitrite ions is lower, this is counteracted by the higher acid concentration, leading to an overall net increase in NO formation with increasing acid concentration over the range studied.

The final experiment was designed to test whether inclusion of an additional substrate in the gassing chemicals could reduce the amount of NO<sub>x</sub> formed. As such, a new solution of NaNO<sub>2</sub> was prepared containing 15 % by mass urea and 25 % NaNO<sub>2</sub>. Urea reacts with nitrous acid to generate N<sub>2</sub> and CO<sub>2</sub>:



It was hypothesised that inclusion of urea could reduce the amount of NO formed, as some of the nitrous acid would be converted instead into N<sub>2</sub>, reducing the extent of nitrous acid decomposition into NO. The experiment was performed without stirring, and with double the mass of CH<sub>3</sub>COOH solution compared to the NaNO<sub>2</sub>/urea solution. The concentration of urea corresponded to a 40 % excess over nitrous acid assuming the stoichiometry of Reaction 12. Figure 15 compares the formation of NO with and without the inclusion of urea. As seen in Figure 15, there was a considerable reduction in the amount of NO produced in the presence of urea, with the final NO concentration being about 55 % of that without urea. Whilst there is a reduction, the initial rate of NO formation is similar for both solutions. Thus, the reaction between nitrous acid and urea is not sufficiently fast to prevent some nitrous acid decomposing to NO.

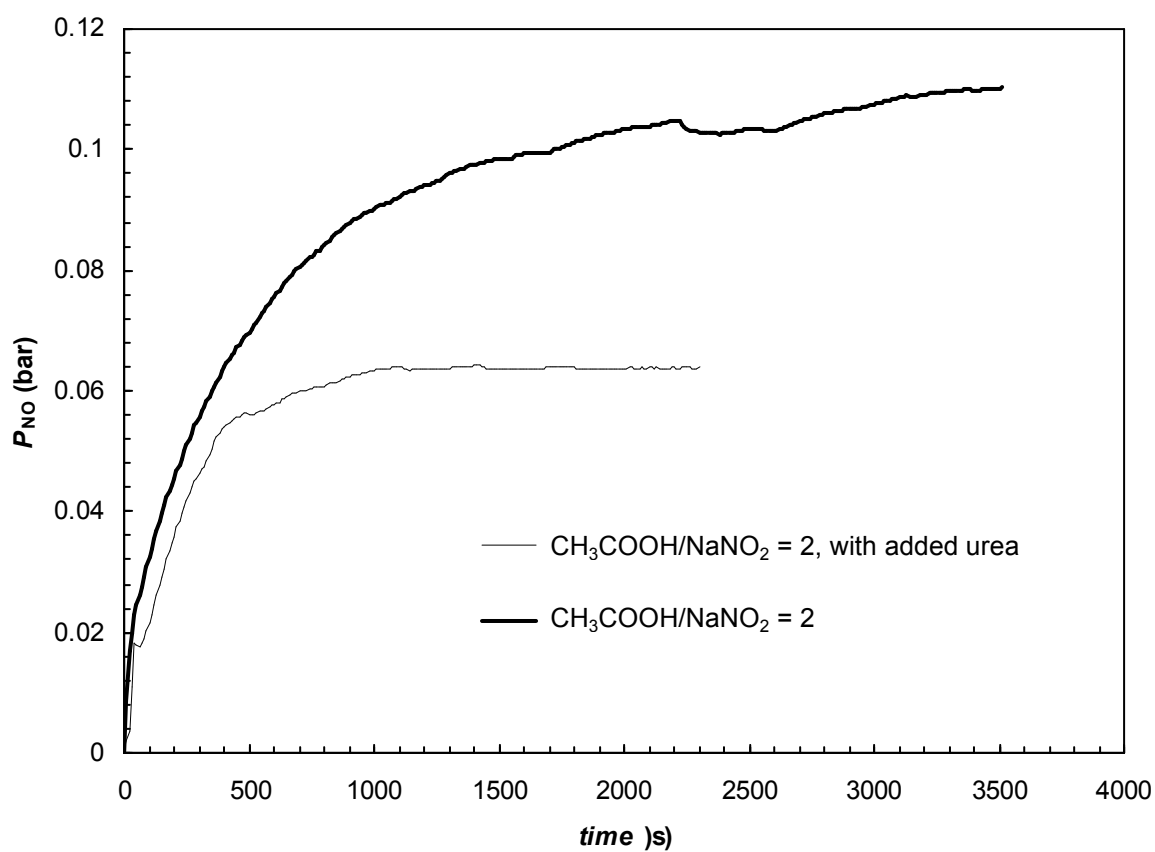


**Figure 15: Effect of urea of NO production from mixing 25 %  $\text{NaNO}_2$  and 45 %  $\text{CH}_3\text{COOH}$  solutions without stirring**

## 9.6 Conclusion

A kinetic model was developed to predict the rates of N<sub>2</sub> and NO formation resulting from the reaction between sodium nitrite and ammonium nitrate under acidic conditions. Experiments with ammonium nitrate solutions showed that the model correctly predicts the rates of NO and N<sub>2</sub> formation, including the effect of thiocyanate ions, which catalyse N<sub>2</sub> formation. This confirmed that the kinetic model includes and correctly accounts for all relevant reactions of the species of interest.

After validating the model in ammonium nitrate solutions, the simulation results were compared to NO<sub>x</sub> measurements from the gassing of an actual emulsion explosive in the laboratory. The experimental results showed an increase in the amount of NO formed with increasing acid concentration, whilst the model predicted a negligible effect of acid concentration on NO production. This discrepancy can be explained by the assumptions in the model that the gassing chemicals were homogeneously distributed throughout the emulsion and the neglect of mass transfer enhancement resulting from chemical reactions near the gas-liquid interface. Simulations showed that inclusion of sulfamate ions in the emulsion could reduce the amount of NO formed, however, a large excess of sulfamate over nitrous acid is required. The levels of NO predicted in the simulations were similar to those observed experimentally, with less than 1 % of the initial nitrite being converted into NO<sub>x</sub>. This confirms nitrous acid decomposition as the sole source of NO during the chemical gassing of emulsion explosives. These low levels are unlikely to result in visible NO<sub>x</sub> emissions during large scale explosive gassing, considering that the exposed surface area for NO<sub>x</sub> evolution is low, and the majority of the gas is trapped within the bubbles of the explosive.

An alternate source of  $\text{NO}_x$  comprises the direct contact between the concentrated acid and nitrite solutions, which results in rapid NO formation. This mechanism is more likely to be a source of  $\text{NO}_x$  in large scale emulsion gassing, where mixing may be less efficient compared to the laboratory experiments. The rate of  $\text{NO}_x$  formation from the concentrated solutions increases with the degree of stirring, with the stoichiometric amount of NO being produced within 5 min when the solution is continuously stirred. Increasing the amount of acid also increases the  $\text{NO}_x$  formation rate. Inclusion of an additional substrate such as urea can reduce the amount of  $\text{NO}_x$  produced by promoting the conversion of nitrous acid into nitrogen rather than NO. However, owing to the rapid rate of nitrous acid decomposition to NO, inclusion of additional reaction substrates cannot completely eliminate  $\text{NO}_x$  formation.

## 9.6 References

1. Rayson, M. S.; Mackie, J. C.; Kennedy, E. M.; Dlugogorski, B. Z., Accurate rate constants for decomposition of aqueous nitrous acid. *Inorg. Chem.* **2012**, *51* (4), 2178-2185.
2. da Silva, G.; Dlugogorski, B. Z.; Kennedy, E. M., Water-in-oil emulsion foaming by thiourea nitrosation: Reaction and mass transfer. *AIChE J.* **2006**, *52* (4), 1558-1565.
3. Schwartz, S. E.; White, W. H., Kinetics of reactive dissolution of nitrogen oxides into aqueous solution. *Adv. Environ. Sci. Technol.* **1983**, *12*, 1-116.
4. da Silva, G. Experimental and theoretical study of nitrosation reactions: Applications in the chemical foaming of concentrated water-in-oil emulsions. PhD Thesis. The University of Newcastle, Australia, Newcastle, 2005.
5. da Silva, G. R.; Dlugogorski, B. Z.; Kennedy, E. M., Elementary reaction step model of the N-nitrosation of ammonia. *Int. J. Chem. Kinet.* **2007**, *39* (12), 645-656.
6. Turner, D.; Dlugogorski, B.; Palmer, T., Factors affecting the stability of foamed concentrated emulsions. *Colloids Surf., A* **1999**, *150* (1-3), 171-184.
7. Vestre, J. A method for preparing a sensitised emulsion explosive 2003.
8. Atkins, P.; de Paula, J., *Elements of Physical Chemistry (5ed)*. Oxford University Press: New York, 2009.
9. da Silva, G.; Dlugogorski, B. Z.; Kennedy, E. M., An experimental and theoretical study of the nitrosation of ammonia and thiourea. *Chem. Eng. Sci.* **2006**, *61* (10), 3186-3197.
10. Park, J. Y.; Lee, Y. N., Solubility and decomposition kinetics of nitrous acid in aqueous solution. *J. Phys. Chem.* **1988**, *92* (22), 6294-302.

11. Beake, B. D.; Moodie, R. B., Role of the reaction of nitric oxide with oxygen in the decomposition of nitrous acid in aqueous acid solution. *J. Chem. Soc., Perkin Trans. 2* **1995**, (6), 1045-8.
12. Partanen, J. I.; Covington, A. K., Determination of stoichiometric dissociation constants of acetic acid in aqueous solutions containing acetic acid, sodium acetate, and sodium chloride at 0 to 60 °C. *J. Chem. Eng. Data* **2003**, 48 (4), 797-807.
13. Hughes, M. N., Kinetic study of the reaction between nitrous acid and sulfamic acid. *J. Chem. Soc. A* **1967**, (6), 902-5.
14. Li, J. C.; Ritter, D. M., Decomposition of nitrosyl disulfonate Ion. IV. The reaction of sulfamate ion with nitrous acid. *J. Am. Chem. Soc.* **1953**, 75, 5828-5830.
15. Dvoeglazov, K. N.; Marchenko, V. I., Oxidation of urea with nitrous acid in nitric acid solutions. *Radiochemistry* **2005**, 47 (1), 58-62.
16. Lasalle, A.; Roizard, C.; Midoux, N.; Bourret, O.; Dyens, P., Removal of NO<sub>x</sub> from flue gases using the urea acidic process: Kinetics of the chemical reaction of nitrous acid with urea. *Ind. Eng. Chem. Res.* **1992**, 31, 777-780.
17. Knopf, D. A.; Luo, B. P.; Krieger, U. K.; Koop, T., Thermodynamic dissociation constant of the bisulfate ion from Raman and ion interaction modeling studies of aqueous sulfuric acid at low temperatures. *J. Phys. Chem. A* **2003**, 107 (21), 4322-4332.
18. da Silva, G.; Kennedy, E. M.; Dlugogorski, B. Z., Ab Initio procedure for aqueous-phase pK<sub>a</sub> calculation: The acidity of nitrous acid. *J. Phys. Chem. A* **2006**, 110, 11371-11376.



19. Everett, D. H.; Wynne-Jones, W. F., The dissociation of the ammonium ion and the basic strength of ammonia in water. *Proc. R. Soc. London, Ser. A* **1938**, *169*, 190-204.
20. Bunton, C. A.; Llewellyn, D. R.; Stedman, G., Oxygen exchange between nitrous acid and water. *J. Chem. Soc.* **1959**, 568-573.
21. Lewis, R. S.; Deen, W. M., Kinetics of the reaction of nitric oxide with oxygen in aqueous solutions. *Chem. Res. Toxicol.* **1994**, *7*, 568-574.
22. Stedman, G.; Whincup, P. A. E., The equilibrium constant for the formation of nitrosyl thiocyanate in aqueous solution. *J. Chem. Soc.* **1963**, 5796-5799.
23. McCabe, W.; Smith, J.; Harriott, P., *Unit operations of chemical engineering*. McGraw Hill: New York, 2004.
24. Magrabi, S. A.; Dlugogorski, B. Z.; Jameson, G. J., Bubble size distribution and coarsening of aqueous foams. *Chem. Eng. Sci.* **1999**, *54* (18), 4007-4022.
25. Mahfud, L.; Ronze, D.; Wehrer, A.; Zoulalian, A., Reduction of nitrous acid by an aqueous solution of urea or sulfamic acid for treatment of NO<sub>x</sub> from a flue gas. *Chem. Eng. J. (Lausanne)* **1998**, *70* (2), 85-92.
26. Roizard, C.; Wild, G., Mass transfer with chemical reaction: the slow reaction regime revisited. *Chem. Eng. Sci.* **2002**, *57* (16), 3479-3484.
27. Parulekar, S. J.; Saidina, A. N. A., Complex gas-liquid reactions: feedback from bulk liquid to liquid-side film. *Chem. Eng. Sci.* **1996**, *51* (10), 2079-2088.
28. van Swaaij, W. P. M.; Versteeg, G. F., Mass transfer accompanied with complex reversible chemical reactions in gas-liquid systems: an overview. *Chem. Eng. Sci.* **1992**, *47* (13-14), 3181-95.



## **CHAPTER 10**

### **Conclusions and recommendations**

## **Table of Contents**

10.1	Conclusions	297
10.2	Recommendations	303
10.3	References	305

## 10.1 Conclusions

A detailed study on the rates and mechanisms of chemical reactions leading to the formation of toxic nitrogen oxides during explosive sensitisation was undertaken. The study employed stopped flow UV-vis spectrophotometry to investigate the kinetics of the decomposition of nitrous acid and nitrosyl thiocyanate, with the thermodynamic feasibility of the reaction mechanisms investigated through high level quantum chemistry calculations. New experimental techniques, including membrane inlet chemiluminescence NO analysis, were developed to determine the effect of ammonium nitrate concentration on the solubility of nitric oxide and the equilibrium associated with nitrous acid decomposition. A comprehensive kinetic model was developed to describe the formation of both nitric oxide and nitrogen gas during explosive sensitisation, and the model predictions compared to experimental measurements of  $\text{NO}_x$  formation during gassing of emulsion explosives.

Significant disagreement regarding the rate constant for nitrous acid decomposition exists in the literature. To resolve these discrepancies, the decomposition of nitrous acid, including the reverse reaction between nitrous acid and nitrate ions was studied by stopped flow spectrophotometry. The value determined for the rate constant ( $K_4^2 k_5 = 1.34 \pm (0.06) \times 10^{-6} \text{ L mol}^{-1} \text{ s}^{-1}$ ), is of higher accuracy than those previously reported in the literature as it does not depend on the rate of parallel reaction pathways or on the rate of interphase mass transfer of gaseous reaction products. The activation energy associated with  $K_4^2 k_5$  is 107 kJ, the majority of this being attributable to the endothermic nature of the reaction  $2\text{HONO} \rightleftharpoons \text{NO} + \text{NO}_2 + \text{H}_2\text{O}$ .

The mechanism of the decomposition of nitrosyl thiocyanate involves a complex system of reactions, with the rate suppressed by the accumulation of the product, nitric oxide, and catalysed by thiocyanate ions. Potential reaction mechanisms were examined by fitting the kinetic parameters to the experimental measurements, and subjecting these kinetic parameters to thermodynamic and kinetic scrutiny, to identify three parallel pathways for the decomposition of ONSCN. The first two pathways, which describe the kinetics at high thiocyanate ion concentrations comprise a reaction that is second order in ONSCN to generate NO and  $(\text{SCN})_2$  and a reaction between ONSCN and  $\text{SCN}^-$  to form NO and  $(\text{SCN})_2^-$ , with the latter pathway being reversible. The rate limiting step in the mechanism corresponds to the consumption of  $(\text{SCN})_2^-$  radicals by ONSCN, which could occur via either radical substitution or S-nitrosation. The third reaction pathway, which becomes significant at low thiocyanate concentrations, involves the formation of a previously unreported species, ONOSCN, via reaction between ONSCN and HOSCN, the latter being an intermediate in the hydrolysis of  $(\text{SCN})_2$ . ONOSCN contributes to NO formation via homolysis of the O-NO bond and subsequent dimerisation and hydrolysis of OSCN. The proposed kinetic mechanism provides an excellent fit to the experimental measurement, allowing the rate of NO formation from the decomposition of ONSCN to be modelled accurately. Comparison of the kinetics of nitrosyl thiocyanate and nitrous acid decomposition indicates that the decomposition of nitrous acid is the dominant  $\text{NO}_x$  formation pathway under conditions relevant to emulsion explosives, with decomposition of ONSCN being insignificant at  $\text{pH} > 2$ .

Quantum chemistry calculations were performed to investigate the thermodynamic feasibility of the ONSCN decomposition mechanism proposed on the basis of kinetic experiments. The calculation procedure involved computing the gas phase reaction free

energy with the CBS-QB3 and G3B3 compound methods, and combining these results with solvation free energies calculated using DFT methods by means of a thermochemical cycle. To ascertain the accuracy of the calculations, the performance of a variety of solvation models was evaluated by comparing the computed reaction free energies to experimental results with experimentally established equilibrium constants, for six reactions. The PCM model yielded the best agreement with the experimental data set, with a mean absolute deviation ranging from 6-8 kJ, depending on the choice of atomic radii and the method employed for computing the free energies of the gas phase reaction.

The calculations confirmed that the first decomposition pathway for ONSCN proceeds via the reaction between  $\text{SCN}^-$  and ONSCN, yielding  $(\text{SCN})_2^-$ , with subsequent oxidation of this species by ONSCN. The formation of SCN radicals from ONSCN homolysis was shown to be energetically unfeasible, and does not contribute to ONSCN decomposition. The decomposition pathway second order in ONSCN could proceed via reaction of two ONSCN molecules, or, alternatively, could involve initial formation of  $\text{ON}(\text{SCN})_2^-$  and its subsequent nitrosation. Formation of ONOSCN was demonstrated to be plausible, with dissociation of this species into NO and OSCN radicals exhibiting a low free energy change relative to the homolysis of ONSCN. The ensuing dimerisation and hydrolysis of OSCN was shown to be thermodynamically favourable. Production of  $\text{N}_2\text{O}$  via hydrolysis of ONCN appears to be feasible, however, the corresponding reaction of ONSCN is highly energetically unfavourable.

The solubility of nitric oxide in solutions of sodium and ammonium nitrate was examined for salt concentrations ranging up to the saturation limit at 25 °C. The

Henry's constant decreased considerably with increasing salt concentration, as predicted from the Sechenov Equation. The enthalpy of solvation of NO decreased considerably with increasing salt concentration, indicating that the effect of temperature on the solubility diminishes with increasing salt concentration. The effect of sodium nitrate on NO solubility was significantly greater than that of ammonium nitrate, in agreement with previous literature results, which show that sodium ions have a much greater effect on gas solubility than ammonium ions. The solubility data yielded the activity coefficients of NO, which were observed to increase exponentially with increasing salt concentration. A model was developed to describe the solubility of NO as a function of salt concentration and temperature. The model predicted the solubility of NO in 13 mol L<sup>-1</sup> NH<sub>4</sub>NO<sub>3</sub> (as found in emulsion explosives) to be 5 times lower than in water at 25 °C, and largely independent of temperature.

Experiments were conducted to determine the observed equilibrium constant for nitrous acid decomposition in ammonium and sodium nitrate solutions, and the results interpreted in terms of the activity coefficients of the species involved. An initial increase in the observed equilibrium constant was caused by a decline in the activity coefficient of nitrate ions, whilst a decrease at higher concentrations arose as a result of increases in the activity coefficients of NO and H<sup>+</sup> relative to that of HNO<sub>2</sub>. Models were developed to describe the effect of NH<sub>4</sub>NO<sub>3</sub> concentration on the HNO<sub>2</sub>, NO and H<sup>+</sup> activity coefficients, permitting extrapolation of the results to supersaturated ammonium nitrate solutions relevant to emulsion explosives, where direct measurements are not possible. It was shown that the effect of the activity coefficients on the equilibrium concentration of aqueous NO is small, however, under the conditions employed for the simulation, the reduced solubility of NO in 13 mol L<sup>-1</sup> ammonium



nitrate results in a gas phase nitric oxide concentration four times larger than would be predicted without accounting for the effects of non-unity activity coefficients.

A kinetic model was developed to predict the rates of  $N_2$  and NO formation resulting from the reaction between sodium nitrite and ammonium nitrate under conditions relevant to explosive sensitisation. Experiments with ammonium nitrate solutions confirmed that the model correctly predicts the rates of NO and  $N_2$  formation, including the effect of thiocyanate ions, which catalyse  $N_2$  formation. Simulation results were then compared to  $NO_x$  measurements from the gassing of an actual emulsion explosive in the laboratory. The experimental results showed an increase in the amount of NO formed with increasing acid concentration, whilst the model predicted a negligible effect of acid concentration on NO production. This discrepancy can be explained by the assumptions in the model that the gassing chemicals were homogeneously distributed throughout the emulsion and there was no mass transfer enhancement resulting from chemical reactions near the gas-liquid interface. Simulations showed that inclusion of sulfamate ions in the emulsion could reduce the amount of NO formed, however, a large excess of sulfamate over nitrous acid is required. The levels of NO predicted in the simulations were similar to those observed experimentally, with less than 1 % of the initial nitrite being converted into  $NO_x$ . This confirms nitrous acid decomposition as the sole source of NO during the chemical gassing of emulsion explosives. These low levels are unlikely to result in visible  $NO_x$  emissions during large scale explosive gassing, considering that the exposed surface area for  $NO_x$  evolution is low, and the majority of the gas is trapped within the bubbles of the explosive.

An alternate source of  $\text{NO}_x$  during explosive sensitisation comprises the direct contact between the concentrated acid and nitrite solutions employed for commercial chemical gassing, which results in rapid NO formation. This mechanism is more likely to be a source of  $\text{NO}_x$  in large scale emulsion gassing, where mixing may be less efficient compared to the laboratory experiments. The rate of  $\text{NO}_x$  formation from the concentrated solutions increases with the degree of stirring, with the stoichiometric amount of NO being produced within 5 min when the solution is continuously stirred. Increasing the amount of acid also increases the  $\text{NO}_x$  formation rate. Inclusion of an additional substrate such as urea can reduce the amount of  $\text{NO}_x$  produced by promoting the conversion of nitrous acid into nitrogen rather than NO. However, owing to the rapid rate of nitrous acid decomposition to NO, inclusion of additional reaction substrates cannot completely eliminate  $\text{NO}_x$  formation.

## 10.2 Recommendations

The present study has demonstrated that employing nitrous acid as an oxidant in the chemical gassing process results in formation of nitric oxide, with the amount of NO dependent on the conditions employed. Inclusion of additional reaction substrates such as sulfamate can increase the rate of desired  $N_2$  forming reactions, reducing NO formation. However, NO formation can not be completely eliminated, even for very high substrate concentrations. As such, potential for  $NO_x$  formation will exist so long as nitrous acid is employed in the chemical gassing system. A possible way to eliminate the potential for  $NO_x$  formation is to employ an alternate oxidant, such as NaOCl or  $NaMnO_4$ , in place of  $HNO_2$ , as described by Dlugogorski et al (2008)<sup>1</sup>. NaOCl however suffers the drawback that the reaction with  $NH_3$  produces significant amounts of nitrate, increasing the chemical requirement, whilst  $MnO_4^-$  exhibits poor diffusivity through the emulsion oil lamellae. As such, it is suggested that further research efforts be directed to resolve these issues, for example, by employing additional reaction substrates to improve the yield of  $N_2$ , or in the case of  $MnO_4^-$ , development of phase transfer catalysts or rapidly diffusing reaction substrates.

It has been demonstrated in laboratory experiments, wherein the gassing chemicals are mixed thoroughly into the emulsion, that the amount of  $NO_x$  formed during gassing corresponds to less than 1% of the total gas produced. As such, the visible  $NO_x$  emissions from gassed emulsions on the bulk scale were proposed to occur due to the direct contact between the acid and nitrite gasser solutions. To avoid this possibility, it is recommended that the emulsion formulation be modified to incorporate the acid component into the oxidiser phase, eliminating the need to add acid during the gassing

process. This would eliminate the risk of a concentrated acid solution being mixed with the nitrite, as an acid solution would not be required in the gassing process. Sulfamate has been predicted to reduce the amount of NO produced, and could be included in the oxidiser phase to further diminish the risk of NO formation. Alternatively, the process of adding the gasser components into the emulsion could be investigated, and alternative mixer designs investigated to improve mixing and reduce the likelihood of contact between the concentrated acid and nitrite solutions.

The formation of a previously unreported nitrosyl compound, ONOSCN, was proposed as a product of the nitrosation of HOSCN by ONSCN. High level quantum chemistry calculations showed that formation of ONOSCN from hypothiocyanate ions ( $\text{OSCN}^-$ ), the conjugate base of HOSCN, was highly energetically favourable, with a predicted equilibrium constant in the range of  $10^5$ - $10^8 \text{ L}^2 \text{ mol}^{-2}$ . Furthermore, the dissociation of ONOSCN to NO and OSCN radicals exhibits a small free energy change of reaction of 5-15 kJ, and represents a low energy pathway to NO formation.  $\text{OSCN}^-$  is produced in the human body via the oxidation of  $\text{SCN}^-$ , and as such, formation and subsequent decomposition of ONOSCN is a potential source of NO in biological systems. It is recommended that further investigation of ONOSCN be undertaken, including an experimental study of  $\text{OSCN}^-$  nitrosation and subsequent decomposition kinetics, to establish if the reactions could contribute to NO formation in the human body. Furthermore, electron paramagnetic resonance spectroscopy (EPR) could be employed to detect radicals such as  $\text{SCN}_2^-$  and OSCN, to unequivocally prove the presence of these species during ONSCN decomposition.

### 10.3 References

1. Dlugogorski, B. Z.; Kennedy, E. M.; Rayson, M. S.; da Silva, G. *Method for gassing explosives especially at low temperatures*. PCT/AU2008/000013. 2008.



## **APPENDIX A**

### **Supporting information for Chapter 4**

## Table of Contents

A1.	Derivation of rate law for nitrous acid decomposition	309
A2.	Derivation of equations used to determine $\text{HNO}_2$ and $\text{NO}_2^-$ from UV-Vis absorbance data	310
A3.	Derivation of integrated form of Equation 2 used for kinetic fitting	311
A4.	Derivation of Equation 13 from the main text of the paper	313
A5.	Temperature dependence of nitrous acid decomposition and reverse reaction	316
A6.	Calculated geometries and vibrational frequencies of species involved in $\text{HNO}_2$ decomposition (B3LYP/6-31G(d) level)	317



### A1. Derivation of rate law for nitrous acid decomposition

Reaction stoichiometry:



Overall:



The total concentration of nitrous acid is defined as the sum of the nitrite and nitrous acid concentrations:

$$[\text{HNO}_2]_T = [\text{HNO}_2] + [\text{NO}_2^-]$$

Assuming reaction (4) is at equilibrium, and reaction (5) is irreversible and rate limiting:

$$\frac{d[\text{HNO}_2]_T}{dt} = 3k_5[\text{NO}_2]^2 \quad (\text{A2})$$

$$K_4 = \frac{[\text{NO}][\text{NO}_2]}{[\text{HNO}_2]^2} \quad (\text{A3})$$

$$[NO_2] = \frac{K_4[HNO_2]^2}{[NO]} \quad (A4)$$

Substituting (S4) into (S2)

$$\frac{d[HNO_2]_T}{dt} = \frac{3K_4^2k_5[HNO_2]^4}{[NO]^2} \quad (A5)$$

**A2. Derivation of equations used to determine  $HNO_2$  and  $NO_2^-$  from UV-Vis absorbance data**

$$A_1 = C_a \varepsilon_{a,1} + C_b \varepsilon_{b,1} \quad (A6)$$

$$A_2 = C_a \varepsilon_{a,2} + C_b \varepsilon_{b,2} \quad (A7)$$

where  $A$  is absorbance,  $C$  is concentration, and  $\varepsilon$  is the molar extinction coefficients, the subscripts  $a$  and  $b$  refer to species  $a$  and  $b$  and the number subscripts refer to the wavelength 1 and 2 respectively. Substituting (S7) into (S6) for  $C_a$ :

$$A_1 = \frac{A_2 \varepsilon_{a,1} - C_b \varepsilon_{a,1} \varepsilon_{b,2}}{\varepsilon_{a,2}} + C_b \varepsilon_{b,1} \quad (A8)$$

hence

$$C_b = \frac{A_1 \varepsilon_{a,2} - A_2 \varepsilon_{a,1}}{\varepsilon_{b,1} \varepsilon_{a,2} - \varepsilon_{a,1} \varepsilon_{b,2}} \quad (\text{A9})$$

$$C_a = \frac{A_2 - C_b \varepsilon_{b,2}}{\varepsilon_{b,1}} \quad (\text{A10})$$

Table S1 shows the molar extinction coefficients for each species determined in the present work and employed in Equations S9 and S10:

**Table A1: Molar extinction coefficients of  $\text{HNO}_2$  and  $\text{NO}_2^-$  at selected wavelengths**

<i>Wavelength (nm)</i>	$\varepsilon_{\text{HNO}_2} (\text{M}^{-1})$	$\varepsilon_{\text{NO}_2^-} (\text{M}^{-1})$
357.5	54.32	22.40
371	56.41	15.56
386	32.97	5.234

### A3. Derivation of integrated form of Equation 2 used for kinetic fitting

Rate law for  $\text{HNO}_2$  decomposition

$$-\frac{d[\text{HNO}_2]_T}{dt} = \frac{3K_4^2 k_5 [\text{HNO}_2]^4}{[\text{NO}]^2} \quad (\text{A5})$$

The nitrous acid concentration can also be written in terms of the total concentration of nitrous acid, the acidity and the dissociation constant:

$$[HNO_2] = \frac{[HNO_2]_T [H^+]}{K + [H^+]} \quad (A11)$$

Owing to the excess of hydrogen ions used in the experiments, the ratio  $[H^+]/(K+[H^+])$  is constant and defined as the variable  $a$ , which can be determined with Equations S9 and S10.

$$a = \frac{[H^+]}{K + [H^+]} \quad (A12)$$

$$[HNO_2] = a[HNO_2]_T \quad (A13)$$

The nitric oxide concentration can be written in terms of the initial total nitrous acid concentration and the total nitrous acid concentration:

$$[NO] = \frac{2}{3}([HNO_2]_{T,initial} - [HNO_2]_T) \quad (A14)$$

The rate law then becomes:

$$-\frac{d[HNO_2]_T}{dt} = \frac{k[HNO_2]_T^4}{([HNO_2]_{T,initial} - [HNO_2]_T)^2} \quad (A15)$$

where:

$$k = \frac{27a^4 K_4^2 k_5}{4} \quad (\text{A16})$$

Separating variables:

$$\int_{[HNO_2]_{T,initial}}^{[HNO_2]_T} \frac{([HNO_2]_{T,initial} - [HNO_2]_T)^2}{[HNO_2]_T^4} d[HNO_2]_T = \int_0^t -k dt \quad (\text{A17})$$

After integration and rearrangement:

$$t = -\frac{1}{k} \left( \frac{-([HNO_2]_{T,initial})^2 + 3[HNO_2]_{T,initial} [HNO_2]_T - 3[HNO_2]_T^2}{3[HNO_2]_T^3} + \frac{1}{3[HNO_2]_{T,initial}} \right) \quad (\text{A18})$$

$$t = \frac{1}{3} \frac{([HNO_2]_{T,initial} - [HNO_2]_T)^3}{k[HNO_2]_{T,initial} [HNO_2]_T^3} \quad (\text{A19})$$

#### A4. Derivation of Equation 13 from the main text of the paper

Definition of the equilibrium constant:

$$K = \exp\left(\frac{-\Delta G}{RT}\right) \quad (\text{A19})$$

$$\ln(K) = \left(\frac{-\Delta G}{RT}\right) \quad (\text{A20})$$

Multiply S12 by two:

$$2 \ln(K) = 2 \frac{-\Delta G}{RT} \quad (\text{A21})$$

$$\ln(K_4^2) = -\frac{2\Delta G_{(4)}}{RT} \quad (\text{A22})$$

Arrhenius equation:

$$k_5 = A \exp\left(\frac{-E_{A(5)}}{RT}\right) \quad (\text{A23})$$

$$\ln(k_5) = \frac{-E_{A(5)}}{RT} + \ln(A) \quad (\text{A24})$$

Summing equations (S16) and (S14)

$$\ln(K_4^2) + \ln(k_5) = -\frac{2\Delta G_{(4)}}{RT} - \frac{E_{A(5)}}{RT} + \ln(A) \quad (\text{A25})$$

$$\ln(K_4^2 k_5) = -\frac{2(\Delta H_{(4)} - T\Delta S_{(4)})}{RT} - \frac{E_{A(5)}}{RT} + \ln(A) \quad (\text{A26})$$

$$\ln(K_4^2 k_5) = -\frac{(2\Delta H_{(4)} + E_{A(5)})}{RT} + \frac{\Delta S_{(4)}}{R} + \ln(A) \quad (13)$$

**A5. Temperature dependence of nitrous acid decomposition and reverse reaction**

**Table A2: Temperature dependence of nitrous acid decomposition**

<i>Experiment</i>	<i>NaNO<sub>2</sub> (M)</i>	<i>HClO<sub>4</sub> (M)</i>	<i>NaClO<sub>4</sub> (M)</i>	<i>T (K)</i>	<i>K<sub>4</sub><sup>2</sup>k<sub>5</sub> (M<sup>-1</sup>s<sup>-1</sup>)</i>
12	0.02	0.04	0.04	308.15	$5.77 \times 10^{-6}$
13	0.02	0.04	0.04	293.15	$6.82 \times 10^{-7}$
14	0.02	0.04	0.04	293.15	$6.82 \times 10^{-7}$
15	0.02	0.04	0.04	303.55	$3.44 \times 10^{-6}$
16	0.02	0.04	0.04	313.35	$1.16 \times 10^{-5}$
17	0.02	0.04	0.04	287.75	$2.73 \times 10^{-7}$
18	0.02	0.04	0.04	288.15	$4.22 \times 10^{-7}$
19	0.02	0.1	0.08	308.15	$6.51 \times 10^{-6}$
20	0.02	0.04	0.04	288.15	$2.35 \times 10^{-7}$

**Table A3: Temperature dependence of reverse reaction determined in 0.02 M NaNO<sub>2</sub>, 0.1 M H<sup>+</sup> and 0.1 M NO<sub>3</sub><sup>-</sup>**

<i>Experiment</i>	<i>T (K)</i>	<i>k<sub>-5</sub> (M<sup>-2</sup>s<sup>-1</sup>)</i>
29	308	$1.44 \times 10^{-2}$
30	308	$1.18 \times 10^{-2}$
31	318	$3.91 \times 10^{-2}$
32	318	$4.59 \times 10^{-2}$
33	328	$9.45 \times 10^{-2}$
34	328	$1.06 \times 10^{-1}$



**A6. Calculated geometries and vibrational frequencies of species involved in  
HNO<sub>2</sub> decomposition (B3LYP/6-31G(d) level)**

***cis*-HNO<sub>2</sub>**

Center Number	Atomic Number	Atomic Type	Coordinates (Angstroms)		
			X	Y	Z
1	7	0	0.000000	0.551088	0.000000
2	8	0	1.088193	0.065533	0.000000
3	8	0	-1.017487	-0.389393	0.000000
4	1	0	-0.565653	-1.266736	0.000000

Moments of inertia: 21.70234 135.94458 157.64692

Frequencies -- 649.0997 739.5585  
919.6412  
1369.1921 1728.5844  
3520.7427

***trans*-HNO<sub>2</sub>**

Center Number	Atomic Number	Atomic Type	Coordinates (Angstroms)		
			X	Y	Z
1	7	0	0.171496	0.492520	-0.000053
2	8	0	1.105817	-0.225959	0.000041
3	8	0	-1.040812	-0.260023	-0.000043
4	1	0	-1.720515	0.440209	0.000381

Moments of inertia: 19.53117 143.68656 163.21773

Frequencies -- 599.7799 630.6753  
863.9376  
1325.1947 1794.6324  
3698.4640

**NO**

Center Number	Atomic Number	Atomic Type	Coordinates (Angstroms)		
			X	Y	Z
1	7	0	0.000000	0.000000	-0.617977
2	8	0	0.000000	0.000000	0.540730

Moments of inertia: 0.00000 35.79798 35.79798

Frequencies -- 1991.0549

## NO<sub>2</sub>

Center Number	Atomic Number	Atomic Type	Coordinates (Angstroms)		
			X	Y	Z
1	7	0	0.000000	0.000000	0.328016
2	8	0	0.000000	1.106847	-0.143507
3	8	0	0.000000	-1.106847	-0.143507

Moments of inertia: 7.73299 139.95380 147.68679

Frequencies -- 748.9003 1404.3162  
1721.1053

## H<sub>2</sub>O

Center Number	Atomic Number	Atomic Type	Coordinates (Angstroms)		
			X	Y	Z
1	8	0	0.000000	0.000000	0.119720
2	1	0	0.000000	0.761560	-0.478879
3	1	0	0.000000	-0.761560	-0.478879

Moments of inertia: 2.29054 4.17466 6.46520

Frequencies -- 1712.7968 3728.4714  
3850.6127

## N<sub>2</sub>O<sub>3</sub>

Center Number	Atomic Number	Atomic Type	Coordinates (Angstroms)		
			X	Y	Z
1	7	0	-0.712024	-1.077808	0.000000
2	7	0	0.000000	0.636056	0.000000
3	8	0	1.207767	0.609247	0.000000
4	8	0	-0.781588	1.556106	0.000000
5	8	0	0.196842	-1.778820	0.000000

Moments of inertia: 145.47627 418.87032 564.34659

Frequencies -- 146.8842 218.9720  
294.3661 462.7442 667.4194  
808.7758 1395.0423 1762.1034  
1937.9829

**N<sub>2</sub>O<sub>4</sub>**

Center Number	Atomic Number	Atomic Type	Coordinates (Angstroms)		
			X	Y	Z
1	7	0	-0.000204	0.891809	0.000000
2	7	0	0.000204	-0.891809	0.000000
3	8	0	-0.000204	-1.352416	1.104066
4	8	0	0.000204	1.352416	1.104066
5	8	0	0.000204	1.352416	-1.104066
6	8	0	-0.000204	-1.352416	-1.104066

Moments of inertia: 278.50299 497.43019 775.93316

Frequencies -- 96.0361 229.2779  
 298.6682  
 433.8216 500.1918  
 681.2027  
 756.1365 838.4744  
 1329.7985  
 1461.0943 1829.8512  
 1856.8592

**HNO<sub>3</sub>**

Center Number	Atomic Number	Atomic Type	Coordinates (Angstroms)		
			X	Y	Z
1	7	0	0.147892	0.037115	0.000060
2	8	0	-1.128129	-0.563375	-0.000058
3	1	0	-1.728587	0.209358	0.000316
4	8	0	1.057381	-0.749560	0.000000
5	8	0	0.157416	1.254289	-0.000034

Moments of inertia: 140.12864 149.83009 289.95873

Frequencies -- 507.6597 581.1593  
 651.4895  
 769.2530 916.0211  
 1346.4844  
 1373.4176 1803.2813  
 3669.3812

**NO<sub>3</sub><sup>-</sup>**

Center Number	Atomic Number	Atomic Type	Coordinates (Angstroms)		
			X	Y	Z
1	7	0	0.000000	0.000000	0.000000
2	8	0	0.000000	1.264276	0.000000
3	8	0	1.094896	-0.632138	0.000000
4	8	0	-1.094896	-0.632138	0.000000

Moments of inertia: 136.94778 136.94778 273.89557

Frequencies --	706.2626	706.2669
837.9729		
	1076.5545	1469.6907
	1469.7133	

**Table A4: Calculated gas phase G3B3 and CBS-QB3 free energies (hartrees)**

	<b>G3B3</b>	<b>CBS-QB3</b>
cisHONO	-205.6313	-205.4983
trans HONO	-205.6324	-205.4990
NO	-129.8563	-129.7685
NO <sub>2</sub>	-205.0074	-204.8759
H <sub>2</sub> O	-76.4014	-76.3551
N <sub>2</sub> O <sub>3</sub>	-334.8626	-334.6418
N <sub>2</sub> O <sub>4</sub>	-410.0178	-409.7187
HNO <sub>3</sub>	-280.7810	-280.6050
NO <sub>3</sub> <sup>-</sup>	-280.2634	-280.0896

**Table A5: Calculated gas phase enthalpies at G3B3 and CBS-QB3 (hartrees)**

	<b>G3B3</b>	<b>CBS-QB3</b>
cisHONO	-205.6032	-205.4702
trans HONO	-205.6042	-205.4708
NO	-129.8329	-129.7452
NO <sub>2</sub>	-204.9801	-204.8487
H <sub>2</sub> O	-76.3799	-76.3337
N <sub>2</sub> O <sub>3</sub>	-334.8285	-334.6078
N <sub>2</sub> O <sub>4</sub>	-409.9827	-409.7187
HNO <sub>3</sub>	-280.7507	-280.5748
NO <sub>3</sub> <sup>-</sup>	-280.2355	-280.0616

**Table A6: Calculated free energies and heats of solvation at B3LYP/6-31G(d,p), PCM solvent model with UAHF radii. All quantities are in kJ/mol**

	<b><math>\Delta H_{s, 298}</math></b>	<b><math>\Delta G_{s, 298}</math></b>
cisHONO	-27.8	-27.7
trans HONO	-31.1	-31.0
NO	-1.5	-1.5
NO <sub>2</sub>	-4.4	-4.4
N <sub>2</sub> O <sub>3</sub>	-16.1	-16.2
N <sub>2</sub> O <sub>4</sub>	-14.9	-16.0
HNO <sub>3</sub>	-37.4	-37.4
NO <sub>3</sub> <sup>-</sup>	-272.1	-273.8



## **APPENDIX B**

### **Supporting information for Chapter 5**

## Table of Contents

B1.	Initial rates data	325
B2.	Experimental conditions for kinetic fitting	326
B3.	Kinetic data for ONSCN decomposition	327
B4.	Typical UV-Vis spectrum for ONSCN solution	331
B5.	Simulation results showing oxidation of NO exclusively to $\text{NO}_2^-$	332
B6.	Detailed description of apparatus for preparing NO saturated solution	333
B7.	Typical FTIR spectrum of product gases	334
B8.	Experiments to determine equilibrium constant of ONSCN	335
B9.	Additional graphs for the fit of Pathways 1 and 2 to measurements at high SCN <sup>-</sup>	337
B10.	Derivation of Equation 19 from the main text	339



**B1. Initial rates data****Table S1: Effect of  $[\text{SCN}^-]$  on initial rate.  $[\text{H}^+] = 1 \text{ M}$  and  $[\text{HNO}_2] = 2 \text{ mM}$  in all experiments. All concentrations in units of  $\text{moles L}^{-1}$  and time in s.**

$[\text{SCN}^-]$	$[\text{ONSCN}^-]/[\text{HNO}_2]_{\text{Total}}$	$d[\text{HNO}_2]_{\text{Total}}/dt$	$\sigma$	$d[\text{HNO}_2]/dt \text{ corr}$
0.1	0.772	4.78E-05	6.46E-06	6.20E-05
0.15	0.840	7.75E-05	7.61E-06	9.23E-05
0.2	0.875	1.12E-04	1.08E-05	1.28E-04
0.25	0.897	1.46E-04	2.13E-05	1.63E-04

**Table S2: Effect of  $[\text{HNO}_2]$  on initial rate. Concentrations of  $\text{SCN}^-$  and  $\text{H}^+$  are constant in all runs at 0.1 and 1 M, respectively/ All concentrations in units of  $\text{moles L}^{-1}$  and time in s.**

$[\text{HNO}_2]_{\text{T}}$	$d[\text{HNO}_2]_{\text{T}}/dt$	$\sigma$
0.001	1.97E-05	5.93E-07
0.002	4.78E-05	6.46E-06
0.003	6.69E-05	3.06E-06
0.004	8.80E-05	3.08E-06

**B2. Experimental conditions for kinetic fitting****Table S3: List of experiments and concentrations**

<b>Experiment number</b>	<b>[H<sup>+</sup>] (M)</b>	<b>[NaNO<sub>2</sub>] (M)</b>	<b>[NaSCN] (M)</b>	<b>[NO] (mM)</b>
1 (6)	0.4	0.01	0.05	0
2 (5)	0.3	0.01	0.05	0
3 (4)	0.2	0.01	0.05	0
4 (18)	0.1	0.005	0.3	0
5 (19)	0.3	0.005	0.3	0
6 (20)	0.5	0.005	0.3	0
7 (16)	0.3	0.002	0.3	0
8 (17)	0.5	0.002	0.3	0
9 (15)	0.5	0.002	0.5	0
10 (11)	0.05	0.01	0.05	0
11 (10)	0.1	0.01	0.05	0
12 (9)	0.2	0.003	0.1	0.62
13 (7)	0.2	0.003	0.1	0
14 (13)	0.2	0.003	0.2	0.62
15 (8)	0.2	0.003	0.2	0
16 (12)	0.02	0.01	0.2	0
17 (1)	0.1	0.01	0.1	0
18 (2)	0.1	0.01	0.15	0
19 (3)	0.1	0.01	0.2	0
20 (14)	0.3	0.0093	0.05	0.62

**B3. Kinetic data for ONSCN decomposition****Table S4: Kinetic Data (Concentrations in mol L<sup>-1</sup>)**

	1	2	3	4	5	6	7
time (s)	[HNO <sub>2</sub> ]T	[HNO <sub>2</sub> ]T	[HNO <sub>2</sub> ]T	HNO <sub>2</sub> T	HNO <sub>2</sub> T	HNO <sub>2</sub> T	HNO <sub>2</sub> T
0.1	0.01	0.01	0.01	0.00520	0.00520	0.00520	0.00200
5.0	0.009675	0.009753	0.009759	0.00476	0.00456	0.00432	0.00171
10.0	0.009486	0.009587	0.009642	0.00453	0.00421	0.00397	0.00161
15.0	0.009333	0.00947	0.009555	0.00437	0.00397	0.00372	0.00153
20.0	0.009203	0.009349	0.009463	0.00424	0.00378	0.00353	0.00146
25.0	0.009092	0.009258	0.009403	0.00413	0.00363	0.00337	0.00140
30.0	0.008996	0.009202	0.009356	0.00403	0.00351	0.00324	0.00135
35.0	0.008906	0.009129	0.009298	0.00395	0.00339	0.00311	0.00131
40.0	0.008824	0.009065	0.009239	0.00387	0.00329	0.00301	0.00127
45.0	0.008747	0.009001	0.009196	0.00380	0.00320	0.00292	0.00124
50.0	0.008667	0.008931	0.009139	0.00373	0.00311	0.00283	0.00121
55.0	0.008595	0.00888	0.009093	0.00367	0.00303	0.00275	0.00118
60.0	0.008533	0.008832	0.00906	0.00361	0.00296	0.00268	0.00116
65.0	0.008469	0.008778	0.009018	0.00356	0.00289	0.00261	0.00113
70.0	0.008404	0.008716	0.00897	0.00351	0.00283	0.00255	0.00111
75.0	0.008342	0.008672	0.008944	0.00346	0.00277	0.00249	0.00109
80.0	0.008292	0.008622	0.008915	0.00342	0.00271	0.00244	0.00107
85.0	0.008232	0.008579	0.008863	0.00337	0.00266	0.00239	0.00105
90.0	0.008174	0.008539	0.008831	0.00333	0.00261	0.00234	0.00103
95.0	0.008124	0.008495	0.008813	0.00329	0.00256	0.00229	0.00102
100.0	0.008077	0.008446	0.008761	0.00325	0.00252	0.00225	0.00100
105.0	0.008027	0.008409	0.008745	0.00321	0.00248	0.00221	0.00098
110.0	0.007981	0.008366	0.008714	0.00318	0.00244	0.00217	0.00096
115.0	0.007931	0.008329	0.008689	0.00314	0.00240	0.00213	0.00095
120.0	0.00788	0.008296	0.008654	0.00311	0.00236	0.00209	0.00093
125.0	0.007841	0.008284	0.008631	0.00308	0.00233	0.00205	0.00092
130.0	0.007798	0.008249	0.008588	0.00303	0.00229	0.00202	0.00091
135.0	0.007752	0.008232	0.008579	0.00300	0.00226	0.00199	0.00090
140.0	0.007712	0.008202	0.008535	0.00297	0.00222	0.00196	0.00089
145.0	0.007673	0.008162	0.00852	0.00295	0.00220	0.00193	0.00088
150.0	0.007634	0.008118	0.00849	0.00292	0.00217	0.00190	0.00087
155.0	0.007595	0.008086	0.008457	0.00289	0.00213	0.00187	0.00086
160.0	0.007554	0.008048	0.008427	0.00287	0.00211	0.00185	0.00085
165.0	0.00751	0.008011	0.008413	0.00284	0.00208	0.00182	0.00084
170.0	0.007474	0.007986	0.008392	0.00282	0.00206	0.00180	0.00082
175.0	0.007438	0.00795	0.008368	0.00279	0.00203	0.00177	0.00082
180.0	0.007403	0.007914	0.008343	0.00277	0.00201	0.00175	0.00081
185.0	0.007366	0.007876	0.008308	0.00275	0.00198	0.00173	0.00080
190.0	0.007333	0.007854	0.008291	0.00272	0.00196	0.00171	0.00079
195.0	0.007291	0.007831	0.008277	0.00270	0.00194	0.00168	0.00078
200.0	0.007251	0.007804	0.00825	0.00268	0.00191	0.00167	0.00077
205.0	0.007228	0.00777	0.008229	0.00266	0.00189	0.00164	0.00076
210.0	0.007189	0.007748	0.008212	0.00264	0.00187	0.00163	0.00076

215.0	0.007153	0.007718	0.008185	0.00262	0.00185	0.00161	0.00075
220.0	0.007122	0.007697	0.008156	0.00260	0.00183	0.00159	0.00074
225.0	0.007094	0.007667	0.008132	0.00258	0.00181	0.00157	0.00073
230.0	0.007066	0.007627	0.008124	0.00256	0.00180	0.00155	0.00073
235.0	0.007031	0.007602	0.008103	0.00254	0.00178	0.00154	0.00072
240.0	0.006996	0.007569	0.008087	0.00252	0.00176	0.00152	0.00072
245.0	0.006961	0.007547	0.008062	0.00250	0.00174	0.00150	0.00071
250.0	0.006933	0.007526	0.008037	0.00249	0.00172	0.00149	0.00070
255.0	0.006906	0.007492	0.008024	0.00247	0.00171	0.00147	0.00069
260.0	0.006885	0.007477	0.008005	0.00245	0.00169	0.00146	0.00069
265.0	0.006853	0.007454	0.007981	0.00243	0.00168	0.00144	0.00068
270.0	0.006828	0.007458	0.007965	0.00242	0.00167	0.00143	0.00068
275.0	0.006794	0.007429	0.007935	0.00240	0.00165	0.00142	0.00067
280.0	0.006779	0.007415	0.007938	0.00238	0.00163	0.00140	0.00067
285.0	0.006751	0.007386	0.007909	0.00236	0.00162	0.00139	0.00066
290.0	0.006722	0.007369	0.007882	0.00235	0.00160	0.00138	0.00065
295.0	0.006693	0.007348	0.007864	0.00233	0.00159	0.00137	0.00065

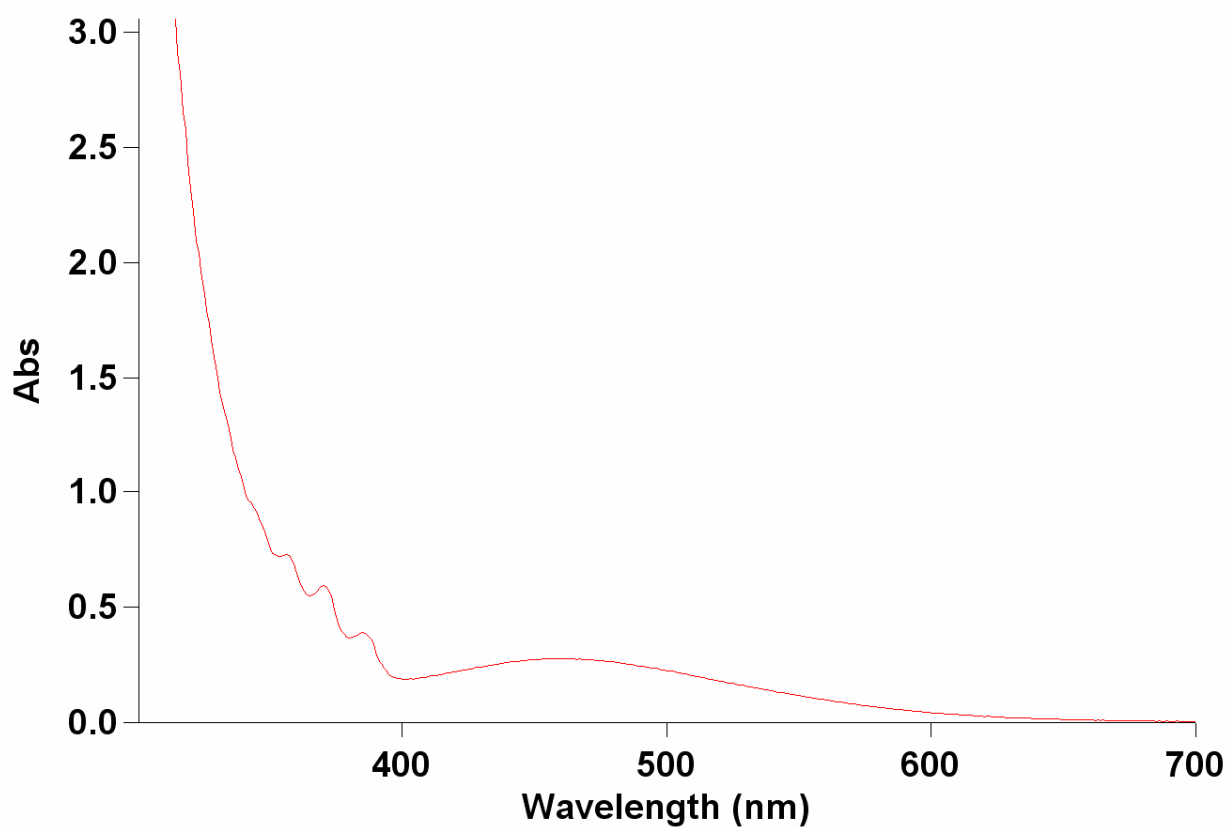
	8	9	10	11	12	13	14
time (s)	HNO <sub>2</sub> T	[HNO <sub>2</sub> ]T	[HNO <sub>2</sub> ]T	[HNO <sub>2</sub> ]T	[HNO <sub>2</sub> ]T	[HNO <sub>2</sub> ]T	[HNO <sub>2</sub> ]T
0.1	0.00200	0.001862	0.01	0.01	0.003	0.003	0.003
5.0	0.00164	0.001544	0.009901	0.009932	0.002981	0.002894	0.002924
10.0	0.00153	0.001388	0.009861	0.009887	0.002949	0.00285	0.002846
15.0	0.00144	0.001277	0.009839	0.009859	0.002933	0.002814	0.002784
20.0	0.00136	0.001196	0.009806	0.009826	0.002907	0.002785	0.002728
25.0	0.00130	0.001129	0.009807	0.009801	0.002884	0.002748	0.002675
30.0	0.00126	0.001075	0.009782	0.009765	0.002869	0.002717	0.002629
35.0	0.00121	0.001027	0.009778	0.00972	0.002855	0.002685	0.002581
40.0	0.00118	0.000986	0.009759	0.009692	0.002829	0.002655	0.00254
45.0	0.00114	0.000951	0.009746	0.009652	0.002814	0.002629	0.002502
50.0	0.00111	0.00092	0.009731	0.009636	0.002791	0.002601	0.002466
55.0	0.00108	0.00089	0.009714	0.009603	0.002773	0.002579	0.002431
60.0	0.00105	0.000865	0.009703	0.009575	0.002759	0.002558	0.002395
65.0	0.00103	0.000841	0.009693	0.009537	0.002739	0.002538	0.002365
70.0	0.00101	0.000815	0.009682	0.009524	0.002724	0.002518	0.002338
75.0	0.00099	0.000797	0.009668	0.009512	0.002708	0.0025	0.002309
80.0	0.00097	0.000778	0.009649	0.009488	0.00269	0.00248	0.002283
85.0	0.00095	0.00076	0.009643	0.009474	0.002677	0.002462	0.002255
90.0	0.00093	0.000743	0.009634	0.009448	0.002662	0.00245	0.002229
95.0	0.00091	0.000727	0.009634	0.009434	0.002647	0.002431	0.002205
100.0	0.00090	0.000712	0.009618	0.009406	0.002629	0.002415	0.002182
105.0	0.00088	0.000699	0.009603	0.009383	0.002619	0.002402	0.002157
110.0	0.00087	0.000684	0.0096	0.009367	0.002607	0.002389	0.002137
115.0	0.00085	0.000673	0.009588	0.009358	0.002589	0.002374	0.002115
120.0	0.00084	0.000661	0.009586	0.009338	0.002579	0.00236	0.002095
125.0	0.00083	0.000649	0.009567	0.009323	0.002567	0.002347	0.002075
130.0	0.00082	0.000637	0.009568	0.009308	0.002553	0.002334	0.002055
135.0	0.00080	0.000627	0.009556	0.009293	0.002543	0.002323	0.002036
140.0	0.00079	0.000619	0.009557	0.009275	0.002524	0.002313	0.002018
145.0	0.00078	0.000608	0.00954	0.009271	0.002518	0.002299	0.002
150.0	0.00077	0.000599	0.009543	0.009254	0.002507	0.002286	0.001981

155.0	0.00076	0.000591	0.009534	0.009245	0.002499	0.002276	0.001965
160.0	0.00075	0.000582	0.009523	0.009231	0.002484	0.002264	0.001948
165.0	0.00074	0.000574	0.009522	0.009215	0.002473	0.002253	0.00193
170.0	0.00073	0.000568	0.00951	0.009195	0.002467	0.002243	0.001914
175.0	0.00073	0.000558	0.009506	0.009184	0.002455	0.002235	0.001899
180.0	0.00071	0.00055	0.009498	0.009173	0.002439	0.002223	0.001884
185.0	0.00071	0.000545	0.009498	0.009166	0.002432	0.002215	0.001868
190.0	0.00070	0.000536	0.009489	0.009142	0.002422	0.002203	0.001855
195.0	0.00069	0.000531	0.009484	0.009133	0.002412	0.002195	0.001842
200.0	0.00068	0.000524	0.009475	0.009125	0.002404	0.002185	0.001829
205.0	0.00067	0.000519	0.009464	0.009108	0.002398	0.002179	0.001814
210.0	0.00066	0.000513	0.009466	0.009101	0.002388	0.002166	0.001803
215.0	0.00066	0.000508	0.009457	0.00909	0.002381	0.002157	0.001787
220.0	0.00065	0.000501	0.009459	0.009076	0.002367	0.002152	0.001776
225.0	0.00065	0.000496	0.009445	0.009063	0.002361	0.002144	0.001763
230.0	0.00064	0.000492	0.009444	0.009062	0.002349	0.002131	0.001751
235.0	0.00063	0.000487	0.009437	0.009045	0.002343	0.002123	0.001738
240.0	0.00063	0.000482	0.009429	0.009041	0.002333	0.002117	0.001727
245.0	0.00062	0.000478	0.009419	0.009017	0.002326	0.002111	0.001716
250.0	0.00061	0.000473	0.009416	0.009012	0.002316	0.0021	0.001705
255.0	0.00061	0.000468	0.009408	0.009003	0.002309	0.002093	0.001694
260.0	0.00060	0.000463	0.009404	0.008977	0.002303	0.002086	0.001682
265.0	0.00060	0.000458	0.0094	0.008969	0.002293	0.002077	0.00167
270.0	0.00059	0.000456	0.009405	0.008972	0.002287	0.00207	0.001661
275.0	0.00059	0.00045	0.009406	0.008951	0.002279	0.002065	0.001649
280.0	0.00058	0.000448	0.009397	0.00895	0.002264	0.002057	0.001639
285.0	0.00058	0.000443	0.009392	0.008926	0.002256	0.002046	0.001631
290.0	0.00057	0.00044	0.009385	0.008922	0.002252	0.002043	0.00162
295.0	0.00057	0.000436	0.009382	0.008915	0.002242	0.002036	0.001609

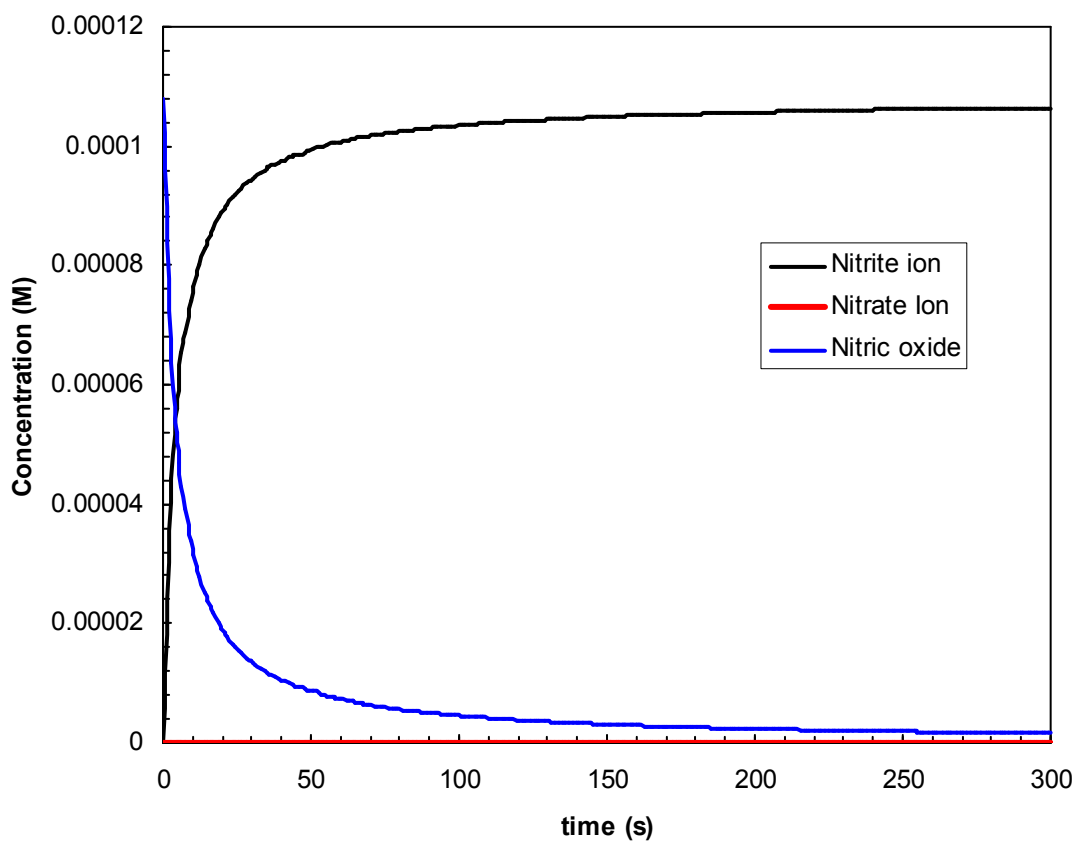
	15	16	17	18	19	20
time	[HNO <sub>2</sub> ]T	[HNO <sub>2</sub> ]T	[HNO <sub>2</sub> ]T	[HNO <sub>2</sub> ]T	[HNO <sub>2</sub> ]T	[HNO <sub>2</sub> ]T
0.01	0.003	0.01	0.01	0.01	0.01	0.009214
5.00	0.00277	0.009925	0.00975	0.009566	0.009586	0.009142
10.00	0.002664	0.009889	0.009631	0.009337	0.009271	0.009041
15.00	0.002571	0.009858	0.009511	0.009157	0.009058	0.008954
20.00	0.002495	0.009831	0.009416	0.00902	0.008873	0.008875
25.00	0.002432	0.009811	0.009332	0.008897	0.008733	0.008802
30.00	0.002381	0.009788	0.009286	0.008813	0.008617	0.008739
35.00	0.00233	0.009757	0.009226	0.008715	0.008502	0.008681
40.00	0.002283	0.009737	0.009166	0.008626	0.008392	0.00862
45.00	0.002242	0.009715	0.009111	0.008551	0.008289	0.008568
50.00	0.002203	0.009693	0.009058	0.008475	0.008194	0.008516
55.00	0.002167	0.009674	0.00901	0.008409	0.0081	0.008469
60.00	0.002135	0.009653	0.008964	0.008333	0.008019	0.008418
65.00	0.002103	0.009639	0.008923	0.008275	0.007938	0.008374
70.00	0.002074	0.009623	0.008878	0.008219	0.00786	0.008328
75.00	0.002044	0.009611	0.008834	0.008154	0.007783	0.008284
80.00	0.002016	0.009593	0.008798	0.008095	0.007719	0.008242
85.00	0.001991	0.009582	0.008754	0.008047	0.007651	0.008201
90.00	0.001967	0.009568	0.008727	0.007992	0.007581	0.00816

95.00	0.001947	0.009553	0.008705	0.007938	0.007526	0.008121
100.00	0.001922	0.00954	0.008667	0.007894	0.007456	0.008085
105.00	0.001901	0.009528	0.00863	0.007845	0.007399	0.008049
110.00	0.00188	0.009518	0.008597	0.007797	0.007347	0.008013
115.00	0.001861	0.009509	0.008565	0.007757	0.007291	0.007976
120.00	0.001843	0.009496	0.008537	0.007711	0.007234	0.007942
125.00	0.001822	0.009483	0.008505	0.007672	0.007184	0.00791
130.00	0.001805	0.009474	0.008487	0.007622	0.007134	0.007876
135.00	0.001786	0.009462	0.00845	0.00758	0.007084	0.007843
140.00	0.00177	0.009454	0.008428	0.007542	0.007031	0.007812
145.00	0.001753	0.00944	0.008405	0.007505	0.006983	0.007781
150.00	0.001738	0.009433	0.008377	0.007465	0.006937	0.007749
155.00	0.00172	0.009424	0.008351	0.00743	0.006895	0.00772
160.00	0.001705	0.009413	0.008321	0.007395	0.006851	0.007689
165.00	0.001692	0.009403	0.008299	0.007358	0.006801	0.007664
170.00	0.001678	0.009391	0.00827	0.007316	0.006765	0.007632
175.00	0.001665	0.00939	0.008248	0.007288	0.006721	0.007603
180.00	0.00165	0.00938	0.008221	0.007248	0.00668	0.007577
185.00	0.001635	0.009369	0.008202	0.00722	0.006641	0.007553
190.00	0.001623	0.009361	0.008186	0.007188	0.006603	0.007524
195.00	0.00161	0.009353	0.008154	0.007156	0.006567	0.007495
200.00	0.001596	0.009344	0.008138	0.00712	0.006526	0.007469
205.00	0.001585	0.009336	0.008118	0.007088	0.006484	0.007443
210.00	0.001573	0.009327	0.008087	0.007057	0.006454	0.007415
215.00	0.001562	0.009319	0.008075	0.007029	0.006416	0.007387
220.00	0.001552	0.009311	0.008046	0.006998	0.006381	0.00737
225.00	0.001536	0.009305	0.008027	0.006967	0.006348	0.007345
230.00	0.001528	0.009298	0.008013	0.006937	0.00632	0.00732
235.00	0.001518	0.009287	0.007995	0.00691	0.006281	0.007296
240.00	0.001508	0.009283	0.007974	0.006882	0.006241	0.007271
245.00	0.001496	0.009272	0.00795	0.006857	0.006213	0.007249
250.00	0.001487	0.009268	0.007931	0.006828	0.006177	0.007226
255.00	0.001477	0.009259	0.007917	0.006804	0.006147	0.007203
260.00	0.001466	0.009252	0.007892	0.006775	0.006115	0.007178
265.00	0.001456	0.009245	0.007884	0.006746	0.006086	0.007159
270.00	0.001444	0.009238	0.007854	0.006722	0.006054	0.007136
275.00	0.001439	0.009232	0.007846	0.0067	0.006034	0.007117
280.00	0.001431	0.009223	0.007826	0.006674	0.006001	0.007087
285.00	0.001422	0.009219	0.00781	0.006647	0.005974	0.007068
290.00	0.001411	0.009213	0.007786	0.006619	0.005944	0.007044
295.00	0.001401	0.009203	0.007771	0.006598	0.005914	0.007029

**B4. Typical UV-Vis spectrum for ONSCN solution**



**Figure S1. Typical spectrum of ONSCN solution (0.4 M HClO<sub>4</sub>, 0.01 M NaNO<sub>2</sub>, 0.05 M NaSCN)**

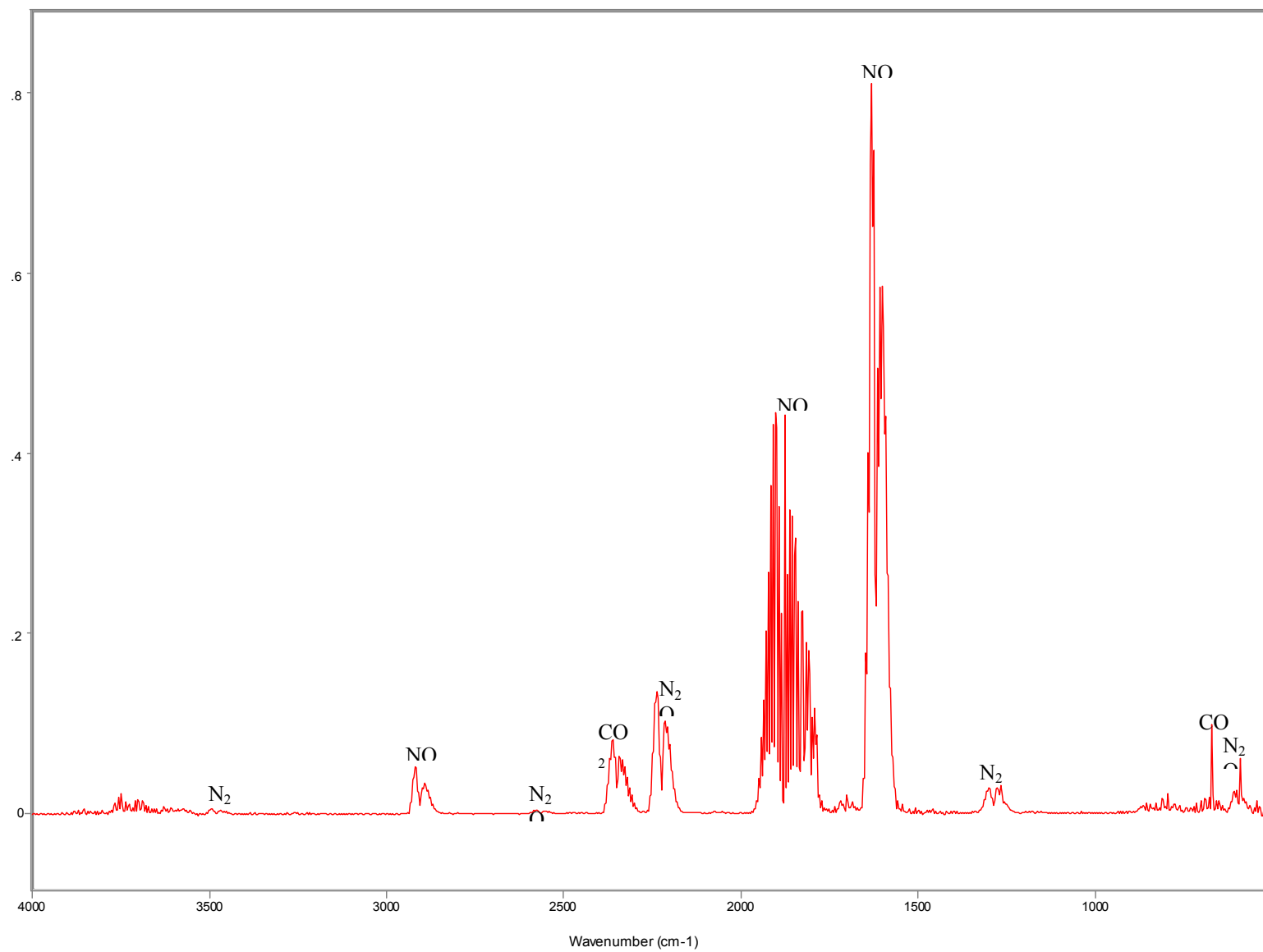
**B5. Simulation results showing oxidation of NO exclusively to  $\text{NO}_2^-$** 

**Figure S2: Simulations for oxidation of NO by dissolved oxygen ( $\text{NO}_{\text{initial}} = 0.1 \text{ mM}$ ,  $\text{O}_2 \text{ initial} = 0.27 \text{ mM}$ )**



**B6. Detailed description of apparatus for preparing NO saturated solution**

The apparatus assembled to generate the NO solutions consisted of a 50 mL reaction flask, with the inlet connected to a supply of high purity nitrogen. The reactor was filled with 40 mL of a solution containing approximately 0.3 M ascorbic acid (Sigma Aldrich) and 0.7 M HClO<sub>4</sub>, prior to purging the system of air using N<sub>2</sub>. A steady flow of NO was initiated by adding a 25% solution of sodium nitrite dropwise to the reactor containing ascorbic acid via a syringe inserted through a rubber stopper. The NO flowed through a scrubber containing a 0.1 M NaOH solution to trap any traces of NO<sub>2</sub> formed in the first reactor, before bubbling into a 10 mL reactor with septum side port containing the target solution. To ensure that the solution was indeed saturated with NO, test runs were performed wherein a small sample of NO solution reacted with a known mass of deionized water in a sealed UV-Vis cuvette. Oxygen in the water oxidized NO to nitrite according to Equations 1.2 and 1.3 (Scheme 1 in Results), and the concentration determined by the UV absorbance of nitrite at 220 nm. Results agreed with literature values<sup>25</sup> for NO saturation in water ( $1.9 \times 10^{-3} \text{ M atm}^{-1}$ ), and in 1 M NaClO<sub>4</sub> ( $1.2 \times 10^{-3} \text{ M atm}^{-1}$ ). Simulations were performed using the rate constants recommended by Schwartz and White<sup>30</sup> to confirm that nitrite was the sole product of the reaction under these conditions (Figure S2).



**B7. Typical FTIR spectrum of product gases**

**B8. Experiments to determine equilibrium constant of ONSCN**

Accurate knowledge of the equilibrium constant for the formation of ONSCN is an important factor in elucidating the kinetics of ONSCN decomposition, as it allows the concentration of ONSCN to be predicted under a given set of experimental conditions and serves as a check on the value determined spectrophotometrically. The equilibrium constant and molar absorptivity of ONSCN has been previously determined by Stedman and Whincup<sup>17</sup> by hand-mixing ONSCN solutions using standard spectrometer cells, and extrapolating back to the time of mixing to estimate the initial absorbance. Using equation 8 below, that study determined the equilibrium constant to be  $32 \text{ M}^{-2}$  at  $20^\circ\text{C}$  in perchloric acid medium, with appropriate corrections made for the activities of the ionic species. The molar absorptivity was also determined to be  $100 \pm 5 \text{ M}^{-1}\text{cm}^{-1}$ . The value of the equilibrium constant can be determined at different temperatures using the enthalpy change of reaction, with the value being  $29 \text{ M}^{-1}$  at  $25^\circ\text{C}$ <sup>29</sup>.

$$\frac{1}{A_{460}} = \frac{1}{\epsilon L K_{\text{ONSCN}} [\text{SCN}^-][\text{H}^+][\text{HNO}_2]_T} + \frac{1}{\epsilon L [\text{HNO}_2]_T} \quad (8)$$

We have performed similar experiments, determining the absorbance at 460 nm for a range of concentrations of  $\text{H}^+$  and  $\text{SCN}^-$  for a fixed total nitrite concentration of 0.01 M. As noted above, all experiments were performed at a constant ionic strength of 1.0 M, adjusted with sodium perchlorate. Using 0.05 M NaSCN, the  $\text{HClO}_4$  concentration was varied from 0.1 to 0.4 M, and the apparent equilibrium constant determined to be  $22.1 \pm 0.7 \text{ M}^{-2}$  assuming a molar absorptivity of  $100 \text{ M}^{-1}\text{cm}^{-1}$ . It should be noted that all values of  $K_{\text{ONSCN}}$  in this study were determined from concentration data without correction for the effect of non-unity activity coefficients, and should thus be regarded as apparent

equilibrium constants. Equation 8 was also used to determine simultaneously  $\epsilon$  and  $K_{ONSCN}$ , with values of  $108 \text{ M}^{-1}\text{cm}^{-1}$  and  $20.1 \text{ M}^{-2}$  respectively. The extinction coefficient is in reasonable agreement with the value determined by Stedman and Whincup<sup>17</sup>, and for consistency with past studies of ONSCN, we have continued to use the value determined in that study in conjunction with  $K_{ONSCN} = 22 \text{ M}^{-2}$ .

A set of experiments was performed using higher concentrations of  $\text{SCN}^-$  and correspondingly lower concentrations of  $\text{H}^+$  to produce the same concentrations of ONSCN used to determine  $K_{ONSCN}$  with 0.05 M NaSCN above. The absorbance was seen to be significantly higher in the experiments with higher  $\text{SCN}^-$  concentrations, despite having the same ONSCN concentration according to (4). This can be explained by the presence of an adduct between ONSCN and  $\text{SCN}^-$ ,  $\text{ON}(\text{SCN})_2^-$  which has previously been investigated by Doherty et al<sup>20</sup>.

**B9. Additional graphs for the fit of Pathways 1 and 2 to measurements at high [SCN<sup>-</sup>]**

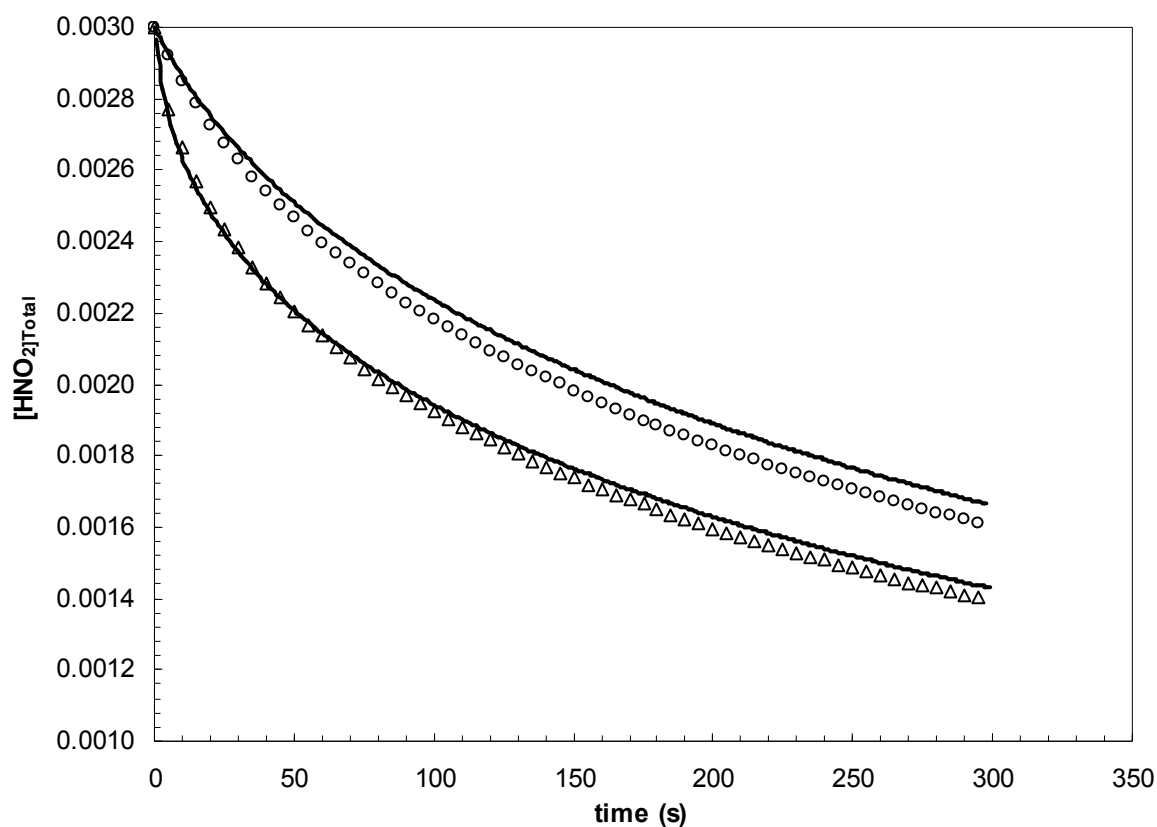


**Figure S4: Fit of Pathways 1 and 2 to experiments 8 and 13**

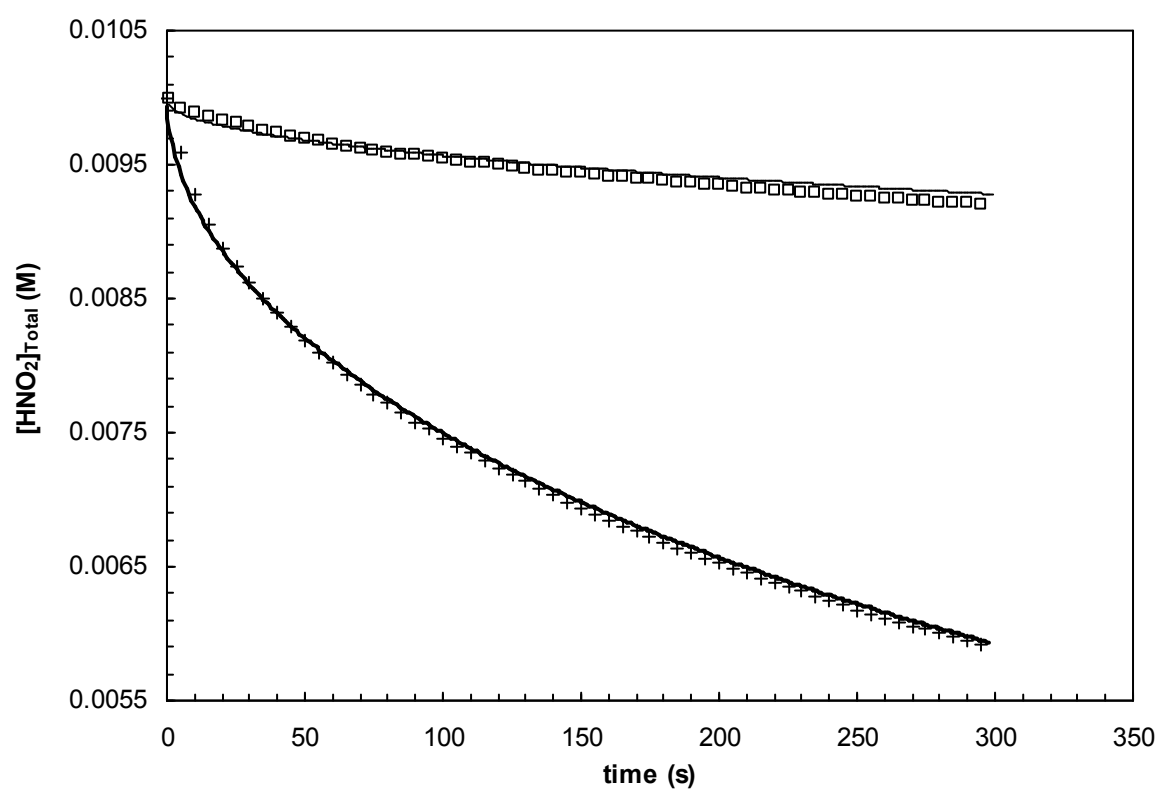


**Figure S4: Fit of Pathways 1 and 2 to experiments 12 and 3**

**B10. Derivation of Equation 19 from the main text**

$$-\frac{d[HNO_2]_{Total}}{dt} = \frac{k_a[ONSCN]^2}{[NO]} + \frac{k_b[SCN^-][ONSCN]^2}{[NO]} + k_c[ONSCN]^2 \quad (19)$$

*Pathway 3-(i)*

If Reaction 16 is the rate limiting step in pathway 3-(i), (i.e. reaction of SCN radicals with  $SCN^-$  is rapid and irreversible), and Reaction 14 is at equilibrium, then the rate of formation of NO and  $(SCN)_2^-$  is given by:

$$forward\ rate = k_{16}[ONSCN] + k_{14}[ONSCN][SCN^-]$$

and the backward rate would be:

$$backward\ rate = k_{-14}[NO][(SCN)_2^-]$$

Equating the forward and backward rates provides an expression for the concentration of  $(SCN)_2^-$ , which can then be substituted into the rate law for Reaction 15, which is assumed to be irreversible and rate limiting:

$$[(SCN)_2^-] = \frac{k_{16}[ONSCN]}{[NO]k_{-14}} + \frac{k_{14}[SCN^-][ONSCN]}{[NO]k_{-14}}$$

$$-\frac{d[HNO_2]_{Total}}{dt} = k_{15}[(SCN)_2^-][ONSCN] = \frac{k_{15}k_{16}[ONSCN]^2}{k_{-14}[NO]} + \frac{k_{15}k_{14}[SCN^-][ONSCN]^2}{k_{-14}[NO]}$$

*Pathway 3-(ii)*

If Reaction 14 is sufficiently rapid to be at equilibrium, the  $(SCN)_2^-$  concentration is given by:

$$[(SCN)_2^-] = \frac{k_{14}[SCN^-][ONSCN]}{[NO]k_{-14}}$$

$(SCN)_2^-$  is consumed in two parallel Reactions (15 and 18) and the rate of reaction is given by:

$$\begin{aligned} -\frac{d[HNO_2]_{Total}}{dt} &= k_{15}[(SCN)_2^-][ONSCN] + k_{18}[(SCN)_2^-][HNO_2][H^+][ONSCN] \\ &= \frac{k_{15}k_{14}[SCN^-][ONSCN]^2}{k_{-14}[NO]} + \frac{k_{18}k_{14}[SCN^-][HNO_2][H^+][ONSCN]}{k_{-14}[NO]} \\ &= \frac{k_{15}k_{14}[SCN^-][ONSCN]^2}{k_{-14}[NO]} + \frac{k_{18}k_{14}[ONSCN]^2}{K_{ONSCN}k_{-14}[NO]} \end{aligned}$$

The third term in Equation 19 is associated with Reaction 5.



## **APPENDIX C**

### **Supporting information for Chapter 6**

## Table of Contents

C1.	Calculated geometries and vibrational frequencies of species involved in ONSCN decomposition (B3LYP/6-31G(d) level)	343
C2.	Gas phase species enthalpies and free energies computed at G3B3 and CBS-QB3 (in Hartrees/particle)	355
C3.	Solvation free energies computed with various solvent models (kJ mol <sup>-1</sup> )	356

**C1. Calculated geometries and vibrational frequencies of species involved in  
ONSCN decomposition (B3LYP/6-31G(d) level)**

***cis*-HNO<sub>2</sub>**

Center Number	Atomic Number	Atomic Type	Coordinates (Angstroms)		
			X	Y	Z
1	7	0	0.000000	0.551088	0.000000
2	8	0	1.088193	0.065533	0.000000
3	8	0	-1.017487	-0.389393	0.000000
4	1	0	-0.565653	-1.266736	0.000000

Moments of inertia: 21.70234 135.94458 157.64692

Frequencies -- 649.0997 739.5585 919.6412  
1369.1921 1728.5844  
3520.7427

***trans*-HNO<sub>2</sub>**

Center Number	Atomic Number	Atomic Type	Coordinates (Angstroms)		
			X	Y	Z
1	7	0	0.171496	0.492520	-0.000053
2	8	0	1.105817	-0.225959	0.000041
3	8	0	-1.040812	-0.260023	-0.000043
4	1	0	-1.720515	0.440209	0.000381

Moments of inertia: 19.53117 143.68656 163.21773

Frequencies -- 599.7799 630.6753 863.9376  
1325.1947 1794.6324 3698.4640

**NO<sub>2</sub><sup>-</sup>**

Center Number	Atomic Number	Atomic Type	Coordinates (Angstroms)		
			X	Y	Z
1	7	0	0.000000	0.000000	0.470720
2	8	0	0.000000	1.076533	-0.205940
3	8	0	0.000000	-1.076533	-0.205940

Moments of inertia: 5.92516 132.39292 148.31808

Frequencies -- 792.7212 1339.2136 1377.6180

**NO**

Center Number	Atomic Number	Atomic Type	Coordinates (Angstroms)		
			X	Y	Z
1	7	0	0.000000	0.000000	-0.617977
2	8	0	0.000000	0.000000	0.540730

Moments of inertia: 0.00000 35.79798 35.79798

Frequencies -- 1991.0549

**H<sub>2</sub>O**

Center Number	Atomic Number	Atomic Type	Coordinates (Angstroms)		
			X	Y	Z
1	8	0	0.000000	0.000000	0.119720
2	1	0	0.000000	0.761560	-0.478879
3	1	0	0.000000	-0.761560	-0.478879

Moments of inertia: 2.29054 4.17466 6.46520

Frequencies -- 1712.7968 3728.4714 3850.6127

***cis*-ONSCN**

Center Number	Atomic Number	Atomic Type	Coordinates (Angstroms)		
			X	Y	Z
1	6	0	-1.193438	-0.156010	0.001303
2	16	0	-0.137374	1.146717	-0.000135
3	7	0	-1.833213	-1.135412	-0.000771
4	7	0	1.584527	-0.026732	-0.000346
5	8	0	1.387426	-1.159551	0.000269

Moments of inertia: 292.47879 466.74533 759.22389

Frequencies -- 92.5242 206.7628 287.3390  
400.0356 412.2788 617.9152  
727.1657 1885.1095 2240.5145

***trans*-ONSCN**

Center Number	Atomic Number	Atomic Type	Coordinates (Angstroms)		
			X	Y	Z
1	6	0	1.465858	-0.110929	0.000004
2	16	0	0.093666	0.869768	-0.000003
3	7	0	2.424921	-0.777290	0.000010
4	7	0	-1.226610	-0.692139	-0.000041
5	8	0	-2.335249	-0.370589	0.000030

Moments of inertia: 148.91240 773.85657 922.76897

Frequencies --	112.7675	148.9827	276.6890
	385.8533	406.2546	618.6320
	729.0243	1864.5566	2260.5263

### **cis-ONNCS**

Center Number	Atomic Number	Atomic Type	Coordinates (Angstroms)		
			X	Y	Z
1	6	0	-0.480668	0.482648	0.000173
2	16	0	-1.864254	-0.266788	-0.000112
3	7	0	0.593713	1.065965	0.000400
4	7	0	1.977641	0.208467	-0.000732
5	8	0	1.839074	-0.943537	0.000384

Moments of inertia: 127.95374 813.09736 941.05101

Frequencies --	82.8488	85.5858	282.6954
	493.0229	580.9033	681.3420
	945.8102	1782.2271	
	1953.7165		

### **trans-ONNCS**

Center Number	Atomic Number	Atomic Type	Coordinates (Angstroms)		
			X	Y	Z
1	6	0	0.607043	0.221458	0.000018
2	16	0	2.139910	-0.122199	-0.000015
3	7	0	-0.567724	0.567920	0.000028
4	7	0	-1.694919	-0.484093	0.000048
5	8	0	-2.755291	0.004956	-0.000051

Moments of inertia: 31.65519 1132.01732 1163.67251

Frequencies --	100.3745	128.9446	349.2063
	492.4499	560.8980	692.0284
	957.4153	1754.8676	1974.5990

### **SCN-**

Center Number	Atomic Number	Atomic Type	Coordinates (Angstroms)		
			X	Y	Z
1	16	0	0.000000	0.000000	1.036524
2	6	0	0.000000	0.000000	-0.639965
3	7	0	0.000000	0.000000	-1.820656

Moments of inertia: 0.00000 305.97629 305.97629

Frequencies -- 477.7348 477.7348 731.5966  
2174.6995

## HNCS

Center Number	Atomic Number	Atomic Type	Coordinates (Angstroms)		
			X	Y	Z
1	16	0	0.035976	-1.082290	0.000000
2	6	0	0.000000	0.498265	0.000000
3	7	0	-0.155442	1.696355	0.000000
4	1	0	0.512476	2.452561	0.000000

Moments of inertia: 1.72107 310.13967 311.86074

Frequencies -- 453.4947 482.2170 668.4997  
876.4141 2066.7100 3675.5163

## SCN

Center Number	Atomic Number	Atomic Type	Coordinates (Angstroms)		
			X	Y	Z
1	16	0	0.000000	0.000000	1.020105
2	6	0	0.000000	0.000000	-0.617191
3	7	0	0.000000	0.000000	-1.802647

Moments of inertia: 0.00000 297.63106 297.63106

Frequencies -- 360.6485 425.2803 756.7012  
1999.7619

## (SCN)<sub>2</sub>

Center Number	Atomic Number	Atomic Type	Coordinates (Angstroms)		
			X	Y	Z
1	6	0	1.843450	0.463561	-0.039786
2	7	0	2.585573	1.258075	-0.461509
3	16	0	0.838318	-0.724224	0.655396
4	16	0	-0.838402	-0.724386	-0.655294
5	6	0	-1.843540	0.463525	0.039675
6	7	0	-2.585303	1.258388	0.461371

## Appendix C – Supporting information for Chapter 6

Moments of inertia: 416.045471239.791111416.83473

Frequencies --	54.1812	136.8965	152.6040
	369.2474	376.3663	408.9742
	433.5653	468.6660	674.0060
	681.1842	2269.9742	2275.4160

(SCN)<sub>3</sub><sup>-</sup>

Center Number	Atomic Number	Atomic Type	Coordinates (Angstroms)		
			X	Y	Z
1	6	0	-3.287299	-0.513385	0.283159
2	7	0	-4.007598	-0.682603	1.192580
3	16	0	-2.295930	-0.288330	-1.060255
4	16	0	2.296788	-0.281333	1.061673
5	6	0	3.286850	-0.515110	-0.281232
6	7	0	4.006405	-0.690279	-1.190114
7	16	0	0.000134	-0.187487	0.001045
8	6	0	-0.000340	1.517025	-0.003546
9	7	0	-0.000397	2.684770	-0.006707

Moments of inertia: 957.21094 4141.78998 4287.37054

Frequencies --	18.3695	25.3239
53.7751		
	77.3719	115.9896
	130.3647	
	185.8887	191.3186
	205.0725	
	413.9475	416.7501
	433.1031	
	437.0925	438.7003
	449.4439	
	683.6490	707.7289
	709.7947	
	2220.6742	2220.7683
	2259.1774	

(SCN)<sub>2</sub><sup>-</sup>

Center Number	Atomic Number	Atomic Type	Coordinates (Angstroms)		
			X	Y	Z
1	6	0	-2.331751	0.072289	0.348129
2	7	0	-3.129894	0.670992	0.972834
3	16	0	-1.228765	-0.799231	-0.556188
4	16	0	1.228769	0.799291	-0.556108
5	6	0	2.331748	-0.072327	0.348124
6	7	0	3.129887	-0.671096	0.972769

Moments of inertia: 367.01725 1966.15974 1981.85580

Frequencies --	16.2585	54.8870	59.9883
	156.6999	424.7975	425.6748

446.4474                      450.3691                      718.3583  
719.3215                      2157.3267                      2159.0847

**ON(SCN)<sub>2</sub><sup>-</sup>**

Center Number	Atomic Number	Atomic Type	Coordinates (Angstroms)		
			X	Y	Z
1	6	0	-2.751220	0.197001	0.236807
2	7	0	-3.328775	1.121029	0.678208
3	16	0	-1.849306	-1.056612	-0.398915
4	16	0	1.642227	-0.862292	0.480248
5	6	0	2.948027	0.109724	0.063655
6	7	0	3.863585	0.787728	-0.224774
7	7	0	0.009190	0.502067	-0.700347
8	8	0	-0.209447	1.498293	-0.171965

Moments of inertia: 548.06505 2797.06272 3147.48318

Frequencies --    19.7146                      38.4347                      54.0122  
                         83.9575                      86.9583                      171.2311  
                         244.7832                      410.3290                      434.1048  
                         445.9274                      449.4938                      457.2045  
                         481.5075                      714.7235                      731.9198  
                         1865.3461                      2196.1025                      2199.5953

**ON(SCN)<sub>2</sub><sup>-</sup> S-S isomer**

Center Number	Atomic Number	Atomic Type	Coordinates (Angstroms)		
			X	Y	Z
1	6	0	2.798458	-0.532648	0.000014
2	7	0	3.237377	-1.625528	0.000000
3	16	0	2.149808	1.013460	0.000017
4	16	0	-0.582930	-0.398021	-0.000040
5	6	0	-1.333541	1.111292	-0.000014
6	7	0	-1.968839	2.093185	-0.000004
7	7	0	-2.318057	-1.440133	0.000003
8	8	0	-3.314115	-0.813945	0.000049

Moments of inertia: 693.21834 2592.26634 3285.48468

Frequencies --    27.8091                      28.0686                      49.2544  
                         73.3747                      118.3690                      131.1605  
                         216.4265                      253.3578                      401.6417  
                         427.2519                      462.2869                      463.2636  
                         605.4363                      716.3802                      726.2500  
                         1743.9408                      2188.0326                      2243.5304



**Transition State - ONSCN + SCN<sub>2</sub><sup>-</sup> (Reaction 3)**

Center Number	Atomic Number	Atomic Type	Coordinates (Angstroms)		
			X	Y	Z
1	6	0	2.620302	-1.240441	-0.531498
2	16	0	2.232964	0.363908	-0.238494
3	7	0	2.992877	-2.340121	-0.688765
4	7	0	4.142274	0.723985	0.804068
5	8	0	4.788421	-0.228725	0.960148
6	7	0	-0.869236	2.915774	-0.078980
7	6	0	-0.905365	1.746891	-0.177977
8	16	0	-0.905231	0.074185	-0.324459
9	7	0	-4.591491	-1.030841	1.814178
10	6	0	-4.142124	-0.744875	0.766881
11	16	0	-3.544308	-0.351921	-0.748242

Moments of inertia: 1426.39139 7264.0231 77901.00662

Frequencies --	-112.2763	13.9687	17.8514
	19.5816	33.2703	44.1854
	58.3008	76.0628	86.2808
	98.4557	121.7772	170.7852
	192.9883	404.1114	419.4992
	420.3088	426.6295	433.5555
	442.1293	522.0227	709.0989
	713.7846	721.3709	1803.4797
	2179.5985	2197.3244	2222.3744

**HOSCN**

Center Number	Atomic Number	Atomic Type	Coordinates (Angstroms)		
			X	Y	Z
1	6	0	-1.063705	-0.003872	-0.002367
2	7	0	-2.169779	0.368994	-0.001915
3	16	0	0.527046	-0.621568	0.012743
4	8	0	1.445135	0.782333	-0.119867
5	1	0	1.576863	1.126698	0.782662

Moments of inertia: 93.24749 446.75274 534.29623

Frequencies --	179.2007	345.2882
461.7098		
	480.4340	673.5766
	754.6833	
	1237.7169	2259.9169
	3692.6075	

**OSCN<sup>-</sup>**

Center Number	Atomic Number	Atomic Type	Coordinates (Angstroms)		
			X	Y	Z

## Appendix C – Supporting information for Chapter 6

1	6	0	-0.678262	-0.837994	0.000000
2	7	0	-1.219234	-1.885025	0.000000
3	16	0	0.000000	0.763166	0.000000
4	8	0	1.575527	0.751560	0.000000

Moments of inertia: 61.27003 481.10488 542.37491

Frequencies -- 180.8809 383.2474 462.3440  
583.7802 893.3145 2139.6332

### ONOSCN

Center Number	Atomic Number	Atomic Type	Coordinates (Angstroms)		
			X	Y	Z
1	6	0	1.529219	0.274313	0.035432
2	7	0	2.332044	1.088700	0.265608
3	16	0	0.407554	-0.946361	-0.370083
4	8	0	-0.815477	-0.670086	0.744636
5	7	0	-1.845748	0.431411	0.366993
6	8	0	-1.572054	1.026975	-0.584570

Moments of inertia: 337.08967 817.778521000.57959

Frequencies -- 59.2972 148.3758 240.9967  
302.2691 331.2749 398.4179  
475.7885 680.5049 695.1809  
819.1690 1868.1771 2268.2410

### OSCN

Center Number	Atomic Number	Atomic Type	Coordinates (Angstroms)		
			X	Y	Z
1	6	0	-0.658595	-0.821594	0.000000
2	7	0	-1.169108	-1.870251	0.000000
3	16	0	0.000000	0.793530	0.000000
4	8	0	1.516916	0.665605	0.000000

Moments of inertia: 65.06611 454.34112 519.40723

Frequencies -- 175.4341 308.6695 456.0728  
620.7165 1013.8773 2253.5268

### 1,1-S (ON)2SCN<sup>+</sup>

Center Number	Atomic Number	Atomic Type	Coordinates (Angstroms)		
			X	Y	Z

## Appendix C – Supporting information for Chapter 6

1	6	0	-0.001012	0.939712	0.594846
2	16	0	0.000625	-0.700289	0.884421
3	7	0	-0.002856	2.056781	0.237466
4	7	0	-2.036851	-0.835227	-0.465141
5	8	0	-2.347631	0.177141	-0.804655
6	7	0	2.038313	-0.833397	-0.464528
7	8	0	2.348360	0.179015	-0.804644

Moments of inertia: 581.47846 1247.89011 1423.63975

Frequencies -- 43.9482 53.9524 76.3671  
 145.8657 150.8320 218.5200  
 220.3047 387.4934 388.4019  
 462.4993 480.0750 737.5590  
 2107.3697 2141.3104 2213.8027

### ONSCNNO<sup>+</sup>

Center Number	Atomic Number	Atomic Type	Coordinates (Angstroms)		
			X	Y	Z
1	6	0	-0.043977	-0.559527	0.249866
2	16	0	1.418263	-1.217571	-0.066683
3	7	0	-1.045136	0.002364	0.555988
4	7	0	2.499471	0.818889	-0.174241
5	8	0	1.855669	1.718233	0.008077
6	7	0	-2.747965	-0.099397	-0.477160
7	8	0	-3.527286	0.504929	0.021375

Moments of inertia: 431.47491 1913.30002 2281.62593

Frequencies -- 34.0278 36.7008 71.4184  
 92.1174 142.6137 216.5331  
 262.2593 426.7201 438.9115  
 513.8663 530.8342 801.4477  
 2028.7669 2091.8086 2195.3236

### HCN

Center Number	Atomic Number	Atomic Type	Coordinates (Angstroms)		
			X	Y	Z
1	6	0	0.000000	0.000000	-0.502001
2	1	0	0.000000	0.000000	-1.572523
3	7	0	0.000000	0.000000	0.654933

Moments of inertia: 0.00000 40.82558 40.82558

Frequencies -- 766.8245 766.8245 2214.3701  
 3480.7274

**ONCN**

Center Number	Atomic Number	Atomic Type	Coordinates (Angstroms)		
			X	Y	Z
1	6	0	0.000000	0.672559	0.000000
2	7	0	-0.196172	1.821840	0.000000
3	7	0	0.530668	-0.646336	0.000000
4	8	0	-0.292684	-1.532986	0.000000

Moments of inertia: 20.62352 340.75633 361.37986

Frequencies -- 217.2971 270.9288 628.5306  
824.9824 1611.3301 2274.9044

**ONH**

Center Number	Atomic Number	Atomic Type	Coordinates (Angstroms)		
			X	Y	Z
1	7	0	0.063505	0.582770	0.000000
2	8	0	0.063505	-0.624899	0.000000
3	1	0	-0.952574	0.919800	0.000000

Moments of inertia: 3.28567 42.54712 45.83279

Frequencies -- 1586.7995 1685.5680  
2821.2600

**HO<sub>2</sub>SCN**

Center Number	Atomic Number	Atomic Type	Coordinates (Angstroms)		
			X	Y	Z
1	6	0	-1.256406	-0.034639	-0.023181
2	7	0	-2.407407	-0.017693	0.145163
3	16	0	0.507715	-0.145314	-0.428692
4	8	0	0.887057	1.361550	0.160026
5	1	0	0.767587	1.381547	1.132351
6	8	0	1.050349	-1.202154	0.446181

Moments of inertia: 237.09970 536.25394 694.87751

Frequencies -- 144.4792 173.8944 289.5645  
402.2188 438.1668 494.8915  
597.1770 740.1541 1144.4894  
1217.8521 2296.6429 3639.7588

**SS-(OSCN)<sub>2</sub>**

Center Number	Atomic Number	Atomic Type	Coordinates (Angstroms)		
			X	Y	Z
1	6	0	2.123705	0.271486	-0.051677
2	7	0	3.032265	0.968397	0.162059
3	16	0	0.801712	-0.837814	-0.472296
4	8	0	0.830251	-1.992465	0.470254
5	8	0	-0.827873	1.992451	-0.461152
6	16	0	-0.801537	0.834284	0.477087
7	6	0	-2.123628	-0.271889	0.047843
8	7	0	-3.035451	-0.959967	-0.180127

Moments of inertia: 791.80840 1611.70684 2244.75120

Frequencies -- 18.2362 58.4032 105.9426  
 112.3681 165.8389 170.2866  
 182.4636 296.9611 336.0343  
 422.2978 441.1074 456.6100  
 592.2195 598.4417 1124.5709  
 1143.2804 2277.0847 2278.5852

**HOCN**

Center Number	Atomic Number	Atomic Type	Coordinates (Angstroms)		
			X	Y	Z
1	6	0	0.179817	-0.005052	-0.000160
2	8	0	-1.119900	-0.110863	0.000051
3	1	0	-1.528806	0.772955	0.000039
4	7	0	1.344158	0.020609	0.000073

Moments of inertia: 2.71728 171.69824 174.41552

Frequencies -- 431.5893 487.5029 1103.3088  
 1253.2315 2389.2491 3702.2924

**N<sub>2</sub>O<sub>2</sub>**

Center Number	Atomic Number	Atomic Type	Coordinates (Angstroms)		
			X	Y	Z
1	7	0	-0.167557	0.572119	0.000000
2	7	0	0.167557	-0.572119	0.000000
3	8	0	0.167557	1.741394	0.000000
4	8	0	-0.167557	-1.741394	0.000000

Moments of inertia: 4.51015 380.66148 385.17163

Frequencies --      251.6587                      349.2941                      430.2996  
                          1013.6226                      1527.4107                      2048.9090

**Transition state - 2ONSCN → N<sub>2</sub>O<sub>2</sub> (B3LYP/CBSB7)**

Center Number	Atomic Number	Atomic Type	Coordinates (Angstroms)		
			X	Y	Z
1	6	0	-1.824808	-1.310228	0.128859
2	16	0	-0.604936	-0.525515	0.953797
3	7	0	-2.715276	-1.766303	-0.463542
4	7	0	-1.615248	1.546061	0.321670
5	8	0	-2.480893	1.457696	-0.411672
6	7	0	0.360249	1.654754	-0.681571
7	8	0	1.127074	2.229208	-0.088076
8	7	0	3.376510	0.169806	0.508922
9	6	0	2.529687	-0.484534	0.045789
10	16	0	1.277288	-1.346790	-0.631813

Moments of inertia: 1353.84387      2357.30649      3286.21118

Frequencies --      -156.1409                      24.5561                      46.7585  
                          73.5466                      76.8036                      95.0467  
                          117.0536                      131.9745                      184.6610  
                          213.2193                      223.3759                      237.8628  
                          394.8463                      403.5429                      423.2650  
                          434.8685                      452.9366                      538.6483  
                          717.8299                      720.5469                      1859.9970  
                          1950.1830                      2178.9350                      2218.0236

**C2. Gas phase species enthalpies and free energies computed at G3B3 and CBS-QB3 (in Hartrees/particle)**

Species	CBS-QB3		G3B3	
	Enthalpy	Free energy	Enthalpy	Free energy
cis-HONO	-205.470225	-205.498298	-205.603218	-205.63131
trans-HONO	-205.470839	-205.499027	-205.604177	-205.632388
NO <sub>2</sub> <sup>-</sup>	-204.932197	-204.959104	-205.064011	-205.090949
NO	-129.745164	-129.768458	-129.832945	-129.856256
H <sub>2</sub> O	-76.333703	-76.355129	-76.379945	-76.401392
cis-ONSCN	-620.190939	-620.226707	-620.672172	-620.708113
SCN <sup>-</sup>	-490.53716	-490.563616	-490.929558	-490.956049
HNCS	-491.047701	-491.076161	-491.441354	-491.469887
SCN	-490.406473	-490.433779	-490.798699	-490.826079
(SCN) <sub>2</sub>	-980.887744	-980.927447	-981.671546	-981.711609
(SCN) <sub>3</sub> <sup>-</sup>	-1471.468832	-1471.523757	-1472.642818	-1472.697012
(SCN) <sub>2</sub> <sup>-</sup>	-980.989713	-981.035155	-981.77089	-981.815339
ON(SCN) <sub>2</sub> <sup>-</sup>	-1110.756877	-1110.806737	-1111.631814	-1111.68197
HOSCN	-566.157323	-566.190179	-566.594317	-566.627299
ONOSCN	-695.302549	-695.341302	-695.826358	-695.865322
1,1,S (ON) <sub>2</sub> SCN <sup>+</sup>	-749.624315	-749.669584	-750.195886	-750.241611
OSCN	-565.539341	-565.57231	-565.9737	-566.006829
OSCN <sup>-</sup>	-565.631375	-565.663566	-566.067385	-566.099737
TS (Reaction 3) ONSCN + SCN <sub>2</sub> <sup>-</sup>	-1601.191059	-1601.25631		
ONSCNNO <sup>+</sup>	-749.63547	-749.681778	-750.205568	-750.252266
cis-ONNCS	-620.17505	-620.211258	-620.655432	-620.691786
trans-ONNCS	-620.179944	-620.215213	-620.66051	-620.695747
HCN	-93.284064	-93.306898	-93.374741	-93.397626
CN <sup>-</sup>	-92.727762	-92.750102	-92.817055	-92.839413
ONCN	-222.410033	-222.440719	-222.587826	-222.61863
ONH	-130.3195	-130.344549	-130.408737	-130.433804
HO <sub>2</sub> SCN	-641.289483	-641.325206	-641.769211	-641.80522
NCS(=O)-OSCN	-1131.11089	-1131.156776	-1131.981704	-1132.028281
SS-(OSCN) <sub>2</sub>	-1131.093	-1131.140423	-1131.962511	-1132.01125
NCISOOSCN	-1131.063755	-1131.111808		
trans-ONSCN	-620.187771	-620.223777	-620.669167	-620.705296
ON(SCN) <sub>2</sub> <sup>-</sup> S-S isomer	-1110.747643	-1110.797634	-1111.619926	-1111.670728
N <sub>2</sub> O <sub>2</sub>	-259.463422	-259.492767	-259.641098	-259.670555
TS – 2ONSCN → N <sub>2</sub> O <sub>2</sub>	-1240.335196	-1240.389791		
HO-CN	-168.421072	-168.448509	-168.5552	-168.582763

**C3. Solvation free energies computed with various solvent models (kJ mol<sup>-1</sup>)**

<b>Species/Method</b>	<b>1</b>	<b>2</b>	<b>3</b>	<b>4</b>	<b>5</b>	<b>6</b>	<b>7</b>	<b>8</b>
<i>cis</i> -HONO			-27.7	-7.9	-11.6	-32.6	-17.6	-12.9
<i>trans</i> -HONO	-20.1	-34.9	-30.9	-35.3	-13.2	-38.9	-20.3	-16.6
NO	-2.9	-1.7	-7.9	-7.9	-7.9	-7.9	-2.4	-7.9
H <sub>2</sub> O	-27.3	-34.7	-28.6	-35.0	-37.5	-34.5	-28.3	-39.5
<i>cis</i> -ONSCN	-26.4	-19.1	-17.5	-19.3	-3.1	-18.2	-23.8	-4.0
SCN <sup>-</sup>	-246.5	-242.0	-251.1	-242.1	-223.2	-244.1	-245.9	-223.8
HNCS	-16.0	-32.6	-31.9	-32.9	-8.5	-27.7	-16.7	-10.1
SCN	-16.4	-9.3	-7.8	-9.3	2.0	-11.3	-15.9	2.2
(SCN) <sub>2</sub>	-37.4	-23.4	-20.3	-23.5	1.1	-26.5	-36.1	0.1
(SCN) <sub>3</sub> <sup>-</sup>	-180.0	-172.1	-170.3	-172.1	-141.2	-221.1	-180.5	-144.2
(SCN) <sub>2</sub> <sup>-</sup>	-192.7	-190.4	-194.5	-190.4	-163.7	-196.1	-191.7	-170.4
ON(SCN) <sub>2</sub> <sup>-</sup>	-191.7	-185.7	-189.4	-186.1	-161.7	-213.3	-191.0	-159.4
HOSCN	-35.0	-43.3	-39.3	-43.7	-21.7	-44.7	-34.5	-22.1
ONOSCN	-28.3	-19.0					-25.1	
1,1,S (ON)2SCN <sup>+</sup>	-277.4	-246.5					-274.7	
OSCN	-28.5	-17.0					-27.3	
OSCN <sup>-</sup>	-252.8	-246.9					-251.0	
TS								
ONSCN + SCN <sub>2</sub> <sup>-</sup>	-190.5	-180.3					-185.4	
ONSCNNO <sup>+</sup>	-246.9	-215.8					-241.6	
<i>cis</i> -ONNCS	-18.0	-10.7					-12.1	
<i>trans</i> -ONNCS	-7.9	-6.7					-8.5	
HCN	-23.5	-7.9						
ONCN	-14.8	-10.7					-13.9	
ONH	-15.2	-27.5					-15.2	
HO2SCN	-42.0	-28.6					-41.5	
NCS(=O)-OSCN	-46.5	-24.8					-44.5	
SS-(OSCN) <sub>2</sub>	-52.0						-49.0	
NCSOOSCN		-24.1					-38.9	
<i>trans</i> -ONSCN		-20.9					-26.0	
ON(SCN) <sub>2</sub> <sup>-</sup>								
S-S isomer	-236.9	-224.1	-215.8	-220.1	-187.6	-219.9	-227.8	-188.6
N <sub>2</sub> O <sub>2</sub>		-17.3					-16.8	
TS								
2ONSCN → N <sub>2</sub> O <sub>2</sub>		-40.7					-50.3	
HOCN		-58.8					-41.6	

1. B3LYP/6-311++G(d,p) IEFPCM UFF radii
2. B3LYP/6-31+G(d,p) IEFPCM UAHF radii
3. B3LYP/6-31G(d,p) IEFPCM UAHF radii
4. B3LYP/6-31+G(d,p) CPCM = UAHF
5. B3LYP/6-31+G(d,p) SMD
6. HF/6-31+G(d,p) PCM UAHF radii
7. B3LYP/6-31+G(d,p) IEFPCM UFF radii
8. M052X/6-31+G(d,p) SMD



## **APPENDIX D**

### **Supporting information for Chapter 8**

## **Table of Contents**

D1.	Equations employed by OLI	359
D1.1	Standard state properties	360
D1.2	Excess properties	363
D2.	References	366

**D1. Equations employed by OLI**

This Appendix provides a brief description of the equations employed by OLI. Further details can be found in the associated reference material.<sup>1-4</sup> Thermodynamic properties are divided into two parts, the standard part depending on temperature and pressure only and the excess portion depending on temperature, pressure and composition:

Partial molal Gibbs free energy:

$$\overline{G}_i = \overline{G}_i^o + \overline{G}_i^E \quad (1)$$

Partial molal enthalpy:

$$\overline{H}_i = \overline{H}_i^o + \overline{H}_i^E \quad (2)$$

Partial molal entropy:

$$\overline{S}_i = \overline{S}_i^o + \overline{S}_i^E \quad (3)$$

Partial molal heat capacity:

$$\overline{Cp}_i = \overline{Cp}_i^o + \overline{Cp}_i^E \quad (4)$$

Partial molal volume:

$$\overline{V}_i = \overline{V}_i^o + \overline{V}_i^E \quad (5)$$

where the superscripts <sup>o</sup> and <sup>E</sup> refer to the standard state and excess properties, respectively.

**D1.1 Standard state properties**

OLI employs the Helgeson-Kirkam-Flowers (HKF) equation of state to calculate the standard state thermodynamic properties of species dissolved in water. The HKF equation of state represents the standard state properties of a species using a function with seven terms specific to the species in question.

$$\overline{H_i^o} = \overline{H_i^R} + f_{Hi}(a_1...a_4, c_1, c_2, \omega) \quad (6)$$

$$\overline{G_i^o} = \overline{G_i^R} + \overline{S_i^R}(T - T_R) + f_{Gi}(a_1...a_4, c_1, c_2, \omega) \quad (7)$$

$$\overline{S_i^o} = \overline{S_i^R} + f_{Si}(a_1...a_4, c_1, c_2, \omega) \quad (8)$$

$$\overline{Cp_i^o} = \overline{Cp_i^R} + f_{Cpi}(a_1...a_4, c_1, c_2, \omega) \quad (9)$$

$$\overline{V_i^o} = \overline{V_i^R} + f_{Vi}(a_1...a_4, c_1, c_2, \omega) \quad (10)$$

where the superscript <sup>R</sup> refers to the reference state property (25 °C, 1 bar), the terms  $a_1...a_4$  describe pressure effects, the terms  $c_1$  and  $c_2$  describe temperature effects and  $\omega$  describes the effects of temperature and pressure on the standard state properties of water. The expanded expressions for the HKF equation of state are shown below:

### HKF equation of state

#### Enthalpy:

$$\begin{aligned} \overline{H}_i^o &= \overline{H}_f^R + c_1(T - T_r) - c_2 \left[ \left( \frac{1}{T - \Theta} \right) - \left( \frac{1}{T_r - \Theta} \right) + a_1(P - P_r) + a_2 \ln \left( \frac{\Psi + P}{\Psi + P_r} \right) + \right. \\ &\quad \left. \left( a_3(P - P_r) + a_4 \ln \left[ \frac{\Psi + P}{\Psi + P_r} \right] \right) \left[ \frac{2T - \Theta}{(T - \Theta)^2} \right] + \omega \left( \frac{1}{\varepsilon} - 1 \right) + \omega T Y - T \left( \frac{1}{\varepsilon} - 1 \right) \left( \frac{\partial \omega}{\partial T} \right)_P \right. \\ &\quad \left. - \omega_{Pr,Tr} \left( \frac{1}{\varepsilon_{Pr,Tr}} - 1 \right) \right] - \omega_{Pr,Tr} T_R Y_R \end{aligned} \quad (11)$$

#### Gibbs free energy:

$$\begin{aligned} \overline{G}_i^o &= \overline{G}_i^R + \overline{S}_i^R(T - T_R) - c_1 \left[ T \ln \left( \frac{T}{T_r} \right) - T + T_r \right] + a_1(P - P_r) + a_2 \ln \left( \frac{\Psi + P}{\Psi + P_r} \right) \\ &\quad + \left[ a_3(P - P_r) + a_4 \ln \left( \frac{\Psi + P}{\Psi + P_r} \right) \right] \left( \frac{1}{T - \Theta} \right) \\ &\quad - c_2 \left[ \left( \left( \frac{1}{T - \Theta} \right) - \left( \frac{1}{T_r - \Theta} \right) \right) \left( \frac{\Theta - T}{\Theta} \right) - \frac{T}{\Theta^2} \ln \left( \frac{T_r(T - \Theta)}{T(T_r - \Theta)} \right) \right] \\ &\quad + \omega \left( \frac{1}{\varepsilon} - 1 \right) - \omega_{Pr,Tr} \left( \frac{1}{\varepsilon_{Pr,Tr}} - 1 \right) + \omega_{Pr,Tr} Y_{Pr,Tr} (T - T_r) \end{aligned} \quad (12)$$

#### Entropy:

$$\begin{aligned} \overline{S}_i^o &= \overline{S}_i^R + c_1 \ln \left( \frac{T}{T_r} \right) - \frac{c_2}{\Theta} \left\{ \left( \frac{1}{T - \Theta} \right) - \left( \frac{1}{T_r - \Theta} \right) + \frac{1}{\Theta} \ln \left( \frac{T_r(T - \Theta)}{T(T_r - \Theta)} \right) \right\} \\ &\quad + \left( \frac{1}{T - \Theta} \right)^2 \left[ a_3(P - P_r) + a_4 \ln \left( \frac{\Psi + P}{\Psi + P_r} \right) \right] + \omega Y - \left( \frac{1}{\varepsilon} - 1 \right) \left( \frac{\partial \omega}{\partial T} \right)_P - \omega_{Pr,Tr} Y_{Pr,Tr} \end{aligned} \quad (13)$$

Heat capacity at constant pressure:

$$\begin{aligned} \overline{Cp_i^o} = & c_1 + c_2 \left( \frac{1}{T - \Theta} \right)^2 - \left( \frac{2T}{(T - \Theta)^3} \right) \left[ a_3(P - P_r) + a_4 \ln \left( \frac{\Psi + P}{\Psi + P_r} \right) \right] + \omega TX \\ & + 2TY \left( \frac{\partial \omega}{\partial T} \right)_P - T \left( \frac{1}{\varepsilon} - 1 \right) \left( \frac{\partial^2 \omega}{\partial T^2} \right)_P \end{aligned} \quad (14)$$

Volume:

$$\overline{V_i^o} = a_1 + a_2 \left( \frac{1}{\Psi + P} \right) + \left[ a_3 + a_4 \left( \frac{1}{\Psi + P} \right) \right] \left( \frac{1}{T - \Theta} \right) - \omega Q + \left( \frac{1}{\varepsilon} - 1 \right) \left( \frac{\partial \omega}{\partial T} \right)_T \quad (15)$$

where  $\Theta$  is 228 K,  $\Psi$  is 2600 bar,  $\omega$  is a temperature and pressure dependent term for the electrostatic nature of the electrolytes,  $Q$  is the pressure function of the dielectric constant and  $\varepsilon$  is the dielectric constant of water.

### D1.2 Excess properties

Excess properties are functions of temperature, pressure and composition. The most important excess property is the excess Gibbs free energy. OLI expresses the excess Gibbs free energy as the sum of short, medium and long range interactions:

$$G^E = G_{SR}^E + G_{MR}^E + G_{LR}^E \quad (16)$$

$$\ln \gamma_i = \ln \gamma_i^{SR} + \ln \gamma_i^{MR} + \ln \gamma_i^{LR} \quad (17)$$

$$\frac{G_{LR}^E}{RT} = - \left( \sum_i n_i \right) \frac{4A_x I_x}{\rho} \ln \left( \frac{1 + \rho I_x^{0.5}}{\sum_i x_i [1 + \rho (I_{x,i}^o)^{0.5}]} \right) \quad (18)$$

where  $I_x$  is the mole fraction based ionic strength defined by:

$$I_x = -\frac{1}{2} \sum_i x_i z_i^2 \quad (19)$$

$I_{x,i}^o$  is the ionic strength when the composition is reduced to a pure component (i.e.  $I_{x,i}^o = 0.5z_i^2$ ),  $\rho$  is an empirical constant and the parameter  $A_x$  is given by:

$$A_x = \frac{1}{3} (2\pi N_A d_s)^{0.5} \left( \frac{e^2}{4\pi\epsilon_o\epsilon_s k_B T} \right)^{\frac{3}{2}} \quad (20)$$

where  $N_A$  is the avagadro number,  $d_s$  is the molar density of the solution,  $e$  is the electron charge,  $\epsilon_o$  is the permittivity of a vacuum,  $\epsilon_s$  is the dielectric constant,  $k_B$  is the

Boltzmann constant and  $T$  is the temperature. OLI employs the UNIQUAC model to describe the short range interactions:

$$\frac{G_{SR}^E}{RT} = \frac{G_{combinatorial}^E}{RT} + \frac{G_{residual}^E}{RT} \quad (21)$$

$$\frac{G_{combinatorial}^E}{RT} = \left( \sum_i n_i \right) \left[ \sum_i x_i \ln \frac{\varphi_i}{x_i} + \frac{Z}{2} \sum_i q_i x_i \ln \frac{\theta_i}{\varphi_i} \right] \quad (22)$$

$$\frac{G_{residual}^E}{RT} = - \left( \sum_i n_i \right) \left[ \sum_i q_i x_i \ln \left( \sum_j \theta_j \tau_{ij} \right) \right] \quad (23)$$

$$\theta_i = \frac{q_i x_i}{\sum_j q_j x_j} \quad (24)$$

$$\varphi_i = \frac{r_i x_i}{\sum_j r_j x_j} \quad (25)$$

$$\tau_{ji} = \exp \left( - \frac{a_{ji}}{RT} \right) \quad (26)$$

where  $q_i$  and  $r_i$  are the surface and size parameters of species  $i$ , respectively,  $Z$  a constant,  $a_{ij}$  the binary interaction parameter between species  $i$  and  $j$  ( $a_{ij} \neq a_{ji}$ ). The medium range term arises from ion-ion and ion-molecule interactions not included in the long range term.

$$\frac{G_{MR}^E}{RT} = - \left( \sum_i n_i \right) \sum_i \sum_j x_i x_j B_{ij}(I_x) \quad (27)$$

$$B_{ij}(I_x) = b_{ij} + c_{ij} \exp(-\sqrt{I_x + a_*}) \quad (28)$$

where  $b_{ij}$  and  $c_{ij}$  are adjustable parameters and  $a_*$  is set to 0.01. The parameters  $b_{ij}$  and  $c_{ij}$  are functions of temperature:



$$b_{ij} = b_{0,ij} + b_{1,ij}T + \frac{b_{2,ij}}{T} \quad (29)$$

$$c_{ij} = c_{0,ij} + c_{1,ij}T + \frac{c_{2,ij}}{T} \quad (30)$$

## D2. References

1. Wang, P.; Anderko, A.; Young, R. D., *Fluid Phase Equilib.* **2002**, *203*, 141-176.
2. Wang, P.; Springer, R. D.; Anderko, A.; Young, R. D., *Fluid Phase Equilib.* **2004**, *222-223*, 11-17.
3. Wang, P.; Anderko, A.; Springer, R. D.; Young, R. D., *Journal of Molecular Liquids* **2006**, *125*, 37-44.
4. OLI\_Systems\_Inc., *A guide to using OLI analyser studio 3.2*. OLI Systems Inc.: New Jersey, 2011.

## **APPENDIX E**

### **Supporting information for Chapter 9**

## Table of Contents

E1.	Equations defining kinetic model	369
E2.	Protonation of nitrite ions in ammonium nitrate solutions	377
E2.1	UV-Vis extinction coefficients of $\text{NO}_2^-$ and $\text{HNO}_2$ in ammonium nitrate solution	378
E2.2	UV-Vis spectra of $\text{NO}_2^-$ in ammonium nitrate	378

## E1. Equations defining kinetic model

### Differential equations:

- [1]  $d(A)/d(t) = (k1*B)-(K1*A*H)-(K3*B*A*H)+(k3*C)+(K5*C*D)$
- [2]  $d(B)/d(t)=K1*A*H-k1*B-K3*B*A*H+k3*C-K4*H*B+k4*ON-$   
 $K7a*E*B*H+k7a*F+k7e*N-K7e*O*B*H+2*k10*NO*NO2-$   
 $2*K10*(B^2)+K12*(NO2)^2-k12*B*NO3*H$
- [3]  $d(C)/d(t) = K3*B*A*H-k3*C-K5*C*D$
- [4]  $d(R)/d(t) = k2*D*H-K2*R$
- [5]  $d(D)/d(t) = K2*R-k2*D*H-K5*C*D-K6*ON*D-K8a*F*D-K8e*N*D$
- [6]  $d(E)/d(t) = k7a*F-K7a*E*B*H+K8a*F*D$
- [7]  $d(F)/d(t) = K7a*E*B*H-k7a*F-K8a*F*D$
- [8]  $d(O)/d(t) = -K7e*B*O*H+k7e*N+K8e*D*N$
- [9]  $d(N)/d(t) = K7e*O*B*H-k7e*N-K8e*N*D$
- [10]  $d(ON)/d(t) = K4*B*H-k4*ON-K6*ON*D-K14*ON*U-K15*SA*ON$
- [11]  $d(N2\_N2O3)/d(t) = K5*C*D$
- [12]  $d(N2\_ON)/d(t) = K6*ON*D$
- [13]  $d(N2\_SCN)/d(t) = K8a*F*D$
- [14]  $d(N2\_urea)/d(t) = K14*U*ON$
- [15]  $d(N2\_SA)/d(t) = K15*SA*ON$
- [16]  $d(N2\_SCNH2NH2)/d(t) = K8e*N*D$
- [17]  $d(NO)/d(t) = K10*(B^2)-k10*NO*NO2-rNO-2*K13*(NO^2)*O2$
- [18]  $d(NO2)/d(t)=K10*(B^2)-k10*NO*NO2-rNO2-$   
 $2*K12*((NO2)^2)+2*k12*B*NO3*H+2*K13*(NO^2)*O2$
- [19]  $d(H)/d(t)=-K1*H*A+k1*B+K2*R-k2*H*D-K3*B*A*H+k3*C-$   
 $K4*B*H+k4*ON+K5*C*D+K6*ON*D-K7a*B*E*H+k7a*F+K8a*F*D-$

$$K7e*B*O*H+k7e*N+K8e*O*D-K11*H*AcO+k11*AcOH+K12*(NO2)^2-$$

$$k12*B*NO3*H+K15*ON*SA+K16*HSO4-k16*SO4*H$$

$$[20] \quad d(AcO)/d(t) = -K11*AcO*H+k11*AcOH$$

$$[21] \quad d(AcOH)/d(t) = K11*AcO*H-k11*AcOH$$

$$[22] \quad d(VNO)/d(t) = rNO*24.45$$

$$[23] \quad d(VNO2)/d(t) = rNO2*24.45$$

$$[24] \quad d(V)/d(t)=$$

$$(K5*C*D+K6*ON*D+K8a*F*D+K8e*N*D+K14*ON*U+K15*SA*ON+rNO \\ +rNO2)*(Rg1*T/101.325)$$

$$[25] \quad d(NO3)/d(t) = K12*((NO2)^2)-k12*B*NO3*H$$

$$[26] \quad d(O2)/d(t) = -K13*(NO^2)*O2$$

$$[27] \quad d(U)/d(t) = -K14*ON*U$$

$$[28] \quad d(SA)/d(t) = -K15*SA*ON$$

$$[29] \quad d(HSO4)/d(t) = K15*ON*SA-K16*HSO4+k16*SO4*H$$

$$[30] \quad d(SO4)/d(t) = K16*HSO4-k16*SO4*H$$

Explicit equations:

$$[1] \quad \text{bubbles} = 1.09*10^7$$

$$[2] \quad \text{Sfactor} = 4.8$$

$$[3] \quad \text{Ea1f} = 20$$

$$[4] \quad \text{Ea1b} = 26.7$$

$$[5] \quad \text{Ea2f} = 72$$

$$[6] \quad \text{Ea2b} = 20$$

$$[7] \quad \text{Ea3f} = 20$$

$$[8] \quad \text{Ea3b} = 29.9$$

- [9]  $Ea_{4f} = 65.2$
- [10]  $Ea_{4b} = 20$
- [11]  $Ea_5 = 30$
- [12]  $Ea_6 = 20$
- [13]  $Ea_{7af} = 20$
- [14]  $Ea_{7ab} = 32$
- [15]  $Ea_{7ef} = 0$
- [16]  $Ea_{7eb} = 0$
- [17]  $Ea_{8af} = 36$
- [18]  $Ea_{8ef} = 0$
- [19]  $Ea_{10f} = 65$
- [20]  $Ea_{10b} = 22$
- [21]  $Ea_{11f} = 0$
- [22]  $Ea_{11b} = 0$
- [23]  $radius = (3*(V/(1000*bubbles)))/(4*3.14159))^{(1/3)}$
- [24]  $PNO = VNO/V$
- [25]  $PNO_2 = VNO_2/V$
- [26]  $Ea_{12f} = 20$
- [27]  $Ea_{12b} = 75$
- [28]  $Ea_{13f} = 9.6$
- [29]  $Ea_{14f} = 17$
- [30]  $Ea_{15f} = 9.2$
- [31]  $Ea_{16f} = 1.5$
- [32]  $R_g = 8.314/1000$
- [33]  $K_{mt} = 0.011$

$$[34] \quad k_{\text{HNO}_2} = 4 \cdot 10^{(-2)} / \text{Sfactor}$$

$$[35] \quad k_{\text{HNO}} = 1.95 \cdot 10^{(-3)} / \text{Sfactor}$$

$$[36] \quad \text{Area} = 4 \cdot 3.14159 \cdot (\text{radius}^2) \cdot \text{bubbles}$$

$$[37] \quad r_{\text{NO}} = K_{\text{mt}} \cdot \text{Area} \cdot (\text{NO} - (\text{PNO} \cdot k_{\text{HNO}}))$$

$$[38] \quad \text{total\_N} = \text{A} + \text{B} + \text{D} + \text{R} + \text{NO} + \text{NO}_2 + \text{NO}_3 + \text{C} + \text{F} + (\text{N}_2\_ \text{N}_2\text{O}_3 + \text{N}_2\_ \text{SCN} + \text{N}_2\_ \text{ON}) \cdot 2 \\ + ( \quad \text{VNO} + \text{VNO}_2) / 24.45$$

$$[39] \quad T = 298$$

$$[40] \quad T_o = 298$$

$$[41] \quad r_{\text{NO}_2} = K_{\text{mt}} \cdot \text{Area} \cdot (\text{NO}_2 - (\text{PNO}_2 \cdot k_{\text{HNO}_2}))$$

$$[42] \quad k_{10} = 1 \cdot 10^8 \cdot \exp((E_{a10b} / R_g) \cdot ((1/T_o) - (1/T)))$$

$$[43] \quad k_{12} = 0.0127 \cdot \exp((E_{a12b} / R_g) \cdot ((1/T_o) - (1/T)))$$

$$[44] \quad k_1 = 6.93 \cdot 10^6 \cdot \exp((E_{a1b} / R_g) \cdot ((1/T_o) - (1/T)))$$

$$[45] \quad K_1 = 1 \cdot 10^{10} \cdot \exp((E_{a1f} / R_g) \cdot ((1/T_o) - (1/T)))$$

$$[46] \quad K_2 = 21.5 \cdot \exp((E_{a2f} / R_g) \cdot ((1/T_o) - (1/T)))$$

$$[47] \quad k_2 = 4.3 \cdot 10^{10} \cdot \exp((E_{a2b} / R_g) \cdot ((1/T_o) - (1/T)))$$

$$[48] \quad K_3 = 32000 \cdot \exp((E_{a3f} / R_g) \cdot ((1/T_o) - (1/T)))$$

$$[49] \quad k_3 = 6400 \cdot \exp((E_{a3b} / R_g) \cdot ((1/T_o) - (1/T)))$$

$$[50] \quad K_4 = 12000 \cdot \exp((E_{a4f} / R_g) \cdot ((1/T_o) - (1/T)))$$

$$[51] \quad k_4 = 1 \cdot 10^{12} \cdot \exp((E_{a4b} / R_g) \cdot ((1/T_o) - (1/T)))$$

$$[52] \quad K_5 = 4.3 \cdot 10^6 \cdot \exp((E_{a5} / R_g) \cdot ((1/T_o) - (1/T)))$$

$$[53] \quad K_6 = 3.8 \cdot 10^{11} \cdot \exp((E_{a6} / R_g) \cdot ((1/T_o) - (1/T)))$$

$$[54] \quad K_{7a} = 11700 \cdot \exp((E_{a7af} / R_g) \cdot ((1/T_o) - (1/T)))$$

$$[55] \quad k_{7a} = 366 \cdot \exp((E_{a7ab} / R_g) \cdot ((1/T_o) - (1/T)))$$

$$[56] \quad K_{7e} = 6960 \cdot \exp((E_{a7ef} / R_g) \cdot ((1/T_o) - (1/T)))$$

$$[57] \quad k_{7e} = 1.39 \cdot \exp((E_{a7eb} / R_g) \cdot ((1/T_o) - (1/T)))$$



[58]  $K_{8a} = 8.4 \cdot 10^5 \cdot \exp((E_{8af}/R_g) \cdot ((1/T_o) - (1/T)))$

[59]  $K8e = 2800 * \exp((Ea8ef/Rg)*((1/To)-(1/T)))$

[60]  $K_{10} = 11.6 * \exp((E_{a10}/R_g) * ((1/T_o) - (1/T)))$

[61]  $r_{10} = K_{10} \cdot (B^2) - k_{10} \cdot NO \cdot NO_2$

[62]  $K11 = 1 * 10^{10} * \exp((Ea11f/Rg)*((1/To)-(1/T)))$

[63]  $k_{11} = 1.09 \cdot 10^5 \cdot \exp((E_{a11b}/R_g) \cdot ((1/T_o) - (1/T)))$

[64]  $K_{12} = 1 \cdot 10^8 \cdot \exp((E_{a12}/R_g) \cdot ((1/T_o) - (1/T)))$

[65]  $r_{12} = K_{12} * ((NO_2)^2) - k_{12} * B * NO_3 * H$

[66]  $K13 = 2.1 \cdot 10^6 \cdot \exp((Ea13f/Rg) \cdot ((1/To) - (1/T)))$

[67]  $K14 = 4.83 \cdot 10^7 \cdot \exp((Ea14f/Rg) \cdot ((1/To) - (1/T)))$

[68]  $K_{15} = 1.5 \cdot 10^{11} \cdot \exp((E_{a15f}/R_g) \cdot ((1/T_o) - (1/T)))$

[69]  $K16 = 1.1 \cdot 10^8 \cdot \exp((E_{a16}/R_g) \cdot ((1/T_o) - (1/T)))$

[70] Ea16b = 20

$$[71] \quad k_{16} = 1 \cdot 10^{10} \cdot \exp((E_{a16}/R_g) \cdot ((1/T_o) - (1/T)))$$

```
[72] NOeqm = PNO*kHNO+0.000000000000000000000000000000000000
```

[73]  $E_{qm} \text{ frn} = NO/NO_{eqm}$

[74]  $R_{g1} = R_g^*1000$

[75]  $fHONO = B/(A+B)$

### Definition of variables

<i>Variable</i>	<i>Initial value</i>	<i>Definition</i>
t	0	time
A	0.015	Nitrite ion, NO <sub>2</sub> <sup>-</sup>
B	0	Nitrous acid, HNO <sub>2</sub>
C	0	Dinitrogen trioxide, N <sub>2</sub> O <sub>3</sub>
R	13	Ammonium cation, NH <sub>4</sub> <sup>+</sup>
D	6.80E-05	Ammonia, NH <sub>3</sub>
E	0.024	Thiocyanate anion, SCN <sup>-</sup>

F	0	Nitrosyl thiocyanate, ONSCN
O	0	Thiourea, C=S(NH <sub>2</sub> ) <sub>2</sub>
N	0	Nitroso-thiourea C=S(NH <sub>2</sub> ) <sub>2</sub> NO <sup>+</sup>
ON	0	Nitrosyl cation, ON <sup>+</sup>
N2_N2O3	0	N <sub>2</sub> formed from N <sub>2</sub> O <sub>3</sub> pathway
N2_ON	0	N <sub>2</sub> formed from ON <sup>+</sup> pathway
N2_SCN	0	N <sub>2</sub> formed from ONSCN pathway
N2_urea	0	N <sub>2</sub> formed from urea nitrosation
N2_SA	0	N <sub>2</sub> formed from sulfamic acid nitrosation
N2_SCNH2N	0	N <sub>2</sub> formed from thiourea catalysed nitrosation of ammonia
NO	0	Nitric oxide, NO
NO2	0	Nitrogen dioxide, NO <sub>2</sub>
H	1.00E-05	Hydrogen cation, H <sup>+</sup>
AcO	0	Acetate anion, CH <sub>3</sub> COO <sup>-</sup>
AcOH	0.03	Acetic acid, CH <sub>3</sub> COOH
VNO	0	Volume of nitric oxide gas
VNO2	0	Volume of nitrogen dioxide gas
V	1.00E-07	Total gas volume
NO3	13	Nitrate anion, NO <sub>3</sub> <sup>-</sup>
O2	0	Dissolved oxygen, O <sub>2</sub>
U	0	Urea, C=O(NH <sub>2</sub> ) <sub>2</sub>
SA	0	Sulfamic acid, SO <sub>3</sub> NH <sub>2</sub>
HSO4	0	Bisulfate anion, HSO <sub>4</sub> <sup>-</sup>
SO4	0	Sulfate anion, SO <sub>4</sub> <sup>2-</sup>
bubbles	1.09E+07	Number of gas bubbles per L of emulsion
Sfactor	4.8	Ratio of gas solubility in water compared to NH <sub>4</sub> NO <sub>3</sub>
Ea1f	20	Activation energy
Ea1b	26.7	Activation energy
Ea2f	72	Activation energy
Ea2b	20	Activation energy
Ea3f	20	Activation energy
Ea3b	29.9	Activation energy
Ea4f	65.2	Activation energy
Ea4b	20	Activation energy
Ea5	30	Activation energy
Ea6	20	Activation energy
Ea7af	20	Activation energy
Ea7ab	32	Activation energy
Ea7ef	0	Activation energy
Ea7eb	0	Activation energy
Ea8af	36	Activation energy
Ea8ef	0	Activation energy
Ea10f	65	Activation energy
Ea10b	22	Activation energy
Ea11f	0	Activation energy
Ea11b	0	Activation energy
radius	1.30E-06	Gas bubble radius
PNO	0	Partial pressure of nitric oxide

PNO2	0	Partial pressure of nitrogen dioxide
Ea12f	20	Activation energy
Ea12b	75	Activation energy
Ea13f	9.6	Activation energy
Ea14f	17	Activation energy
Ea15f	9.2	Activation energy
Ea16f	1.5	Activation energy
Rg	0.008314	Gas constant
Kmt	0.011	Mass transfer coefficient
kHNO2	0.008333	Henry's constant for NO <sub>2</sub>
kHNO	4.06E-04	Henry's constant for nitric oxide
Area	2.31E-04	Interfacial area (gas bubbles-emulsion interface)
rNO	0	Rate of nitric oxide mass transfer
total_N	26.01507	Mass balance on nitrogen
T	298	Temperature
To	298	Reference temperature
rNO2	0	Rate of nitrogen dioxide mass transfer
k10	1.00E+08	Reverse rate constant for HNO <sub>2</sub> decomposition
k12	0.0127	Reverse rate constant for NO <sub>2</sub> hydrolysis
k1	6.93E+06	Rate constant for HNO <sub>2</sub> dissociation
K1	1.00E+10	Rate constant for association of NO <sub>2</sub> <sup>-</sup> and H <sup>+</sup>
K2	21.5	Rate constant for ammonium dissociation
k2	4.30E+10	Rate constant for association of NH <sub>3</sub> and H <sup>+</sup>
K3	3.20E+04	Rate constant for N <sub>2</sub> O <sub>3</sub> formation
k3	6400	Rate constant for N <sub>2</sub> O <sub>3</sub> hydrolysis
K4	1.20E+04	Rate constant for ON <sup>+</sup> formation
k4	1.00E+12	Rate constant for ON <sup>+</sup> hydrolysis
K5	4.30E+06	Rate constant for ammonia nitrosation by N <sub>2</sub> O <sub>3</sub>
K6	3.80E+11	Rate constant for ammonia nitrosation by ON <sup>+</sup>
K7a	1.17E+04	Rate constant for ONSCN formation
k7a	366	Rate constant for ONSCN hydrolysis
K7e	6960	Rate constant for nitrosyl thiourea formation
k7e	1.39	Rate constant for nitrosyl thiourea hydrolysis
K8a	8.40E+05	Rate constant for ammonia nitrosation by ONSCN
K8e	2800	Rate constant for ammonia nitrosation by nitrosyl thiourea
K10	11.6	Rate constant for nitrous acid decomposition
r10	0	Rate of reaction 10
K11	1.00E+10	Rate constant for association of CH <sub>3</sub> COO <sup>-</sup> and H <sup>+</sup>
k11	1.09E+05	Rate constant for CH <sub>3</sub> COOH dissociation
K12	1.00E+08	Rate constant for NO <sub>2</sub> hydrolysis
r12	0	Rate of reaction 12
K13	2.10E+06	Rate constant for oxidation of NO by O <sub>2</sub>
K14	4.83E+07	Rate constant for nitrosation of urea
K15	1.50E+11	Rate constant for nitrosation of sulfamic acid
K16	1.10E+08	Rate constant for dissociation of HSO <sub>4</sub> <sup>-</sup>
Ea16b	20	Activation energy
k16	1.00E+10	Rate constant for association of SO <sub>4</sub> <sup>2-</sup> and H <sup>+</sup>
NOeqm	1.00E-25	Equilibrium nitric oxide concentration

Eqm_fr	0	Ratio of nitric oxide concentration to NOeqm
Rgl	8.314	Gas constant
fHONO	0	Fraction of total nitrite as nitrous acid

All concentrations in mol L<sup>-1</sup>

## E2. Protonation of nitrite ions in ammonium nitrate solutions

The proportion of nitrite ions converted into nitrous acid by acetic acid at various concentrations of ammonium nitrate was determined by examining the UV-vis spectra of the solutions. This involved firstly determining the extinction coefficients of nitrous acid and nitrite ions in solutions with different concentrations of ammonium nitrate. These extinction coefficients could then be used to determine the concentrations of nitrite and nitrous acid in a solution containing a known concentration of acetic acid, using the equations derived below:

$$A_1 = C_a \varepsilon_{a,1} + C_b \varepsilon_{b,1} \quad (D1)$$

$$A_2 = C_a \varepsilon_{a,2} + C_b \varepsilon_{b,2} \quad (D2)$$

where  $A$  is absorbance,  $C$  is concentration, and  $\varepsilon$  is the molar extinction coefficients, the subscripts  $a$  and  $b$  refer to species  $a$  and  $b$  and the number subscripts refer to the wavelength 1 and 2 respectively. Substituting (D2) into (D1) for  $C_a$ :

$$A_1 = \frac{A_2 \varepsilon_{a,1} - C_b \varepsilon_{a,1} \varepsilon_{b,2}}{\varepsilon_{a,2}} + C_b \varepsilon_{b,1} \quad (D3)$$

hence

$$C_b = \frac{A_1 \varepsilon_{a,2} - A_2 \varepsilon_{a,1}}{\varepsilon_{b,1} \varepsilon_{a,2} - \varepsilon_{a,1} \varepsilon_{b,2}} \quad (D4)$$

$$C_a = \frac{A_2 - C_b \varepsilon_{b,2}}{\varepsilon_{b,1}} \quad (\text{D5})$$

### E2.1 UV-Vis extinction coefficients of $\text{NO}_2^-$ and $\text{HNO}_2$ in ammonium nitrate solution

	Water		5 mol L <sup>-1</sup> $\text{NH}_4\text{NO}_3$		10 mol L <sup>-1</sup> $\text{NaNO}_3$	
Wavelength (nm)	$\varepsilon_{\text{NO}_2^-}$	$\varepsilon_{\text{HNO}_2}$	$\varepsilon_{\text{NO}_2^-}$	$\varepsilon_{\text{HNO}_2}$	$\varepsilon_{\text{NO}_2^-}$	$\varepsilon_{\text{HNO}_2}$
357.7	22.561	53.25	24.41	53.965	26.717	55.126
371	15.857	55.72	17.37	56.024	19.331	56.313
386	5.35	32.25	6.04	32.892	6.8903	33.27

### E2.2 UV-Vis spectra of $\text{NO}_2^-$ in ammonium nitrate

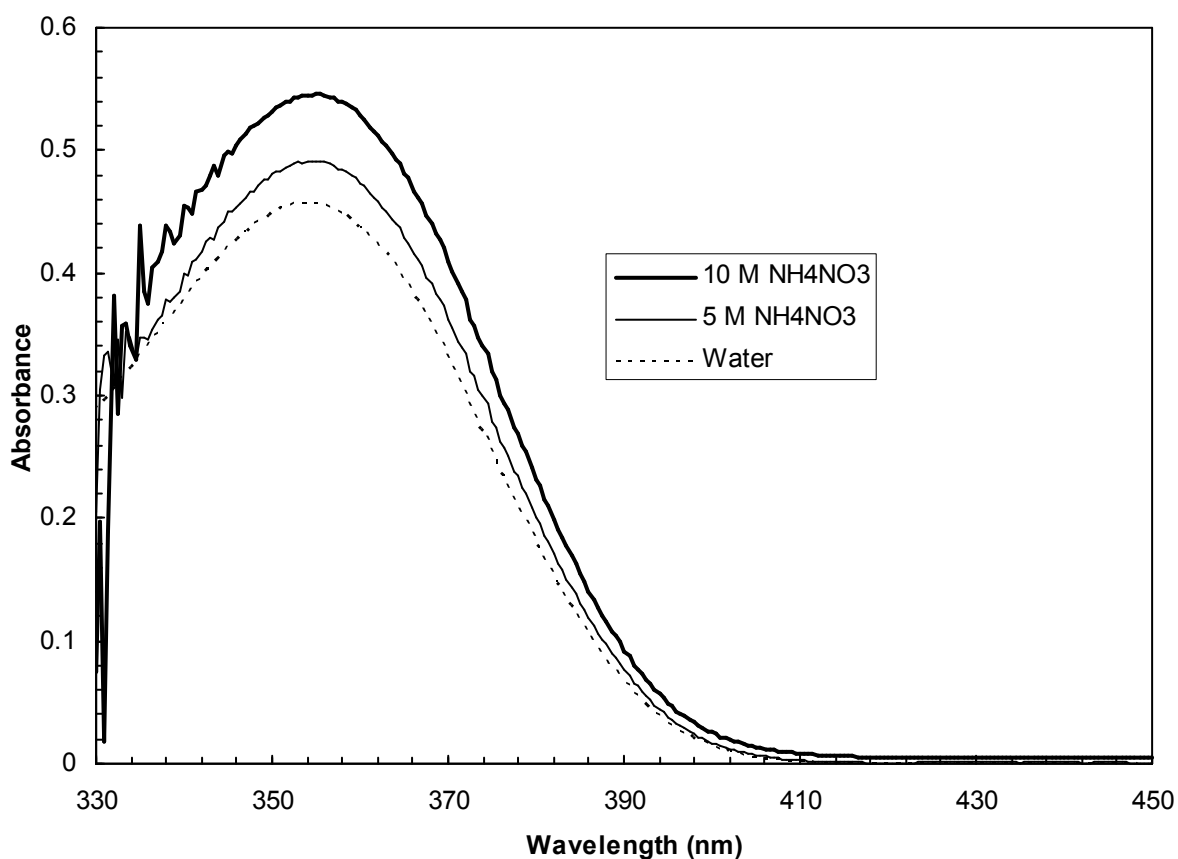


Figure E1. Spectra of 0.02 M  $\text{NO}_2^-$  in 0, 5 and 10 mol L<sup>-1</sup>  $\text{NH}_4\text{NO}_3$

## **APPENDIX F**

### **Publications arising from the present study**

1. Rayson, M. S.; Mackie, J. C.; Kennedy, E. M.; Dlugogorski, B. Z., Experimental study of decomposition of aqueous nitrosyl thiocyanate. *Inorg. Chem.* **2011**, 50 (16), 7440-7452.
2. Rayson, M. S.; Mackie, J. C.; Kennedy, E. M.; Dlugogorski, B. Z., Improved rate constants for nitrous acid decomposition in aqueous solution and kinetic modeling of NO<sub>x</sub> formation from nitrosating agents. *International Conference on Chemical Kinetics.* **2011**, Boston, Massachusetts.
3. Rayson, M. S.; Mackie, J. C.; Kennedy, E. M.; Dlugogorski, B. Z., Accurate rate constants for decomposition of aqueous nitrous acid. *Inorg. Chem.* **2012**, 51 (4), 2178-2185.